Assessing the Potential of Different Oil Seeds for Biodiesel Synthesis Using Green Nano-Catalysts

By

Maria Ameen

Department of Plant Sciences

Quaid-i-Azam University Islamabad, Pakistan

2023

Assessing the Potential of Different Oil Seeds for Biodiesel Synthesis Using Green Nano-Catalysts

A Dissertation Submitted In Partial Fulfillment of the Requirements for the Degree Of

DOCTOR OF PHILOSOPHY (Ph.D)

In

Plant Sciences (Plant Systematics and Biodiversity)

By

Maria Ameen

Department of Plant Sciences

Quaid-i-Azam University Islamabad, Pakistan

2023

In the name of Allah, the Most Merciful, the Most Kind

Then, let man look at his food. That We pour forth water in abundance. And We split earth in clefts. And We cause therein the grain to grow, and grapes and clover plant (i.e. green fodder for cattle). And olives and date-palms. And gardens, dense with many trees. And fruits and Abba (herbage, etc.). (To be) a provision and benefit for you and your cattle

❖ Surah 80: Verses 24-32

This humble effort is dedicated

With

Great love & honor

To

Esteemed and Exalted Messenger of Allah,

Our Holy Prophet

HAZRAT MUHAMMAD ﷺ
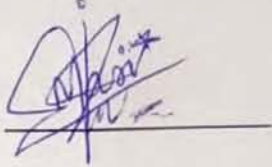
(Blessings and Peace Be Upon Him)

And his Family

The Eternal Source of Guidance for
Humanity

CERTIFICATE OF APPROVAL

This is to certify that research work presented in this thesis, entitled "Assessing the Potential of Different Oil Seeds for Biodiesel Synthesis Using Green Nano-Catalysts" was conducted by **Miss Maria Ameen** under the supervision of **Dr. Muhammad Zafar.** No part of this thesis has been submitted anywhere else for any other degree. This thesis is submitted to the Department of Plant Sciences, Quaid-i-Azam University, Islamabad, Pakistan in partial fulfillment of the requirements for the degree of Doctor of Philosophy in the field of **Plant Sciences (Plant Systematics and Biodiversity),** Department of Plant Sciences, Quaid-i-Azam University, Islamabad, Pakistan.
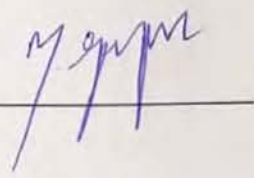
Student name: **Miss Maria Ameen**   Signature: _____
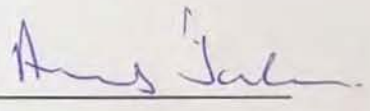
Examination committee

External Examiner 1

Prof. Dr. Muhammad Gulfraz   Signature: _____
Department of Biochemistry
Pir Mehr Ali Shah, Arid Agriculture University,
Rawalpindi

External Examiner 2

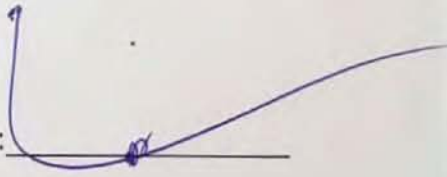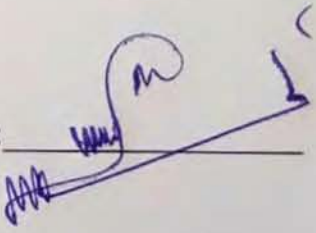**Dr. Asma Jabeen**   Signature _____
Associate Professor
Environmental Sciences Program
Fatima Jinnah Women University
The Mall
Rawalpindi

Supervisor   Signature: _____
Dr. Muhammad Zafar
Associate Professor
Department of Plant Sciences
Quaid-i-Azam University, Islamabad

Chairman   Signature: _____
Prof. Dr. Mushtaq Ahmad
Department of Plant Sciences
Quaid-i-Azam University,
Islamabad

Dated: 30-05-2023

FOREIGN EXAMERS

Prof. Dr. Elizabeth M. Williamson

School of Pharmacy, Pharmacy Practice, Reading University. Whiteknights, Reading UK

Post Code RG6 6AP, United Kingdom

Email: e.m.williamson@reading.ac.uk

Prof. Dr. Geoffrey M. Gadd

Department of Biological Sciences University of Dundee,

Dundee, DD1 4HN Scotland, UK.

E-mail: g.m.gadd@dundee.ac.uk

QUAID-I-AZAM UNIVERSITY

Department of Plant Sciences
Islamabad, Pakistan 45320

No. _____   10 February, 2023

Subject: **Author Declaration**

I Ms. Maria Ameen hereby state that my PhD thesis titled "Assessing the Potential of Different Oil Seeds for Biodiesel Synthesis Using Green Nano-Catalysts" is my own work and has not been submitted previously by me for taking any degree from Department of Plant Sciences, Quaid-i-Azam University, Islamabad or anywhere else in the country/world.

At any time if my statement is found to be incorrect even after my Graduate the university has the right to withdraw my PhD degree.

Student/Author Signature_____

Maria Ameen

No. _____   10 February, 2023

Subject: <u>Plagiarism Undertaking</u>

I solemnly declare that the research work presented in the thesis titled "**Assessing the Potential of Different Oil Seeds for Biodiesel Synthesis Using Green Nano-Catalysts**" is solely my research work with no significant contribution from any other person. Small contribution/help wherever taken has been duly acknowledged and that complete thesis has been written by me.

I understand the zero-tolerance policy of the HEC and Quaid-i-Azam University towards plagiarism. Therefore, I as an author of the above-titled thesis declare that no portion of my thesis has been plagiarized and any material used as reference is property referred/cited.

I undertake that if I am found faulty of any formal plagiarism in the above-titled thesis even after awarding of Ph.D. degree, the University reserves the right to withdraw/revoke my Ph.D. degree and that HEC and the University has the right to publish my mime on the HEC/University website on which name of students are placed who submitted plagiarized thesis

Student/Author Signature_____

Maria Ameen

قائداعظم یونیورسٹی

QUAID-I-AZAM UNIVERSITY

Department of Plant Sciences
Islamabad, Pakistan 45320

SIMILARITY INDEX CERTIFICATE

It is certified that Miss Maria Ameen has completed his Ph.D. research work and compilation of the thesis. The title of her thesis is "Assessing the Potential of Different Oil Seeds for Biodiesel Synthesis Using Green Nano-Catalysts". Her thesis has been checked on Turnitin for similarity index and found 11% that lies in the limits provided by HEC (20%).

Dr. Muhammad Zafar
Supervisor

Turnitin Originality Report

Assessing the Potential of Different Oil Seeds for Biodiesel Synthesis Using Green Nano-Catalysts   by Maria Ameen .

From PhD (PhD DRSML)

- Processed on 07-Feb-2023 11:14 PKT
- ID: 2008344233
- Word Count: 43568

Similarity Index
11%
Similarity by Source

Internet Sources:
        6%
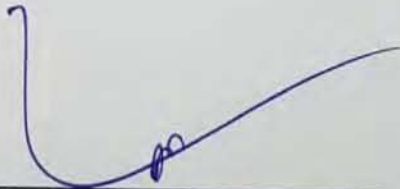Publications:
        9%
Student Papers:
        2%

sources:

1 1% match (Rozina, Mushtaq Ahmad, Lee Keat Teong, Shazia Sultana, Muhammad Zafar. "Sustainable and Eco-friendly Synthesis of Biodiesel from Novel and Non-edible seed oil of Monotheca buxifolia using Green Nano-catalyst of Calcium oxide", Energy Conversion and Management: X, 2021)

Rozina, Mushtaq Ahmad, Lee Keat Teong, Shazia Sultana, Muhammad Zafar. "Sustainable and Eco-friendly Synthesis of Biodiesel from Novel and Non-edible seed oil of Monotheca buxifolia using Green Nano-catalyst of Calcium oxide", Energy Conversion and Management: X, 2021

2 1% match (Rozina, Mushtaq Ahmad, Saira Asif, Jiří Jaromír Klemeš et al. "Conversion of the toxic and hazardous Zanthoxylum armatum seed oil into methyl ester using green and recyclable silver oxide nanoparticles", Fuel, 2022)

Rozina, Mushtaq Ahmad, Saira Asif, Jiří Jaromír Klemeš et al. "Conversion of the toxic and hazardous Zanthoxylum armatum seed oil into methyl ester using green and recyclable silver oxide nanoparticles", Fuel, 2022

3 1% match (Internet from 05-Jan-2023)

http://prr.hec.gov.pk/jspui/bitstream/123456789/18861/1/Anam%20Fatima%20botany%202021%20QAU%20isb.pdf

4 < 1% match (Internet from 05-Dec-2022)
http://prr.hec.gov.pk/jspui/bitstream/123456789/16581/1/21451-Hamza%20Shehzad.pdf

5 < 1% match (Internet from 06-Jan-2023)

http://prr.hec.gov.pk/jspui/bitstream/123456789/15741/1/Farhat%20Rashid%20food%20sci%202020%20uos%20sargoda%20.pdf

6 < 1% match (student papers from 22-Jan-2017)
Submitted to Higher Education Commission Pakistan on 2017-01-22

7 < 1% match (student papers from 13-Oct-2022)
Submitted to Higher Education Commission Pakistan on 2022-10-13

8 < 1% match (student papers from 27-Oct-2020)
Submitted to Higher Education Commission Pakistan on 2020-10-27

9 < 1% match (student papers from 23-Nov-2022)
Submitted to Higher Education Commission Pakistan on 2022-11-23

10 < 1% match (student papers from 23-Sep-2011)
Submitted to Higher Education Commission Pakistan on 2011-09-23

11 < 1% match (student papers from 19-Mar-2012)
Submitted to Higher Education Commission Pakistan on 2012-03-19

12 < 1% match (student papers from 02-Aug-2022)
Submitted to Higher Education Commission Pakistan on 2022-08-02

13 < 1% match (student papers from 08-Apr-2018)
Submitted to Higher Education Commission Pakistan on 2018-04-08

Subject: <u>**Publication of W – Category Miss Maria Ameen (Ph.D. Scholar)**</u>

This is in reference to circular regarding the publication requirement for Ph.D. scholars in Department of Plant Sciences, Faculty of Biological Sciences. It is certified that **Miss Maria Ameen** has published research papers in W-Categories as given below:

Sr. No.	Paper Title	Impact Factor
1.	Ameen, M., Zafar, M., Ramadan, M. F., Ahmad, M., Makhkamov, T., Bokhari, A., ... & Show, P. L. (2023). Conversion of novel non-edible Bischofia javanica seed oil into methyl ester via recyclable zirconia-based phyto-nanocatalyst: A circular bioeconomy approach for eco-sustenance. Environmental Technology & Innovation, 30, 103101.	7.758
2.	Ameen, M., Zafar, M., Ahmad, M., Ramadan, M. F., Eid, H. F., Makhkamov, T., ... & Majeed, S. (2023). Assessing the Bioenergy Potential of Novel Non-Edible Biomass Resources via Ultrastructural Analysis of Seed Sculpturing Using Microscopic Imaging Visualization. Agronomy, 13(3), 735.	3.949
3.	Ameen, M., Zafar, M., Ahmad, M., Shaheen, A., & Yaseen, G. (2018). Wild melon: a novel non-edible feedstock for bioenergy. Petroleum Science, 15, 405-411.	4.757
4.	Ameen, M., Zafar, M., Nizami, A. S., Ahmad, M., Munir, M., Sultana, S.,... & Rehan, M. (2022). Biodiesel Synthesis from Cucumis melo var. Agrestis Seed Oil: Towards Non-Food Biomass Biorefineries. Frontiers in Energy Research, 943.	4.008
5.	Ameen, M., Ahmad, M., Zafar, M., Munir, M., Abbas, M. M., Sultana, S.,... & Kalam, M. A. (2022). Prospects of catalysis for process sustainability of eco-green biodiesel synthesis via transesterification: a state-of-the-art review. Sustainability, 14(12), 7032.	3.889

Dr. Muhammad Zafar
Supervisor

ACKNOWLEDGMENT

I am obliged to **Dr. Mamoona Munir** for her compassion and assistance, many thanks to her for upbringing my research interest.. I pay cordial gratitude to my all lab fellows especially **Farida Anjum.** A huge credit goes to my dear friends **Shaista, Rozina,** and **Nabila** in completion of this project. I am gratified to **Sadia, Wajiha, Uroosa, Iqra** and all PhD and M.Phil fellows. I am also thankful to **Muhammad Sufyan** and **Farooq Ahmad** for their cooperation within this period

Words always seem to shallow whenever it comes to my parents. I wish to express my deepest love to my generous father **Muhammad Ameen Hayat** and loving mother **Riaz Akhtar**, the ones, can never ever be thanked enough for their never-ending prayers and overwhelming love, they bestow upon me and demand nothing for their incessant efforts and difficulties they face while providing me all the possible conveniences and every ease of life.

I owe every success to my caring brother **Muhammad Faisal Ameen** who has constantly assisted me pertaining to my work and intensely longed to see this goal get achieved. I am absolutely nothing without his support and encouragement. How can I forget my younger brother **Muhammad Saad Ameen** whose love and care always makes me happy.

I can't express my unfathomable love for my dear friends **Dr. Mehrin Gul**, **Dr. Hizran Khatoon** and **Rahila Bashar.** How can I neglect the caring attitude of **Roshan Ameen** and **Amina Anwar** who have always understood my feelings and tried their best to provide me every happiness, joy and pleasure? I would not be able to rebuild my potential after each suffering without my sincere friends.

I pay my affable regards to my beloved uncles **M. Saleem Hayat, M. Naeem Hayat, Khalid Mahmood** and **Abdul Ghafoor** (late) and my grandmother. I warmly appreciate my all aunties, uncles and cousins for their nice concern.

I express my deep love to my religious guide and renowned Islamic scholar **Alimah Tahira Yousaf Sahiba** and dear **Dr. Momina Habib** for their giving me a firm belief in Him (SWT) that supports me morally for achieving my every goal.

Last but not least I acknowledge the love of my beloved ones who are no more (Late) especially my grandfather **Maj. Haji Hayat Muhammad**, my virtuous maternal grandfather **Mian Abdullah** and loving maternal grandmother **Ghulam Serwar,** for their deep prayers and mellifluous affection for me and my family. May their souls rest in eternal peace.

Maria Ameen

TABLE OF CONTENTS

LIST OF TABLES

LIST OF FIGURES

LIST OF PLATES

ABSTRACT

The present study is confined to identification of novel oil yielding seeds as potential feedstock for sustainable biodiesel production. In this project, eight different oil seeds were investigated systematically on the basis of considerable oil content. This research is focused on feedstock collection, morphological identification, scanning electron microscopic examination, mechanical oil extraction, free fatty acid value (FFA) determination, biodiesel yield optimization, biodiesel characterization via advance analytical techniques and fuel properties comparison with international standards i.e. ASTM D-6751. Different oil seeds selected in this study include *Bischofia javanica* Blume*, Eryobotrya japonica* (Thunb.) Lindl., *Praecitrulus fistulosus* (Stocks) Pangalo*, Luffa acutangula* (Linn.) Roxb*., Diospyros lotus* L.*, Cucumis melo* var. *Cantalupensis, Solanum surattense* Burm. f. and *Cucumis melo var. agrestis* Naudin. Eight different, affordable, stable and efficient green nano-catalysts were synthesized from same feedstock via biosynthesis method. For this purpose, different plant parts (leaves, seed shells, seed cake, flowers, bark, peel, calyx and seed extract) were used to prepare respective extracts that act as reducing and capping agent. The synthesized green nano-catalysts were characterized by analytical techniques such as X-Ray Diffraction Spectroscopy (XRD), Scanning Electron Microscopy (SEM), Energy Dispersive X-Ray Spectroscopy (EDX) and Fourier Transform Infrared Spectroscopy (FT-IR). All selected seed oils have less than 3% FFA content therefore subjected to single step transesterification directly except non-edible seed oils of *Luffa acutangula* (3.91 mg/KOH) and *Diospyros lotus* (6.91 mg/KOH) that require pretreatment for FFA reduction. Hence, *Luffa acutangula* and *Diospyros lotus* seed oils were subjected to acid esterification with 1% Sulphuric acid (H_2SO_4) followed by transesterification. Furthermore, Response Surface Methodology (RSM) was used to optimize the biodiesel yield by adjusting the reaction variables. Results showed the highest biodiesel yield (98%) recorded for *Cucumis melo* var. *Cantalupensis* using Calcium oxide (CaO) green nano-catalyst (1:9 oil to methanol ratio, 1.05 wt. % catalyst loading at 70°C for 3h). However, the lowest biodiesel yield (87%) was observed in case of *Diospyros lotus* catalyzed by Nickle oxide (NiO) green nano-catalyst (1:9 oil to methanol ratio, 1.25 wt. % of NiO catalyst loading at 65°C for 2h). These outcomes clearly show that all the biosynthesized green nano-catalysts were (ZrO_2, CoO, CuO, CdO, NiO, CaO, Ag_2O and MgO) are renewable, prospective and dynamic for efficient conversion of seed oil

to cost-effective biodiesel. Based on these experimental results, it is recommended that the renewable feedstocks used in this research for synthesis of both green nano-catalyst and biodiesel be employed for industrial implementation at a global level because it is readily available, economically feasible and ecologically viable. The study also suggests mass cultivation of such substantially innovative feedstock for green energy generation on a commercial scale.

CHAPTER: 1

INTRODUCTION

1.1 Biodiesel: A Potential Source of Green Energy

Rising energy demands and exhaustion of fossil fuels have triggered the efforts of researchers to the exploration of renewable energy resources such as biofuel. To resolve the issue of petroleum price hikes, the interest of the scientific community has been diverted towards the utilization of biofuels (biogas, bioethanol, and biodiesel) as an unsurpassed alternate option to finite fossil fuel. Because, biofuel has been proven as a prospective renewable energy source with a high potential to overcome the drastic global concerns and fossil fuel shortage (Sharma *et al.,* 2020). Inadequate petrodiesel can be effectually replaced with sustainable biodiesel as it appears to be the best substitution preference. Biodiesel is referred to as long chains of fatty acid alkyl esters prepared from animal or vegetable oil/fat (triglycerides) via microemulsion, pyrolysis, dilution, and transesterification process (Singh *et al.,* 2020). Among all techniques of biodiesel synthesis, catalyzed transesterification is considered to be an efficient, easy, and cost-effective method. It involves the biodiesel and glycerol production as a result of the reaction of triglycerides and alcohol in the presence of an appropriate catalyst. It is clean-burning fuel having enormous ecological benefits such as being free of Sulphur content as well as aromatic components, biodegradability, non-toxicity and sustainability, and inflammability (Yusuff *et al.,* 2021). The close carbon cycle of biodiesel contributes to CO_2 reduction (78%) in the atmosphere. Physicochemical properties of biodiesel resemble petrodiesel such as phase-changing ability, high combustion ability, energy content, low viscosity, and cetane number. These characteristics make biodiesel a feasible replacement for diesel fuel in combustion engines with little or no modification (Devarajan *et al.,*2020). Hence, biodiesel aids in significant improvement in the rural economy. These wide-ranging advantages have eventually stemmed the global biodiesel industry with 58.4 billion USD (7.3% rise per annum) by 2025 (Sekoai *et al.,* 2019).

The energy demand of various countries (such as Europe, Italy, Germany, Malaysia, France, Brazil, the US, Indonesia, and China) is fulfilled by biodiesel. Hence, biodiesel has been accepted as an impending contender in the energy mix as a substitute for non-renewable fossil-based petroleum fuel. Biodiesel utilization is a dynamic stratagem that may not only cut down hazardous fuel emissions but also alleviate future energy crises (Li *et al.,* 2021).

1.2 Global Perspectives in Renewable Energy

The role of power and energy is irrefutable in running our transportation and industrial sectors. Internationally, energy demand is met via exploitation of fossil fuel reserves such as oil, petroleum and natural as etc. A steady increase in its urgency is expected due to substantial competences offered by modern technologies and implication of reliable energy strategies and ecological regulations. Basically, the need of power and energy is satisfied by coal (carbon containing fossil fuel). Developed countries such as Australia, South Africa and China rely on coal (approx. 68-90%) to fulfil electricity demand. At industrial scale, almost 30% of fossils based energy is used by transportation sector and an increase is accounted for 1.8% per annum by 2005-2035 in industrial sector. World need of energy is reported to be more than 50% by 2030 according to International Energy Agency (IEA) and approximately 45% has already been used by China and India. According to reports by international council of clean transportation and united nation inter government, 45% and 23% GHG emission by vehicle discharge and transportation sector. In addition to this, liquid fossil fuel amount is estimated to rise more than 107 million barrel by 2030. Oil reserves that are prime energy source on earth are deteriorating rapidly to 30% by 2030 because of its non-renewability and unsustainability. The oil reserves would be consumed in near future according to world energy forum (WEF) whereas few others predicted that in less than 45 years, oil reserves would deplete with 3% consumption rate per annum (Srivastava *et al.,* 2018).

To resolve this rising issue of energy crises and to compensate the depletion of petroleum based diesel, biodiesel is most preferable option among various alternate energy resources. It is expected that sources of renewable energy will be prime energy mix by 2030. The shift from non-renewable fuel to renewable is reinforced by sudden elevation in global warming, fossil fuel price, carbon content and modern technological advancement. Biodiesel as substituent energy option is popular across the globe owe to its role in reduction in GHG emission, global warming and fulfilment of energy demands. Figure 1.1 shows the different countries biodiesel production share (%) that will contribute up to 27% liquid fuel supply (Ameen *et al.*, 2022).

US energy information administration reported that seven countries will have almost 100% renewable energy resources such as Brazil (75%), Paraguay (100%),

Austria (80%), Norway (98.5%), Iceland (100%) and Denmark (69.4%) (Sahar *et al.*, 2022)
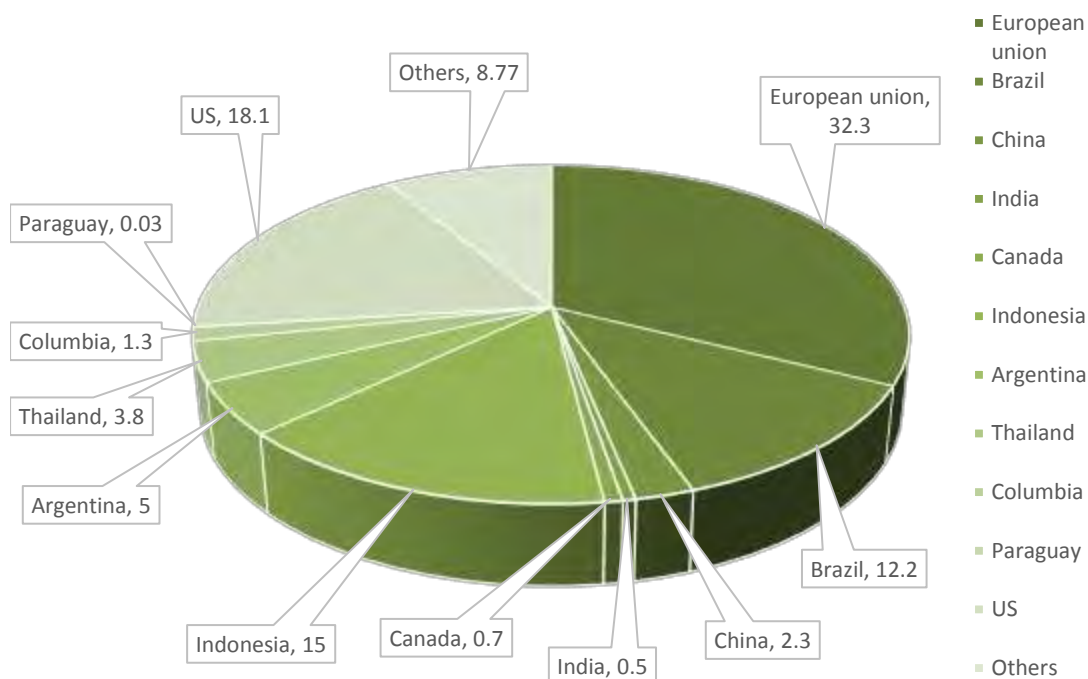
Figure 1.1 World biodiesel production, 2021 (%age refers to production share of countries in the base period) (Ameen *et al.,* 2022)

Pakistan as sixth largest country with highest population in world i.e. 213 million population (2% growth per annum). The ever rising population of Pakistan along with recent economic growth has stemmed high energy consumption and that are fulfilled with conventional fossil fuel reserves. Although initiative has been taken in recent years for promotion of renewable energy yet issue is still unresolved because of dearth of sound policies. Alternative Energy Development Board recognized in 2003 for reduction of GHG emissions and promotion of green technologies under various projects by World Wind Energy Association (WWEA) and International Solar Energy Society (ISES) at international level (Rafique & Rehman, 2017). There is crucial gap between Pakistan energy supply and demand. This gap has been bridged by continuous import of natural petroleum based fuels and a substantial state revenues on these importations are required to be disbursed. In 2014-2015 (fiscal year), petroleum products of 13.57 Milliontons of oil equivalent (MTOE) was imported by Pakistan. There was incredible increase in import bills that eventually put a massive pressure on

country economy (Abdullah 2021). In Pakistan, power generation and transportation are main fossil fuel utilizing sectors. Socioeconomic challenges are faced by consumers due to frequent price hike in transportation cost, all across the country. Currently, almost 15% of total energy required by country may be fulfilled by indigenous resources (Abdullah 2020). Pakistan expends almost 60% currency exchange to overcome energy crises by importation of fossil fuels. This massive expenditure of funds in form of import bills may be reduced by appropriate utilization of indigenous energy resources that are sustainable and cost-effective. Hence, researchers and policymakers are investigating eco-friendly, cheap, green and non-toxic alternate feedstock for renewable energy not only to resolve current energy crises but also for ecological sustainability and economic stability (Rafique & Rehman, 2017).

1.3 Feedstocks for Biodiesel Production

A significant factor in biodiesel synthesis is the easy accessibility of cost-effective feedstock. Therefore, a variety of oil-yielding plants have been recognized as potential future sources for biodiesel production on a worldwide scale. In order to select the feedstock, some major concerns include total energy, land availability, soil erosion, biomass composition and cost, employment power, pesticide injection, farming procedures and water requirement, biodiversity, and climatic impact related to noxious gas emissions etc. Moreover, oil yield (%) is also considered a vital factor to be fulfilled for economic feasibility. The high yield with low cost is a distinctive aspect of ultimate feedstock selection. Feedstock expenses make a noticeable contribution to the overall cost of biodiesel production. i.e. approximately 60-80%. Hence, the selection of easily available and cheap sources is indispensable for economically reasonable biodiesel production. The biodiesel feedstock is basically classified as three generations (Mukhtar *et al.*, 2022)

1. First generation feedstock includes food crops yielding edible oils grown in agricultural lands
2. Second generation feedstock is obtained from animal fat, waste domestic or commercial oil and non-edible oil
3. Third generation feedstock has algal origin or fungal origin.

Since 1890, sunflower, palm, soybean, canola, peanut, and safflower oils that are edible vegetable oils contribute up to >95% in biodiesel industry. However, their excessive

exploitation is not supported by global scientific community owing to forest degradation, inaccessibility to ploughed land, poor soil type, high cost and crucial food vs fuel conflict (Shaah *et al.,* 2021). Therefore, the use of non-edible oils as second generation feedstock for biodiesel synthesis can address this issue. Non-edible seed oils are green, lucrative and ingenious owe to their renewability, non-deleteriousness and non-hazardous ecological effect, sustainability, bulk production capacity. Major non edible oil yielding seeds of *Calophyllum inophyllum*, *Cerbera odollam*, *Pongamia pinnata, Jatropha curcus*, *Madhuca indica, Thevetia peruviana, Vernicia fordii, Datura stramonium, Euphorbia lathyris, Argemona maxicana, Ceiba pentandra, Simmondsia chinensis, Pongamia pinnata, Cucumis melo* var. *agrestis, Silybum marianum, Ricinus communis, Nicotiana tabaccum* (Ameen *et al.,* 2018; Biofuels 2020; Mitra *et al.,* 2021; Tasic 2020). Grease, waste oil and animal fats have also been included in second generation feedstock but their utilization at large scale is associated with disposal exclusion is an additional hurdle that limits their usability for sorting out ecological problems and filling of energy gap. Moreover, the biodiesel obtained from such feedstock (with highly saturated Free Fatty Acids) has low quality therefore it functions meagerly in cold conditions. The consumption of waste cooking oil is accompanied with key constrains at time of collection, carriage and handling that render their utilization as potential feedstock for biodiesel industry (Bandbafha *et al.,* 2022). Recently, biodiesel has been synthesized from fungi and algae as third generation feedstock due to several reasons such as easy cultivation, growth and productivity rate, high oil content (250 times more than soybean and 25 times more than palm oil), photosynthetic capability etc. However, algal pretreatment rises the overall production cost that is the main obstacle for its large scale utilization. Additionally, few plants such as miscanthus, popular, switch grass and big blue stem have been genetically engineered have been utilized as possible resources for the synthesis of biodiesel in recent times but their usability is imperiled by biosafety concerns (Friesen *et al.,* 2022).

1.4 Non-Edible Oil Seeds: A Potential Feedstock for Biodiesel Production

Globally >95% of edible feedstock is used for biodiesel production. Approximately 6.6 million tons biofuel has been produced from edible sources in 2004-2007 that accounts for 34% growth in global biodiesel consumption (Shaah *et al.*, 2021). However, a sharp increase in the use of edible resources has been followed from the 2005 to 2017 trade years. Approximately, 8.6 million tons of edible oil have been

utilized by Europe, the US, Brazil, and Indonesia in 2007. Hence, the unavailability of agricultural land has become a pronounced issue for growing these bioenergy crops. It is reported that 4.4 million hectares of farming land are used by European countries to cultivate edible feedstock for biodiesel production. This continuous practice transformed most of the area into agricultural land and posed these countries with major problems such as food shortage, deforestation, universal incongruity in food supply and demand, the devastation of the soil ecosystem, and food price hikes. For instance, in Malaysia overexploitation of palm oil by biodiesel production industries led to a scarcity of palm oil crops. It resulted in a swift increase in crops global market price i.e. approx. 70% due to the unavailability of palm oil even for cooking. Such discrepancies and vast utilization of agricultural land, water, and soil nutrients have diverted the focus of scientists towards the consideration of non-edible seed oils as a cost-effective and promising source to synthesize biodiesel. Such seeds are wasted every year as have a bitter taste and toxins such as curcin (Jatropha), torphane alkaloids (Datura), and cyanogenic glucosides (Prunus), therefore unfit for human use. But these plants grow best in barren and wasteland (paddock boundaries, irrigation channels, roadsides, etc.) and need low water content for nourishment. Non-edible plants do not create food-fuel dilemmas and land availability competition. For fixing CO_2 emissions, non-edible plants have remarkable roles such as 10t/ha/yr. Furthermore, useful byproducts have lucrative applications such as the seed cake (a byproduct of the oil extraction process) can be used as compost to enhance soil fertility. These plants have high growth and produce tons of seeds per annum because of their high resistance to drought, diseases, and pests. During the biodiesel synthesis process, their accessibility, transportability, biodegradability, and renewability are superfluous recompenses. Little or no aromatic or Sulphur content are the qualitative benefits for upgrading eco-sustainability. Hence, such oil-yielding non-edible plants bear the high potential to be used in biodiesel industries for resolving socioeconomic and ecological concerns on a large scale (Rozina *et al.,* 2021).

Studies have aimed at a variety of non-edible oils in attempt to meet the high competition for practical alternative fuels at the national and global level. (Ahmad *et al.,* 2022; Gebremariam & Marchetti, 2021; Zhang *et al.,* 2021). The preference of non-food oil over edibles is owing to their high oil yield (%) such as *Prunus bokhariensis* (55%) (Dawood *et al.,* 2022), *Raphanus raphanistrum* Linn (40.7%) (Munir *et al.,* 2021), *Capparis spinosa* L. (40.7%) (Liu *et al.,* 2021), *Cucumis melo* var. *agrestis*

(30%) (Ameen *et al.*, 2018), *Zanthoxylum armatum* (36%) (Rozina *et al.,* 2022), *Tribulus terrestris* L. (31%) (Aziz *et al.,* 2022).

While to the best of our knowledge, different seed oils included in this study have not been reported for biodiesel production using green nano-catalysts. These novel potential feedstocks include *Bischofia javanica* Blume*, Eryobotrya japonica* (Thunb.) Lindl.*, Praecitrulus fistulosus* (Stocks) Pangalo*, Luffa acutangula* (Linn.) Roxb.*, Diospyros lotus* L.*, Cucumis melo* var. *Cantalupensis, Solanum surattense* Burm. f. and *Cucumis melo* var. *Agrestis* Naudin.

1.5 Biodiesel Production Techniques

Different oils are much viscous and less volatile with high acidity due to free fatty acid content. These unstable oils are considered as unfeasible for direct use as power fuel in diesel-based engines. Such constraints may lead to grease formation, carbon deposition, and poor fuel combustion in diesel-based engines. There are various techniques have been practiced for years in order to reduce fuel viscosity and attain satisfactory performance in standard engines without any amendment. The use of biodiesel in compression ignition engines with minimal to no modifications ensures better emissions and is a great alternative to petroleum-based diesel fuel. Biodiesel from potential feedstock is produced by pyrolysis, micro-emulsification, dilution, and transesterification using both catalytic and superfluid methods (Table 1.1). Moreover, for the process intensification, microwave technology, and ultrasonication-assisted methods are used (Ameen *et al.,* 2022).

The decomposition of vegetable or animal triglycerides using catalysts without the involvement of air is known as *pyrolysis or catalytic cracking.* The adequate and appropriate catalyst speeds up the thermal breakdown of the raw materials used to make biodiesel and converts long-chain hydrocarbons into short-chain hydrocarbons. The pyrolysis-produced biofuels are acidic and have varying hydrocarbon and water concentrations. In order to use it as an alternative fuel, water must first be removed through a pretreatment procedure.

In *microemulsification,* crude oil is mixed with an emulsifier (any type of alcohol) to create an emulsion that accumulates carbon. Hence, improper combustion results.

A certain quantity of crude oil and diesel are mixed during the *dilution* process. Dilution is achieved by enhancing the solvent and lowering the solute concentration resulting in a decrement in viscosity and density. Conventionally, diesel and ethanol are used as solvents. Although the dilution procedure is simple yet the fuel is unsuitable

for use directly in diesel engines due to its high FFA percentage, viscosity, and acid value, incomplete burning and carbon deposition are some problems associated with its safe utilization.

Transesterification is the most utilized technology in biodiesel synthesis as it is favorable from an economic point of view at industrial-scale production. It involves the reaction between oil/fat obtained from a feedstock and alcohol in presence of a suitable catalyst.

Intensification strategies are used to promote the mass transport effect in overcoming the drawback of the high immiscibility of the solid catalyst with the oil and the alcohol liquid phases in the normal mixing system of the transesterification reaction. Process intensification is achieved by using microwave and ultrasonication technologies. Microwave technology offers a fast rate of reaction and less heat loss. However, after the process catalyst is removed and the conversion process is influenced by catalyst activity. Ultrasonication or acoustic cavitation is considered a promising, ecofriendly, and efficient method for biodiesel production. It involves the utilization of cavity collapse to generate highly disruptive forces that rupture the layer between alcohol and oil and reactant gets uniformly distributed due to the micro-level intermixing hence the reaction yield and rate is enhanced.

When transesterification is used for biodiesel production, one of two routes are supercritical methanol transesterification and catalytic transesterification.

Supercritical fluids (SCF) are used for biodiesel synthesis in the absence of catalysts. It results in fast rate of reaction, high efficiency of conversion; there is no requirement of a catalyst but it requires energy and has a high installation cost. The supercritical transesterification involves single phase mixture, produced at 340 °C temperature and 43 MPa pressure with reduction in dielectric constant of alcohol. The reaction time is 2–4 min at supercritical stage. Though product purification is comparatively easy due to the absence of a catalyst, the production cost is high.

Catalytic transesterification involves interchange of alkyl groups (R) of esters with alkyl groups of alcohols. It results in production of new ester (biodiesel) and alcohol (glycerol). Two basic steps are involved in catalyzed transesterification process. Initially, alcohol and the catalyst react to form alkoxide ion followed by a reaction between an alkoxide ion and triglycerides in oil to produce Fatty Acid Alkyl Esters (FAAEs).

Table 1.1 Various biodiesel synthesis methods Ameen *et al*., 2022; Singh *et al*., 2020)

Biodiesel Methods	Merits	Demerits
Direct use of oil and blends	Liquid based-portability, renewability, readily available, Heat content Retains total power without/little modification to diesel based engine No major operational difficulty	Low cetane, high viscosity, natural gum in oils, low flash point, low volatility. Reaction of unsaturated chains. Gumming and Plugging of lines, filters and injectors. Engine knocking and carbon deposits on engine.
Micro emulsion	Isotropic fluid, stable and clear with aqueous phase, an oil phase and surfactant.	Extensive deposits in exhaust valve of engine. A mass of carbon all over the orifice of injector outlet Partial combustion in 200 h lab screening endurance test. Irregular needle sticking of injector
Pyrolysis	Pyrolyzed oil has satisfactory sulphur amount, sediment, water and copper corrosion value. Undesirable carbon residue amounts, ash, pour point. Short term engine tests.	Equipment is expensive Low moisture is required Products are similar to petroleum diesel fuel. Deoxygenation during pyrolysis removes eco-friendly aspects. Production of low graded materials and less diesel as compared to gasoline.
Dilution	Low viscosity of oil makes it efficient for short term use.	Not recommended for long term usage.

		Heavy carbon deposits on intake valve and appearance of top ring wear.
Transesterification	Fuel properties almost similar to petroleum diesel Low cost High conversion yield efficiency Suitable for large scale production of biodiesel	Low water and FFA content of oil is required (Base catalyzed transesterification) Washing of biodiesel is required that produces pollutants Accompanied by side products
a. Transesterification based on Homogeneous catalysis	Adequate reaction time Efficient conversion and easy to perform Inexpensive	Catalyst recovery not possible Saponification Low quality glycerol is produced
b. Transesterification based on Heterogeneous catalysis	High biodiesel yield Eco-friendly as washing is not required No saponification and hydrolysis	Expensive as compared to Homogeneous catalyzed transesterification Longer reaction time
c. Enzyme catalyzed transesterification	Tolerance to water content in oil No FFA saponification Low energy consumption/input	Very Expensive Enzymes Inhibition via MeOH Much Longer reaction time Enzymes absorb glycerol on its surface
d. Supercritical/Non catalyszed transesterification	No catalyst required Easier product purification Fast reaction time No effect of high FFA and Water	Need of High reaction temperature and pressure Large amount of methanol High energy consumption High capita cost

1.6 Catalytic Transesterification for Biodiesel Production

Catalytic transesterification is the most popular method used across globe that involves the reaction of oil with methanol and suitable catalyst used to speeds up the reaction and facilitates the mixing of alcohol in oil. However, suitable catalytic selection is made on the basis of FFA in oil. Reactions can be one-step (for low FFA) or two-step (for high FFA). Depending on the FFA content of feedstock, basic catalysts give better results at low concentrations in feedstock oil with little FFA content, while acid-catalyzed esterification is preferred for oil with higher FFA content followed by transesterification. Considering that the catalyst is soluble in the medium for the reaction, the catalyst are homogeneous (acid/basic), heterogeneous (acidic/basic) and enzymatic.

The homogeneous catalytic transesterification, the most convenient industrial process, involves the use of liquid acidic or basic type catalyst. Acid-catalyzed processes are mainly used for pretreatment of raw materials with high FFA content, mostly sulfuric acid or hydrochloric acid are used. Esterification and transesterification processes can both be catalyzed by acidic catalysis simultaneously. However, base-catalyzed process, sodium hydroxide or potassium hydroxide, are considered suitable for raw materials with FFA value less than 3 (Lüneburger *et al.,* 2022; Yu *et al.,* 2020). FFA mainly comprise long carbon chain that is needed to be separated from glycerol and result in catalytic inactivation and saponification. With acid catalyzed process, alcohol attacks on protonated carbon and produce tetrahedral intermediates. Protonated carbon is produced by carbonyl protonation in respective oil. The base-catalyzed process, on the other hand, involves the production of alkoxides (nucleophiles) (Aransiola *et al.,* 2014).

However, the problems associated with biodiesel that has been synthesized homogeneously include formation of saponification products, repeated washing with water, hygroscopicity etc. The nature and impracticality of catalyst recovery, serious ecological and engine damage due to corrosion limit its use in the biodiesel industry. Due to specific properties, enzymes have also been used as catalysts for the synthesis of biodiesel. Water and FFA resistance with problem-free removal of biodiesel from a by-product (glycerol). But high cost and long reaction time are major obstacles to the commercialization of enzyme-based transesterification (Ramos *et al.,* 2022).

The catalytic properties of heterogeneous catalysts mainly depend on the availability of catalyst active Site with its volume, nature (acidic / basic or both), pore size, surface area of catalyst. Catalyst performance of selected heterogeneous catalyst can be strengthened via a support that strengthens their active site or with pretreatment to increase the acidity or basicity of the catalyst.

Performance of heterogeneous catalysts is recognized by their basic, acidic, or dual (acidic or basic) ability. Catalyst performance is highly type dependent i.e. active sites and precursors used. For example, the catalytic activity of CaO impregnated with alkaline ions largely depends on the metal salt and metal ions used. Similarly, Li_2O_3 impregnation with CaO produces Li / CaO. A high biodiesel yield was achieved due to its maximum basic strength and surface area (Banković-Ilić *et al.,* 2021). Selection of heterogeneous catalysts as well as homogeneous catalysts for the synthesis of biodiesel Depending on the FFA concentration of raw material, non-edible oils may be used. Basic heterogeneous catalysts give the best results with low FFA feedstock, and vice versa when using acidic catalysts capable for synthesizing biodiesel from high FFA feedstock.

A particular framework of a novel catalytic system is urgently and critically required since homogeneous and heterogeneous catalysts, each have advantages and disadvantages. As with homogeneous system, catalysts should be dynamic, active, and efficient. But they are not readily recovered like heterogeneous catalysts. Utilization of nano-catalysts is a point of convergence and synergistic benefits of both homogeneous and heterogeneous catalysts. Nano catalysts are mild and easily transform various chemicals in a selective and rapid manner. Both catalyst separation and recovery are merit of nano-catalysts that offer a high product yield (Abdullah *et al*., 2022). Because nanoscale catalysts have a large surface area, analogous to homogeneous catalysts and the contact between catalyst and reactant is substantial. Similar to heterogeneous catalysts, nano-catalysts are insoluble. Consequently, nano-catalysts are simple to recover and easily separable. The major technological and scientific issue associated with the use of nanoparticles is to figure out the atomic scale structure (basic understanding) and composition of nano-catalysts that provide the optimum catalytic activity. Nano-particles (1-100 nm) acting as catalysts have a high surface area and effectively increase the rate of reaction, as their nano size has an impact on the biodiesel production (Zhu *et al.,* 2021). The primary challenge in the field of nano-catalysis is the synthesis of nano-particles. The two main modern of practices for creating nano-

catalysts are top-down and bottom-up technologies. The conventional techniques include hydrothermal, sol-gel, co-precipitation, thermal decomposition, solid-state synthesis, and combustion. Spray pyrolysis, microemulsion, pyrolysis (laser and spray), sonochemical, drying, reverse micelle, and biosynthesis are examples of unconventional techniques to synthesize nano-catalysts. The use of poisonous chemicals, high temperatures and pressures, as well as the generation of damaging byproducts are some of the disadvantages associated with chemical and physical techniques of synthesis of nano-catalysts. It is therefore vital to find a different way to make nano-catalysts.

1.7 Green Nano-catalysts for Biodiesel synthesis

Different macro-microscopic species, including plants, bacteria, fungus, seaweeds, and microalgae have been used for the biological synthesis of nanoparticles by advanced techniques. Biological synthesis of nano-catalysts via plant extracts has been proposed as it employs low hazardous toxins and higher temperatures than traditional chemical approaches. Several researchers are interested in investigating the process of bio-reduction and metal ion absorption by the plant because of the enormous benefit of utilizing plant extracts for green synthesis of nano-catalysts. Green Synthesis is non-hazardous and environmentally friendly as it is devoid of harmful compounds and offers natural reduction agents for stabilizing nanoparticles hence it is advised as the ideal and operative method to produce nano-catalysts. Plants based nanoparticles are much more effective, stable, ecofriendly, competitive and quick to function (Dawood *et al.,* 2022) Alkaloids, flavonoids, saponins, steroids, tannins, and other natural chemicals are abundant in plants. These organic substances are obtained from a variety seed, leaf, stem, root, shoot, flower, and bark for biosynthesis of highly selective, efficient recyclable green nano-sized catalysts (Kuppusamy *et al.,* 2016).

There is a great deal of information available on the development of sustainable nano-catalysts currently. Ali *et al*. (2018) used goat bone for the transesterification of wasted cooking oil and catalyzed transesterification reaction by calcination with CaO at a 1:9 Oil: Met ratio at 65 °C for 5 h, and obtained an 84% yield with three reusability cycles (Ali *et al*., 2018) . In a research by Kara *et al*. (2019), with 1:9 oil to methanol molar ratio, 60 °C, 3 hours, and a 3 % catalyst loading, the vegetable oil was converted to biodiesel with a significant conversion efficiency (96%) was attained. Thus, cost-effective and ecologically friendly biodiesel was produced (Kara *et al*., 2019). The

effectiveness of nano-catalyst on transesterification of Jatropha was confirmed under ideal conditions. High conversion yield (96.1%) was achieved using a 9:1 methanol to oil ratio, 6 % wt. per wt. of oil used, and a 3h reaction duration at 70 °C (Nisar *et al.,* 2017).

Similarly, organic waste-based solid catalysts have been effectively employed, such as sugarcane bagasse, ashes, coconut shell, palm trunk, peel, and wood sugarcane bagasse, wood, ash, coconut shell, palm trunk, and peel (Changmai *et al.,* 2020). Oleic acid and methanol were esterified using a solid acid catalyst made from *Sargassum horneri* carbon that had been sulfonated. The esterification reaction for the biodiesel production can be efficiently catalyzed by the layers of amorphous carbon that are created during carbonization and the availability of sulfonic acid groups during sulfonation. To explore the catalyst chemical and physical characteristics, various techniques were used. After two hours of carbonization at 300 °C and five hours of sulfonation at 90 °C, rubber deoiled cake as a waste-derived heterogeneous acid catalyst, which was made from sulfuric acid and chlorosulfuric acid was employed to produce FAME from mixed non-edible oil (Cao *et al.,* 2021).

Gohain *et al*. (2017) created a plant-based catalyst by oven-drying peel for 48 hours at 80 °C and calcined for 4 hours at 700 °C (Gohain *et al.,* 2017). Later, it served as a catalyst for the two-step transesterification of Neem oil. Tucum peels, a fruit that is popularly consumed in the north of Brazil, were calcined at 800 °C and used as a heterogeneous catalyst in the biodiesel production. Due to the high concentration of potassium, phosphorus, calcium, and magnesium ions in tucuma palm peels showed excellent catalytic activity (Mendonça *et al.,* 2019). Waste pine apple leaves have been effectively used to create solid base catalysts, and this phytonano-catalyst was used to produce 98.92% of the biodiesel from soybean oil (Barros *et al.,* 2020). According to earlier investigations, calcination at 900 °C for 4 hours may be used to manufacture an affordable solid base catalyst using chicken bones. With 5 % wt. catalyst loading, a 1:15 oil to methanol molar ratio, a reaction temperature of 65 °C, and a reaction period of 4 hours allowed for an 89.3 % FAME conversion yield from soybean seed oil. This catalyst was utilized efficiently for four rounds to increase process effectiveness. As a result, the catalyst appeared to be useful and a potential replacement for homogeneous catalysts (Farooq *et al.,* 2015). *Bombax ceiba* seed extract was used by Hebbar *et al*. (2018) to produce CaO nanoparticles and applied this green nano-catalyst to achieve

significantly high yield (96.2 %) of the biodiesel from *Bombax ceiba* seed oil. The green nano-catalyst could be used up to five times (Hebbar *et al.,* 2018). Biodiesel production from a novel, inedible seed oil of *Monotheca buxifolia* via green nanoparticles derived from *Boerhavia procumbens* aqueous leaf extract reported by Ahmad *et al*. (2022). High yields of biodiesel (95%) were produced under the ideal conditions of 9:1 methanol to oil molar ratio, 0.83 (wt. %) catalyst loading, 180 minutes of reaction time, and 85 °C reaction temperature (Ahmad *et al.,* 2022). Similarly, *Ixora coccinea* leaf extract was used in the synthesis of zinc oxide nano-catalyst (Yedurkar *et al.,* 2016). Dawood *et al.,* 2022 synthesized phytonano-catalysts from leaf extract of *Monotheca buxifolia* and used it to produce biodiesel from *Prunus bokhariensis* with 1:12 oil: Met, 3.5 wt. % catalyst loading at 130 °C for 2.5 h, the highest (89 %) yield achieved (Dawood *et al*., 2022).

In this research, aqueous extracts of leaves of *Bischofia javanica* Blume, seed shells of *Eryobotrya japonica* (Thunb.) Lindl., seed cake of *Praecitrulus fistulosus* (Stocks) Pangalo*,* flowers of *Luffa acutangula* (Linn.) Roxb., bark of *Diospyros lotus* L.*,* peel of *Cucumis melo* var. *Cantalupensis,* persistent calyx of *Solanum surattense* Burm. f. and seed extract of *Cucumis melo* var. *Agrestis* were used to synthesize green nano-catalysts, such as zirconium oxide, cobalt oxide, copper oxide, cadmium oxide, nickel oxide, calcium oxide, silver oxide and magnesium oxide respectively**.** The produced catalyst was examined through a variety of advanced techniques, including Scanning Electron Microscopy (SEM) and Energy Dispersive X-ray (EDX), X-ray Diffraction (XRD) and Fourier Transform Infra-red Spectroscopy (FT-IR).

1.8 Background Justification of the Project

Production of cleaner biodiesel has been progressively popular worldwide. Scientists are concerned about the potential threat to pertinent ecosystems and believe that climate change will eventually raise the risk of severe ecological instabilities. Several of these climate shifts have already been occurred while others are just going to take place. The search for sustainable biofuels has been prompted by severe natural changes associated with the use of petro-fuels. Moreover, it may be produced in large quantities for a reasonable price rather than use up additional food supplies. Even so, using more potential and prospective raw resources and generating as much sustainable and renewable energy as possible are strongly related (Lalithamba *et al.,* 2022; Tripathi

et al., 2022). Several researchers have selected alternative approaches to develop nano-catalysts over traditional means, such as chemical reduction, ball milling, co-precipitation, and green synthesis, in order to address issues with mass transfer and catalytic activity between the non-miscible reactants of alcohol and oil in a short period of time with much less energy usage. Due to their large surface area and particularly small size, nano-catalysts are of great interest because they exhibit both physical and chemical differences in their properties from the majority of a certain chemical compound, such as catalytic activity, melting point and optical absorption, biological and sterical properties, electrical and thermal conductivity, and mechanical properties (Kumari *et al.,* 2021, Nathani 2021).

The green chemistry method for nano-catalyst production has drawn the attention of the research community towards itself. It is an environmentally friendly method for synthesizing nano-catalysts and is suitable for mass manufacturing. Plants based nano-catalysts are more effective, stable, and quick to function. Many scientists are concerned with studying the process of bio-reduction and metal ion absorption by the plant because of the substantial value of utilizing plant extracts for green synthesis of nano-catalysts (Ameen *et al.,* 2022).

The commercialization of this approach would pave way for considerable economic opportunities, which might be a significant step toward the development of a clean diesel substitute that is relatively stable and comfortable when ignited in the engine. This research demonstrates that biodiesel is an affordable source of energy by emphasizing the effects of bioenergy generation from selected feedstocks.

1.9 Scope of the Study

Over 350 oil-producing plants are estimated to be viable feedstock for biodiesel production. However, a variety of potential feedstocks have not been investigated properly. Homogeneous catalytic transesterification techniques are used on a variety of seed oils. According to a systematic review, there is a significant gap in knowledge on the use of green nano-catalysts for transesterification of seed oils. Pakistan, which is primarily an agriculture-based country, has a considerable area where drought and salt issues are prevalent. The deforestation driven by urbanization, soil erosion, erratic rainfall, floods, intensification of agricultural practices, and anthropogenic activities

has resulted in such physiological stress. Due to these restraints, the bulk of the fertile region has been transformed into semi-desert lands. Pakistan still has a marginal and neglected land area of about 28 million hectares. This land may be utilized firmly for the cultivation of Pongame and Jatropha plants since it is barren and unproductive owing to a lack of water, salinity, and the rising environmental temperatures. Since such plants can thrive in salty soils and extreme climatic conditions.

Current study involves synthesis and characterization of eight green nano-catalysts such as zirconium oxide, cobalt oxide, copper oxide, cadmium oxide, nickel oxide, calcium oxide, silver oxide and magnesium oxide from same feedstock selected for biodiesel synthesis i.e. *Bischofia javanica* Blume, *Eryobotrya japonica* (Thunb.) Lindl., *Praecitrulus fistulosus* (Stocks) Pangalo*, Luffa acutangula* (Linn.) Roxb., *Diospyros lotus* L*., Cucumis melo* var. *Cantalupensis, Solanum surattense* Burm. f. and *Cucumis melo* var. *Agrestis* Naudin*.* Hence, this research work is confined to biodiesel synthesis from eight selected seed oils via eight diverse green nano-catalysts. This work is unique to be reported for the first time because it implements scanning electron microscopy to identify novel non-edible oil seeds. It involves oil content estimation, FFA value determination, green nano-catalytic synthesis, and biodiesel production by transesterification by applying synthesized green nano-catalysts, followed by characterization of catalysts and synthesized biodiesel via SEM, FT-IR, XRD, EDX and GC-MS, NMR, FT-IR respectively.

1.10 Objectives of the Study

- This project is focused on identification and selection of novel oil yielding seeds with high oil contents for the biodiesel production.

- The assessment of oil contents (%) and FFA content (mg KOH/g) in order to use as a prospective feedstock for biodiesel production.

- Synthesis and application of diverse catalysts as solid green nano-catalysts (zirconium oxide, cobalt oxide, copper oxide, cadmium oxide, nickel oxide, calcium oxide, silver oxide and magnesium oxide) as affordable and non-hazardous catalysts for biodiesel production.

- Implication of variety of *in-situ* and advanced techniques for green nano-catalyst characterization such as XRD, SEM, EDX and FT-IR.

- Implementation of operando techniques such as FT-IR, GC-MS and ^{1}HNMR and ^{13}CNMR to have an insight into functional groups of compounds in biodiesel

- Investigation of physicochemical characterization of fuel and comparison with ASTM-D 6751 to recognize if it may be employed as a substitute for petro-diesel.

- Application of statistical methods like Response Surface Methodology (RSM) and ANOVA for biodiesel yield optimization.

CHAPTER: 2

MATERIALS AND METHODS

2.1 Research Outline of Project

The experimental framework, research methods, and several analytical techniques applied for the current study are all outlined as following the schematic flow sheet:
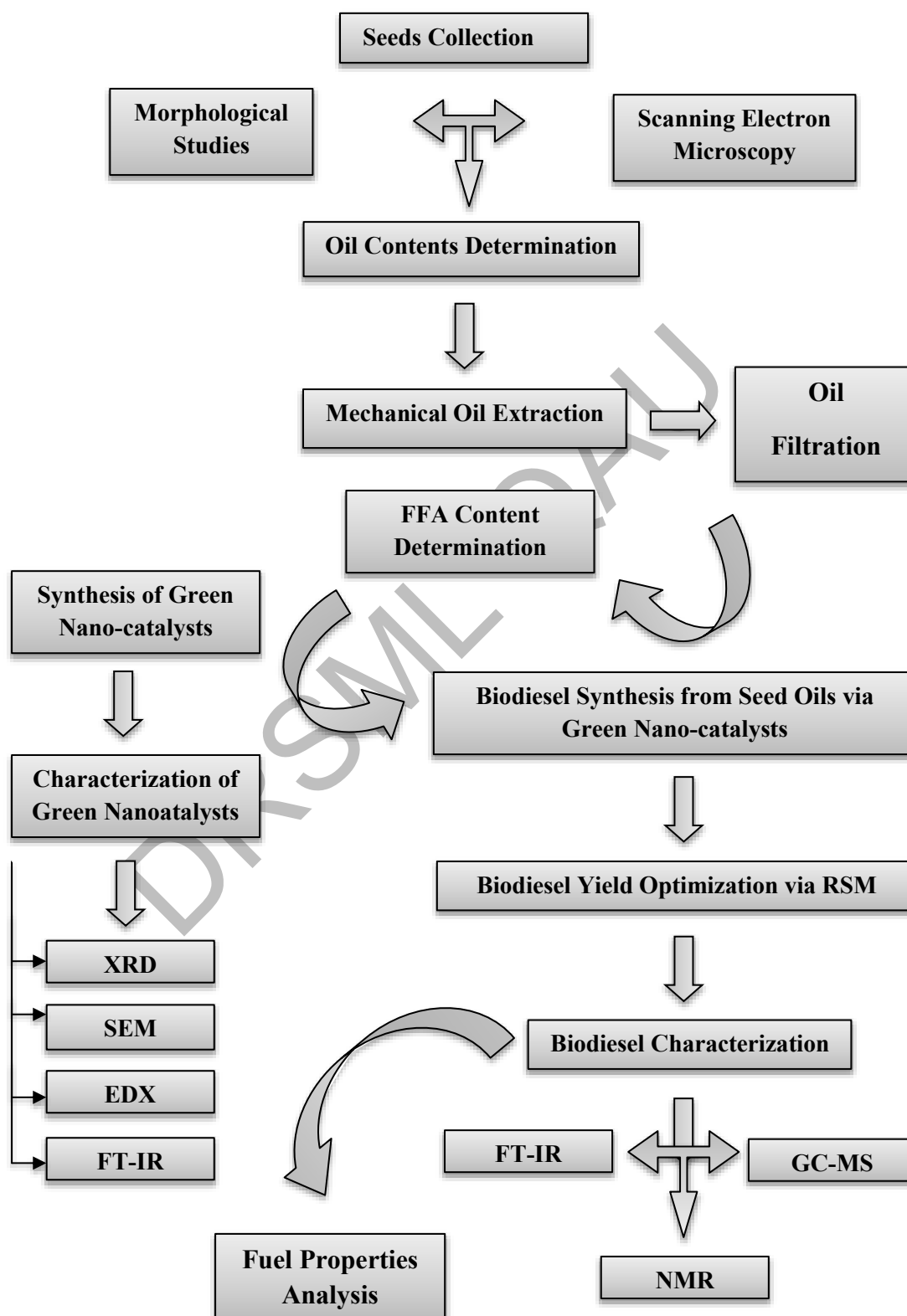
Flow Sheet 1: Outline of project methodology

2.2 Materials

In this study, several chemicals and reagents were employed which include Zirconium (IV) nitrate $Zr(NO_3)_4$, Cobalt (II) nitrate hexahydrate $Co(NO_3)_2.6H_2O$, Copper sulphate pentahydrate ($CuSO_4.5H_2O$), Cadmium nitrate tetrahydrate $Cd(NO_3)_4.4H_2O$, Nickle (II) sulphate hexahydrate ($NiSO_4).6H_2O$, Calcium sulphate dihydrate ($CaSO_4).2H_2O$, Silver nitrate (NO_3), Magnesium Sulphate ($MgSO_4$), Sodium hydroxide (NaOH), Sulphuric acid (H_2SO_4), Isopropyl alcohol, Ethanol, Acetone, Anhydrous methanol (CH_3OH), Phenolphthalein, and chloroform ($CHCl_3$). All of the compounds were of analytical quality and were purchased from Sigma Aldrich (USA) and Merck (Germany).

2.3 Feedstock Collection

All of the selected unique oil-producing seeds were meticulously collected throughout the year during various seasons from different parts of Pakistan. Some seeds were purchased from local market in Rawalpindi, Punjab Pakistan. These seeds were shade-dried and kept at room temperature.
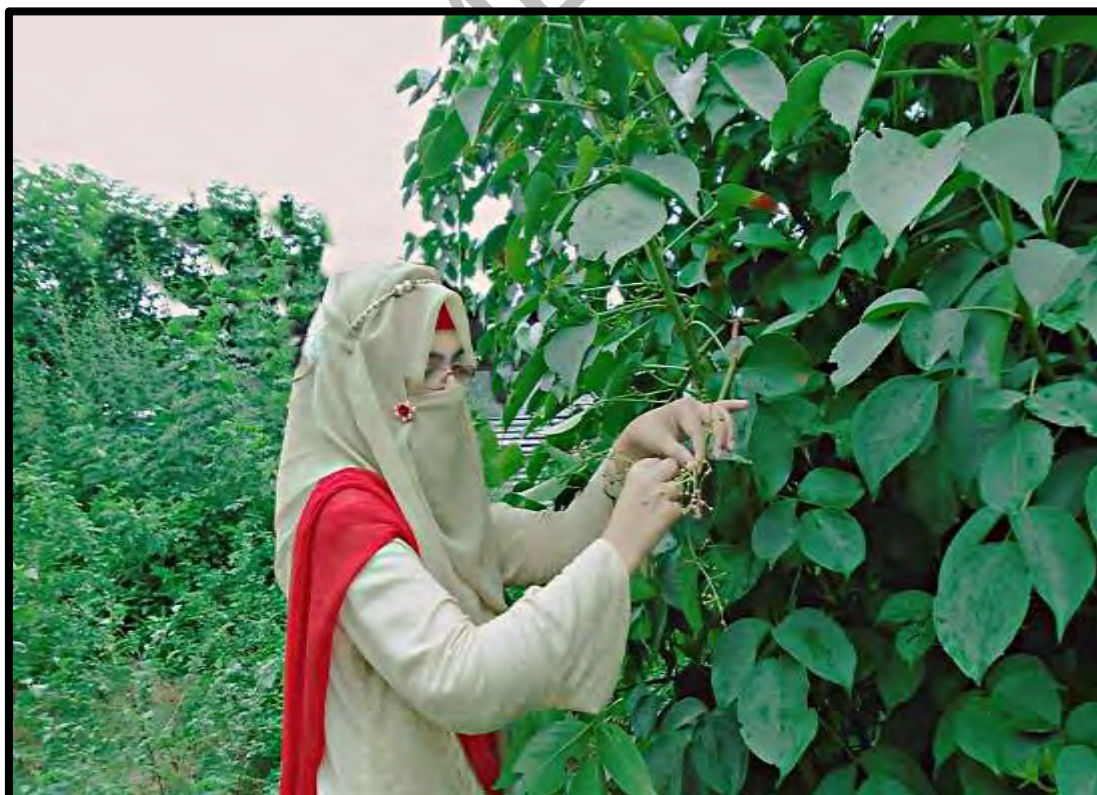
Plate 1: Seed Collection (*Bischofia javanica* blume)

Then collected plant specimens were preserved by drying under presser, poisoned and mounted on herbarium sheets and then for the future reference such specimens were submitted to Herbarium of Pakistan (ISL), Quaid-i-Azam University Islamabad.

Plate 2 Preservation of Plant Specimens

2.4 Morphological Description of Non-edible Oil Seeds

Morphological details of eight oil seed yielding plant species, including *Bischofia javanica* Blume*, Eryobotrya japonica* (Thunb.) Lindl.*, Praecitrulus fistulosus* (Stocks) Pangalo*, Luffa acutangula* (Linn.) Roxb*., Diospyros lotus* L.*, Cucumis melo* var. *Cantalupensis, Solanum surattense* Burm. f. and *Cucumis melo var. agrestis* Naudin were investigated. To analyze the vegetative components of the plants, magnifying glasses were utilized. For validation and accuracy of the recorded mean values, the measurements were repeated three to five times by a dissecting microscope. The components of the flowers were examined with a Stereo Light microscope (Model SF 2 Kyowa) (Ahmad *et al.,* 2022).

The qualitative and quantitative study of morphological characteristics of selected samples was done by comparison with preserved specimens and data was

verified by confirmation from expert taxonomists at Herbarium of Pakistan (ISL), Quaid-i-Azam University Islamabad.

2.5 Micro-morphological Examination of Oil Seeds

SEM is a useful technique for generating intricate high-magnification images of a sample surface topography, which is utilized to ascertain the seed morphological structure. SEM with high resolution and magnification may investigate inherent features at the micro- and nanoscale levels. SEM technology has made it possible to analyze a substance ultra-microscopic structure in detail. In our study, SEM was employed to investigate the micro-morphological properties of both catalyst and specific seeds (Ahmad and Zafar 2021; Arshad *et al.,* 2023).

The seed samples for SEM analysis should be clean and devoid of any dirt. The seeds were washed for 1-3 minutes with a series of ethyl alcohol solutions (from 60 to 80 % purity) and then left to dry at room temperature. The next step is mounting the seed sample using carbon based adhesive tape on the stubs. The mounted sample were next placed in the gold (Au) sputter coater (model CCU-010) to apply a thin layer of gold to the sample. The gold-sputtered seed samples were analyzed with a scanning electron microscope (JEOL JSM-5910) that has been installed in Central Resource Laboratory (CRL), University of Peshawar, Pakistan. Different magnifications were used to analyze the seed samples. The characteristics of the seed surfaces, such as shape, margin, texture, cells, and periclinal wall patterns were observed and photographed on film (Polaroid films, p/n 665) (Munir *et al.,* 2021).

2.6 Oil Contents Determination

The seeds of selected feedstock were ground after being oven dried for 24 hours at 60°C. This was conducted before the oil contents was determined. A thimble filled with dried, finely ground seeds (5g) was placed in the center of the soxhlet apparatus (Behr Labor-Technik^{TM} B00218425, Germany). Petroleum ether was poured in a 250mL round-bottom flask and heated to 65 °C accompanied with the operation of a water-circulating reflux system connected to apparatus. The reaction continued for 5–6 hours and oil drips were clearly visible in the round bottom flask as the reaction progressed (The resulting wet sample (Thimble) was then oven dried to remove the solvent after the predetermined amount of time, and its weight was noted (Plate 3).

The following formula was used to determine the proportion of oil in the seeds (Munir *et al.,* 2021).

Oil Content (%) = (W3 - W1 ÷ W2) × 100   **(1)**

W1= Sample weight;

W2= Empty flask weight

W3= W1+W2

Plate 3 Oil contents determination via soxhlet apparatus

2.7 Oil Extraction

One of the practical methods to get large quantities of seed oils is mechanical extraction. In order to extract crude oil and the valuable byproduct known as seed cake (i.e. animal feed), the electric oil expeller (KEK P0015-10127) was used (Plate 4). Dried seeds were fed in massive quantities through a mechanical press. In order to extract maximum amount of oil in terms of volume from provided feedstock, the seed cakes were run through the expeller several times. Oils were stored in the dark at room temperature in order to prevent their auto photo-oxidation (Ullah *et al.,* 2018).

Plate 4 Mechanical extraction via electric oil expeller

2.8 Crude Oil Filtration

The extracted oils stored in airtight jars to be used in experimentation were then filtered via Whatman grade 1 qualitative filter paper to remove debris from crude oil (Plate 5).

Plate 5 Crude Oil Filtration

2.9 Free Fatty Acid Contents Estimation

The free fatty acid number of the oil was determined using aqueous acid-base titration. There were two different kinds of titrations performed: sample and blank.

2.9.1 Blank Titration

For the blank titration, a 0.025 M KOH solution was made when 0.14 g of KOH was dissolved in 100 mL of distilled water and used to make the solution, which was then taken in a burette. A conical flask containing 10 mL of isopropyl alcohol was then filled with 2 or 3 drops of the phenolphthalein indicator (50%) prepared from 0.5g of phenolphthalein with ethanol. The pink tint appeared after it was titrated against KOH (0.025 M) in a burette. The volume of KOH used at this endpoint was noted. The experiment was carried out three times while keeping track of the quantity of KOH ingested to ensure accurate findings (Ameen *et al.,* 2018).

2.9.2 Sample Titration

A conical flask was filled for sample titration with 9 mL of isopropyl alcohol, 1 mL of oil, and a couple of drops of phenolphthalein indicator. Then, a burette was used to titrate it against 0.025M KOH until the color became pink. The experiment was conducted three times with the exact same volume of KOH in order to calculate the average volume of KOH required to titrate the sample (Ameen *et al.,* 2018).

Acid number = Vol. of KOH used in sample titration 3-Vol. of KOH used in blank titration x Catalytic mass (g/l) ÷Vol. of oil used in sample titration   **(2)**

2.10 Green Nano-catalyst Synthesis

2.10.1 Zirconium Oxide Green Nano-catalyst

(a) Preparation of *Bischofia javanica* Leaf Extract

For phyto-nano-catalyst synthesis by biological technique combined with in situ impregnation, *Bischofia javanica* Blume aqueous leaf extract (BJLE) was used. For this purpose, fresh leaves were collected in the field, and deionized water was used to wash away any remaining dust particles. Leaves of *Bischofia javanica* (10g) were chopped followed by boiling in distilled water (200mL) for 15 minutes at 100°C. Leaf extract

was filtered and utilized as a capping and reducing agent in a solution of metal precursor.

(b) Synthesis of Zirconium Oxide Green Nano-catalyst

Bischofia Javanica Leaf Extract (BJLE) (5mL) was added drop wise in 100 mL of 0.1 M aqueous solution of Zirconium (IV) nitrate $Zr(NO_3)_4$ while continuously heating the mixture at 200°C for 30 min in the dark to produce a green zirconium oxide phyto-nano-catalyst. The solution was filtered after 3 hours of settling, then poured into petri plates and dried in a 60°C oven. After drying, it was scraped and put in a silica crucible for calcination in a muffle furnace (Plate 6). The temperature was set at 500°C for 3 hours (Ahmad & Zafar, 2021; Dawood *et al.,* 2022).

Plate 6 Synthesis of Zirconium Oxide Green Nano-catalyst

2.10.2 Cobalt Oxide Green Nano-catalyst

(a) Preparation of *Eryobotrya japonica* Seed Shells Extract

For green synthesis of Cobalt oxide nanoparticles by biological method combined with in situ impregnation, *Eryobotrya japonica* seed shells extract (EJSSE) was used. Fresh seeds were collected in the field, and deionized water was used to wash

away any remaining dust particles. *Eryobotrya japonica* seeds were oven dried at 60°C until the seed shells were easily separable. Then 10g of seed shells was boiled in distilled water (200mL) for 15 minutes at 100°C. *Eryobotrya japonica* seed shell extract (EJSSE) was formerly filtered to be used as a capping and reducing agent in a solution of metal precursor (Ahmad & Zafar, 2021).

(b) Synthesis of Cobalt Oxide Green Nano-catalyst

For biosynthesis of green nanoparticles of Cobalt oxide, *Eryobotrya japonica* seed shells extract (EJSSE) (5mL) was dropwise added to 0.1 M solution of Cobalt (II) nitrate hexahydrate $(Co(NO_3)_2.6H_2O)$ while stirring the mixture continuously. This reaction mixture (extract and salt soln.) was heated at 200°C for 30 min in the dark to produce a green cobalt oxide (CoO) phyto-nano-catalyst. The solution was filtered after 3 hours of settling, then poured into petri plates and dried in a 60°C oven. After drying, it was scraped and put in a silica crucible for calcination in a muffle furnace (Plate 7). The temperature was set at 300°C for 3 hours (Sharifi *et al.*, 2013).
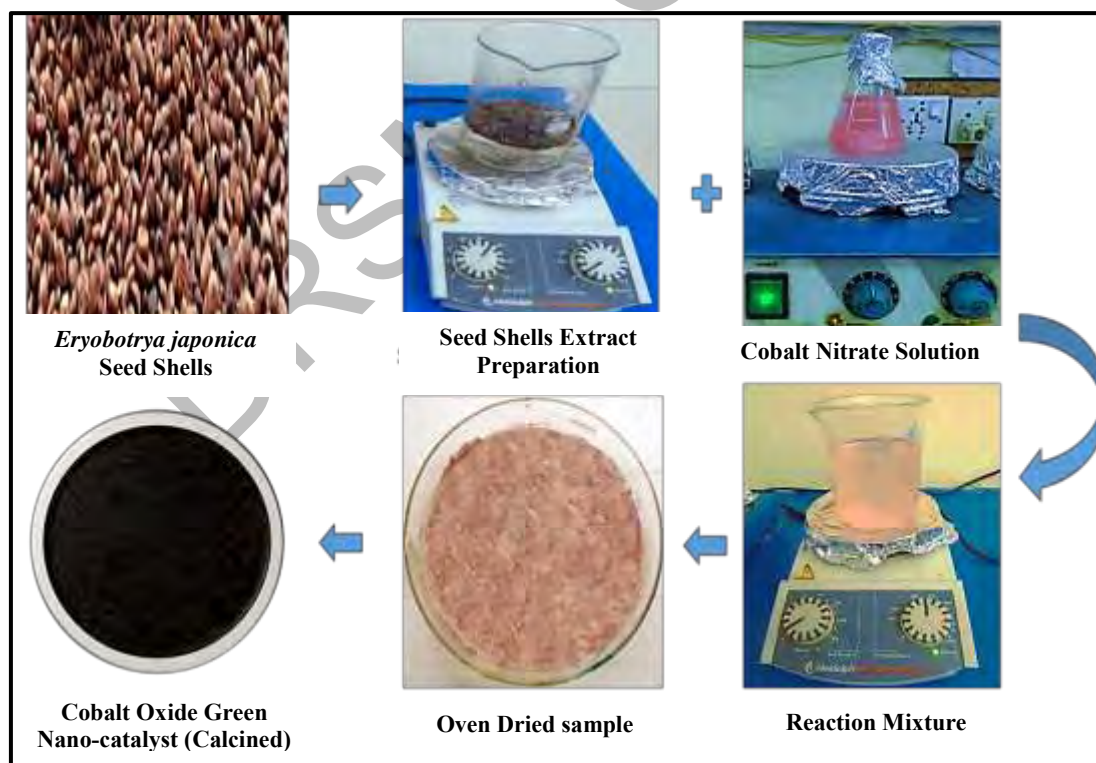
Plate 7 Synthesis of Cobalt Oxide Green Nano-catalyst

2.10.3 Copper Oxide Green Nano-catalyst

(a) Preparation of *Praecitrulus fistulosus* seed cake extract

To synthesize Copper oxide nanoparticles by biological method incorporated with in situ impregnation, *Praecitrulus fistulosus* seed cake extract (PFSCE) was used with some minor modification as represented by earlier studies (Kamel *et al.,* 2018). Fresh seed cake i.e. byproduct of mechanical oil extraction, was collected from oil expeller after oil extraction from seeds. To remove dirt, soil, and dust, PFSCE was thoroughly washed with running tap water three times. After that, it was rinsed with distilled water. PFSCE was cleaned and dried at 60 °C until a consistent weight was obtained. This seed cake was crushed and powder was stored for further use in order to prepare PFSCE by boiling 30g of seed cake in 200 mL of distilled water at 70 °C followed by filtration and storage at 4°C (Dawood *et al.* 2022; Kamel *et al.,* 2018).

(b) Synthesis of Copper Oxide Green Nano-catalyst

The 1.0 M aqueous solution of Copper Sulphate pentahydrate ($CuSO_4.5H_2O$) was prepared in 100mL of double-distilled water in order to produce the copper oxide green nano-catalyst. A 10mL aqueous copper sulphate solution was mixed well by a magnetic stirrer for 2 hours at 200°C after the addition of 6mL of *Praecitrulus fistulosus* seed cake extract (PFSCE). The solution turned from light brown to blackish brown, which was then centrifuged for 20 minutes at 1800 RPM followed by oven drying at 60 °C. The dried copper oxide nano-catalyst was heated to 300 °C for 3h (Plate 8).

Plate 8 Synthesis of Copper Oxide Green Nano-catalyst

2.10.4 Cadmium Oxide Green Nano-catalyst

(a) Preparation of *Luffa acutangula* floral Extract

In the current study, green synthesis of cadmium oxide (CdO) nanoparticles was conducted from Cadmium nitrate tetrahydrate $Cd(NO_3)_4.4H_2O$ and flower of *Luffa acutangula* (Linn.) Roxb (Kaliammal *et al.,* 2021; Tariq *et al.,* 2021). *Luffa acutangula* floral Extract (LAFE) was prepared in deionized and double distilled water extraction medium. Freshly collected yellowish mature flowers were thoroughly washed and dried under shade and in a dust-free environment for 6 days. The purpose of under-shade drying of flowers was to avoid the degeneration of phytochemical constituents that would be used as reducing and capping agent while biosynthesis of green nano-catalyst (Arshad *et al.,* 2023).

Dried flowers were ground over Philips electric grinder to acquire fine particle homogeneity that was further ensured by brass sieve straining(mesh size, 4cm). Then 1g in 150mL kept on a hot plate and magnetic stirrer for 7h at 85±2°C. The reaction mixture is filtered to separate residue and filtrate. Integrated bioextract was placed in airtight sample bottles to be stored at 4 °C in a refrigerator for further experimental purpose (Khan *et al.,* 2020).

(b) Synthesis of Cadmium Oxide Green Nano-catalyst

By following a typical green synthesis of Cadmium oxide green nano-catalyst, 5 mL of aqueous *Luffa acutangula* floral extract (LAFE) was added to a 100 mL aqueous solution 0.1M of $Cd(NO_3)_2.4H_2O$. The mixture was magnetically stirred while keeping the assembly temperature at 85 ± 2 °C for 3 hours at 400 rpm agitation rate. The resulting solid was separated from the reaction mixture when subjected to centrifugation at 3500 rpm for 30 minutes (Kaliammal *et al.,* 2021).

The pellet was separated and is dried in an oven at 150 °C followed by scrapping and calcination at 300 ° C for 3 hours (Tariq *et al.,* 2021).

The ultimate reddish brown powder is indication of synthesis of CdO-NPs that is stored in air tight zipper bag to be used as green nano-catalyst (Plate 9) (Haider *et al.,* 2022; Savale *et al.,* 2022; Arshad *et al.,* 2023).

Plate 9 Synthesis of Cadmium Oxide Green Nano-catalyst

2.10.5 Nickle Oxide Green Nano-catalyst

(a) Preparation of *Diospyros lotus* Bark Extract

Diospyros lotus L. bark was taken, cleaned properly with double-distilled water to remove the pollutants and dust, dried, ground into a fine powder. 40 g of bark powder was solubilized in double distilled water (100mL) which was then heated for 30 minutes at 65°C. The aqueous extract was filtered using Whatman filter paper No. 1 after cooling it at room temperature. The extract was utilized as a stabilizing and reducing agent and kept at 4-6 °C (Dawood *et al.,* 2021).

(b) Synthesis of Nickle Oxide Green Nano-catalyst

For synthesis of green nickle oxide, a known amount of Nickle (II) sulphate hexahydrate (NiSO4).6H2O was dissolved in distilled water (100mL) to prepare 0.1 M aqueous solution. Then *Diospyros lotus* L. bark Extract (DLBE) (25mL) was mixed in it and allowed it to heat at 200 °C for 30 minutes while being constantly stirred. The solution was centrifuged for 15 minutes at 10,000 RPM after 3 hours. To remove any undesired pollutants from the nanoparticle, the pallet was washed four times via double-

distilled water. The pallet was next fully dried at 100 °C in a hot air oven. The oven dried pallet was ground into a fine powder to create a fine crystalline nanostructure, which was employed for more research and the biodiesel synthesis process (Dawood *et al.,* 2021). (Plate 10).

Plate 10 Synthesis of Nickle Oxide Green Nano-catalyst

2.10.6 Calcium Oxide Green Nano-catalyst

(a) Preparation of *Cucumis melo* var. *Cantalupensis* Peel Extract

In order to prepare *Cucumis melo* var. *Cantalupensis* Peel Extract (CMCPE), the fresh fruit was purchased from local market in Islamabad. The fruit was splashed with running tap water to get rid of the dust and peeled off. The obtained peel was again washed with distilled water to remove left over pulp followed by chopping in to small pieces. These peel sections were kept in oven overnight for drying and ground in to fine powder. By using 20 g of peel material, saturated aqueous peel extract was prepared in distilled water (400mL), continuously boiling on a hot plate until half the water had evaporated. The CMCPE was filtered and stored at 4°C for future use (Ahmad and Zafar 2022).

(b) Synthesis of Calcium Oxide Green Nano-catalyst

In next step of calcium oxide green nano-catalyst synthesis, calcium sulphate dihydrate $(CaSO_4).2H_2O$ (5.4456 g) was used to prepare a 0.1 M calcium sulfate solution in 400mL of distilled water. The molar solution was heated at a steady temperature i.e. 65 °C while saturated CMCPE (200mL approx.) was constantly added for 2 hours. This mixture was filtered and allowed to settle followed by centrifugation at 900 rpm. The pellet containing calcium oxide was separated, rinsed with distilled water and then transferred to petri plates. Petri dishes containing sample solution were kept in an oven set at 60°C until it dried completely. Using a scraper, dried calcium oxide green nano-catalyst samples were collected in silica crucibles and subjected to calcination process in muffle furnace at 500 °C for 3 hours (Ahmad and Zafar 2022).

Plate 11 Synthesis of Calcium Oxide Green Nano-catalyst

2.10.7 Silver Oxide Green Nano-catalyst

(a) Preparation of *Solanum surattense* Persistent Calyx Extract

For preparation of *Solanum surattense* persistent calyx extract (SSPCE), the fruit was collected from wild areas of lower Margella hills Islamabad and Talagang district Chakwal Pakistan. Each fruit of *Solanum surattense* is globose berry with acute

4-5mm long, prickly persistent calyx i.e. distinguishing feature of family solanaceae. After collection, mature fruits were washed with distilled water and dried under shade for two days. Completely dried calyces were separated from seeds and boiled in 100 mL of distilled water until half of the water evaporated and 50 mL extract is left over. This freshly prepared extract is filtered and added to a simultaneously synthesized aqueous solution of silver nitrate (NO_3) (Dawood *et al.,* 2022).

(b) Synthesis of Silver Oxide Green Nano-catalyst

To synthesize silver oxide green nano-catalyst, 100mL of 0.1 M aqueous solution of silver nitrate (Ag NO_3) was prepared and 5mL SSPCE was added in to drop wise while continuously stirring the mixture at 200 °C for 30 minutes. The reaction setup was incubated in the dark to prevent silver nitrate from photocativation. When SSPCE reacts with silver ions, the solution color changes from light green to brownish black, suggesting the creation of silver oxide nanoparticles (Plate 12). The solution was filtered, oven-dried, scrapped, ground into a fine powder sequentially. The sample was calcined in muffle furnace at 300°C for three hours to produce fine crystalline nanostructures of silver oxide (Ag_2O) to be used for further research and in the biodiesel synthesis process as green nano-catalyst (Dawood *et al.,* 2022).

Solanum surattense **Persistent Sepals Extract Preparation**

Silver Oxide Green Nano-catalyst (Calcined)   **Oven Dried Sample**   **Reaction Mixture**   **Silver Nitrate Solution**

Plate 12 Synthesis of Silver Oxide Green Nano-catalyst

2.10.8 Magnesium Oxide Green Nano-catalyst

(a) Preparation of *Cucumis melo* var. *Agrestis* Seed Extract

The feedstock for *Cucumis melo* var. *Agrestis* Seed Extract (CMASE) was collected in the district Talagang from the wild and from the sides of roads. Non-edible seeds were cleaned with distilled water to eliminate any remaining pulp, then dried overnight in the oven before being ground into a fine powder. Saturated aqueous seed extract was created in distilled water using 20g of seed powder (400mL). For future use, CMASE was filtered and kept at 4°C. (Ahmad and Zafar 2022).

(b) Synthesis of Magnesium Oxide Green Nano-catalyst

The coprecipitation cum biosynthesis method was adopted with minor modifications (Ahmad and Zafar 2021 and Shaheen *et al.,* 2018). When a basic pH of 10 was reached, 0.1 M (100 mL soln.) magnesium sulphate (MgSO4) with 2 mL seed extract was titrated in the burette against a solution of 0.1 M sodium hydroxide (NaOH) that was continually stirring (500 rpm). Purification was achieved by repeatedly rinsing the viable mixture, which was then dried for 12 hours in a 90 °C oven. For three hours, the dried sample was maintained in an electric furnace at 500 °C. (Ahmad and Zafar 2021; Ameen *et al.,* 2022; Shaheen *et al.,* 2018).

Plate 13 Synthesis of Magnesium Oxide Green Nano-catalyst

Plate 14 Calcination in Muffle Furnace

2.11 Green Nano-catalyst Characterization

The green nano-catalysts were characterized by diverse advanced analytical techniques such as Fourier Transform Infrared Spectroscopy (FT-IR), X-ray Diffraction (XRD), Scanning Electron Microscopy (SEM) and Energy Dispersive X-Ray (EDX) etc. used for the qualitative and quantitative examination of catalyst in this research project. The major challenge to be encountered for implication of these techniques is high expense and lack of professionals. Moreover, single analytical technique cannot satisfy all the characterization requirements. Therefore, while employing a standard technique for analysis, flexibility is required (Dawood *et al.,* 2018).

2.11.1 Fourier Transform Infrared Spectroscopy (FT-IR) of Green Nano-catalyst

The functional groups of catalyst were studied using FT-IR spectroscopy and spectra were recorded at 400–4000 cm^{-1} range with Bruker-Tensor 27. FT-IR is a prospective scientific method that has a built-in computer system that is integrated to examine the catalyst and biodiesel. With distinct absorption peaks that are parallel to the vibration frequency of bonds between the sample atoms and resulting the infrared

spectrum signifies the sample fingerprint. It is among the fine methods for recognizing amorphous surfaces quickly and accurately (Munir *et al.,* 2021)

2.11.2 X-ray Diffraction (XRD) of Green Nano-catalyst

For determination of samples' crystalline phase and to offer precise information on its unit cell dimensions, X-ray diffraction (XRD) analysis is used. For an effective analysis, the sample needs to be homogenized, finely powdered, and thoroughly dry. X-rays are directed to the material during each run, and the diffracted rays are collected on an XRD spectrum. The angle between the incident and diffracted rays is a principle element and key component of the XRD system. For the identification of crystallite size and phase of the crystalline material (inorganic chemicals and minerals), this approach is frequently used (Abbasi *et al.,* 2022).

For crystallographic investigation of as-synthesized raw catalyst, a powder diffractometer with 20 scans rate in 2θ/min (2θ = 50-70°) and Cu-K=1.54 A° was used.

2.11.3 Scanning Electron Microscopy (SEM) of Green Nano-catalyst

An efficient method for producing complicated high-magnification images of a sample surface topography is scanning electron microscopy (SEM). The morphological structure of the seed and green nano-catalyst was determined via scanning electron microscopy. The implementation of SEM technology has provided a breakthrough trend for detailed analysis of ultra-microscopic structure of a substance. Using this method, the micro-morphology of selected eight seeds was also determined. Hence, for an accurate and comprehensive examination of morphological aspects at the micro- and nano-scale level, scanning electron microscopy employs high resolution and magnification (Munir *et al.,* 2021).

In this study, Scanning electron microscopy (SEM) was used to analyze the morphological structure and particle size of the produced green nano-catalysts. In a 20 kHz with 750W ultrasonic processor (Sonics Corp., USA), 10 mg/L of manufactured nano-catalyst was sonicated for 30 minutes. The glass slide was coated with 1-2 drops of a sonicated nano-catalysts dispersion, dried on a hot plate at 60°C for 2-3 minutes, mounted to the stub using carbon tape, and then placed in a gold sputtering machine. Following that, a scanning electron microscope was used to examine the gold-coated samples (JOEL JSM-5910) (Ahmad *et al.,* 2022).

2.11.4 Energy Dispersive X-Ray (EDX) of Green Nano-catalyst

Energy dispersive X-ray spectroscopy (EDX) is used to determine chemical composition and elemental analysis of chemical compounds. It is based on how the excited X-ray source and sample interact. It is also utilized to look at a nano-chemical structure of a catalyst. Using EDX analysis, it is possible to determine unique atomic structure, which allows for a specific set of peaks on the electromagnetic emission spectrum. Hence, the purity and elemental composition of a substance is thoroughly investigated. In current research project, SEM (JOEL JSM-5910) fixed with EDX equipment was implicated (Arshad *et al.,* 2023).

2.12 Biodiesel Synthesis via Green Nano-catalyst

A single step (transesterification) and a double step (esterification and transesterification) were used for biodiesel synthesis depending on the selected feedstocks' acid value (Ahmad and Zafar 2021).

2.12.1 Esterification

Biodiesel feedstock with an acid value more than 3 mg/KOH should be acid-pretreated prior to transesterification reaction by esterification by an acid to lower its acid value. In round-bottom flask (250 mL), esterification was carried out using 1% H_2SO_4 (w/w), 6:1 (methanol to oil ratio), at 60–65 °C for 1–1.5 hours. When the process is completed, the reaction mixture was decanted into a separating funnel for the physical separation of top layer (alcohol and water) from bottom layers (esterified oil) followed by rinsing of esterified oil via hot double distilled water for catalyst removal. This pretreated oil was dried in the oven at 100 °C for an hour. Anhydrous sodium sulphate was used to remove moisture from pretreated esterified oil (Hasni *et al.,* 2017).

2.12.2 Transesterification

An appropriate catalyst was utilized to transesterify the pre-treated esterified oil. Specific concentration of catalyst was dispersed in a known volume of methanol (30-minute agitation) to form methoxide followed by transfer in to preheated oil. Process was conducted with an altered ratio of catalyst and methanol-oil at the desired temperature while stirring for the particular time span followed by centrifugation at 4000 rpm for 5-7 minutes. Using a rotary evaporator, the solution was processed for

catalyst removal in order to evaporate any excess alcohol i.e. methanol. The mixture that resulted was poured to funnel for separating the glycerol and biodiesel phases (Ullah *et al.,* 2020). The biodiesel yield was calculated by using the provided equation

$$\text{Biodiesel Yield (\%)} = \text{Biodiesel Produced (g)} \div \text{Oil Used (g)} \tag{3}$$

2.13 Biodiesel Characterization

Biodiesel synthesized via green nano-catalyst was by Fourier Transform Infrared Spectroscopy (FT-IR), Gas Chromatography and Mass Spectroscopy (GC-MS), Nuclear Magnetic Resonance (NMR) i.e. ^{1}HNMR & ^{13}CNMR (Ullah *et al.,* 2020)

2.13.1 Fourier Transform Infrared Spectroscopy (FT-IR)

FT-IR spectrum of synthesized biodiesel was acquired on Bruker-Tensor 27 in 4000-400 cm^{-1} range to get insight about the functional groups and structural arrangement of Fatty Acid Methyl Esters (Chia *et al.,* 2022).

2.13.2 Gas Chromatography and Mass Spectroscopy (GC-MS)

The FAMEs were tested using a GC-MS (type GC-MS QP 2010 ultra by SHIMADZU) equipped with a quadrupole mass spectrometer and a dual inlet differential vacuum system. Helium flowed at a rate of 1.44 mL/min as the carrier gas. From 120 to 250 C at a rate of 80 C/min, the column temperature was programmed. The injector temperature was set to 120°C, while the detector temperature was set to 250°C. Utilizing a split mode with a split ratio of 1:3, 0.1 L of sample volume in MTB in CHCL3 was injected. With the Electron Impact (EI) method of ionization, the mass spectrometer was programmed to scan in the m/z value range of 50–1000. The duration of the entire program was 31 minutes (Awang *et al.,* 2021; Shaheen *et al.,* 2018).

2.13.3 Nuclear Magnetic Resonance (NMR)

Nuclear Magnetic Resonance (NMR) i.e. ^{1}HNMR & ^{13}CNMR offers the overall distribution of methyl esters. The yield of transesterification reaction was observed using NMR analysis, specifically ^{1}HNMR & ^{13}CNMR. Utilizing an Avan CE 300 MHz spectrometer, using 5.05 mm BBO probes operating at 7.05 T. Tetramethylsilane (internal standard) with deuterated chloroform (TMS) as a solvent were utilized. Spectra of NMR (300 MHz) were captured using 30° of pulse duration, 1s of recycle delay, and 8 scans (Akhtar *et al.,* 2022).

2.14 Fuel Properties Determination

Synthesized biodiesel quality and impact on diesel engines were measured in terms of the fuel properties. The physicochemical properties were compared with the ideal conditions of the international biodiesel standard (ASTM D-6751) in order to investigate color, total acid number, kinematic viscosity, sulphur content, density, cloud, flash and pour point (Ullah *et al.,* 2020; Wang *et al.,* 2022).

2.15 Biodiesel Yield Optimization via Response Surface Methodology (RSM)

Biodiesel yield was optimized via Response Surface Methodology (RSM) using Design-Expert 13 (Stat-Ease Inc, Minneapolis, USA). This method was used to statistically examine the data and determine that the ploy quadratic approach seemed to be fitted and response appeared to be related to dependent factor i.e. yield (Y) and the investigational factors i.e. methanol to oil molar ratio (A), catalyst loading (B), reaction time (C) and reaction temperature (D). Results from 30 experimental runs were evaluated to determine how well they fit the predicted model. The optimal values of four autonomous reaction parameters were examined using the regression equation, and additional factors like the Fisher test (F-value), correlation coefficient (R), and probability value (p-value) were also computed from statistical analysis of the model (Munir *et al.,* 2021; Akhtar *et al.,* 2022; Arshad *et al.,* 2023)

CHAPTER: 3

RESULTS AND DISCUSSION

SECTIONS

1. Morphological description and SEM of oil yielding seeds
2. Biodiesel Synthesis from *Bischofia javanica* Seed Oil using Zirconium Oxide Green Nano-catalyst
3. Biodiesel Synthesis from *Eryobotrya japonica* Seed Oil using Cobalt Oxide Green Nano-catalyst
4. Biodiesel Synthesis from *Praecitrullus fistulosus* Seed Oil using Copper Oxide Green Nano-catalyst
5. Biodiesel Synthesis from *Luffa acutangula* Seed Oil using Cadmium Oxide Green Nano-catalyst
6. Biodiesel Synthesis from *Diospyros lotus* Seed Oil using Nickle Oxide Green Nano-catalyst
7. Biodiesel Synthesis from *Cucumis melo* var. *Cantalupensis* Seed Oil using Calcium Oxide Green Nano-catalyst
8. Biodiesel Synthesis from *Solanum surattense* using Seed Oil Silver Oxide Green Nano-catalyst
9. Biodiesel Synthesis from *Cucumis melo* var. *Agrestis* Seed Oil using Magnesium Oxide Green Nano-catalyst

This chapter is comprised on results with discussion of nine following sections involving morphological description, seed identification via scanning electron microscopy, application and characterization of green nano-catalysts, analysis of sustainable biodiesel fuel synthesized from eight different oil yielding seeds

SECTION I: Morphological description and SEM of oil yielding seeds

SECTION II: Biodiesel Synthesis from *Bischofia javanica* Blume Seed Oil using Zirconium Oxide Green Nano-catalyst

SECTION III: Biodiesel Synthesis from *Eryobotrya japonica* (Thunb.) Lindl. Seed Oil using Cobalt Oxide Green Nano-catalyst

SECTION IV: Biodiesel Synthesis from *Praecitrullus fistulosus* (Stocks) Pangalo Seed Oil using Copper Oxide Green Nano-catalyst

SECTION V: Biodiesel Synthesis from *Luffa acutangula* (Linn.) Roxb. Seed Oil using Cadmium Oxide Green Nano-catalyst

SECTION VI: Biodiesel Synthesis from *Diospyros lotus* L. using Seed Oil Nickle Oxide Green Nano-catalyst

SECTION VII: Biodiesel Synthesis from *Cucumis melo* var. *Cantalupensis* Seed Oil using Calcium Oxide Green Nano-catalyst

SECTION VIII: Biodiesel Synthesis from *Solanum surattense* Burm. f. Seed Oil using Silver Oxide Green Nano-catalyst

SECTION XI: Biodiesel Synthesis from *Cucumis melo* var. *Agrestis* Naudin Seed Oil using Magnisium Oxide Green Nano-catalyst

Biodiesel Feedstock

Morphological Studies

Scanning Electron Microscopy

Green Nano-catalysts Synthesis and Characterization

Biodiesel Synthesis and Characterization

Biodiesel Yield Optimization via RSM

Fuel Properties Estimation and Comparison with ASTM
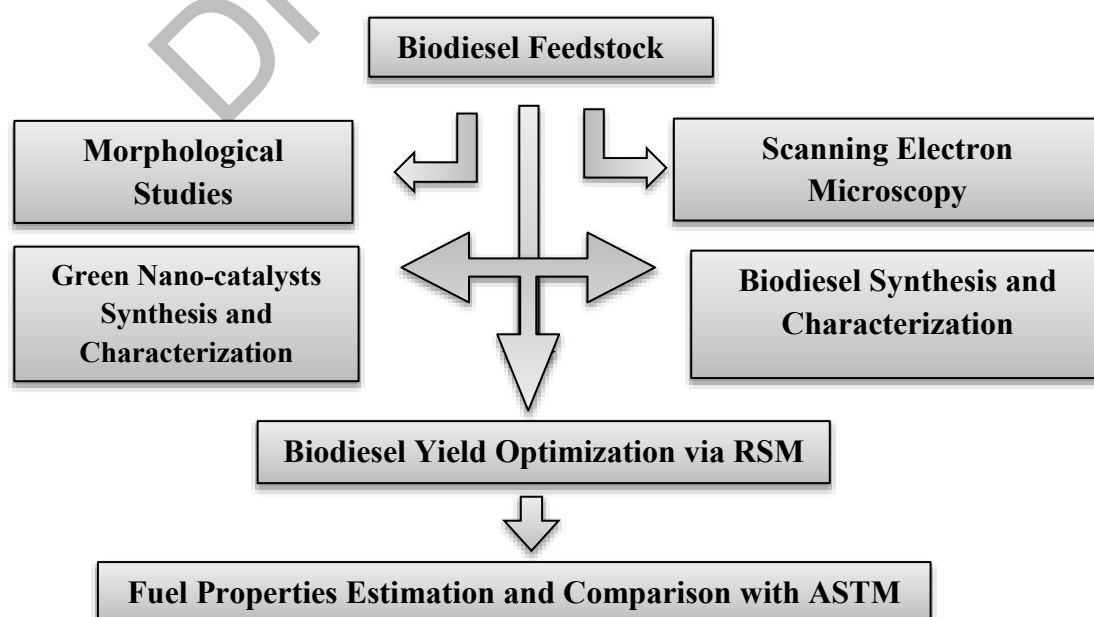
Flowsheet 2: Schematic Representation of Chapter 3

SECTION: I

Morphological description and SEM of oil yielding seeds

3.1 Morphological description and SEM of oil yielding seeds

This Section includes a detailed investigation of the micro-morphological characteristics of seeds as energy crops using scanning electron microscopy (SEM) along with the morphological description of eight different oil-yielding plants. By examining minute morphological characteristics of seeds. The current technology of scanning electron microscopy (SEM) has been widely employed to resolve taxonomic issues, assisting in the species identification and authenticity of oil seeds. The diagnostic tools to distinguish between various species are the micromorphological characteristics of seeds, along with size and form. These factors demonstrate the direct relationship that exist between various plant species at the taxonomy level. Since oil content, free fatty acid content (FFA), and their availability have a significant role in the selection of feed stock for the biodiesel industry. Researchers are now considering seed oils with an advantage as a potential feedstock for the future energy sector if it is cost-effective, can grow easily in waste land, solves the food vs fuel dilemma, and is environmentally friendly. Therefore, the current work is an attempt to introduce some novel oil-producing seeds and their micromorphological content to the scientific community. These seeds have the potential to be used in the future energy sectors as promising biodiesel feedstock. The biodiesel yield, distribution, and micromorphological characteristics of seeds as determined by SEM, coupled with the percentage of oil and FFA among understudied oil-producing seeds (Table 3.1.1 and 3.1.2).

3.1.1 *Bischofia javanica* blume

Bischofia javanica blume belongs to family Phyllanthaceae and is widely distributed in Southeast Asia, India, Southern China, Malesia, Southern Japan, Taiwan and Myanmer. *Bischofia javanica* is evergreen tree with fissured, shallow and narrow bark, having heartwood in dark brown and reddish stem, straight cylindrical trunk that grows fast even up-to 35 m in height with smooth, dense, glabrous, round head branches with milky sap. Leaves are shiny, bright green, membranous, palmate, 3 or 5 foliate, stipulate, petiolate, lanceolate, pulvinate, leaflets 7-15×4-8 cm, broad base obtuse to cuneate having lateral nerves (12-16), papery, glabrescent, obovate, elliptic, oblong, ovate. Inflorescence dioecious (separate female and male flowers) paniculate, green, raceme with many floral clusters, without petal, axillary, greenish-yellow. Female

flower has ovate-oblong sepals, membranous margins, with 15-27cm long peduncle, having exerted, glabrous and smooth, tri-locular ovary with three entire, linear styles. Male flower (2.5 mm diameter) is also without petals having sepals that are semi-orbicular, membranous, outside pubescent abaxially, concave adaxially, ladle shaped and five stamen, short filaments, peltate, pistillode, lengthwise dehiscing large anthers, 13cm long, glabrous, pubescent, peduncle is present. Fruit is reddish brown, smooth berry (1.2-1.5 cm diameter), subglobose or globose with fleshy mesocarp and leathery to horny pericarp and shinning surface. 3-4 shiny non-edible seeds (4-5mm in length and 2-3 mm in width) are embedded in colorless fruit pulp (edible) (Ajaib & Zaheer-ud-din, 2012).

The seeds are light brown outside and brown to black inner surface, smooth, two flat and one rounded side, ovoid to oblong in shape and 60-100 thousand seeds are estimated to be present in per kilogram (Figure 3.1.1a, b).

SEM micrograph shows that surface sculpturing is verrucate, very thick and raised wall ornamentation, cell arrangement is irregular with buttressed anticlinal wall pattern and periclinal walls are concave with thick and raised elevation, hilum is not visible, sub-terminal and depressed whereas a lateral compression is present (Figure 3.1.1 c, d) Seeds have high oil content i.e. 29.7% wt. /wt. and FFA value with 1.95 mg KOH/g. and was found as favorable potential feedstock for biodiesel production as represented by our results.

The phytochemical and physicochemical properties of *Bischofia javanica* oil yielding seeds include 5.93% moisture content, 6.83% ash content, 18.91% carbohydrates, Protein content 18.69%, fiber content 5.32 %, total phenolics 0.59%, total tannins 9.65%, and total alkaloid 0.22% (Rai *et al.,* 2013; Lee *et al.,* 2021; Chowdhury *et al.,* 2020).

Figure 3.1.1: *Bischofia javanica* **(a)** Plant **(b)** Seeds **(c, d)** SEM Micrographs of seed and sculpturing

3.1.2 *Eryobotrya japonica* (Thunb.) Lindl.

Eryobotrya japonica (Thunb.) Lindl. belongs to family rosaceae, is a medium-sized tree, located in mildly temperate areas. The tree small to 10 m with brownish or yellowish brown branches and rusty gray tomentose; is most well-known for its fruit, which has numerous health advantages. The orange, oval loquat fruit is frequently referred to as a Japanese plum. The fruits have huge, brown seeds and are between one and two inches long. Stipule is pubescent, subulate, acuminate apex, 1-1.5 cm. A short, 6-10 mm, greyish brown tomentose petiole or virtually absent; leaf blade 12-30 3-9 cm, leathery, lanceolate, oblanceolate, obovate, or elliptic-oblong; 11 to 12 pairs of lateral veins; abaxially thickly grey rusty tomentose; adaxially glossy; cuneate; entire basally; remotely serrate apically; acute or acuminate. Thickly rusty tomentose peduncle; panicle 10 to 19 cm, many flower; pedicel 2-8 mm, tomentose rust; subulate, 2-5 mm, heavily rusty tomentose bracts; shallowly cupular and tomentose on the abaxial side in hypanthium; floral scent, 1.2-2 cm in diameter. Triangular-ovate, 2-3 mm, abaxially heavily tomentose in rust, acute apex sepals are present. Petals are white, oblong or ovate, 5-9×4-6 mm, with an obtuse or emarginate apex; with two ovules per locule and a rusty pubescent apex, the ovary has five free styles; 20 stamens; globose or obovate, yellow or orange pome i.e. 1-1.5 cm in diameter, glabrescent and rusty tomentose, fruiting pedicel is 0.3-0.8 cm, glabrescent and rusty tomentose. Flowering june; and fruiting period, july to august. Fruits are spherical to pear-shaped, 3–4 cm long, orange–yellow, and delicious (ranging from sweet to sour). They ripen in the winter and spring (Inoue *et al.,* 2017).

One of the commercial crops that is widely grown in East Asia is *Erybotrya japonica.* It is a subtropical evergreen tree with the potential to flourish in a variety of climatic conditions. With an annual production of 1,000,000 tonnes, China is the primary loquat producer, followed by Spain (40,000 tonnes), Pakistan (30,000 tonnes), and Turkey (20,000 tonnes) as the other major producers globally. A little fruit harvested in the summer called a loquat is considered as a functional fruit because of its unique nutritional qualities (Per 100 gm of loquat fruit contains 0.4gm proteins, 1gm fat, 7gm carbohydrate, 0.8 mg dietary fiber, 0.5 mg ash, 22 mg calcium, 32 mg phosphorus, 1.33 mg carotenoids, and 3 mg vitamin C). More than half of a total fruit volume is made up of its seeds (Inoue *et al.,* 2017)

SEM micrographs show that seeds have reticulate wall sculpturing whereas wall ornamentation is buttressed with irregular epidermal cell arrangement, regular thickened anticlinal wall pattern whereas periclinal walls are thick, raised and convex, seed hilum is visible, terminal and raised while the lateral compression is present (Figure 3.1.2 c, d).

Our results represent that *Eryobotrya japonica* has 24% seed oil and 1.56 mg/g KOH content and was found as favorable potential feedstock for biodiesel production as depicted by our results and correlate with the findings of Henmi et al. (2019) for fatty acid composition and applications of *Eryobotrya japonica* seed oil (Henmi *et al.* 2019)
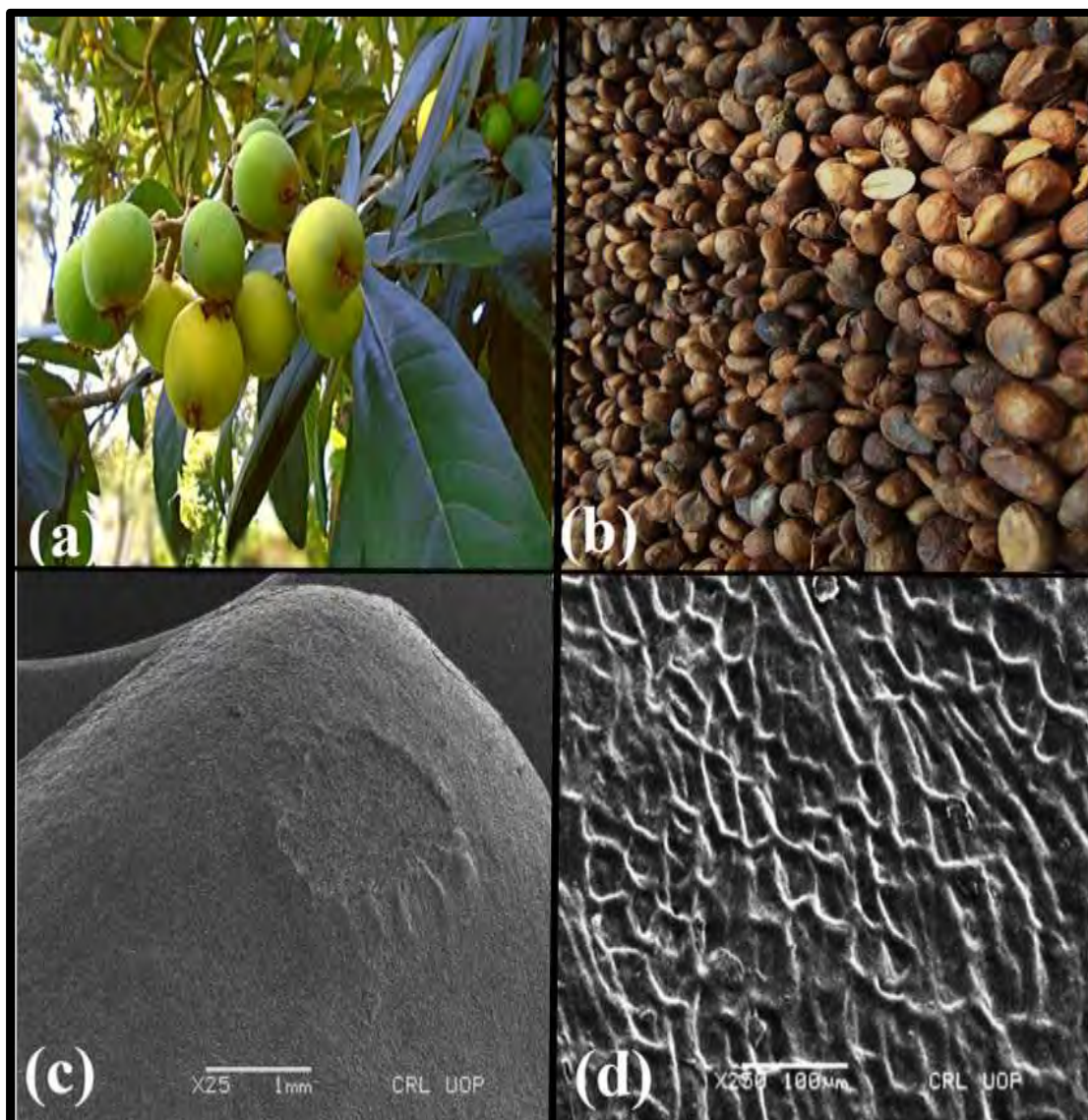
Figure 3.1.2: *Eryobotrya japonica* **(a)** Plant **(b)** Seeds **(c, d)** SEM Micrographs of seed and sculpturing

3.1.3 *Praecitrullus fistulosus* (Stocks) Pangalo

Praecitrullus fistulosus belongs to family cucurbitaceae, commonly known as Indian squash, round melon, Apple gourd, squash melon and is cultivated in two forms (light green and dark green) for its fruit to be used as vegetable and it is grown in Asia especially in north-west of India, Pakistan, Afghanistan, Africa, as export commodity in Kenya and Ghana for UK and US (cultivated at small scale). The plant is trailer or climbing herb that grows annually having hispid to villous robust stem and 2-3fid, slender stem. Leaves are apparently entire, meticulously denticulate margins, veins and veinlets on lower surface that are dense hispid and villous, lightly hispid lamina, hirsute petiole and sparingly pinnatifid leaves. *Praecitrullus fistulosus* is monoecious plant having yellowish, solitary and smaller flowers. Female flower has villous, hairy and soft ovary with campanulate lobed calyx, lanceolate, 5mm in length. Male flowers are pedicellate (1mm in length) have three stamens, two connate and a free have obconic lobes, campanulate and hairy calyx. Flowering period is march to September and its fruit is spherical (6 cm diameter) and seeds are dark brown in color whereas inner surface is smooth, pale yellow or whitish oblong to ovate, 8-9 mm in length and 4-5mm in width (Figure 3.1.3 a, b).

SEM micrographs illustrate that seeds have wrinkled wall sculpturing whereas wall ornamentation is thick and raised with irregular epidermal cell arrangement, irregular thickened anticlinal wall pattern whereas periclinal walls are convex with depressed elevation and seed hilum is not visible, terminal and raised while the lateral compression is present (Figure 3.1.3 c, d). Seeds have high oil content i.e. 34% wt. /wt. and FFA value with 2.01 mg KOH/g. Our current results are in accordance with Tyagi et al. (2012) who reported considerable percentage of fatty oil in seeds (52.8%)with following composition linoleic 50.80, oleic 21.23, stearic 10.70, palmitic 11.85 and myristic 1.74% with saponification and iodine value 192.5 and 126.5 respectively (Tyagi *et al.,* 2012).
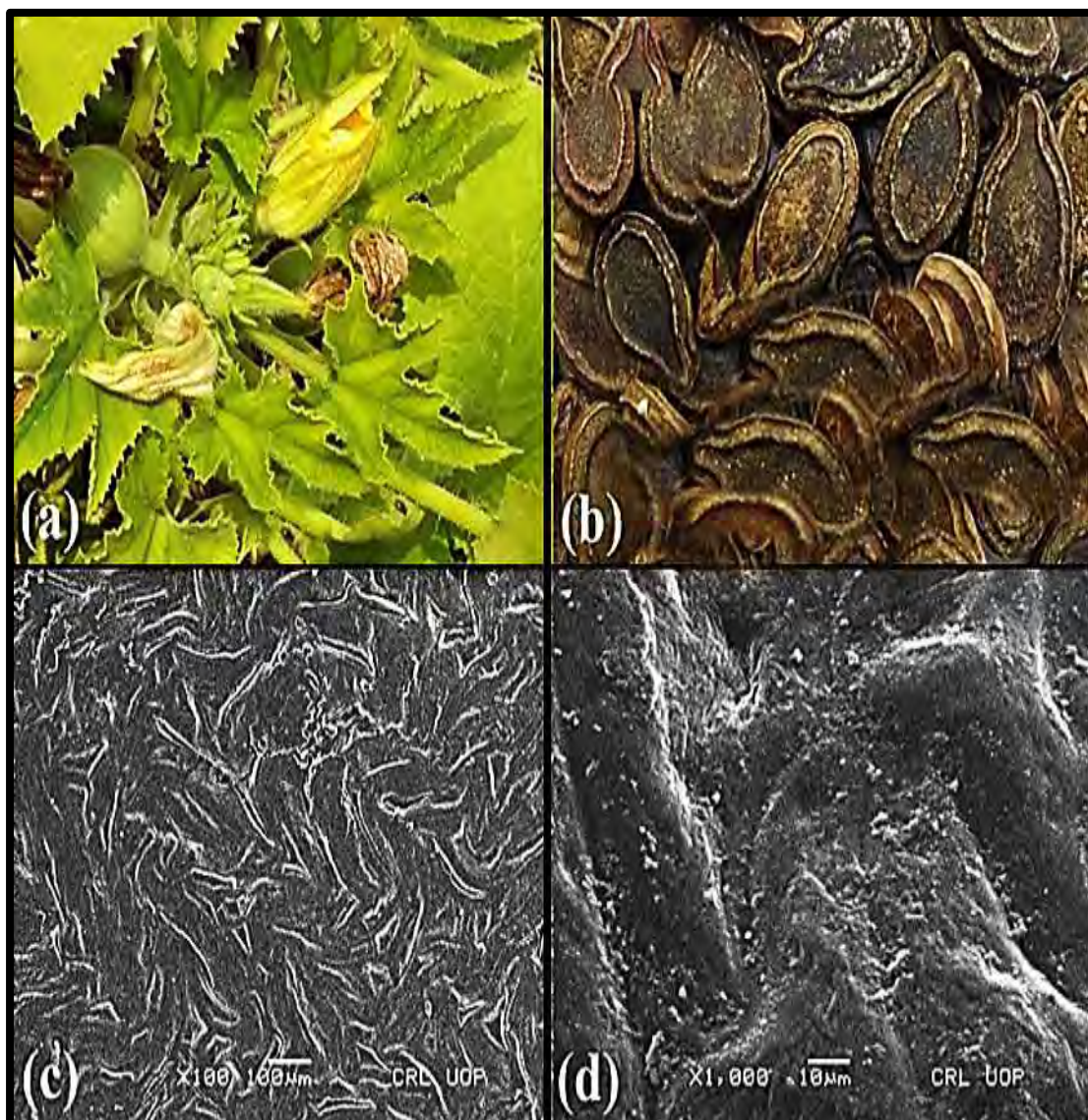
Figure 3.1.3: *Praecitrullus fistulosus* **(a)** Plant **(b)** Seeds **(c, d)** SEM Micrographs of seed and sculpturing

3.1.4 *Luffa acutangula* (Linn.) Roxb.

Luffa acutangula commonly known as Angled Loofah, Ridged Gourd, and Chinese Okra belongs to family Cucurbitaceae widely distributed in Tropical South Asia, India, Pakistan, China, Russia, Tropical Africa, West Indies, Mexico, Islands in Pacific, Tropical America. *Luffa acutangula* is annual climber and creeper vine with herbaceous green, five angled scabrous (along ribs) stem (grows up to 5-10m), glabrous, having trifid axillary sub-scabrous, 2-3 inches long tendrils. Leaves are scabrous, pale green, palmatilobed (5-7 lobed that are more or less deep), glabrous, chartaceous, alternate, acuminate or acute apex, 15-20 cm across blade, hastate or cordiform base, denticulate or sinuate-dentate margins, petiolate (8-12 cm in length). *Luffa acutangula* is monoecious or unisexual, pedicellate, pale yellow flowers, 4.5 cm across, actinomorphic. Calyx slightly hairy, pentagonal tube, slightly long lobes as compared to tube. Staminate or male flowers are elongated, racemes, deep lobes, corolla pale yellow, obtuse, 10-20 flowered, axillary, erect, three stamens with 4 mm long free filaments, villous, 10-15 cm in length. Petals are 2 cm long and 2.5 cm wide, obcordate, pale yellow, emarginate or may not be. Pistillate or female flowers are found in same axil as staminate flowers, have less than 1cm hypanthium and are solitary, having globose stigma, short style, tri-carpellate, 10 angled, inferior, claviform, ovary with many horizontal ovules. Fruit is dehiscent from apical pores and has crustose pericarp, 10 angled, longitudinal ribs, acute, 15-30 cm long and 6-10 cm diameter. Seeds of *Luffa acutangula* are soft, pale white, and lighter yellow in color when immature and dark brown or blackish and hard when mature while inner seed surface is still yellowish in color, elliptic (1/16th of inch thick and ¼ to 3/8th of inch long, 1/8th to ¼ of inch wide), 11-12 mm in length and 6-8mm in width, emarginated, smooth and slightly rugose. Seeds are ovate to obovate, numerous, more than 30 seeds are present per mature fruit (Al-Snafi, 2019). (Figure 3.1.4 a, b). Our SEM images show verrucate surface sculpturing and very thick and raised wall ornamentation, cell arrangement is irregular with buttressed anticlinal wall pattern and concave periclinal walls have thick and raised elevation, *Luffa acutangula* seeds have visible, terminal and raised hilum whereas dorsoventral compression is present (Figure 3.1.4 c, d). Seeds have high oil content i.e. 48 % wt. /wt. and FFA value with 3.91 mg KOH/g. In general, seed morphological patterns found to be supportive in distinguishing the different species of Cucurbitaceae (Schaefer & Renner, 2011)
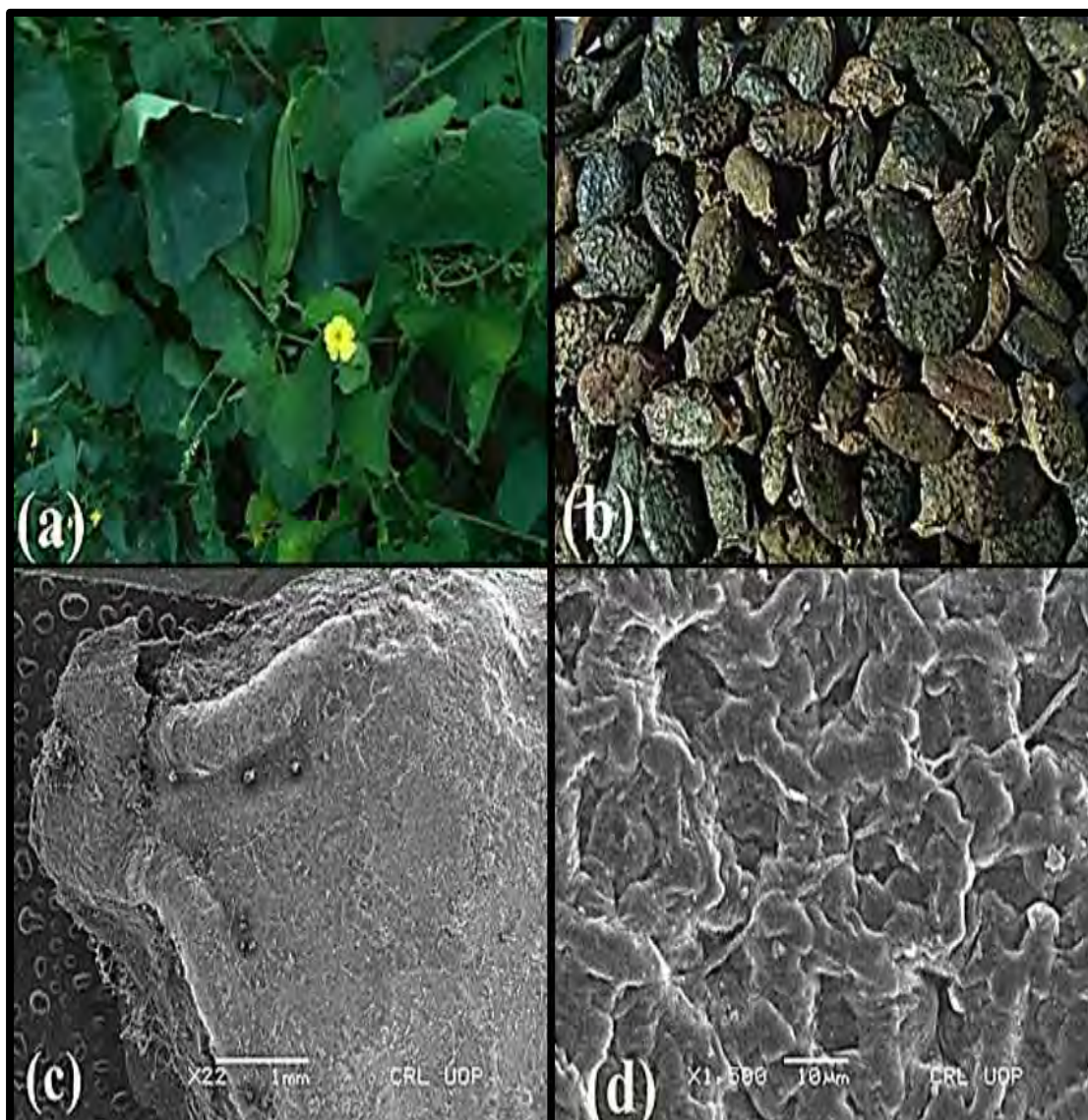
Figure 3.1.4: *Luffa acutangula* **(a)** Plant **(b)** Seeds **(c, d)** SEM Micrographs of seed and sculpturing

3.1.5 *Diospyros lotus* L.

Diospyros lotus belongs to family Ebenaceae commonly known as date-plum, Caucasian persimmon, or lilac persimmon, Japanese persimmon and is distributed in Iran, Japan, India, Pakistan, Afghanistan, China and Mediterranean region, Caucasia, Japan, Balkans, Anatolia. *Diospyros lotus* is 2-20 m tall tree with glabrous or pubescent stem having petiolate (4-10mm petiole length) leaves that are elliptic, acuminate, lanceolate, rounded base, undulate at margins and pubescent on lower or both sides. *Diospyros lotus* flowers are sessile and sometimes pedicellate with dense pubescent and short pedicel. Corolla reflexed, 7mm long, yellowish brown petals with rounded lobes and inside hairy or ciliated. Female flower is solitary and larger than male, has persistent calyx, single row of eight staminodes, 4-6 styles, persistent, ovary is glabrous below and hairy at apex whereas male flowers have 2.5 mm long calyx, cymes (2 or 3 flowered), two opposite rows of sixteen stamens, having 3mm long anthers, connective pilose, short filaments, 4-5 triangular lobes, pubescent, subacute to obtuse and rudimentary ovary. Fruit is glaucous berry ovoid to globose, when unripen mealy white in color and when ripens it is dark purple to blackish in color and has13-22 mm diameter. Seeds of *Diospyros lotus* are dark brown on outer surface and greyish at inner side, semi-spheroid, 11-15 mm long and 6-8 mm in width (Figure 3.1.5 a, b). SEM micrographs show striate wall sculpturing, thin and raised wall ornamentation, undulate and rough anticlinal wall pattern, asymmetric slightly depressed but convex periclinal wall pattern whereas hilum is visible and depressed and laterally compressed as shown in (Figure 3.1.5 c, d). Seeds have 20.3% oil content that has high FFA value with 6.91 mg KOH/g. Too high FFA makes the oil unfit for human consumption therefore it can be considered as non-edible seed oil with good potential for biodiesel production.

Our SEM results are in accordance with Sodeifian *et al.,* 2019 who evaluated seeds' surface via SEM images that revealed uneven rough appearance with uniformly spread oil layers and interlacing in both non-extracted solid portion and oil. However, on oil extraction these layers appeared cracked and surface became deflated, highly porous and oil depleted representing higher extraction efficacy (Sodeifian *et al.,* 2019; (Moghaddam *et al.,* 2012)
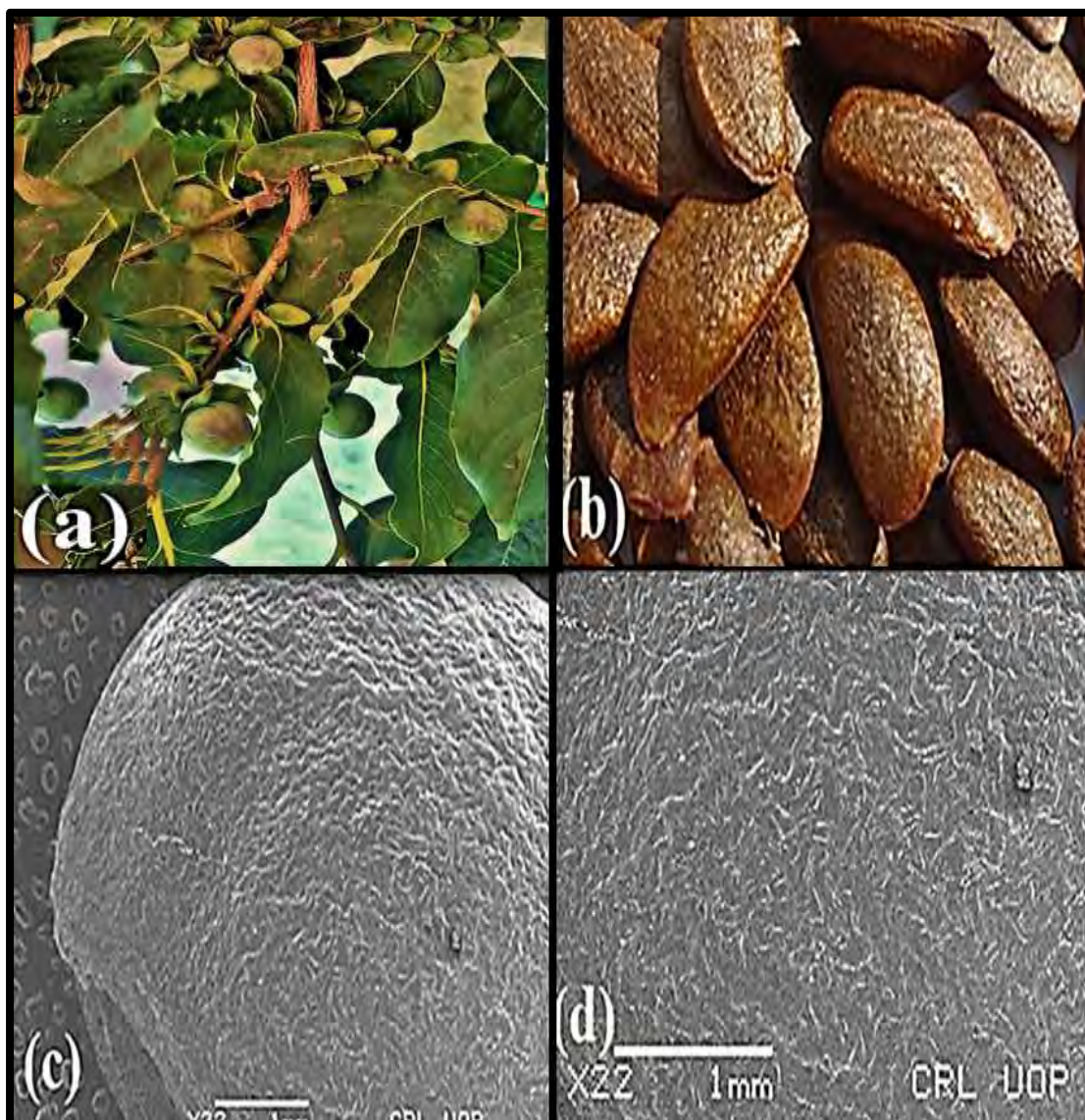
Figure 3.1.5: *Diospyros lotus* **(a)** Plant **(b)** Seeds **(c, d)** SEM Micrographs of seed and sculpturing

3.1.6 *Cucumis melo var. cantalupensis*

Cucumis melo var. cantalupensis belongs to family Cucurbitaceae commonly known as Charentias Cantaloupe, Musk Melon, Netted Melon, Person Melon, Nutmeg Melon and Rock Melon. *Cucumis melo* is distributed in all of the *Cucumis melo var. cantalupensis* is likely restricted to Afghanistan, Iran, China, Turkey, Bangladesh, Pakistan, and to a lesser extent, India. Many cultivated forms and types with varying fruit shapes, sizes, and colors are grown across the world. *Cucumis melo var. cantalupensis* is an annual climber reaching 1.5 metres (5ft)., softly hairy leaves with flowers typically 2-3 cm long, while the peduncle is typically 2 cm long and large, ovoid, spherical, or elliptical fruits.The thickness, colour, and markings on the fruit surface varies noticeably from one another. The inside flesh likewise varies in hue, flavour, thickness, and appearance. The flesh is greenish white and has a thick, wrinkled rind. Plants creeping, puberulent, scabrous, or hispid branched stem; tendrils puberulent and filiform; petiole is setose and 7-12cm. Leaf blade adaxially scabrous, undivided or 3–7 lobed, 6–15 cm×6–15 cm, suborbicular or reniform, papery, dentate; sinus truncate or rounded. Monoecious plants and bisexual flowers, one or more male flowers, fasciculate; filiform, 0.5–4 cm, pubescent pedicels; the calyx tube is narrowly campanulate, 3-8 mm, white villous and thickly hispidulous; corolla yellow; tube 1-2 mm; segments broadly ovate, obovate, ovate-oblong, obtuse, 3-24×2.5-20 mm; anthers flexuous. Female flowers are solitary whereas ovary is fusiform or ellipsoid, 4-11×2-5 mm, densely covered in villous, white lanate or pubescent; stigma 2–2.5, 3 mm. Size, shape, colour, odour, and taste of fruit are all highly diverse. Numerous, smooth, ovate-oblong, yellow-white, emarginate seeds with a sharp, rounded base; flowering and fruiting period is May to September (Ameen *et al.,* 2018)

Our experimental work showed that seeds are dark brown in color, seeds were 6 mm in length, 3.2 mm wide and 10-12 seeds in a gram (Figure 3.1.6 a, b). SEM micrograph shows seeds are broad ovate-oblong in shape, regular epidermal cell arrangement, anticlinal wall irregularly thickened and convex wall ornamentation. Seeds have striate surface sculpturing, hilum is visible, terminal and depressed with lateral compression (Figure 3.1.6 c, d) Seeds have high oil content i.e., 35% wt. and FFA value with 0.78 mg KOH/g and research.
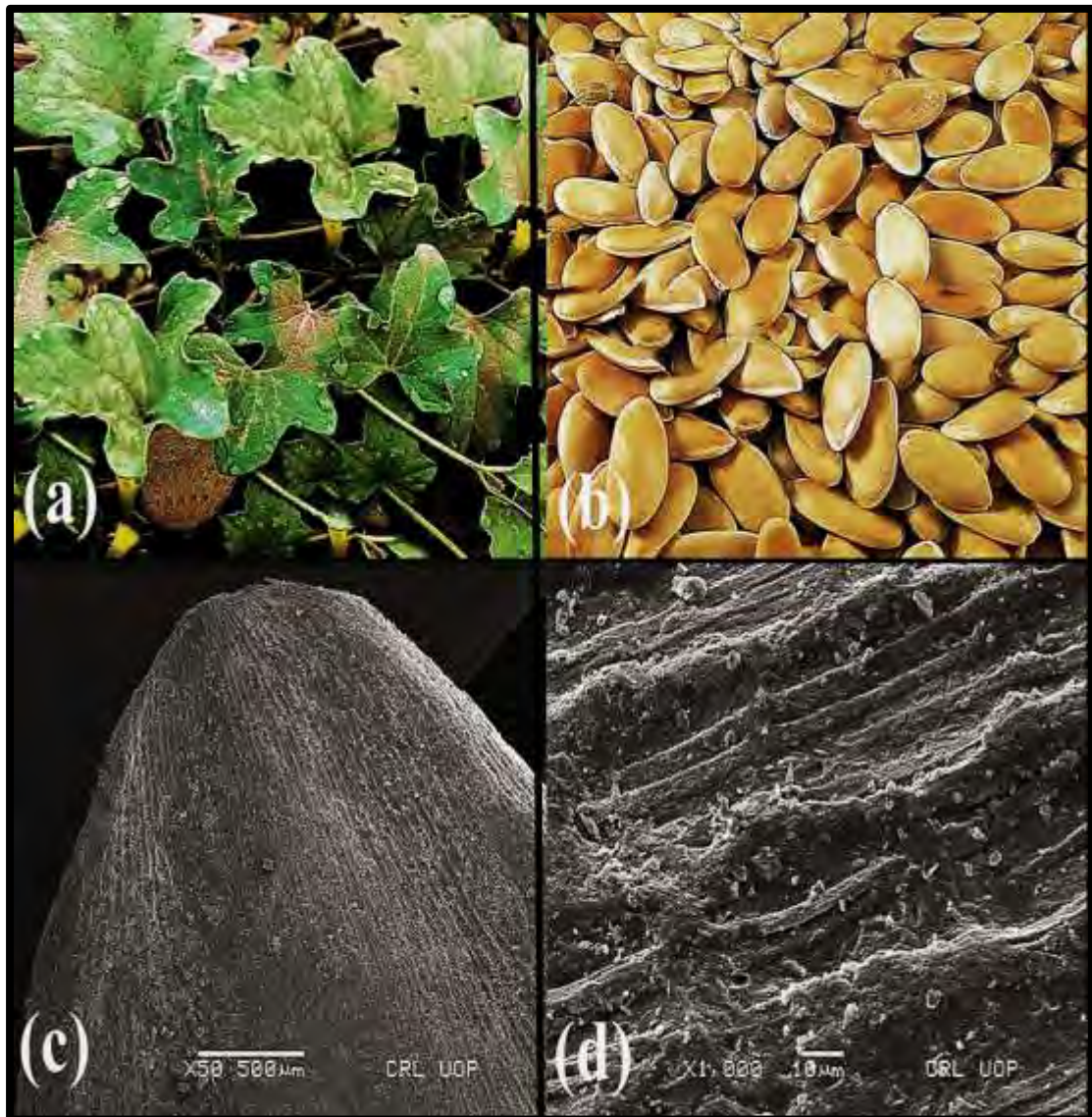
Figure 3.1.6: *Cucumis melo var. cantalupensis* **(a)** Plant **(b)** Seeds **(c, d)** SEM Micrographs of seed and sculpturing

3.1.7 *Solanum surattense* **Burm. f.**

Solanum surattense belongs to family Solanaceae, commonly known as Yellow-fruit nightshade, Thai striped eggplant (from the unripe fruit), Indian Nightshade and is distributed as weed or wild plant in South and South East Asia, especially Pakistan, India North Africa, Polynesia and Australia. Plant is herbaceous, perennial, prostrate with approximately 15mm long prickles therefore it is diffuse prickly herb with pubescent stem and branches that are stellate to glabrous. Leaves are dark green, elliptic to oblong, lobulated with unequal lobes, deeply lobed to sinuate, often toothed, acute or obtuse and 30-80×25-50 mm in size. Flowers are purple in color, peduncle cymes, 10-20 mm long peduncle, 2-4 in number, corolla limb is 10-12 mm long, 2-2.8 cm broad, triangular to ovate and stamen has elongated 7.5 mm long anthers. Whereas calyx is also prickly, acute and 5mm long lobes. Fruit is fleshy, 15-20 mm diameter and globose berry however seeds are orange to yellow in color on outer surface and yellow at inner side, 3 mm in length and 2 mm in width, smooth, obovate to discoid, faintly reticulate (Mali & Harsh, 2015; Tekuri *et al.*, 2019) (Figure 3.1.7 a, b).

SEM illustrate that seeds have ruminate surface sculpturing with thick and raised wall ornamentation, irregular asymmetric cell arrangement, buttressed anticlinal wall, rough, thickened and concave periclinal walls, seed hilum is visible, terminal and depressed and laterally compressed (Figure 3.1.7 c, d).

Seeds have considerable oil content i.e. 21% wt. /wt. and FFA value with 3.91 mg KOH/g.

Kumar (2021) reviewed the presence of active phytochemicals in *Solanum surattense* such as glycosides, ascorbic acid, steroids, flavonoids, phenols, gums, sterols etc (Kumar 2021).
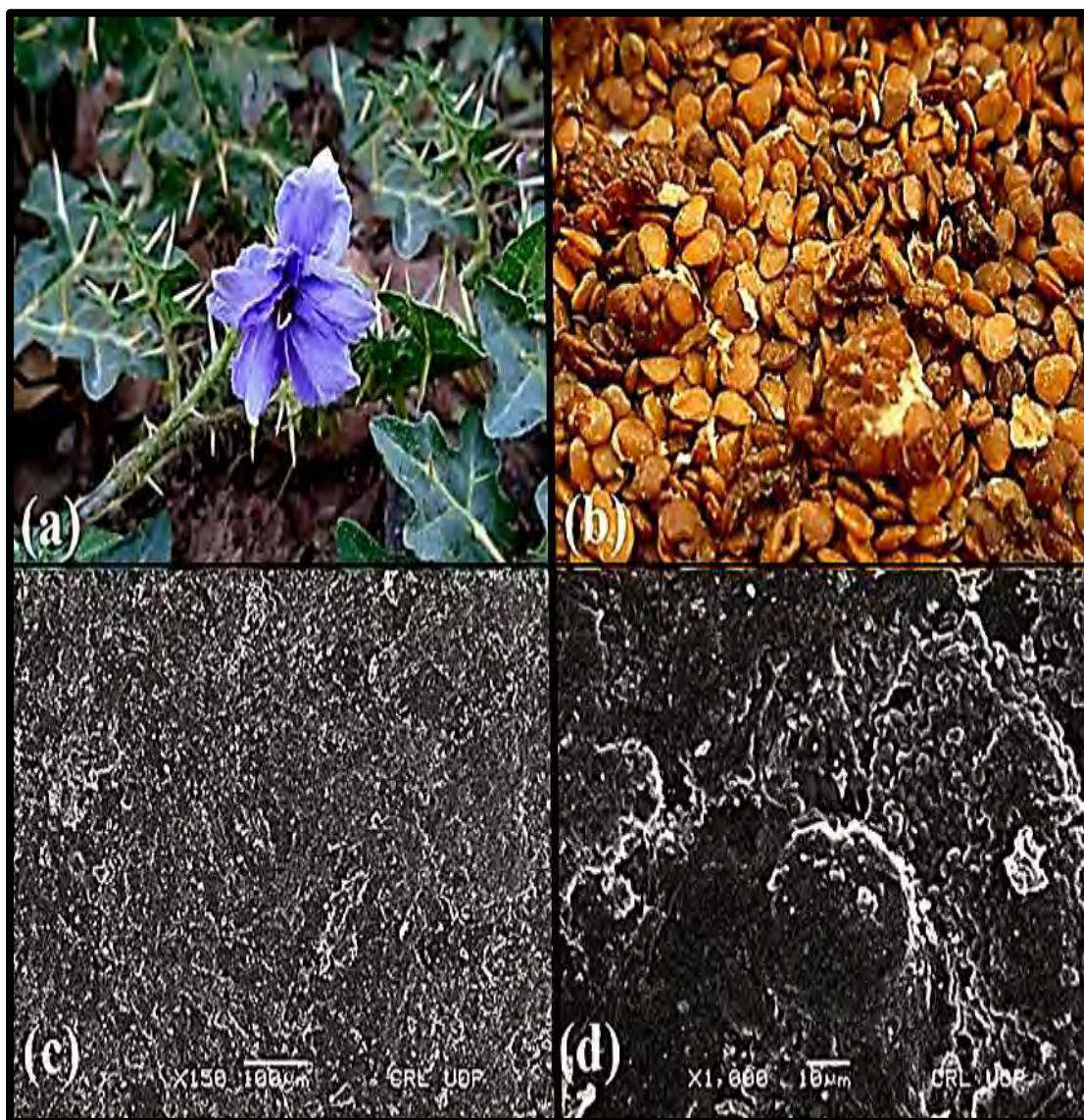
Figure 3.1.7: *Solanum surattense* **(a)** Plant **(b)** Seeds **(c, d)** SEM Micrographs of seed and sculpturing

3.1.8 *Cucumis melo* **var.** *Agrestis* **Naudin**

It is perennial or annual branched climbing herb and invasive weed, commonly known as wild musk melon, small gourd or wild melon throughout the old world tropics. It is distributed in arid zone, pastures, fields of soybean, alfalfa, sugarcane etc. railroad banks, marsh landscapes, trash dumps, vacant lots, disturbed areas and abandoned home sites, creek beds and waste marshy lands where other plants seedlings are unable to germinate, infests maize, cotton, pearl millet, cotton, sorghum as well as cyprus heads. Scabrid stem is prostrate with hairs (Scabrous hairy stem) with 3-5(-7) lobed, ovate, triangular leaves, calyx subulate (1.5mm), petiolate (1-6cm), corolla yellowish, ovate-oblong, 6-8mm in length, solitary flower with peduncle (5-10mm) sometimes in pairs or three in number, densely hipsid. *Cucumis melo* var. *agrestis* has rounded (2.5-5cm diameter) ellipsoidal fruit that is consumed as vegetable in Pakistan whereas poisonous seeds remain unused and wasted. Memon *et al.,* 2018 demonstrated nutritional profile of fruit (3.8% ash content, 31.2% carbohydrate, 18.9% protein, 80.9% moisture content) of this non-conventional vegetable (Memon *et al.,* 2018).

Our experimental work showed that seeds are dark brown in color, seeds were 12 mm in length, 6 mm wide and 11-13 seeds in a gram SEM micrograph shows seeds are broad ovoid in shape, irregular epidermal cell arrangement, anticlinal wall irregularly thickened, wall ornamentation is thick and raised and ruminate surface sculpturing, seed's hilum is visible, terminal and raised with lateral compression, as shown in Figure . Seeds have high oil content i.e. 30% wt. /wt. and FFA value with 0.63 mg KOH/g and was found as promising feedstock (96%) for biodiesel production. Previous study by Ameen et al., 2018 showed the wild melon as source of bioenergy and fuel properties meet the international standards (ASTM)
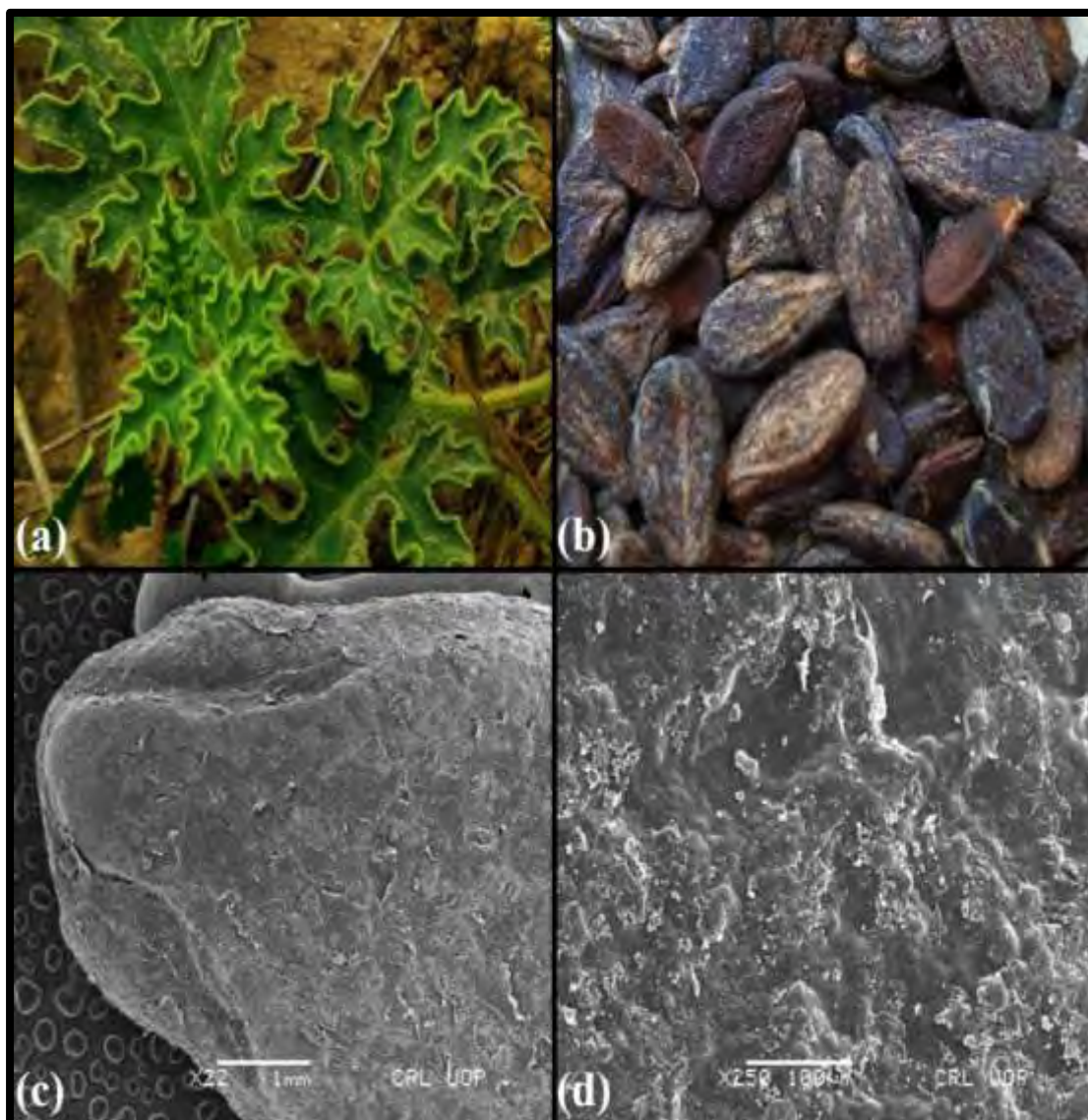
Figure 3.1.8 *Cucumis melo* var. *Agrestis* **(a)** Plant **(b)** Seeds **(c, d)** SEM Micrographs of seed and sculpturing

Table 3.1.1 Qualitative characters of non-edible oil seeds

Plant name	Family	Common name	Seed color	Inner color	Seed shape	Surface Sculpturing	Wall Ornamentation	Hilum			Compression
								Occurrence	Position	Level	
Bischofia javanica blume	Phyllanthaceae	Bishop Wood, Java cedar, Toog tree	Light Brown	Brown	Ovoid-oblong	Verrucate	Very thick and raised	Not visible	Sub-terminal	Depressed	Lateral
Eryobotrya japonica (Thunb.) Lindl.	Rosaceae	Japanese Medlar, Japanese Plum	Dark Brown	Yellow	Obovoid-Oblong	Reticulate	Buttressed	Visible	Terminal	Raised	Lateral
Praecitrullus fistulosus (Stocks) Pangalo	Cucurbitaceae	Indian squash, round melon, Apple gourd, squash melon,	Dark brown	Pale Yellow	Ovate-oblong	Wrinkled	Thick and Raised	Not visible	Terminal	Raised	Lateral

Luffa acutangula (L.) Roxb	Cucurbitaceae	Angled Loofah, Ridged Gourd, Chinese Okra	Black	Yellow	Ovate-Obovate	Verrucate	Very thick and raised	Visible	Terminal	Raised	Dorso-ventral
Diospyros lotus .L.	Ebenaceae	date-plum, Caucasian persimmon, or lilac persimmon	Dark brown	Grey	Semi-spheroid	Striate	Thin and raised	Visible	Terminal	Depressed	Lateral
Cucumis melo var. *cantalupensis*	Cucurbitaceae	Charentias Cantaloupe, Musk Melon,	Off white	yellow	Ovate-Oblong	Striate	Thickened	Visible	Terminal	Depressed	Lateral
Solanum surattense Burm. f.	Solanaceae	Yellow-fruit nightshade, Thai striped eggplant	Orange to Yellow	yellow	Discoid-obovate	Ruminate	Thick and Raised	Visible	Terminal	Depressed	Lateral
Cucumis melo var. *agrestis* Naudin	Cucurbitaceae	Wild melon	Dark brown	Off white	Ovoid	Ruminate	Thick and Raised	Visible	Terminal	Raised	Lateral

Table 3.1.2 Quantitative characters of non-edible oil seeds

Plant name	Seed length(mm)	Seed width(mm)	Length/Width ratio	No. of Seeds/ kilogram	Seed Oil Content (%)	FFA content(mg KOH/g)	Biodiesel Potential (%)
Bischofia javanica blume	3-4 (3.5)	2-3 (2.5)	1.4	205000-207000	29.7	1.95	95.8
Eryobotrya japonica (Thunb.) Lindl.	14-16 (15)	11-13(12)	1.25	2120-3000	24	1.56	96
Praecitrullus fistulosus (Stocks) Pangalo	9-11 (10)	5-6 (5.5)	1.81	4000-4500	40	2.01	91
Luffa acutangula (L.) Roxb	11-13 (12)	6-7 (6.5)	1.84	5000-6000	48	3.91	93
Diospyros lotus .L.	13-15 (14)	5-6 (5.5)	2.54	7000-9000	20.3	6.91	87
Cucumis melo var. *cantalupensis*	4-8 (6)	2.4-4 (3.2)	1.87	8000-10000	35	0.78	98
Solanum surattense Burm. f.	3-4 (3.5)	2-2.5 (2.25)	1.5	250000-260000	21	3.91	89
Cucumis melo var. *agrestis Naudin*	10-12 (11)	5-6 (5.5)	2	1000-11000	30	0.63	96

SECTION: II

Biodiesel Synthesis from *Bischofia javanica* Seed oil using Zirconium oxide Green Nano-catalyst

3.2. Biodiesel Synthesis from *Bischofia javanica* Seed oil using Zirconium oxide Green Nano-catalyst

3.2.1 Characterization of Zirconium Oxide Green Nano-catalyst (ZrO$_2$)

(a) XRD of ZrO$_2$

XRD was performed in order to find their size and crystalline structure of green nano-catalyst. Results depicted pure ZrO$_2$ NPs with good crystalline structure supporting the high pureness attained via green nanotechnology. Using the Debye Scherer, average particle size was calculated.

$$D = \frac{K \, x \, \lambda \, (nm)}{FWHM \cos \theta} \hspace{3cm} (4)$$

Where; D = Crystalline Size in nanometer

λ = Wavelength in nanometer;

FWHM = Full Width at Half Maximum

θ = Braggs angle θ.

ZrO$_2$ has intense peak for 2θ value of 30.29°, 35.10°, 50.32°, 60.07° correspond to (111), (200), (220) and (311) plane (Figure 3.2.1). Particle size was found to be 40nm and all sharp diffraction peaks indexed for a pure crystalline nature of nanoparticles (NPs) efficiently stabilized by *Bischofia javanica* leave extract. Our results are in close agreement with previous studies when peaks at 30.23°(111), 50.63°(220) and 60.09°(311). Our results are also accordant with erstwhile work of stabilization of zirconia based NPs (spherical in shape) from leaves of G. Speciosa (Muthulakshmi *et al*., 2022).

(b) SEM of ZrO$_2$

Scanning electron microscopic analysis was done for topographic examination of cross sections of nano-sized ZrO$_2$ particles. SEM micrographs present good crystallite surface and overlapping or agglomeration is reason for appearance of large sized particles. SEM also shows the uniform sized particles with spherical shape

(Anandan *et al.,* 2017). Figure 3.2.2 portray the SEM micrographs of ZrO_2 taken at different resolutions. Our results in close accordance with previous literature where spherical NPs were prepared (Alsaiari *et al*., 2022; Muthulakshmi *et al*., 2022).

(c) EDX of ZrO_2

Energy dispersive X-ray spectroscopy was performed for elemental identification and chemical composition of nano-sized catalyst. EDX spectrum revealed the presence of Zr and O as 66.7% and 33.2% respectively having total content closer to 100%. Our results depict the purity of ZrO2 nanoparticles (Figure 3.2.3).

(d) FT-IR of ZrO2

FT-IR can be used to investigate a wide variety of materials in bulk or thin films, liquids, solids, pastes, powders, fibres, and other forms. When coupled with appropriate standards, FT-IR analysis can provide quantitative (quantity) examination of materials in addition to qualitative (material identification) analysis. FT-IR can be used to measure the top 1µm layer or the bulk of samples with a diameter of up to 11mm. The biomolecules that could be responsible for responsible of capping and effective stability of the metal nanoparticles produced *by Bischofia javanica* leaf extract were investigated using FT-IR measurements. The FT-IR spectrum of naon-sized zirconium oxide nanoparticles is shown in figure 3.2.4. Signals from 3000 to 3650 cm^{-1} were detected in the samples, and they could be attributed to either hydroxyl groups or the stretching vibration of the -OH bond in the adsorbed water such as 1383.67 cm^{-1} peak represent –OH group. The water molecule bending mode may be identified by the bands seen for each sample at 1533.67 and 1031.63 cm^{-1}. A prominent peak at 596.94 cm^{-1} and neighboring strong signal of 655.10 cm^{-1} and 740.82 cm^{-1} signifies the Zr-O stretch and Zr-O-Zr vibration mode indicate its nanocrystalline nature. Our results resemble the research done by (Anandan *et al.,* 2017)

3.2.2 Characterization of *Bischofia javanica* biodiesel (BJBD)

(a) FT-IR of BJBD

To determine the chemical composition of BJBD, FT-IR (400-4000 cm^{-1} wavelength) was performed for function group identification within BJBD with appearance of various characteristic peaks of particular bond vibrations. Wavelengths

500-1500 cm^{-1} showed a wide range of peaks depicting ester formation. Specifically, peaks of 1159.97 cm^{-1} and 1238.16 cm^{-1} are within the range of 1320-1000 (cm^{-1}) corresponding to presence of C-O stretch of methoxycarbonyl group of biodiesel. Similarly, a clear and strong peak 1743.11 cm^{-1} appeared in biodiesel spectrum lie within wavelength range (1735-1750 cm^{-1}) that corresponds to C=O stretch showing the methyl ester synthesis. The major vibrational bond (R1-C (OCH3) =O) Moreover, two large peaks detected around 2853.52 cm^{-1} and 2922.95 cm^{-1} lie within the range of 3300-2500 cm^{-1} representing O-H stretch of carboxylic acids and 3000-2850 cm^{-1} C-H stretch of Alkanes (Figure 3.2.5).

(b) GC-MS of BJBD

Chemical constituents were identified via GC-MS leading to analytical characterization of FAME quantification in *Bischofia javanica* Blume biodiesel. GC-MS depicted ester profile in form a spectrum. These peak identification as well as confirmation of different esters was done by NIST 11 software and MS analysis. A total of six peaks representing FAMEs were observed as shown in figure 3.2.6. He was carrier, temperature adjusted at 300°C for 40 minute reaction time. The quantified esters in BJBD using GC/MS from peak 5 to 10 included Hexadecanoic acid, methyl ester ($C_{17}H_{34}O_2$), 9,12-Octadecanoic acid, methyl ester ($C_{19}H_{34}O_2$), Elaidic acid methyl ester ($C_{19}H_{36}O_2$), Stearic acid, methyl ester ($C_{19}H_{38}O_2$), Linolenic acid, methyl ester ($C_{19}H_{32}O_2$), Eicosenoic acid, methyl ester ($C_{21}H_{40}O_2$) with retention time 20.49, 22.58, 22.67, 22.94, 24.25, 24.88 respectively (Indra *et al.,* 2013; Wang *et al.,* 2013).

(c) NMR of BJBD

^{1}H NMR has been subsequently used to assess the percent yield of BJBD using ^{1}H NMR Spectroscopy, as shown in figure 3.2.7a. The use of ^{1}H NMR is comparatively easy and expedient when examining the reaction process. The methylene protons of newly produced esters are used to determine the product yield. Absence of 3.45 ppm signal (representing free CH_3OH) is clear endorsement of purity of biodiesel sample (Ibrahim *et al.,* 2022). Peak area ranging from 0.8496-0.904 ppm presents terminal -CH_3 protons. The characteristic peak appeared at 3.649 ppm depicting a singlet of –OCH_3 and α-CH_2 appeared at 2.315 ppm. Presence of –OCH_3 and α-CH_2 reflects the existence of FAMEs in sample fuel. β- CH_2 perceived at 1.294-1.993 ppm as a confirmation of H-atoms in 3-carbon of aliphatic chain. However, Olefinic protons (-

HC=CH-) are illustrated by 5.274-5.413 ppm. In order to confirm the conversion percentage in biodiesel sample, the position of carbonyl (C=O) group is determined via ^{13}CNMR. The distinctive chemical shifts in this spectrum include 174.19 ppm (-COO-), 129.85 ppm (-CH=CH-), 77.07 ppm (-C-O) and 29.32 ppm (-CH$_2$-)$_n$. Figure 3.2.7b illustrates the existence of characteristic peaks of 127.87 and 130.12 ppm endorse the occurrence of unsaturated esters. However, existence of terminal methyl carbon is attributed to the signal appearance at 34.14ppm and 24.85ppm (Muhammad *et al*., 2019; Raud *et al*., 2019).

3.2.3 Biodiesel Yield Optimization via Response Surface Methodology

The collective impact of reaction parameters has been illustrated as 3D graphs plotted via response surface methodology (Figure 3.2.8 a-f). Such plots aid in understanding collective interaction among various variables hence locate the optimized limits of each parameter for peak response as described under following subsections (Table 3.2.2). The polynomial equation is as follows:

Yield $=93.68+5.75*A+8.3358*B-2.605*C+12.98*D-3.51*AB\ 6.44*AC+6.3*AD-2.55*BC+1.51*BD-8.3*CD-10.20*A²-25.126*B²-18.33*C²-20.61*D²$ **(5)**

3.2.3.1 Interaction between methanol to oil molar ratio and catalyst loading

Two substantial reaction parameters that influence biodiesel production throughout the transesterification process. To transform oil/fat into biodiesel and drive the process forward, an excessive amount of methanol is necessary. When alcohol (3 mol) combines with oil (1 mol), according to stoichiometric calculations, the biodiesel and glycerol are produced (3 mol and 1 mol respectively). Collective impact of both A and B is depicted by 3D-plot (Figure 3.2.8a). The maximum yield was achieved at 6:1 (Met: Oil) with 2.5 wt. % catalyst loading and maximum yield (95.8%) was achieved (run 8). When molar ratio was increased to 9:1, a minor yield reduction up to 94.6% was noticed (run 28). This decline in conversion yield in attributed to glycerolysis (backward reaction) leading to glycerol solublization and recombination with methyl esters resulting monolglyceride reformation (Miyuranga *et al.,* 2022).

Catalytic dilution is also a significant factor that lowers the FAME yield by interference in the byproduct removal from reaction mixture. When molar ratio was decreased to 3:1 and by adjusting other variables, the yield was decreased to 64.5% (run

10). Similarly with increase in catalyst concentration up to 4% the decrease in biodiesel yield was noticed at 92.8% (run 27) and the reason for yield declination is the synthesis of unwanted byproducts. When the catalyst amount was decreased to 1%, the yield was decreased to 93.5% (run 15). ANOVA showed insignificant results with p-value greater than 0.05 (0.053523). However, the separate molar ratio and catalyst loading were found significant (<0.05).

3.2.3.2 Interaction between methanol to oil molar ratio and reaction temperature

The interaction of molar ratio and reaction temperature (AC) is mentioned as 3D plot (Figure 3.2.8b). The methyl ester yield was noticed at maximum i.e. 95.8% at 6:1 molar ratio and 70°C. However, a further elevation in reaction temperature (>70°C) such as at 80°C, a significant decline in FAME yield up to 63.79% (run 29). Reactants require a specific amount of kinetic energy for proper reaction with high productivity in short time. In our optimizations, the low temperature i.e. 60 °C resulted in yield decline to 91.7% (run 26) because of reduction in miscibility of methoxide in oil at low reaction temperature. ANOVA outcomes depict this significant interactive effect with p-value < 0.05 (0.001706). Hence, it is confirmed that the combined impact is necessary to be considered in optimizing the transesterification reaction (Orege *et al.,* 2022).

3.2.3.3 Interaction between oil to methanol molar ratio and reaction time

Molar ratio (Met: Oil) and reaction time (AD) both collectively influence the FAME yield as a critical optimization parameter. In our study, the interactive influence is depicted by (Figure 3.2.8c) at constant variables i.e. 70°C, 0.5 wt. % catalyst amount with 1:9 molar ratio, the sudden declination in yield (49.6%) was noticed after 1 h of reaction time (run 11) because in less time reaction fails to attain the equilibrium state. Similarly, the low molar ratio (1:3) and short reaction time (1 h) at constant 70°C temperature and 0.5 wt. % catalyst amount, gave considerably smaller yield (50.6 %) as happened in run 2. This fall in FAME yield is attributed to insufficient reaction time lead to incomplete trans-esterification. With optimum molar ratio (1:6) and 2h reaction time, the maximum yield 95.8% was achieved due to rise in transesterification reaction due to enhanced reaction between excess of methanol and triglycerides. When both parameters were increased such as molar ratio (1:9) along with reaction time (3 h) then the yield achieved was (88.7%). The reason could be that the reaction shifted in

backward direction due to formation of unwanted byproducts and as a result of dilution, the separation becomes difficult (run 20). The ANOVA results depicted a highly significant and a strong correlation between these two parameters with p- value < 0.05 (i.e. 0.002014).

3.2.3.4 Interaction between catalyst load and reaction temperature

Combined interactive influence between catalyst amount and reaction temperature (BC) is represented by 3D plot of Figure 3.2.8 d. The most high biodiesel yield (95.8%) appeared with 0.5 wt. % catalyst and 70 °C that is attributed to high kinetic energy of molecules leading to their effective collisions and eventually convert them to their respective methyl esters as a result of a steady increase in reaction rate. Moreover, as the catalyst amount is increased from 1 wt. % to 2.5 wt. %, it fastens the reaction rate by lowering the activation energy of reactant thus more triglycerides get converted into respective methyl esters and more biodiesel is produced. However, up to a certain limit, the upsurge in catalyst concentration e.g. 4 wt. % drops the ester yield due to unwelcome process of saponification. When both molar ratio and time were kept constant (1:6 and 2 h) and the catalyst loading and reaction temperature were increased up to 4 wt. % and 80 °C respectively, the sudden decrease in yield was noticed i.e. 51.5% in run 3. Similarly, the high temperature results in evaporation of methanol (B.P 64.7°C) as most of it remains in vaporized state therefore its reaction with oil becomes problematic (Ameen *et al.,* 2022; Ahmad and Zafar 2022; Munir *et al.,* 2021).

When both catalyst conc. and reaction temperature were decreased to 1 wt. % and 60°C respectively, just 44.8% yield was achieved (run 1). At this stage, low concentration of catalyst is insufficient to lower the activation energy barrier and rate of reaction is also slow due to unavailability of catalytic active sites required to accommodate large no. of substrate (reactant) molecules hence product yield is considerably low. Similarly at low temperature the kinetic energy of molecules is not enough to support their effective collisions resulting in low rate of reaction with noticeably low FAME yield. Our outcomes are as per former studies (Abbah *et al.,* 2016). ANOVA results show their non-significant mutual effect by having p-value (>0.05).

3.2.3.5 Interaction between catalyst loading and reaction time

Interactive effect of amount of catalyst and reaction time (BD) has been mention as 3D RSM graph (Figure 3.2.8e). The highest biodiesel yield was attained with 0.5 wt. % catalyst and 2h reaction time. When both catalyst amount and reaction time were decreased below the optimized level i.e. from 2.5 to 1 wt. % and from 120 min to 60 min respectively, a remarkable reduction in biodiesel yield (29.8%) was noticed even under same 1:6 molar ratio and 70 °C (run 25). The low amount of catalyst is not enough to enhance the rate of chemical reaction. Similarly, time period has also a pronounced impact on biodiesel yield. Less time does not permit the proper reaction between catalyst and oil as a result the reactants partially convert into products. Moreover, increase in catalyst concentration enhances the side reaction leading to soap formation thus lower the FAME yield. When the time limit exceeds the optimal level the reversible transesterification reduces the product concentration in the reaction mixture. Run 16 clearly demonstrated the combined influence of both catalyst conc. and time. With rise in both catalyst (4 wt. %) and time (3 h), an obvious drop in biodiesel yield (74.1%) happened ANOVA results depict the non-significant mutual influence of catalyst loading and reaction time (p-value > 0.05) i.e. 0.377504 (Table 3.2.3).

3.2.3.6 Interaction between reaction temperature and reaction time

The interactive effect of reaction temperature and reaction time (CD) has been mention as 3D RSM graph. The combined effect of increase or decrease in both parameters was systematically studied (while keeping both molar ratio and catalytic load constant at 1:6 and 2.5 wt. % respectively). It was noticed that under both extreme conditions, the biodiesel yield drops suddenly as depicted by Figure 3.2.8 f. When reaction temperature and reaction time were set at maximum i.e. 80 °C and 3 h reaction time, a reduction in FAME yield i.e. (54.5%) occurred. Because, the high temperature for long time resulted in vaporization of methanol prevent the chemical reaction of two liquids (oil and methanol) under given conditions (run 21). Nevertheless, when the reaction conditions (temp. and time) were set at lower extremes i.e. 60 °C for 1 h the lowest yield of all conducted experiments, was recorded i.e. 32.4.% (run 7). The minimum yield was due to poor mixing of catalyst, methanol and oil (as viscosity of oil is high at low temp.). Hence, the reactant molecules neither have enough energy nor sufficient reaction time to react properly and convert in to respective products. Our

findings are in accordance with (Takase *et al*., 2014) who achieved maximum yield in 2h with zirconia based nano-catalyst from non-edible seed oil. Our results are in contradiction with Stavarache *et al.,* (2005) who reported high biodiesel yield just after 10 minutes using ultrasonic strategy. Our ANOVA results depict the significant mutual influence of reaction temperature and reaction time (p-value < 0.05) i.e. 0.0002.

3.2.4 Fuel Properties of BJBD

Fuel properties were compared to international standards American Society of Testing Materials with method ASTM D-6751 to ensure biodiesel (B100) purity before its utilization in either pure or blended form (biodiesel-petrodiesel). Fuel properties are given in Table3.2.1.

The density has a massive concern associated with biodiesel and it was found to be 0.8623Kg/L that lie within the range (0.86-0.90) g/cm^3. Due to composition of FAMEs and biodiesel purity, density is higher as compared to regular petro-diesel.

The Kinematic Viscosity checked according to ASTM D-445 and results (5.32 @ 40 °C c. St.) were found within the range (1.9-6.0). Temperature effects the kinematic viscosity inversely as it goes on decreasing with an increase in the temperature (Munir *et al*., 2021). Kinematic viscosity is affected by degree of saturation ($-CH_2-$) and unsaturation (double and triple bonds) in carbon chain as it is high in former case while low in later, respectively. Moreover, due to its origin from organic compounds, biodiesel is environment friendly owe to low emission of CO from engine.

Both pour point (min. temp. at which liquid loses its flow property) and cloud point (min. temp. at which wax crystal formation occurs) were -11°C (Table3.2.1). Flash point (PMCC) of BJBD is 80 °C. The biodiesel combustion is highly affected by its flash point. Higher flash point is assurance of feasibility and safety of biodiesel in terms of storage, handling and usability in transportation.

Total Acid No. was matched with ASTM D-4294 standard and was found as 0.203 mg KOH/gm.

BJBD has remarkably low sulphur content (0.00047wt. %) compared with ASTM D-974. Less than 1ppm Sulphur in biodiesel makes it immensely beneficial over conventional petrodiesel that causes ecofriendly and pollution free fuel combustion.

Moreover, the reduced SO_2 emissions (during biodiesel combustion in vehicle engine) are attributed to this negligible Sulphur content making it ecologically sustainable.

The fuel properties were found compatible with physicochemical characteristics of already reported non-edible feedstock such as safflower (Thiyagarajan *et al*., 2020), jatropha (Singh *et al*., 2021), cottonseed (Sharma *et al.,* 2019) pongamia (Perumal & Ilangkumaran, 2018) and rubber seed oil (AVSL *et al*., 2021).
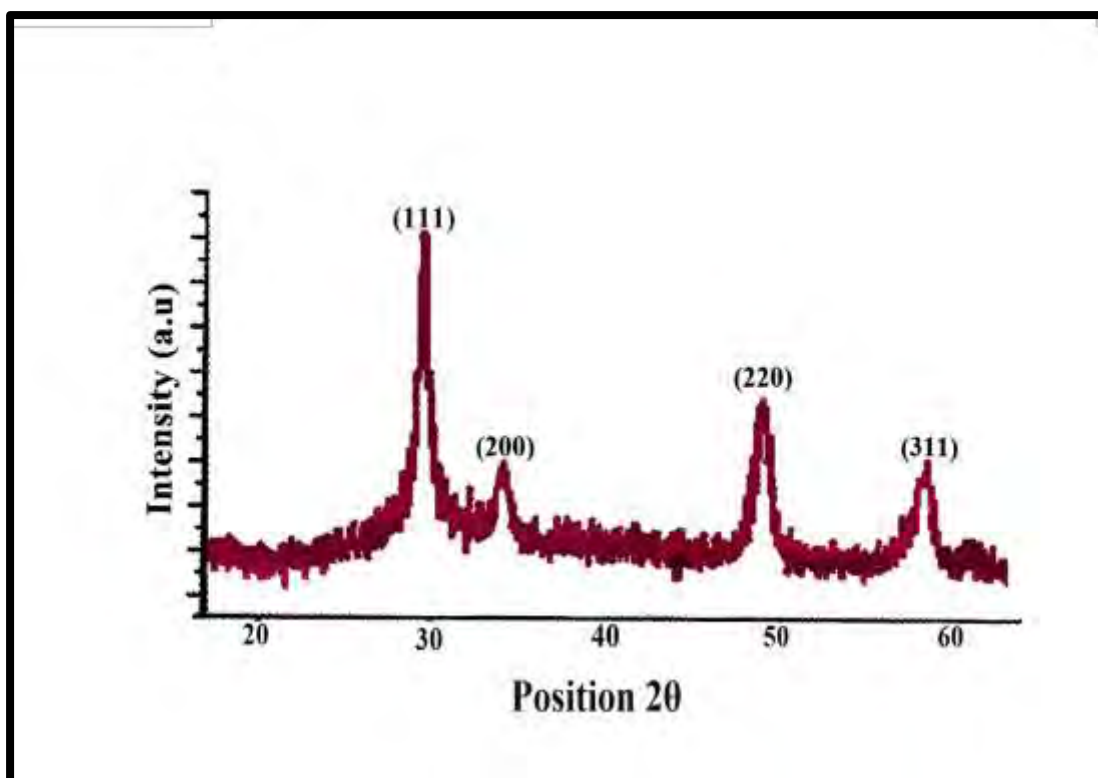
Figure 3.2.1 XRD of ZrO$_2$ green nano-catalyst
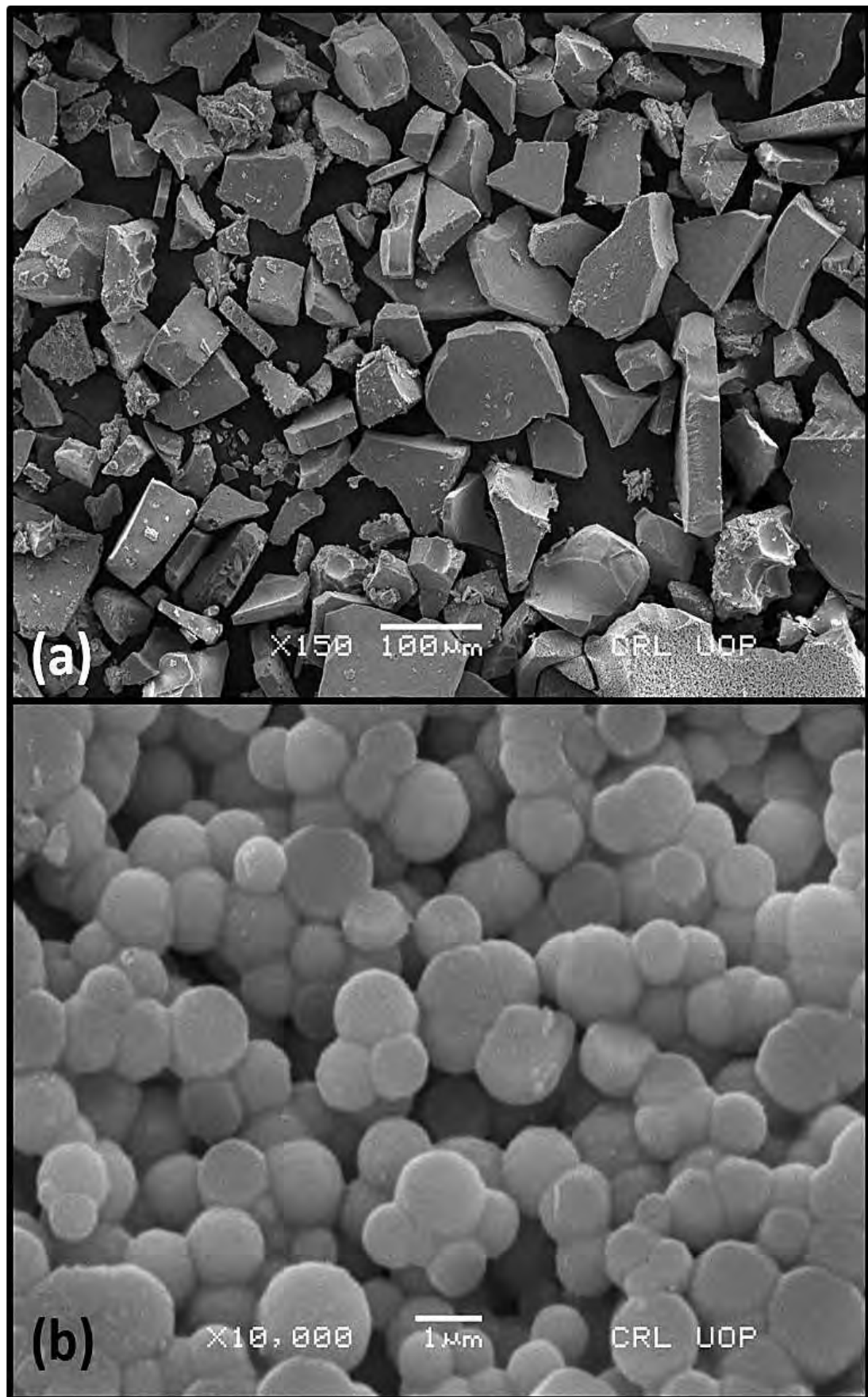
Figure 3.2.2 SEM of ZrO_2 green nano-catalyst
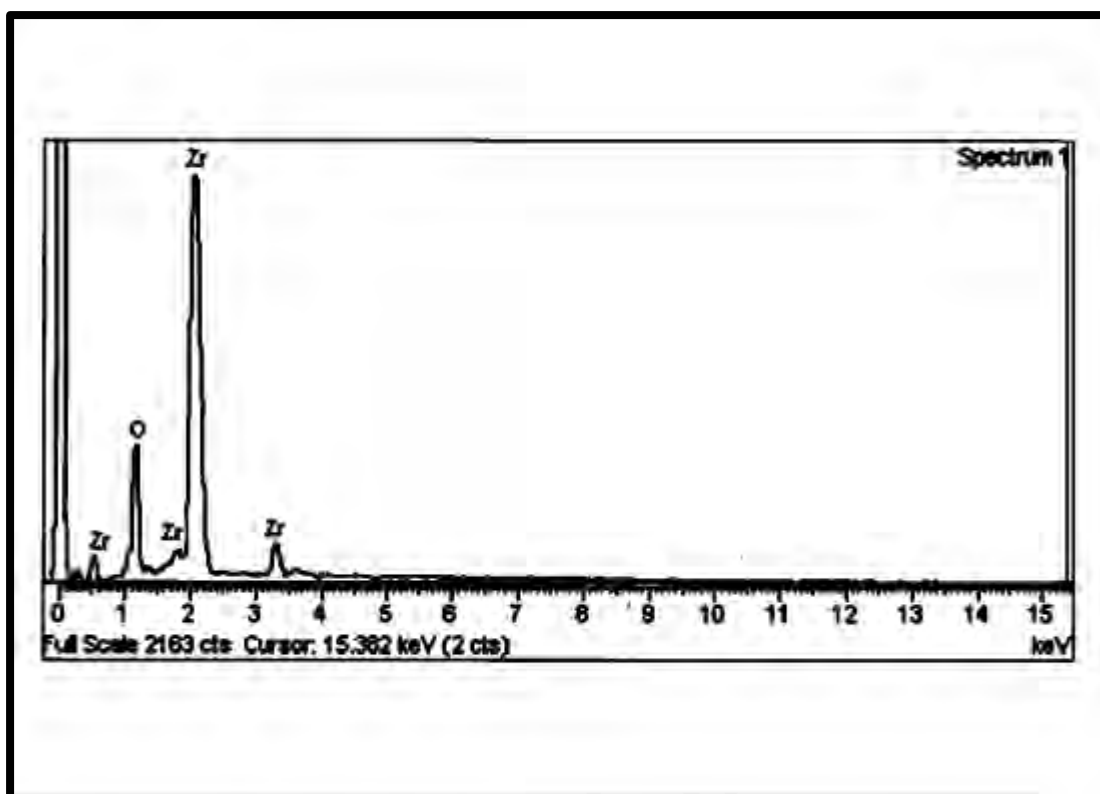
Figure 3.2.3 EDX of ZrO$_2$ green nano-catalyst
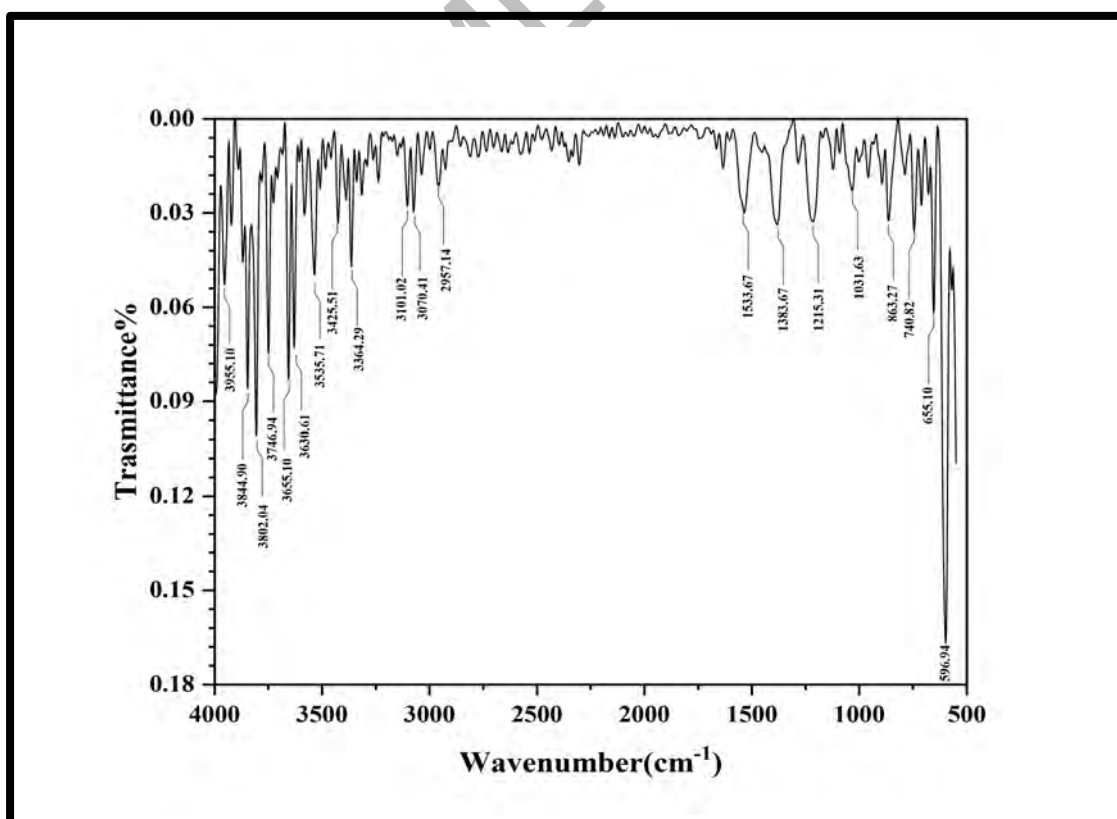
Figure 3.2.4 FT-IR of ZrO$_2$ green nano-catalyst
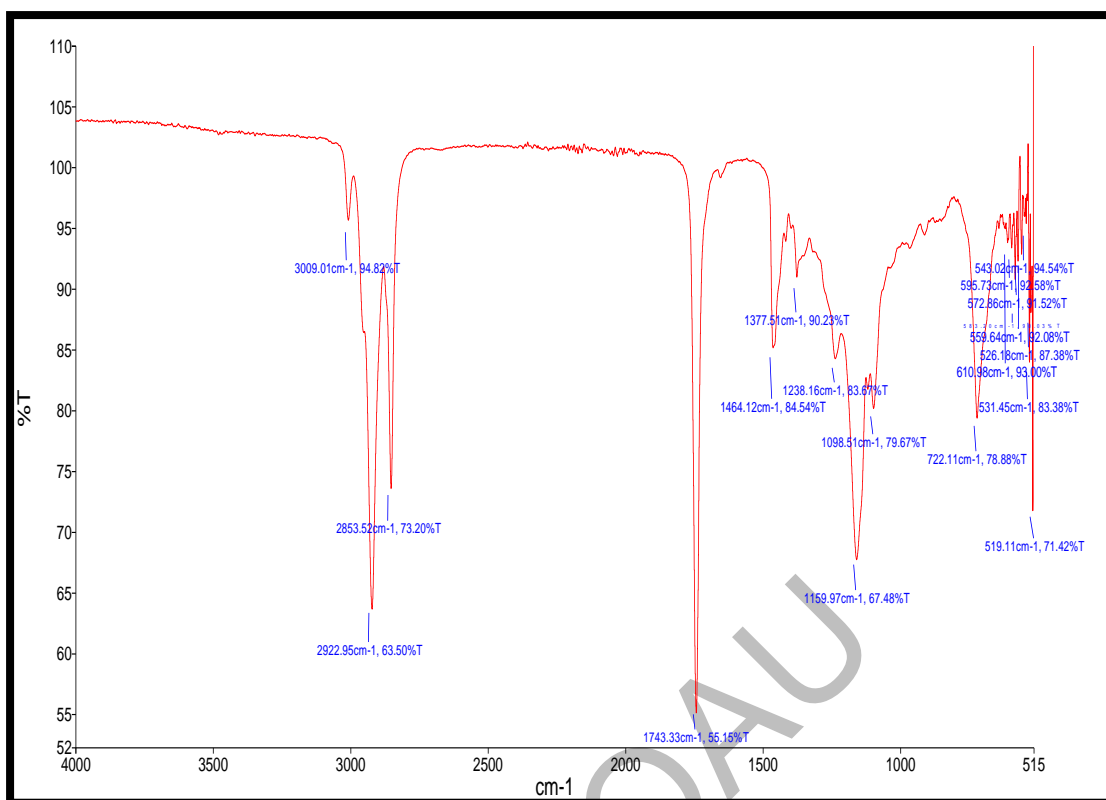
Figure 3.2.5 FT-IR spectrum of BJBD
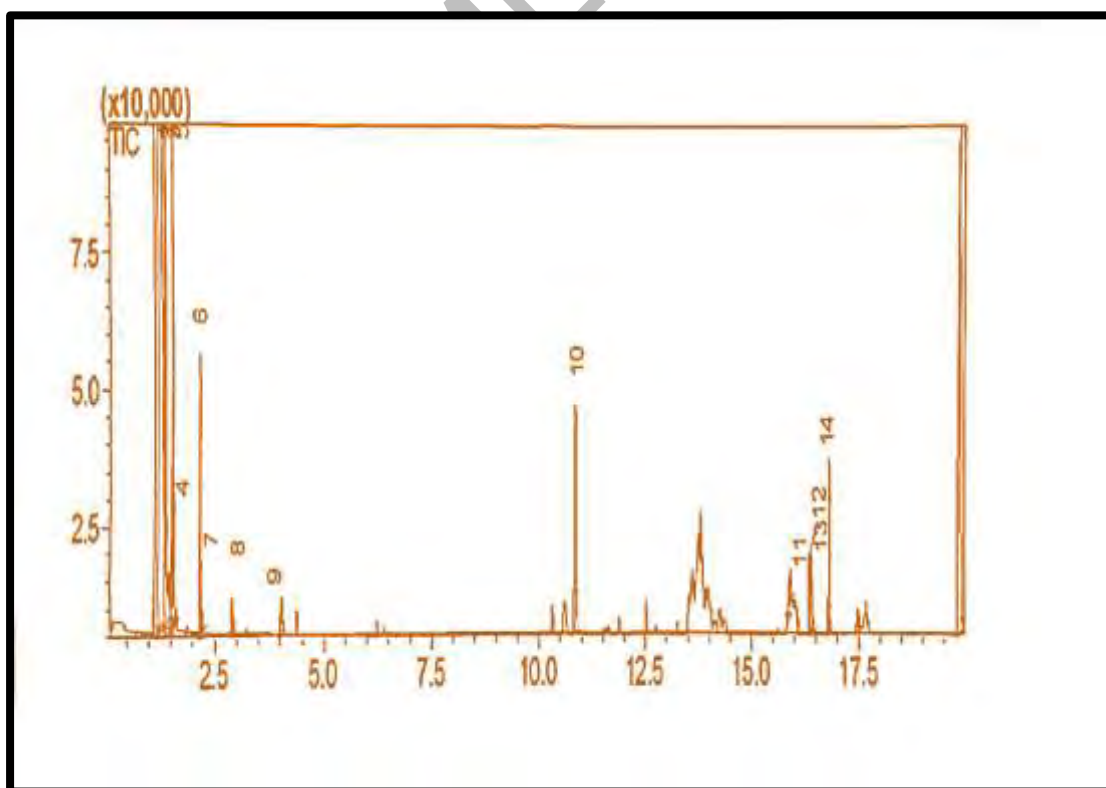
Figure 3.2.6 GC-MS spectrum of BJBD
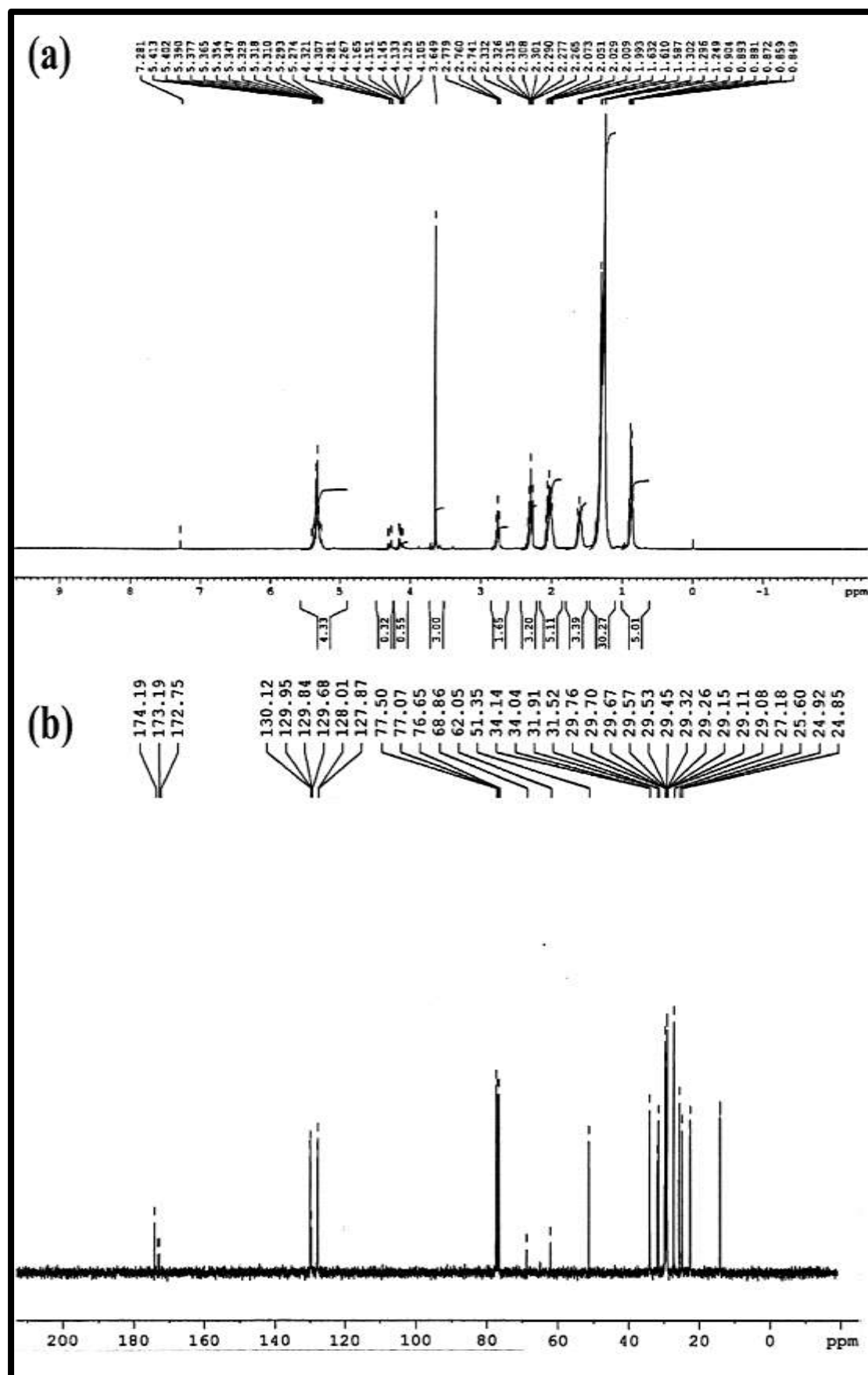
Figure 3.2.7 (a) ^{1}HNMR and (b) ^{13}CNMR spectrum of BJBD
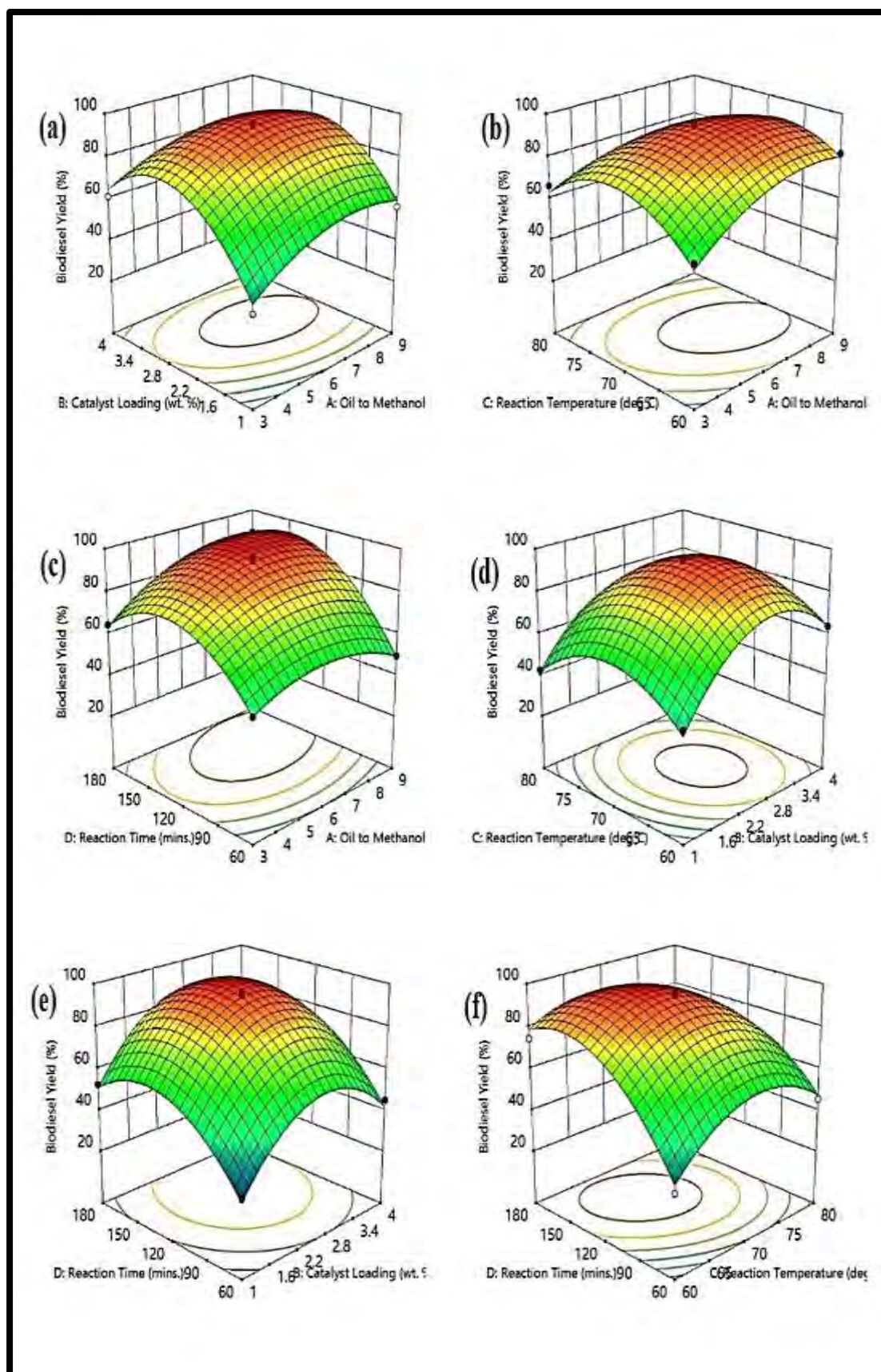
Figure 3.2.8 (a-f) The influence of reaction variables on BJBD
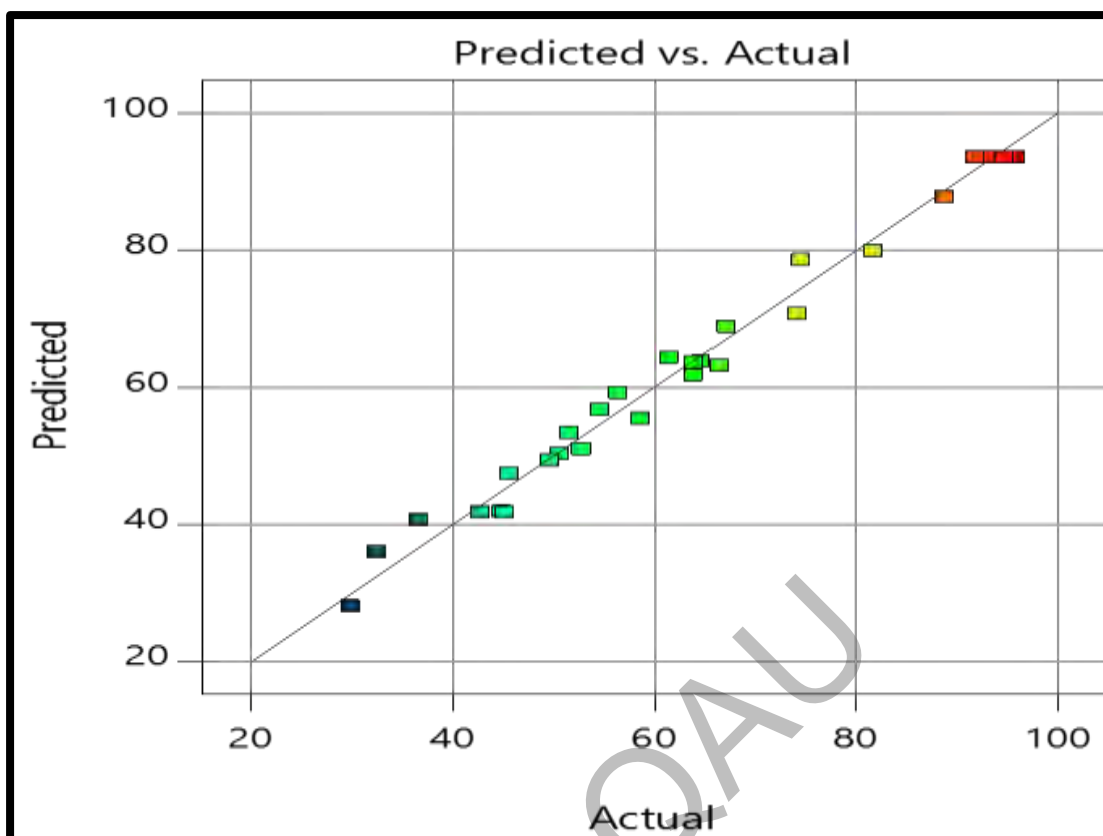
Figure 3.2.9 Predicted yield vs actual yield of BJBD

Table 3.2.1 Fuel properties of BJBD

TESTS	METHOD	BJ B-100
Color	Visual	2
Density @ 15 °C Kg/L	ASTM D-1298	0.8623
Kinematic Viscosity @ 40 °C c St	ASTM D-445	5.32
Pour point °C	ASTM D-97	-11
Flash point °C(PMCC)	ASTM D-93	80
Cloud point °C	ASTM D-2500	-11
Total Acid No. mg KOH/gm	ASTM D-4294	0.203
Sulphur % wt.	ASTM D-974	0.00047

Table 3.2.2 Experimental yield of BJBD

Run	Methanol to Oil Molar Ratio	Catalyst Loading (wt. %)	Reaction Temp. (°C)	Reaction Time (min)	BJBD Yield (%)
1	6	1	60	120	44.8
2	3	2.5	70	60	50.6
3	6	4	80	120	51.5
4	3	4	70	120	61.4
5	3	2.5	60	120	58.6
6	9	1	70	120	56.37
7	6	2.5	60	60	32.4
8	6	2.5	70	120	95.8
9	6	1	70	180	52.7
10	3	2.5	70	120	64.5
11	9	2.5	70	60	49.6
12	9	2.5	60	120	81.7
13	6	2.5	60	180	74.5
14	6	4	70	60	45.13
15	6	1	70	120	93.5
16	6	4	70	180	74.1
17	6	2.5	80	60	45.6
18	3	2.5	80	120	66.45
19	6	4	60	120	63.8
20	9	2.5	70	180	88.7
21	6	2.5	80	180	54.5
22	9	4	70	120	67.1
23	3	1	70	120	36.63
24	6	1	80	120	42.7
25	6	1	70	60	29.8
26	6	2.5	60	120	91.7
27	6	4	70	120	92.8
28	9	2.5	70	120	94.6
29	6	2.5	80	120	63.79

Table 3.2.3 Analysis of Variance (ANOVA) of BJBD

Source	Sum of	df	Mean	F-value	p-value	
Model	10668.1	14	762.0072517	68.71822	1.99E-10	significant
A-Oil to Methanol	397.6705	1	397.6705333	35.86214	3.32E-05	
B-Catalyst Loading	833.8334	1	833.8334083	75.19554	5.29E-07	
C-Reaction Temperature	81.4323	1	81.4323	7.343608	0.016925	
D-Reaction Time	2024.621	1	2024.621408	182.5814	2.01E-09	
AB	49.2804	1	49.2804	4.444132	0.053523	
AC	165.8944	1	165.8944	14.96044	0.001706	
AD	158.76	1	158.76	14.31706	0.002014	
BC	26.01	1	26.01	2.345596	0.147918	
BD	9.211225	1	9.211225	0.830673	0.377504	
CD	275.56	1	275.56	24.85015	0.0002	
A$\hat{A}^2$	674.9092	1	674.9091903	60.86367	1.83E-06	
B$\hat{A}^2$	4095.239	1	4095.239207	369.3108	1.85E-11	
C$\hat{A}^2$	2181.27	1	2181.270407	196.7081	1.23E-09	
D$\hat{A}^2$	2756.393	1	2756.392653	248.5729	2.63E-10	
Residual	155.2442	14	11.08886845			
Lack of Fit	145.1762	10	14.51761583	5.767825	0.052946	not significant
Pure Error	10.068	4	2.517			
Cor Total	10823.35	28				
Std. Dev.	3.329995		R$\hat{A}^2$	0.985657		
Mean	62.94379		Adjusted R$\hat{A}^2$	0.971313		
C.V. %	5.290427		Predicted R$\hat{A}^2$	0.921286		
			Adeq Precision	27.36979		

SECTION: III

Biodiesel Synthesis from *Eryobotrya japonica* Seed oil using Cobalt Oxide Green Nano-catalyst

3.3. Biodiesel Synthesis from *Eryobotrya japonica* Seed oil using Cobalt Oxide Green Nano-catalyst

3.3.1 Characterization of Cobalt Oxide Green Nano-catalyst

(a) XRD of CoO

Size, phase, and crystallinity of the produced powder are determined by the analytical technique known as X-ray diffraction pattern (XRD). It demonstrates from the acquired spectrum that the peaks in the XRD spectrum are well-defined and correspond to face-centered cubic (FCC) structures. The primary peaks that indicate the lattice scattering planes (111), (200), (220), and (222) for the CoO crystal (Figure 3.3.1), were observed at 37.45°, 43.67°, 64.12°, and 78.04°. According to calculations using the well-known scherrer equation as previously mentioned, the crystallite size was estimated to be just 9 nm. In this spectrum, the sharp and intense peak defines that the grown powder particles exhibit good crystallinity with small particles size. The spectrum shows only CoO peaks without any organic and additive impurities, which further confirms that the prepared powder of CoO is pure and nanosized material. In this case, the X-ray diffraction patterns show the appearance of specific peaks that matches well with cubic face centered shaped CoO nanostructures without any contaminations. The (111) facet of the material is being exposed preferentially while others are being subjected to typical features and a minor increase in the crystallinity of the material, as seen by the X-ray diffraction (Adekunle *et al* 2020). This supported and was in strong accord with published literature on cobalt oxide. (Abbasi *et al* 2021; Deori & Deka, 2013; Gul *et al* 2020)

(b) SEM of CoO

Scanning Electron Microscopy (SEM) was used to determine the size and surface morphology of synthesized green CoO nano-catalysts. The surface morphology of cobalt oxide is depicted in (Figure 3.3.2) at various magnifications. According to the SEM findings, cobalt oxide nanoparticles have a face-centered cubic structure, a smooth surface, and they aggregate to form clusters and the crystalline size of cobalt oxide (i.e. 9nm) nanoparticles revealed their nano-nature. SEM and XRD results of CoO are in agreement that green nanoparticles 9 nm. Figure 3.3.3 illustrates the cobalt oxide nanoparticle SEM micrograph. The morphology of cobalt oxide nanoparticles

was uniform as they had a face centered cubic shape. As a result of the polar and electrostatic pull of nanoparticles towards one another, a cluster of particles was observed in the SEM image. The findings of this study are consistent with earlier research (Abbasi *et al* 2021).

(c) EDX of CoO

As illustrated in Figure 3.3.3 an EDX examination of a cobalt oxide nano-catalyst reveals the presence of two distinct elements cobalt and oxygen. Discrete and specifically, typical points were selected on the surface of the catalyst while subjected to EDX analysis. The peaks that closely approximate the optical absorption of the fabricated nano-catalyst were identified by EDX analysis. The nano-elemental analysis of cobalt oxide green nano-catalyst showed that it contained 80.25 % cobalt and 19.75 % oxygen, making it the purest form that could be developed. Previous researches by Hafeez *et al* 2020 and Vijayanandan & Balakrishnan, 2018 are in agreement with this study, in which values were predicted theoretically via the compositional information from the EDX that demonstrate good compositional uniformity across the green nanoparticles (Hafeez *et al* 2020; Vijayanandan & Balakrishnan, 2018).

(d) FT-IR of CoO

In order to ascertain the chemical functional detail of CoONPs, investigations of the fingerprints and signals from FT-IR in the 400–4000 cm^{-1} range is performed. Figure 3.3.4 displays the FT-IR spectrum of cobalt oxide nanoparticles contained some characteristic peaks which indicated that cobalt oxide nanoparticles had been synthesized. As a characteristic band at 563.27 cm^{-1} corresponding to *v* (Co–O) while the corresponding vibration of the O-Co-O bond could be assigned to the peak at 618.37 cm^{-1}. Hence our acquired FT-IR spectrum depict that significant peaks, found at 1677.5 cm^{-1}, 1151.02 cm^{-1}, and 563.27 cm^{-1}, attributed to the carbonyl group, C-O stretch of organic compounds in leaf extract, and CoO, respectively. The peak values at 1343.88 cm^{-1} were attributed to O-H stretching of the moisture content and the hydroxyl group of phenolic substances is represented by a distinctive peak at 3480.61 cm^{-1}. A sharp peak at 3373.47 cm^{-1} corresponds to medium N-H stretch of 1°, 2° amides or amines. Our results are in close agreement with published FT-IR data of cobalt oxide nanoparticles (Iravani & Varma, 2020; Luisetto *et al.,* 2008; Moradpoor *et a.,l* 2019).

3.3.2 Characterization of *Eryobotrya japonica* Biodiesel (EJBD)

(a) FT-IR of EJBD

One of the frequently used methods for examining the structural constitution of biodiesel is FT-IR spectroscopic analysis. Once transesterification is complete, FT-IR aids in the confirmation of methyl ester production. Figure 3.3.5 displays a graphical analysis of a variety of functional group bands and stretches in the triglycerides of *Eryobotrya japonica* seed oil (EJSO) and *Eryobotrya japonica* Biodiesel (EJBD). The carbonyl group (C=O) represented by 1743.31 cm^{-1} depicts a band for methyl esters. Another characteristic peak corresponding to methyl group (CH3) could be seen at a wavelength of 1464.31 cm^{-1}. The appearance of these two bands is a proof that methyl ester formed at the end of transesterification. At 1377.57 cm^{-1} (CH3) and 1464.31 cm^{-1} (CH2) can be seen in IR spectrum. However, changing from the methyl ester (biodiesel) to other ester groups significant effect on the spectrum. Hence, it is possible to comprehend every aspect of the carbonyl group for biodiesel i.e. R1- C(OCH3) = O. The strong peaks at 2853.32 and 2922.82 cm^{-1} was observed that depict the CH and C-H with sp2 and sp3 hybridization. In the biodiesel spectrum, the carbonyl group is supposed to be the most susceptible to chemical and molecular changes. The 1159.67 cm^{-1} of O=C-O-C represent the presence of aliphatic esters and stretch of 1098.61 cm^{-1} is attributed to the C-H$_2$ wagging frequency that support the transesterification of oil triglycerides into methyl esters. Reported results of previous studies are in consistent with our most recent findings (Ameen *et al.,* 2018, Chaudhry *et al.,* 2022; Rezania *et al* 2022).

(b) GC-MS of EJBD

The EJBD biodiesel FAMEs have been quantified for their chemical composition, structure, and various fragmentations using the widely used and highly acceptable analytical technique known as GC-MS. The EJBD has seven prominent peaks (Figure 3.3.6). Using Library Match Software (NO. NIST02), the recognized peaks (3-9) include Hexadecanoic acid methyl ester (C$_{17}$H$_{34}$O$_2$), 2, 6 Dihexadecanoate (C$_{38}$H$_{68}$O$_8$), 9, 12 Octadecadienoic acid methyl ester (C$_{19}$H$_{34}$O$_2$), 9, octadecadienoic acid methyl ester (C$_{19}$H$_{34}$O$_2$), octadecanoate (C$_{18}$H$_{36}$O$_2$), Methyl 9-octadecenoate (C$_{19}$H$_{36}$O$_2$), Octadec-9-enoic acid (C$_{18}$H$_{34}$O$_2$) with retention time (min) 25.94, 26.88,

28.82, 28.95, 29.0, 29.29, 29.55. Our GC-MS analysis is in line with the work done by Ala'a and coworkers (Ala'a *et al*., 2021).

(d) NMR of EJBD

Figure 3.3.7a displays the ^{1}HNMR spectrum of EJBD corresponds to three unsaturated FAMEs such as two monounsaturated and another diunsaturated with conjugated and non-conjugated double bonds, 5.301 ppm corresponds to unsaturated moieties i.e. –**CH**=**CH**- and –**CH**=CH-CH=**CH**- from double bonds (non-conjugated and isolated) and two outer hydrogens respectively. However, two inter hydrogens produced a signal at 7.281ppm corresponding to the –CH=**CH**-**CH**=CH- in biodiesel sample. Distinct signals 2.01ppm, 2.276ppm and 2.748ppm correspond to –C**H**2- as adjacent to double bond, carbonyl group and as methylene between two double bonds (noon-conjugated) respectively while the aliphatic -CH2- signals are seen at 1.616 and 1.299 ppm. The chemical shifts of these compounds are not affected by the ester group or double bonds. At the end of the chain, the aliphatic -CH3 caused the appearance of peak at 0.854 ppm whereas the signal of methyl ester -CH3 is at 3.662 ppm. Figure 3.3.7b displays the 13CNMR spectrum of EJBD. The carbonyl carbon signal (-COO-) is detected at 174.33 ppm. The signals for the non-conjugated (-CH=CH-CH2-CH=CH-) and unsaturated (—CH=CH-) outer and inner carbons are at 129.71 ppm and 127.88 ppm, respectively. The signal for the methyl ester carbon (-O-CH3) is at 51.41 ppm. The signal for the terminal chain methyl (-CH3) carbon is at 24.93 ppm, while the signals for the aliphatic methylene carbons (-CH2-s) ranged from 34.07 to 27.18 ppm. By applying the formula as stated earlier (Killner *et al* 2015). The overall conversion in EJSO for EJBD was 93%, which is objectively close to the actually achieved yield.

3.3.3 Biodiesel Yield Optimization via Response Surface Methodology

To illustrate the combined impact of reaction parameters, 3D graphs have been created using the response surface methodology (Figure 3.3.8 a-f). The optimum limits for each parameter for peak response are established using such graphs, which take into account the overall interaction between different factors that are listed in the following subsections Table 3.3.2. Using four distinct transesterification variables with varying values, like the Met: Oil (A) 3:1–11:1, catalyst load (B) 0.1-2 wt.% (B), reaction time (C) 1–5 h and reaction temperature (D) 50–70 °C, the Central Composite Design (CCD)

for our current study was created by DOE (Design of Experiment). The comparison of the predicted and actual transesterification yield is depicted in Figure 3.3.9. The straight line has remarkably close distribution of actual and predicted values, indicating strong connection. The response surface quadric model statistical analyses of variance (ANOVA) is shown in Table 3.3.3. The quadric model has a low p-value (0.0009), indicating significance of model. In comparison to pure error, the experimental model lack of fit F-value (0.8349) was not statistically significant. A good lack of fit value for the quadric model is one that is not statistically significant and has an 83.49% chance of noise-cause. Based on the findings in Table 3.3.3, the predicted R^2 value found to be 0.594 and adjusted R^2 0.6290 with a variance of <0.2. The model adequate precision was found as to be >4 i.e. (5.8705). The efficiency of the experimental model to estimate biodiesel yield to a higher value of precision was demonstrated. In the quadric model, the following polynomial equation is employed (Alsaiari *et al.,* 2022).

Yield $=+79.46+8.32*A-7.43*B+2.14*C+1.31*D+3.92*AB+0.7179*AC+5.31*AD-5.33*BC-4.79*BD+4.20*CD-12.12*A^2+4.20*B^2-9.13*C^2-7.23*D^2$ **(6)**

3.3.3.1 Interaction between methanol to oil molar ratio and catalyst loading

The molar ratio and catalyst loading (AB) are significant reaction parameters that influence the biodiesel synthesis process i.e. transesterification. The course of turning oil or fat into biodiesel is sped up by using an excessive amount of methanol. A 3D-plot shows the combined impact of the catalyst loading and molar ratio (Figure 3.3.8a). The maximum yield (96%) was attained at 7:1 (Met: Oil) with 0.1 wt. % catalyst loading (run 3). The slight rise in catalyst concentration to 1.05% while keeping other parameters constant the biodiesel yield decreases (85%). The methyl ester yield was decreased to 72% with decrease in molar ratio (3:1) with same amount of catalyst (run 16). Even with an increase in catalyst load to 1.05 with all same conditions as in run 16, the biodiesel yield reduces further to 64% (run 13). This continuous decline in yield from 75% to 64% is ascribed to low molar ratio, as it is a fundamental reaction parameter that promotes biodiesel yield. Hence, this is testified that low molar ratio does not favors the methyl ester FAME yield. When both molar ratio and catalyst load increased to 11:1 and 1.05% respectively, the biodiesel yield was 77% (run 8). Glycerolysis, which causes glycerol to solubilize and recombine with methyl esters to create monolglycerides, is responsible for this decline in conversion yield. With a p-

value less than 0.05, the combined interaction between the molar ratio and catalyst loading (0.0396) was significant.

3.3.3.2 Interaction between oil to methanol molar ratio and reaction time

As a fundamental optimization parameter, the molar ratio (Met: oil) and the reaction time (AC) both jointly affect the FAME production. Figure 3.3.8b illustrates the interactive influence. The highest yield (96%) was achieved at 7:1 (Met: Oil) and 3 h reaction time and maximum yield was achieved (run 3). It was noticed the yield was significantly lower (68%) due to the high molar ratio (11:1), short reaction time (1 h), constant 60°C temperature, and 0.1 wt. % catalyst quantity. The inadequate reaction time that led to the incomplete transesterification process leading to decrease in FAME production. Low molar ratio (1:3) and more reaction time (5h) as compared to optimized conditions, a low biodiesel yield (65%) was noticed. The reaction may have moved backward and made the separation more difficult as a result of the production of unfavourable byproducts (run 30). The ANOVA findings showed a highly significant and robust association (p-value < 0.05) between these two factors (i.e. 0.0157). Our results are in accord with Ahmad et al., 2019 and Munir *et al.,* 2019 where insufficient reaction time affected conversion rate (Ahmad et al., 2019; Munir *et al.,* 2019) .

3.3.3.3 Interaction between methanol to oil molar ratio and reaction temperature

The collective influence of molar ratio (Met: Oil) and reaction temperature (AD) is mentioned as RSM 3D plot (Figure 3.3.8c). With optimized 7:1 (Met: Oil) and 60°C reaction temperature, the highest yield (96%) was obtained (run 3). A decrease in reaction temperature to 50°C while keeping other parameters constant, resulted in sudden declination in methyl ester yield i.e. 80% (run 11) and when molar ratio was also decreased to 3:1, a remarkable yield reduction was noticed i.e. 68% (run 27). Low molar ratio and low temperature hindered the rate of reaction. However, higher temperatures up to 60°C, accelerated the mass transfer between the immiscible phases i.e. catalyst, oil, and methanol, giving the reacting molecules more kinetic energy and boosting productivity. But further increase in reaction temperature up to 70°C resulted in evaporation of methanol, although molar ratio is increased to 11:1 yet the yield is low i.e.85% (run 23). Our ANOVA results show that this interacting effect is significant with a p-value of <0.05. (0.0434). Therefore, it is clear that maximization of

transesterification product i.e. biodiesel requires consideration of the combined impact of molar ratio and reaction temperature (Ahmad and Zafar 2022).

3.3.3.4 Interaction between catalyst loading and reaction time

Interactive effect of amount of catalyst and reaction time (BC) has been mention as 3D RSM graph (Figure 3.3.8d). The highest biodiesel yield was attained with 0.1 wt. % catalyst and 3 h reaction time (run 3). Under the constant conditions of 7:1 molar ratio, 3 hs of reaction time, and 60 °C, a considerable reduction in biodiesel output (65 %) was seen when catalyst amount was increased above the optimal level, i.e. from 1.05 to 2 wt. % (run 7). An increase in catalyst concentration 1.05 wt. % furnished 70% yield in 1 h (run 24) but further increase in catalyst amount up to 2 wt. % reduced the yield (68%) under same reaction conditions (run 14). This sudden declination is attributed to soap formation making the product separation process difficult (Dawood *et al.,* 2021). Another reason is short reaction time being insufficient for the completion of transesterification. However, long duration provided to reaction mixture also results in low FAME yield, for instance, an increase in the catalyst amount to 1.05% and reaction time to 5 h while keeping other parameters constant, a remarkable reduction in biodiesel yield (65%) was noticed (run 26). ANOVA results depict the significant mutual influence of catalyst loading and reaction time (p-value < 0.05) i.e. 0.0264 (Table 3.3.3)

3.3.3.5 Interaction between catalyst loading and reaction temperature

In a 3D plot, the overall interactive relationship between the amount of catalyst and the reaction temperature (BD) has been illustrated (Figure 3.3.8e). The maximum biodiesel yield (96%) was achieved with 0.1 wt. % catalyst and 60 °C. By keeping all three optimization parameters constant, a high catalyst amount (2 wt. %) resulted in yield declination i.e. 87 % (run 21). However, when temperature was increased to 70°C by keeping other factors constant, the biodiesel yield was 88% (run 29). When both catalyst conc. and reaction temperature were increased from 0.1 wt. % to 1.05 % and reaction temperature from 60 to 70°C respectively, just 69 % yield was achieved (run 12). The reason is saponification and methanol evaporation that resulted in low product yield. ANOVA results show their significant mutual effect by having p-value (<0.05) i.e. 0.0328 (Arshad *et al.,* 2023).

3.3.3.6 Interaction between reaction time and reaction temperature

A thorough investigation of the combined effects of a change in either of the aspects was conducted (while keeping both molar ratio and catalytic load constant at 7:1 and 0.1 wt. % respectively). The relationship between reaction temperature and reaction time (CD) has been mentioned as a 3D RSM graph (Figure 3.3.8f). The maximum biodiesel yield (96%) was achieved in 3 h and 60 °C. When the reaction parameters (reaction time and reaction temperature) were set at lower extremities, i.e. 1 h and 50 °C, a considerably low yield (60%) was recorded (run 19). Low yield was caused by improper mixing of three essential components i.e. catalyst, methanol, and oil (as viscosity of oil is high at low temp.). Due to low kinetic energy and a quick reaction time, the reactant molecules are unable to react correctly and transform into their desired products. However with an increase in temperature up to 70°C, a conversion yield of 75% was obtained (run 28). This yield is comparatively higher than results of run 19 (with the same reaction conditions except temperature) because the reactant molecules have enough kinetic energy to collide and convert in to products however, short time duration (1 h) and high temperature (70°C) are the reasons for low conversion yield due to insufficient time period for reaction completion and methanol vaporization correspondingly. Increase in reaction time to 5 h while keeping other parameters constant (7:1 molar ratio, 0.1% catalyst concentration and 60°C reaction temperature), yield is comparatively low (90%) due to reversible reaction of glycerolysis (run 17). However, when temperature is decreased to 50°C with 5 h reaction time, a decline in conversion percentage (73%) was observed (run 15). Our ANOVA show our results are significant with p-value (0.0178).

3.3.4 Fuel Properties of EJBD

For physicochemical analysis of biodiesel, following characteristics of the EJBD were measured: color, flash point, pour point, cloud point, sulphur content, density, kinematic viscosity, cetane number, and acid value. These quality metrics are comparable to the ASTM standard (American Society of Testing Materials). Before being utilized in its pure form or blended with petroleum-based diesel fuel, biodiesel (B100) must meet this criterion, which ensures its purity. As shown in Table 3.3.1 the density of EJBD was examined and contrasted with ASTM D-1298. According to data in the table, EJBD has a density of 0.827 kg/liter. Biodiesel has a density that ranges

from 0.86 to 0.90 g/cm3. Because it depends on the fatty acid methyl esters in the fuel and its purity, biodiesel has a higher density than ordinary diesel fuel made from petroleum. According to ASTM D-445, the kinematic viscosity of EJBD was evaluated. as 4.87 at 40 °C. The results under investigation fall between 1.9 and 6.0 levels. Our results are in concurrence with previous research on the kinematic viscosity of various fatty acid methyl esters (Mohan & Raj, 2022; Zamberi *et al* 2022).

This feature of biodiesel is inversely affected by temperature. The Kinematic viscosity of EJBD reduces with rising temperature and vice versa. The saturation and unsaturation of the carbon atoms in the fuel chain also affect its kinematic viscosity. With more saturated carbon atoms, kinematic viscosity is higher (-CH2-). In contrast, kinematic viscosity would be low if the carbon chain contains many double and triple bonds. Because biodiesel comes from organic components, it has a significantly lower CO emission, making it environmentally benign. As measured by ASTM D-93, the EJBD B100 has a Flash Point of 97 °C. The biodiesel flash point is a characteristic that affects how fuel burns. Higher flash point makes biodiesel advantageous in terms of safety during handling, storage, and transportation because this fuel can be stored at ambient temperature without risk. Low temperature flow properties, which are expressed in terms of cloud point and pour point temperatures, are a significant issue with biodiesel. In comparison to ASTM D-97 and ASTM D-2500, the pour point (PP) and cloud point (CP) of EJBD are -10°C and -14°C, are relatively close to the ASTM D-6571 range at -15 to 16 and -3 to 12 ° C, respectively, The different types of feedstock used to make biodiesel account for the variance in pour point and cloud point (Danlami *et al*2022).

The total acid no. (mg KOH/gm) was measured according to ASTM D-974 and was found to be 0.183. Biodiesel prepared from *Eryobotrya japonica* has very low Sulphur content which is checked according to ASTM standard D-4294. BJ-B$_{100}$ has 0.0067 wt. % sulphur content. The trace amount of Sulphur in EJOB is the actual reason for reduction in emissions of SO2; hence, negligible amount of Sulphur in *Eryobotrya japonica* biodiesel makes it environmentally friendly (Akhtar *et al.,* 2017).
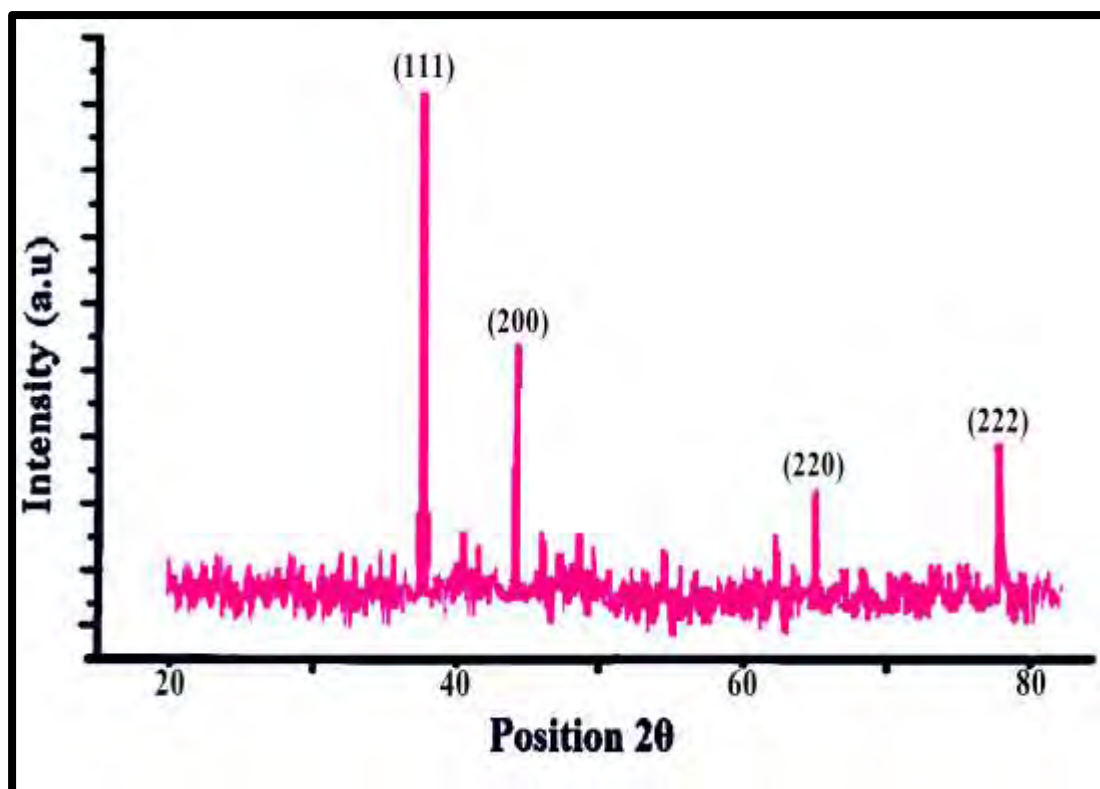
Figure 3.3.1: XRD of CoO green nano-catalyst
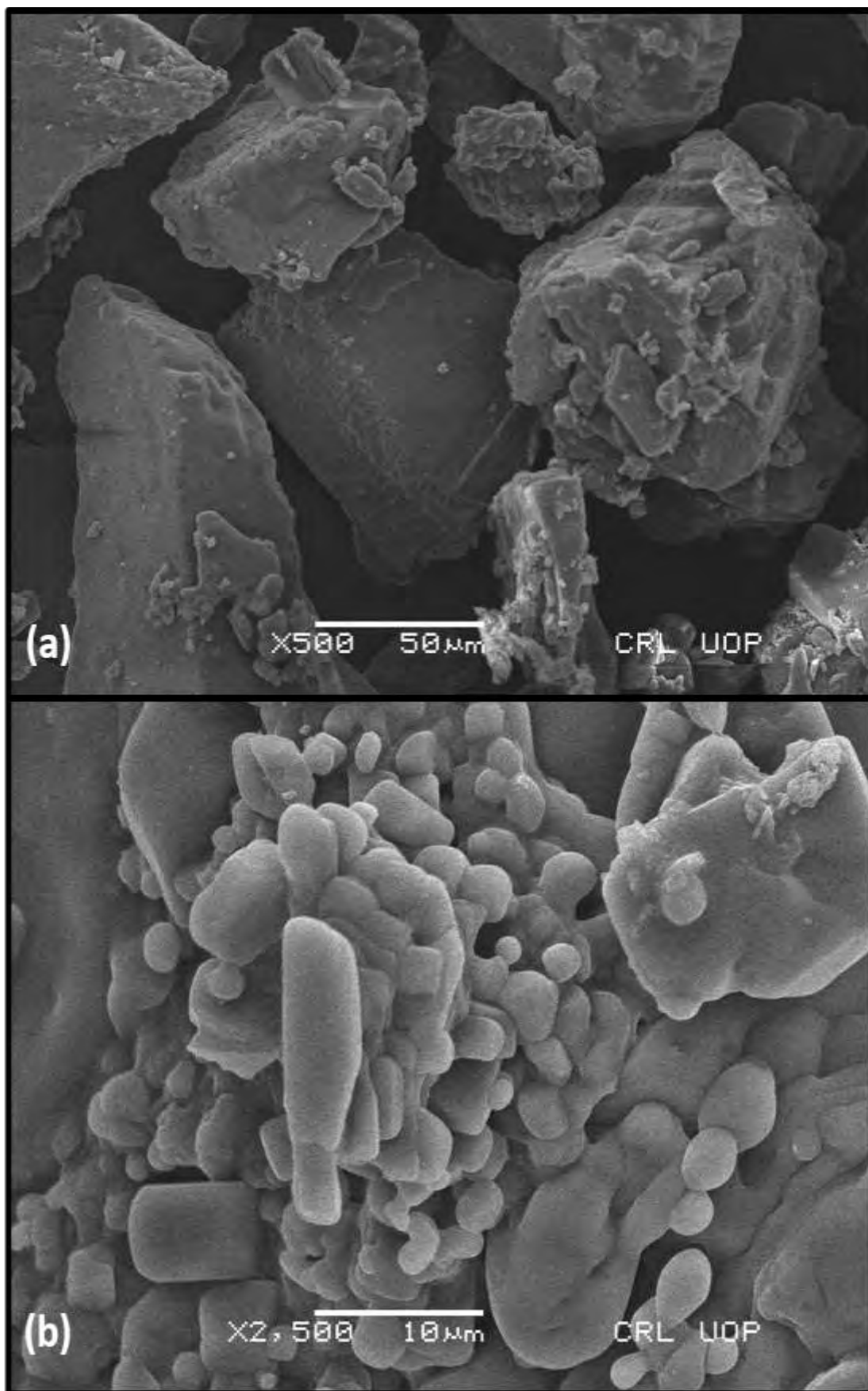
Figure 3.3.2: SEM of CoO green nano-catalyst
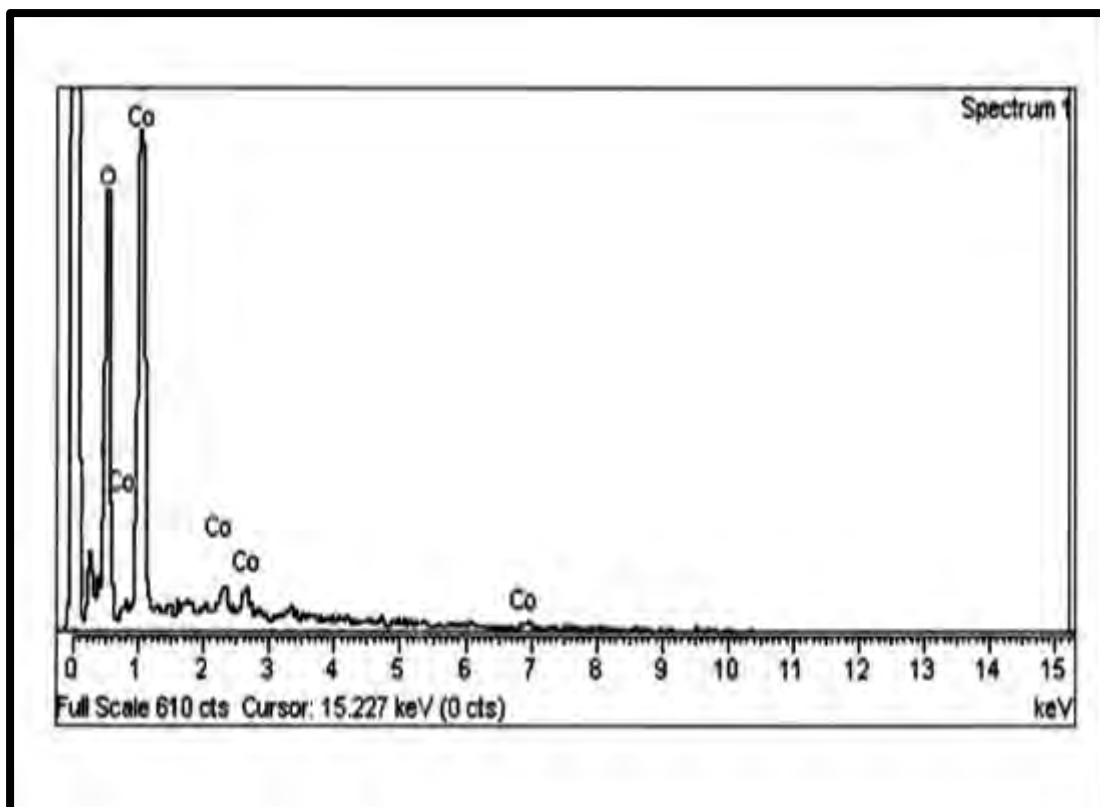
Figure 3.3.3: EDX of CoO green nano-catalyst
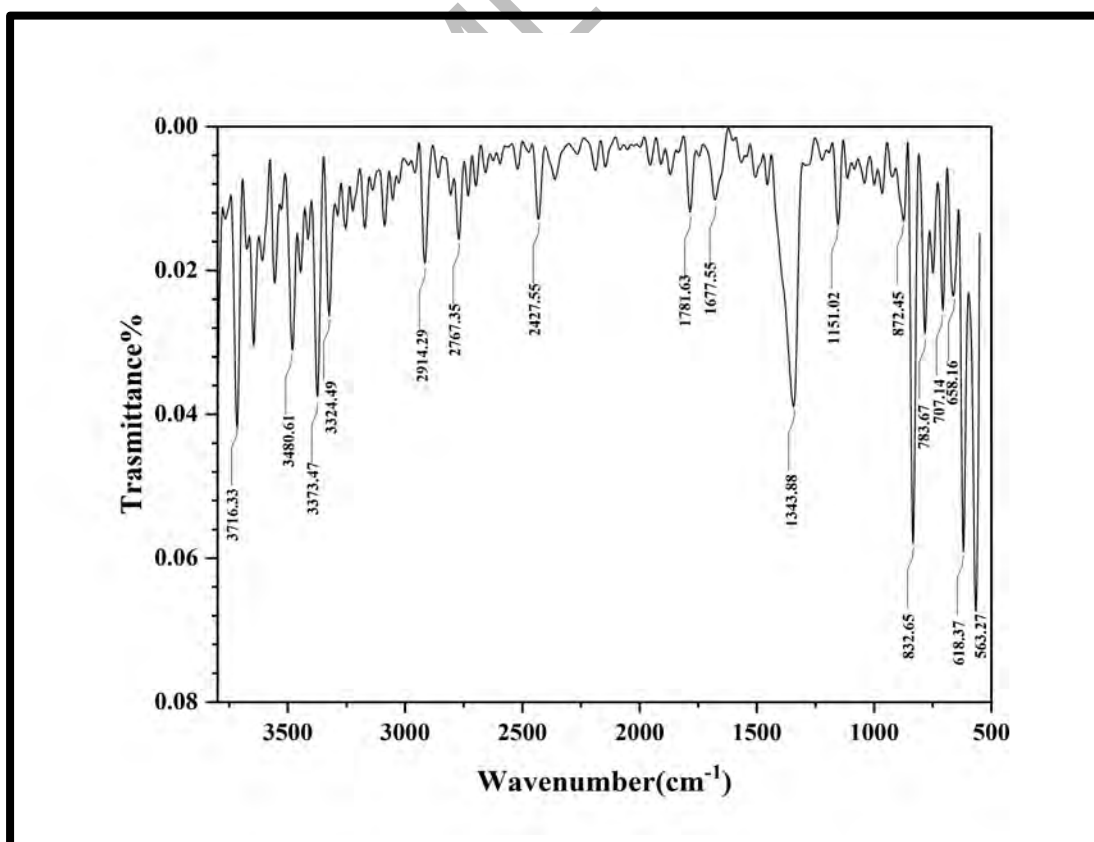
Figure 3.3.4: FT-IR of CoO green nano-catalyst
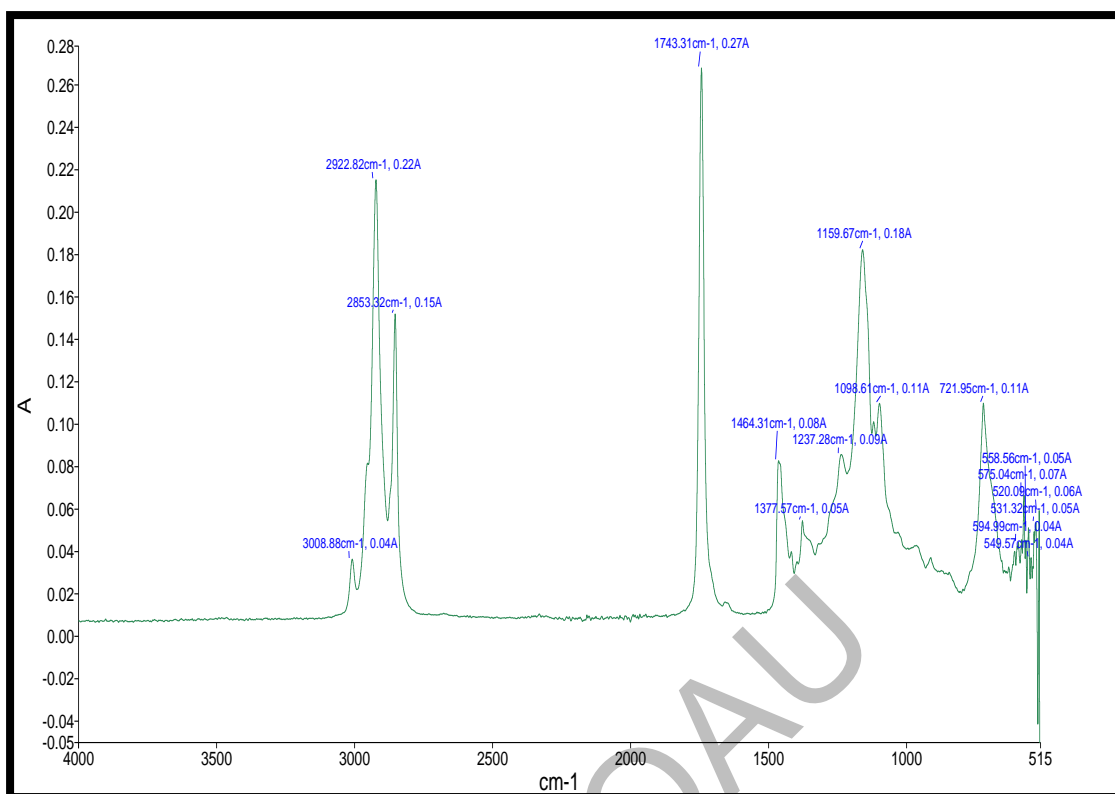
Figure 3.3.5: FT-IR spectrum of EJBD
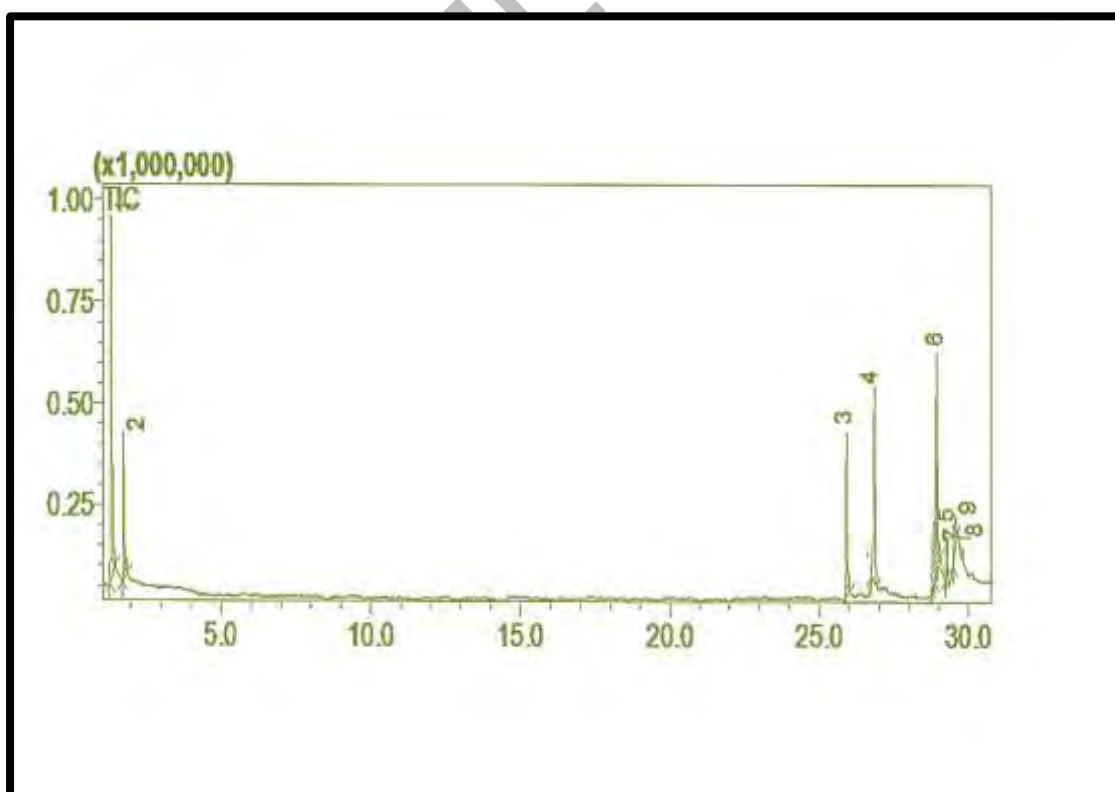
Figure 3.3.6: GC-MS spectrum of EJBD
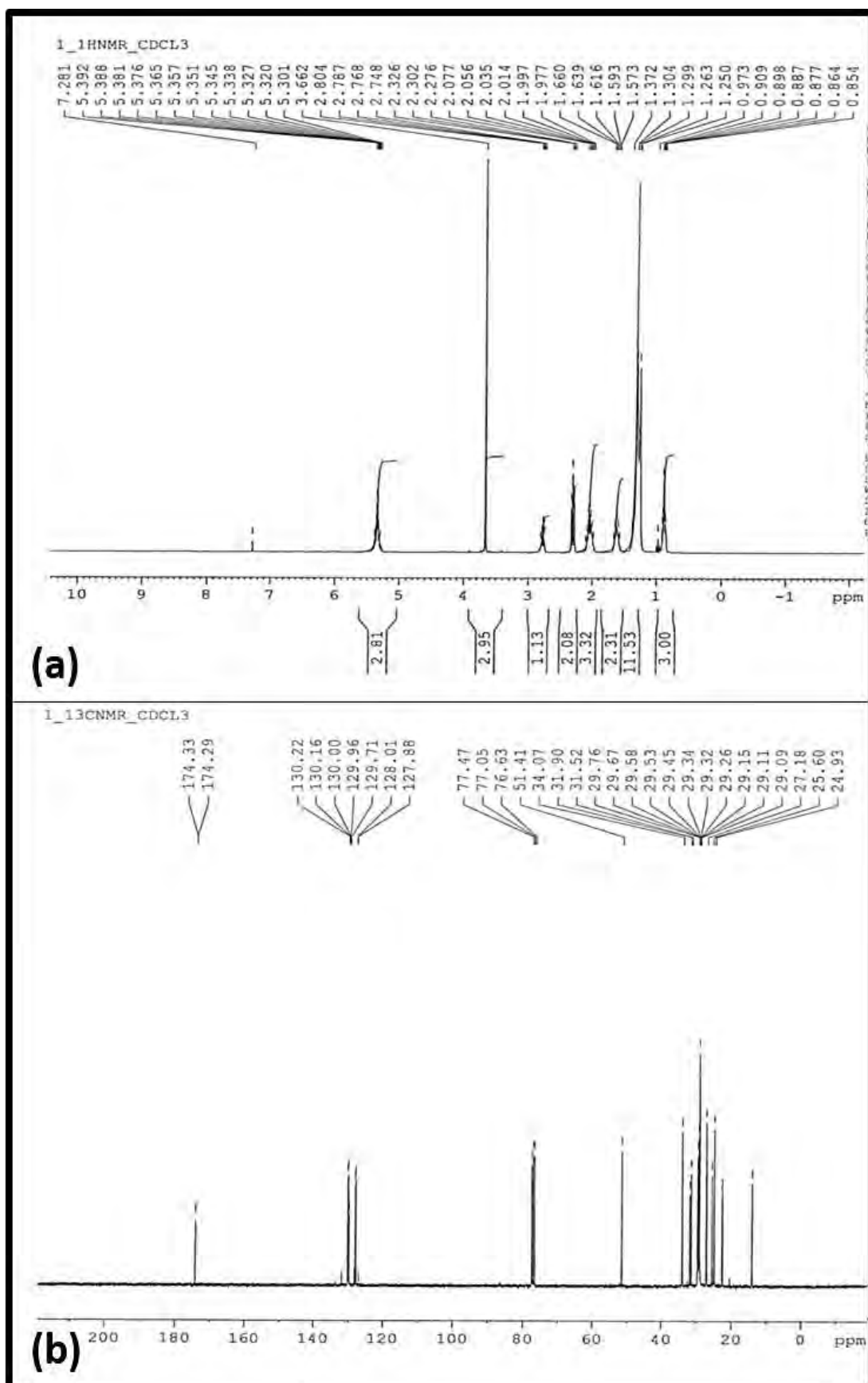
Figure 3.3.7: (a) ^{1}HNMR **(b)** ^{13}CNMR spectra of EJBD
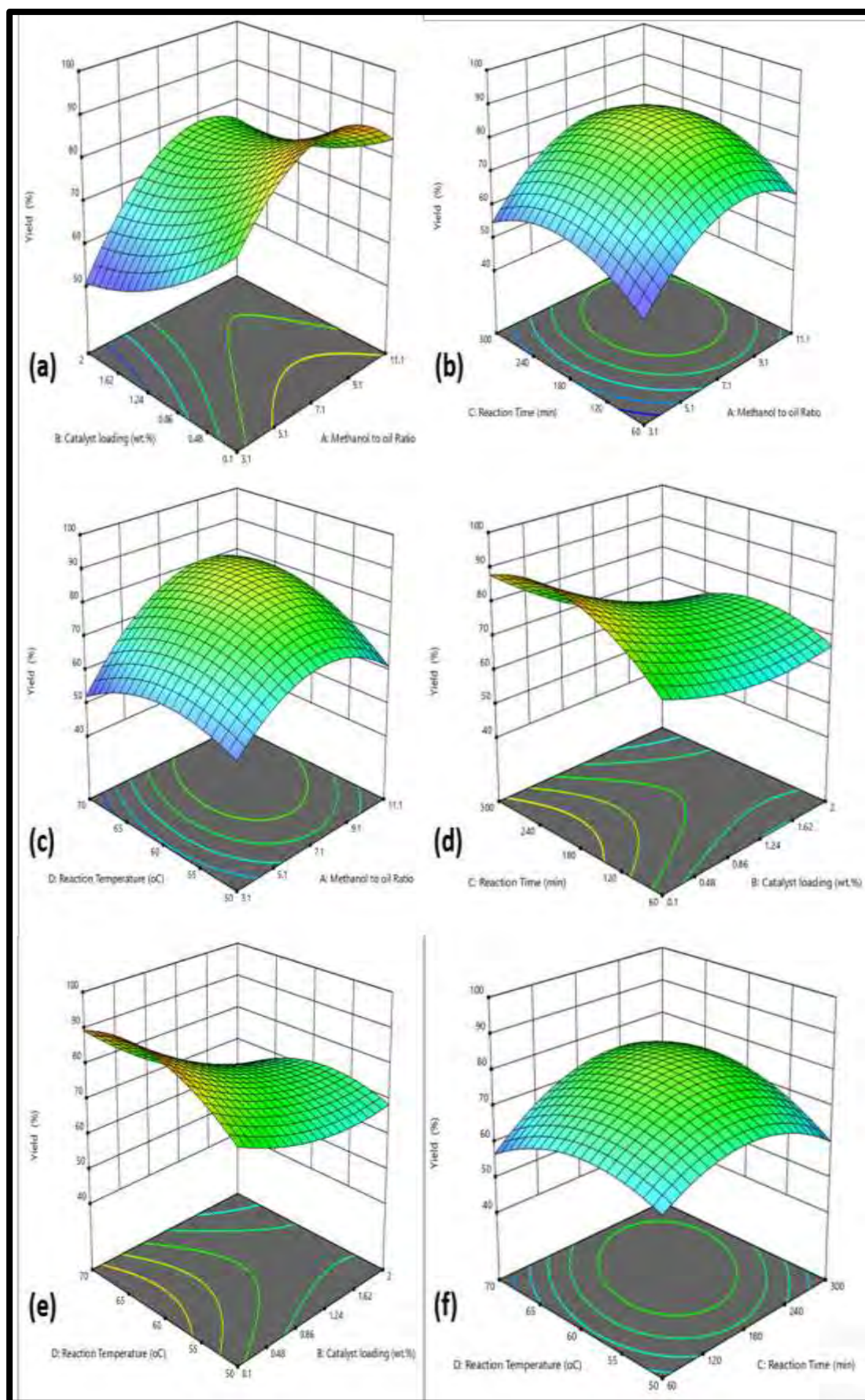
Figure 3.3.8 (a-f) The influence of reaction variables on EJBD
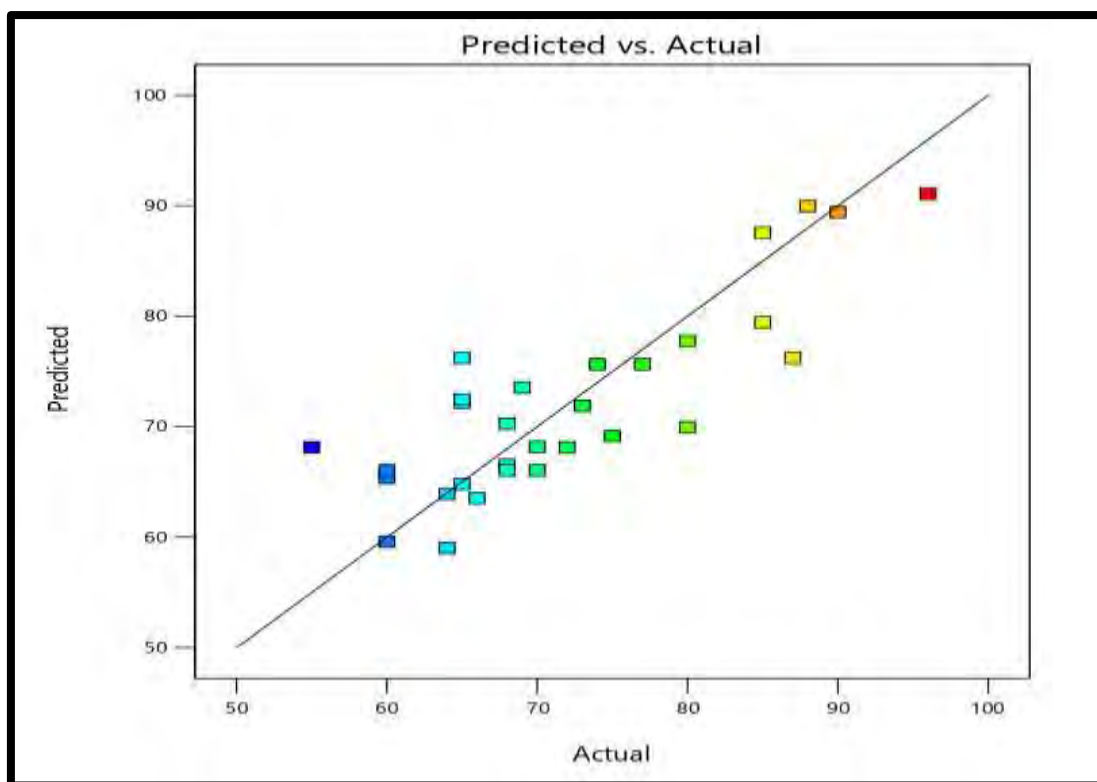
Figure 3.3.9: Predicted yield vs actual yield of EJBD

Table 3.3.1: Fuel properties of EJBD

TESTS	METHOD	EJ B-100
Color	Visual	2
Density @ 15 °C Kg/L	ASTM D-1298	0.827
Flash point °C(PMCC)	ASTM D-98	97
Kinematic Viscosity @ 40 °C c St	ASTM D-445	4.87
Pour point °C	ASTM D-97	-10
Cloud point °C	ASTM D-2500	-14
Total Acid No. mg KOH/gm	ASTM D-974	0.183
Sulphur % wt	ASTM D-4294	0.0067

Table 3.3.2: Experimental yield of EJBD

Run	Methanol to Oil Molar Ratio	Catalyst Loading (wt. %)	Reaction Time (min)	Reaction Temp. (°C)	EJBD Yield (%)
1	3.1	0.1	300	70	80
2	11.1	1.05	180	50	74
3	7.1	0.1	180	60	96
4	7.1	1.05	180	60	85
5	11.1	2	300	70	66
6	11.1	0.1	300	50	60
7	7.1	2	180	60	65
8	11.1	1.05	180	60	77
9	11.1	2	60	50	65
10	11.1	0.1	60	60	70
11	7.1	0.1	180	50	80
12	7.1	1.05	180	70	69
13	3.1	1.05	180	60	64
14	7.1	2	60	60	68
15	7.1	0.1	300	50	73
16	3.1	0.1	180	60	72
17	7.1	0.1	300	60	90
18	7.1	2	300	60	64
19	7.1	0.1	60	50	60
20	11.1	0.1	60	60	68
21	7.1	2	180	60	87
22	11.1	0.1	60	70	60
23	11.1	0.1	180	70	85
24	7.1	1.05	60	60	70
25	3.1	0.1	180	70	55
26	7.1	1.05	300	60	65
27	3.1	0.1	180	50	68
28	7.1	0.1	60	70	75
29	7.1	0.1	180	70	88
30	3.1	0.1	300	60	65

Table 3.3.3: Analysis of Variance (ANOVA) of EJBD

Source	Sum of Squares	df	Mean Square	F-value	p-value	
Model	2136.16	14	152.58	2.56	0.0009	significant
A-Methanol to oil Ratio	333.61	1	333.61	5.59	0.0320	
B-Catalyst loading	454.27	1	454.27	7.61	0.0146	
C-Reaction Time	37.52	1	37.52	0.6286	0.0402	
D-Reaction Temperature	6.20	1	6.20	0.1040	0.0516	
AB	46.85	1	46.85	0.7849	0.0396	
AC	1.28	1	1.28	0.0214	0.0157	
AD	128.20	1	128.20	2.15	0.0434	
BC	200.97	1	200.97	3.37	0.0264	
BD	59.78	1	59.78	1.00	0.0328	
CD	63.74	1	63.74	1.07	0.0178	
A²	751.19	1	751.19	12.59	0.0029	
B²	68.39	1	68.39	1.15	0.0014	
C²	415.21	1	415.21	6.96	0.0187	
D²	175.52	1	175.52	2.94	0.1070	
Residual	895.31	15	59.69			
Lack of Fit	448.31	10	44.83	0.5015	0.8349	not significant
Pure Error	447.00	5	89.40			
Cor Total	3031.47	29				

SECTION: IV

Biodiesel Synthesis from *Praecitrullus fistulosus* Seed oil using Copper Oxide Green Nano-catalyst

3.4 Biodiesel Synthesis from *Praecitrullus fistulosus* Seed oil using Copper Oxide Green Nano-catalyst

3.4.1 Characterization of Copper Oxide Green Nano-catalyst

(a) XRD of CuO

Transesterification studies have indicated that the usage of green copper oxide nanoparticles is a strong contender. Due to its unique catalytic and optical properties, green copper oxide (CuO) has gained significant importance. Figure 3.4.1 shows the XRD spectrum of copper oxide green nano-catalyst. There are numerous diffraction peaks in the XRD spectrum that may be clearly seen. At 2θ angle, several diffraction spots were observed for copper oxide at 32.78°, 37.10°, 39°, 48.89°, 53.80°, 58.75°, 61.81°, 66.50°, and 68.59° (JCPDS 80-1268) and average particle size was calculated about 82 nm. No strong peaks from other phases could be found, proving the great purity of the product created using this approach. Our results are in close accordance with previous researches (Ayoman *et al.,* 2015). Leaf extract of *Euphorbia chamaesyce* has been used to discern effective catalytic characteristics of CuO nanoparticles (Maham *et al.,* 2017). Using *Phoenic dactylifera* leaf extract, Berra *et al*. (2018) created green copper oxide nanoparticles, and their XRD results showed that the particles have a crystalline structure with an average size of 22–28 nm (Berra *et al*., 2018). Using floral extract from Bougainvillaea, copper oxide nanoparticles were produced and synthesized particles were shown to be very stable, spherical, and with an average diameter of 12±4 nm according to the X-ray diffraction (XRD) results. (Shammout & Awwad, 2021)

(b) SEM of CuO

SEM was used to determine the size and surface morphology of green CuO nano-catalysts that had been synthesized. The surface morphology of polydispersed copper oxide nanoparticles is depicted in Figure 3.4.2 at various magnifications. SEM images show that produced nanoparticles were roughly heterogeneous in structure, roughly cubic to hexagonal shape and had diameters in the nanometer range. While the majority of the nanoparticles were present in agglomerated form, others were well separated from one another. These SEM findings thus validated the nanostructure behavior of the created particles. The outcomes are consistent with earlier reports with a few minor

variations brought by chemical composition (Akintelu *et al*., 2020) The copper oxide nanoparticles have a smooth surface and cluster, according to the SEM data. The catalyst has a foliated structure, a porous surface, and flakes that are firmly packed together to give it a fluffy appearance. Particles reorient themselves after calcination and emerge as agglomerated porous structures with numerous catalytic active sites on the surface of big flakes. A significant concentration of accessible sites on a porous surface led to improved catalytic activity. This is corroborated by the catalytic potential for exceptional biodiesel conversion efficiency with high optimized yield. Similar results were achieved by Siddiqui *et al.,* 2021 CuO nanoparticles made with pomegranate (*Punica granatum*) extract had an apparent well-distributed, spherical shape distribution (Siddiqui *et al.,* 2021).

(c) EDX of CuO

The EDX analysis of copper oxide nano-catalyst, as shown in Figure 3.4.3 clearly shows that the manufactured nano-catalyst was composed of two separate elements, namely copper and oxygen. Several points on the catalyst surface were considered. The peaks that closely approximate the optical absorption of the generated nano-catalyst were identified by EDX analysis. The elemental analysis of the nano-catalyst revealed that it contains the greatest levels of purity possible, with 85.25% of copper and 14.75% of oxygen. The high purity and various shapes of the synthesized NPs have been confirmed by EDX. Our findings closely align with previous studies involving SEM with EDX analysis of biosynthesized CuO nano-catalyst from *Galeopsidis herba* extract (Alagarasan *et al*., 2021; Dobrucka, 2018)

(d) FT-IR of CuO

To identify the functional groups that make up CuO nanoparticles, FT-IR analysis was done. The spectrum for CuO NPs is illustrated in Figure 3.4.4. The bands detected are generated by lattice vibrational modes that represent the functional groups of supporting biomolecules. The spectrum shows a band at 3143.88 cm^{-1}, which is attributable to free hydroxyl groups and associated intra- and intermolecular H-bonds in polyphenolic compounds and this band spans the range of 3100 to 3385 cm^{-1}. The OH stretching frequency associated with the broad band at 3397.96 cm^{-1}. The Cu-O bond stretching vibration in the CuO green nano-catalyst is represented by the distinctive band at 593.88 cm^{-1} and 1071.43 cm^{-1}. Our FT-IR results are in accordance

with the outcomes of FT-IR analysis of copper oxide bond (Cu-O) of a green nano-catalyst by (Barman *et al.,* 2021; Veisi *et al.,* 2021).

3.4.2 Characterization of *Praecitrullus fistulosus* Biodiesel (PFBD)

(a) FT-IR of PFBD

Due to its potential to serve as a "fingerprint technique" that aids in the identification of chemical bonds and functional groups in biodiesel samples, FT-IR is a contemporary analytical approach for the quick and simple detection of FAMES. The FT-IR spectra of PFBD (Biodiesel) is overlaid in Figure 3.4.5 in the mid-infrared region (400- 4000 cm-1) and around 722.36 cm^{-1} (C-H bend rocking). 1160.40 cm^{-1} (C-O stretching vibration), 1464.52 cm^{-1} (C-H scissoring), 2852.58 cm^{-1} (sp3C-H stretching) and 2922.98 cm^{-1} (sp2C-H stretching), the primary peaks reflecting several functional groups appears. Nevertheless, the methoxy carbonyl and C=O stretching in the methyl ester of fatty acids resulted in two unique absorption bands i.e. a peak appeared at 1711.67 cm^{-1}, the (sp3C-H) stretch, which is one of the distinctive C=O peaks of the ester group in PFBD and other signals detected at 2853.60 cm^{-1}, and the (sp2C-H) signal a strong peak almost appears at 2922.98 cm^{-1}. These powerful peaks were caused by the ester group C=O stretch in the FT-IR spectrum. The CH3, CH2 bending vibrations almost exhibit peaks at 1377.68 cm^{-1} and 1464.52 cm^{-1}. The change from an ester group to a methyl ester (biodiesel) has a significant impact on the IR spectrum. It is easy to see all of the carbonyl group characteristics. This can be written as R1- C(OCH3) = O for the ester group of biodiesel. The ester control signal area surrounding the broad and strong signal at 1160.40 cm^{-1} exhibits the other frequently seen alteration during transesterification. There is no longer a supply of the typical energy associated with the triple ester group in oils. All of the aforementioned rationalization of peaks confirms the biodiesel synthesis (Ameen *et al.,* 2022).

(b) GC-MS of PFBD

After being transformed into their corresponding FAMEs can be analyzed using gas chromatography to determine their composition. GC-MS results showed presence of twelve methyl esters. Running standards under experimental circumstances and comparing the respective retention time data allowed researchers to confirm the presence of the identified fatty acid methyl esters. The results (Figure 3.4.6) depict the

presence of twelve peaks for methyl esters such as three Lauric acid methyl esters ($C_{13}H_{26}O_2$), Myristic acid methyl ester ($C_{14}H_{28}O_2$), Palmitic acid methyl ester($C_{17}H_{34}O_2$), Linoleic acid methyl ester ($C_{19}H_{34}O_2$), Eicosenoic acid methyl esters ($C_{21}H_{36}O_2$), Cyclopropane butanoic acid methyl ester($C_{25}H_{42}O_2$), two17- octadecynoic acid methyl ester ($C_{19}H_{34}O_2$), Isopropyl linoleate and n-propyl linoleate ($C_{21}H_{38}O_2$) at various retention time per minute i.e. 9.94 , 12.34, 15.38, 16.27, 16.31, 16.49, 19.28, 20.29, 20.59, 21.04, 21.37, 23.70 respectively. Specific methyl esters present in PFBD have also been reported in cucurbitaceae family (Ameen *et al.*, 2018; Aziz *et al.*, 2022; Du *et al.*, 2022; Karaye *et al.*, 2021).

(c) NMR of PFBD

In order to monitor the transesterification reaction based on the presence of the distinctive signal in the NMR spectrum, ^{1}H and ^{13}C-NMR are useful spectroscopic techniques. Figure 3.4.7 displays the key characteristics of the ^{1}H -NMR and ^{13}C-NMR spectra for the PFBD. The emergence of a new singlet peak of the methoxy group at 3.659 ppm confirms the conversion of triglycerides in to fatty acid methyl esters (Chatterjee *et al.*, 2021; Doudin 2021). Other distinctive signals and chemical shifts δ (ppm) can be seen in the ^{1}HNMR spectrum of biodiesel PFBD (Figure 3.7.6a).

Other distinctive signals and chemical shifts can be seen in the 1H-NMR spectra of biodiesel DBD (Figure 3.7.6a): δ (ppm): The peak positions of 5.33 (m,-CH = CH-), 2.32 (t, - CH2-COO-), 1.61 (m, -CH2-CH2-), 1.25 (m, -CH3), and 0.94 (t, -CH3) are in accordance with other research. The chemical shift and signal of biodiesel depicted in ^{13}C-NMR δ (ppm): 174.33 (-COO-), 129.97 (-CH=CH-), 77.07 (-CCH-), and 29.31 (-CH2-)n. Using the equation provided by (Ahmad *et al.*, 2022) the theoretical PFBD yield was 92%, which was found to be close to the experimental yield (91%), which can be raised by extending the settling time of the product mixture or by centrifugations (Munir *et al.*, 2021).

3.4.3 Biodiesel Yield Optimization via Response Surface Methodology

The response surface methodology (RSM) has been used to construct 3D graphs to show the overall impact of reaction parameters (Figure 3.4.8 a-f). Using several graphs, which consider the overall interaction between many factors that are given in

the following subsections, the ideal limits for each parameter for peak response are determined (Table 3.4.2)

During the transesterification procedure, reaction parameters are regularly used. In order to produce highest biodiesel, it is required to analyze the ideal transesterification reaction conditions. Using four independent transesterification variables with lower and higher values, such as the molar ratio of 3:1–15:1 (A), the catalyst concentration of 0.1-2.5 wt. % (B), the reaction time of 1–4 h (C), and the temperature of 55–90 °C (D), the Central Composite Design (CCD) for our current study was created by DOE (Design of Experiment). The comparison of the predicted and actual transesterification yield is shown in Figure 3.4.8a The distribution of the predicted and actual values is discovered to be close to the straight line, indicating a strong correlation between them. The results of the response surface quadric model statistical analyses of variance (ANOVA) are shown in Table 3.4.3. A low p-value of (< 0.0001) indicated that the quadric model was significant (less than 0.05). The lack of fit F-value of experimental model, which has a value of 0.8662, was not statistically significant compared to pure error. For the quadric model, a good lack of fit value is one that is not statistically significant and has a chance of noise-cause of 86.62%. The predicted R^2 value was 0.5163, which is closer to the adjusted R^2 value of 0.7871 with a variance < 0.2, based on the results in Table 3.4.3. The model adequate precision was found to be more than 4. (12.0354). The current experimental model higher value of acceptable precision showed how effectively it can be used to estimate biodiesel yield. The following is the polynomial equation used in the quadric model.

Yield = +72.95-1.94*A-7.18*B-6.39*C-3.24*D+1.89*AB+0.0635*AC-1.77*AD-4.01*BC+1.63*BD-2.97*CD-15.13*A²+6.51*B²-9.29*C²   **(7)**

3.4.3.1 Interaction between methanol to oil molar ratio and catalyst loading

Significant reaction parameters that affect the transesterification step of the biodiesel synthesis process are the Molar ratio and catalyst loading (AB). The process of converting oil or fat into biodiesel is accelerated by having excess methanol. The combined effect of the catalyst loading and Molar ratio is depicted in a 3D plot (Figure 3.4.8a. The maximum yield (91%) was attained at 9:1 (Met: Oil) with 0.1 wt. % catalyst loading (run 19). In order to study the combined influence of Molar ratio and catalyst loading, other reaction parameters such as reaction time and reaction temperature were

kept constant at 2.5 h and 55°C respectively. When catalyst concentration was raised slightly from o.1 to 1.3%, biodiesel yield reduced to 88% (Run 17). When methanol to oil ratio was reduced to 1:3 with same conditions (i.e. 1.3 wt. %, 2.5 h and 55°C), methyl ester yield declined to 77% (Run 11). However, keeping the molar ratio and catalyst load at upper extreme limit i.e. 1:3 and 2.5 wt. % by fixing other parameters, biodiesel yield dropped to 55% (Run 4). This can be explicated by the fact that the production of undesired products is favored by the higher catalyst concentration (soap formation).Moreover, a significant factor driving the biodiesel yield is the oil to methanol ratio. Due to the fact that transesterification is a double-sided reaction, more methanol is required to accelerate the reaction (Chuah *et al*., 2015). With a slight modification in reaction conditions as in run 11, methanol to oil ratio was increased to 1:15, FAME yield dropped to 60% (Run 7). This is because the monoglycerides compel the mixing and solubility of glycerol in FAME. This reversible process takes place, which makes it easier for FAME and glycerol to combine again and produce monoglycerides (Loy *et al*., 2019). Our findings are consistent with previous research, which found that using excessive methanol rendered the reversible reaction faster and lowered the amount of biodiesel that could be achieved (Verma *et al*., 2016). The combined effect of the catalyst concentration and the oil to methanol ratio, however, had a highly significant effect, according to the ANOVA results, with a P-value of 0.0087<0.05.

3.4.3.1 Interaction between oil to methanol molar ratio and reaction time

The molar ratio of methanol to oil (Met: oil) and the reaction time (AC) both simultaneously affect the formation of FAME which makes them efficient optimization parameters. Figure 3.4.8 b in our study demonstrates the interaction influence. Highest product yield (91 %) was attained at 9:1 (Molar ratio), 2.5 h of reaction time, while keeping catalyst concentration and reaction temperature constant at 0.1% and 55 °C (run 19). Through variation in methanol to oil ratio (3:1, 9:1 and 15:1), the combined effect on biodiesel yield was checked in 1 h of reaction time and the recoded results were 70%, 85% and 66% in runs 25, 29 and 15 respectively. The cause of low yield is methanol inadequacy (not enough to drive transesterification) or overabundance (stimulates reversible reaction and hinders product removal). When the molar ratio and reaction time were increased to 15:1 and 4 h, respectively, only 64% of biodiesel was

produced (Run 12). This was due to reversible reactions marked by glycerolysis and problematic product purification as a result of solubilization, which was caused by an excessive methanol fraction and prolonged reaction time. Hence, higher methanol concentrations hinder the separation of glycerol and consequently lower FAME output. The ANOVA results revealed a strong and significant connection between two variables with p-value 0.0356 (< 0.05)

3.4.3.3 Interaction between methanol to oil molar ratio and reaction temperature

The relationship between molar ratio (Met: Oil) and reaction temperature (AD) and is established as RSM 3D plots (Figure 3.4.8). The maximum yield (91%) was achieved in run 19 via an optimized 9:1 (Molar ratio) and reaction temperature of 55°C. When catalyst concentration and reaction time were kept constant at 0.1 wt. % and 2.5 h reaction time then a sudden increase in molar ratio result in decline in the biodiesel yield to 76%, due to intermixing of glycerol in biodiesel due to high methanol content (run 23). Moreover, in our optimization reactions, by keeping reaction temperature at 90°C, the interactive effect by lowering and increasing the Molar ratio was checked. The results depicted that low molar ratio (3:1) is not enough to drive transesterification whereas higher methanol concentrations (15:1) produce hurdle in glycerol separation hence declination in biodisel yield to 74% (run 6) and 65% (run 14) respectively. Our ANOVA results show the combined effect of Molar ratio and reaction temperature is significant with p- value <0.05 i.e. 0.0250 (Table 3.2.3)

3.4.3.4 Interaction between catalyst loading and reaction time

Interactive effect of amount of catalyst and reaction time (BC) has been mention as 3D RSM graph (Figure 3.4.8d). The highest biodiesel yield (91%) was attained at optimal levels of catalyst concentration and reaction time with 0.1 wt. % and 2.5 h owing to reaction equilibrium (run 19). However, beyond the optimum values of catalyst concentration and reaction time (1.3%, 1 h), a sudden drop in yield (68%) was observed as shorter reaction time did not favor the completion of reaction resulting in reduced biodiesel yield (run 22). When catalyst concentration was increased to 2.5% by keeping other parameters constant, a biodiesel yield reduction to 75% was detected (run 27). The longer process duration (4 h) and high catalyst concentration (2.5 wt. %), however, cause a reversible transesterification reaction and saponification, which limit

the biodiesel output. According to ANOVA results, catalyst loading and reaction time have a significant mutual influence (p-value <0.05) 0.0604 (Table 3.4.3)

3.4.3.5 Interaction between catalyst loading and reaction temperature

A 3D plot shows the overall interactive relationship between the amount of catalyst and the reaction temperature (BD) (Figure 3.4.8 e). The maximum biodiesel yield (91%) was achieved with 0.1 wt. % catalyst and 55 °C (run19).When temperature was increased to 90°C by keeping other factors at their optimal level (i.e. 9:1 molar ratio, 0.1 wt. % catalyst, 2.5 h time), the biodiesel yield was 68% (run 18). This is the prevailing view since when the temperature rises over the methanol boiling point, glycerin saponification increases before methanol decomposition, which lowers the biodiesel production. When both catalyst conc. and reaction temperature were increased from 0.1 wt. % to 1.3 wt. % and from 55°C to 72.5°C respectively, a decline in biodiesel yield (75%) was noticed (run 8). With further increase in optimization limits of in both variables to 2.5 wt. % and 90 °C, just 72% was achieved. The reason of yield reduction is saponification and methanol evaporation that resulted in low product concentration. ANOVA results show their significant mutual effect with p-value (0.0604) <0.05.

3.4.3.6 Interaction between reaction time and reaction temperature

The collective influence of reaction time and reaction temperature (CD) has been mentioned as a 3D RSM graph (Figure 3.4.8e). The maximum biodiesel yield (91%) was achieved in 2.5 h and 55 °C. When the reaction time was set at 1 h and reaction temperature was increased to 72.5°C, a substantially low yield (80%) was recorded (run 1). However, with further rise in reaction temperature to 90 °C resulted in too lower yield (75%). Low yield was caused by methanol evaporation at higher temperatures and a quick reaction time as the reactant molecules are unable to react correctly and transform into their desired products. However, upsurge in reaction time to 4 h, methyl ester conversion yield (84%) reduction was observed due to reversible transesterification and glycerolysis (run 9). However by increasing both reaction time and reaction temperature to 4 h and 72.5 °C respectively, a decline in biodiesel yield to 76% was detected owing to reversible transesterification (as a result of long reaction time) and methanol vaporization (as a result of high reaction temperature). Our ANOVA show our results are not significant with p-value (0.1684) > 0.05.

3.4.4 Fuel Properties of PFBD

The fuel properties of PFBD were quantified and evaluated to ASTM standards. A significant aspect in the determination of quality of methyl esters is the density. According to Table 3.4.1, the density of PFBD at 15 °C was 0.89 Kg/L, while the density of conventional high speed diesel was 0.834. According to this finding, the PFBD is just similar to high speed diesel with negligible difference. Kinematic viscosity is the metric used to gauge how sticky biodiesel or fuel is. The kinematic viscosity of biodiesel must adhere to ASTM standards since fuel with lower viscosity levels could obstruct engine lubrication. The kinematic viscosity of PFBD was discovered to be 4.52 Kg/L, which is within ASTM standard tolerance. In comparison to the standard high speed diesel, this value is higher at 4.22 Kg/L. Flash point is the maximum temperature at which fuel can ignite. It is a measurement of a propensity of substance to combine with air to generate a flammable mixture. The flash point is an element that has practical importance. During handling, shipping, and storage, high flash points are secure. The ASTM D-93 criteria are met by the flash point of PFBD, which was measured to be up to 70 °C (Table 3.4.1) and makes it a safer fuel. The typical high-speed diesel flash point value is between 60 and 80 °C. The cloud point was recorded as -12 °C while the pour point value was -12 °C,) and found within the range of ASTM requirements i.e. (-15-16°C). Acid value refers to how many free fatty acids are present in a fuel sample. The amount of KOH needed to neutralize 1 g of fatty acid methyl esters is expressed in mg KOH/g. High acid value is detrimental to engine efficiency. In this work, according to the ASTM testing procedure D-974, the PFBD acid value was found to be 0.36 mg KOH/mg, which was extremely low and suitable for commercial use, in the transportation industry in particular. As stated and proven from the conclusions that biodiesel is preferable than high-speed diesel since it has negligible or no Sulphur content. Sulfur was present in PFBD at a level of accordance to the ASTM standard D-4294, 00.0063 ppm by %weight was discovered ().
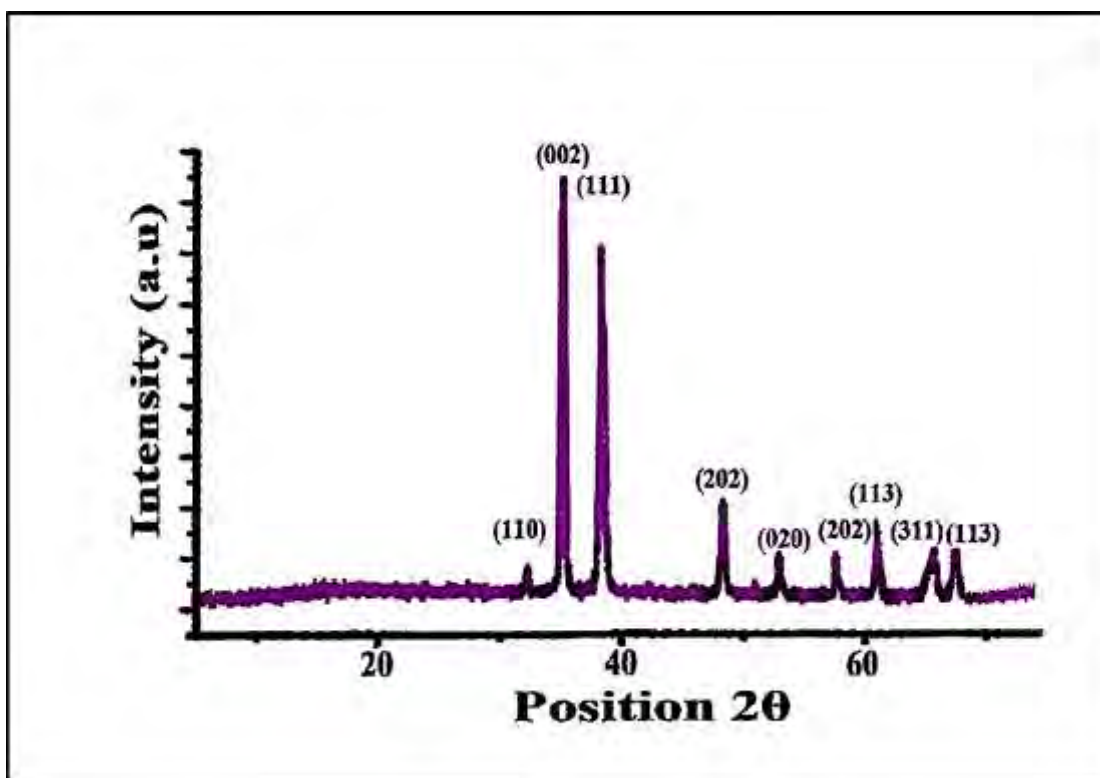
Figure 3.4.1: XRD of CuO green nano-catalyst
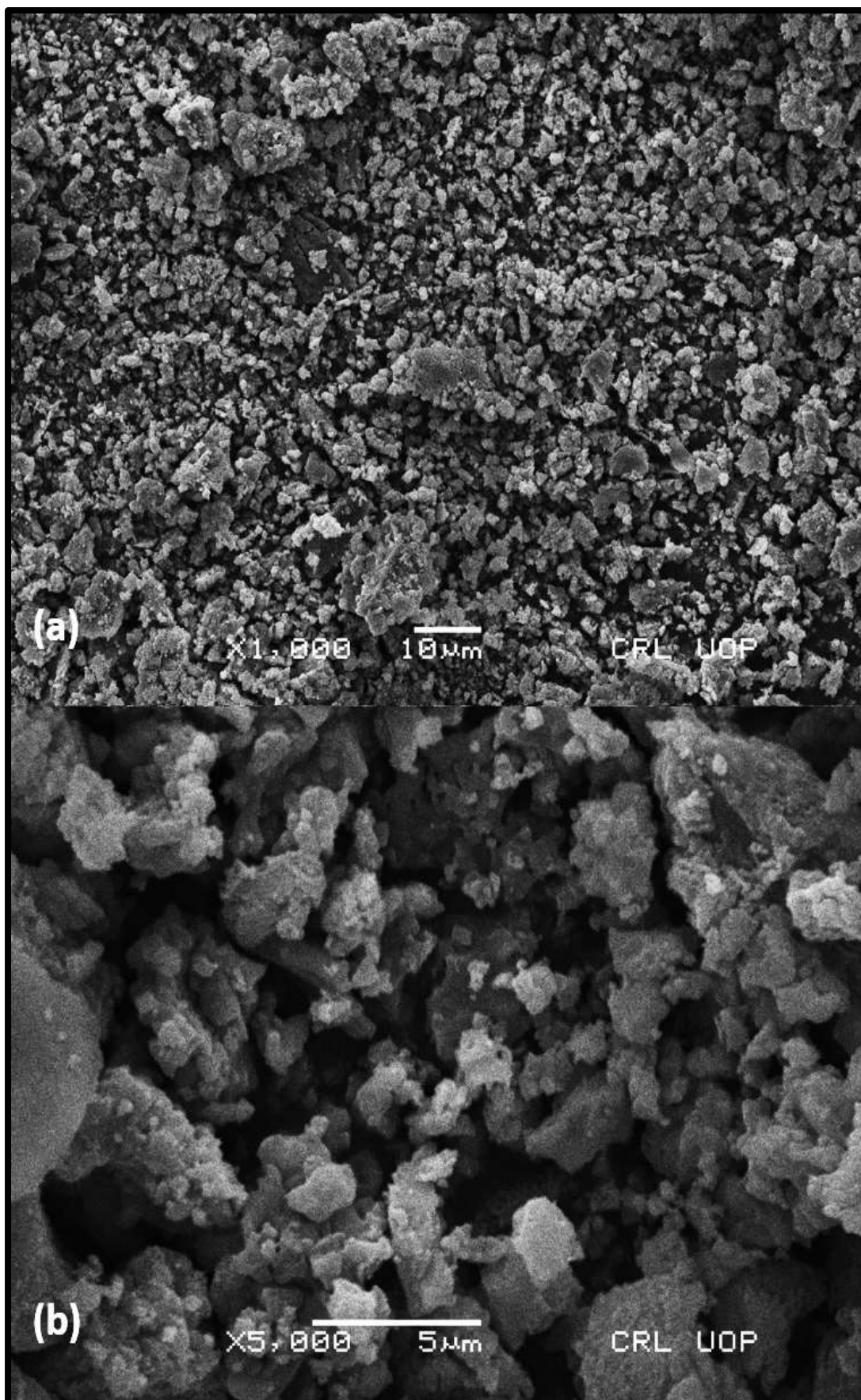
Figure 3.4.2: SEM of CuO green nano-catalyst
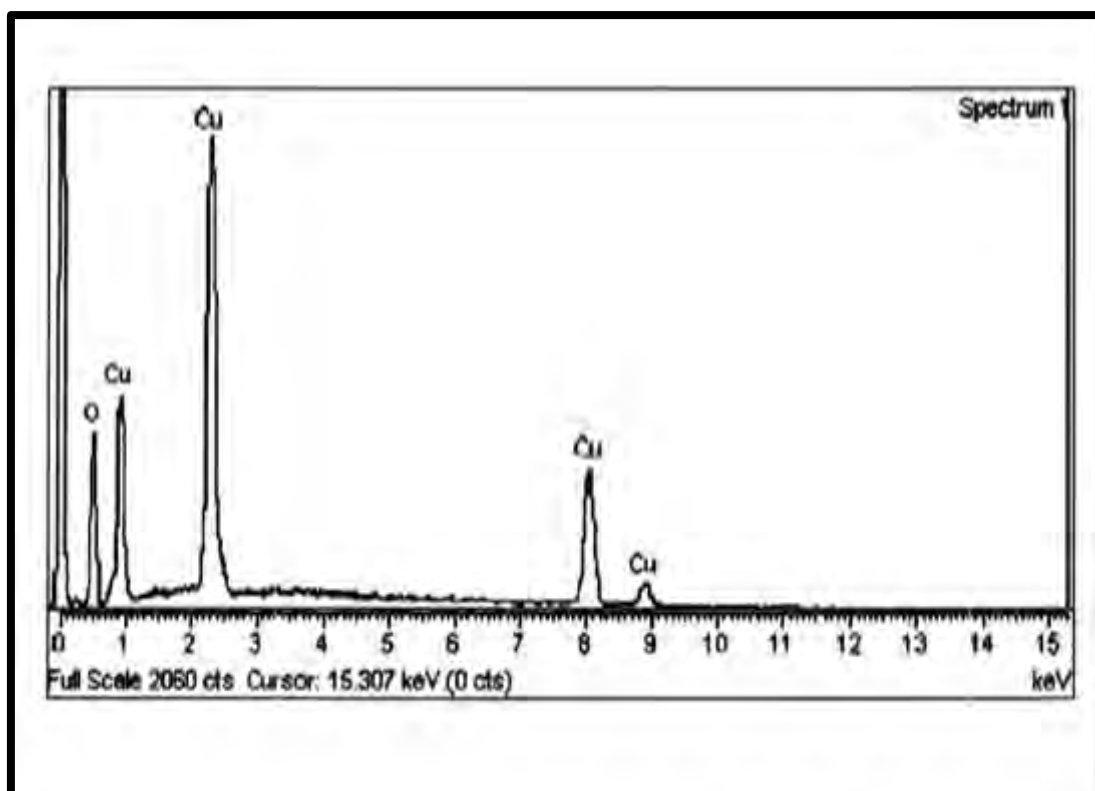
Figure 3.4.3 EDX of CuO green nano-catalyst
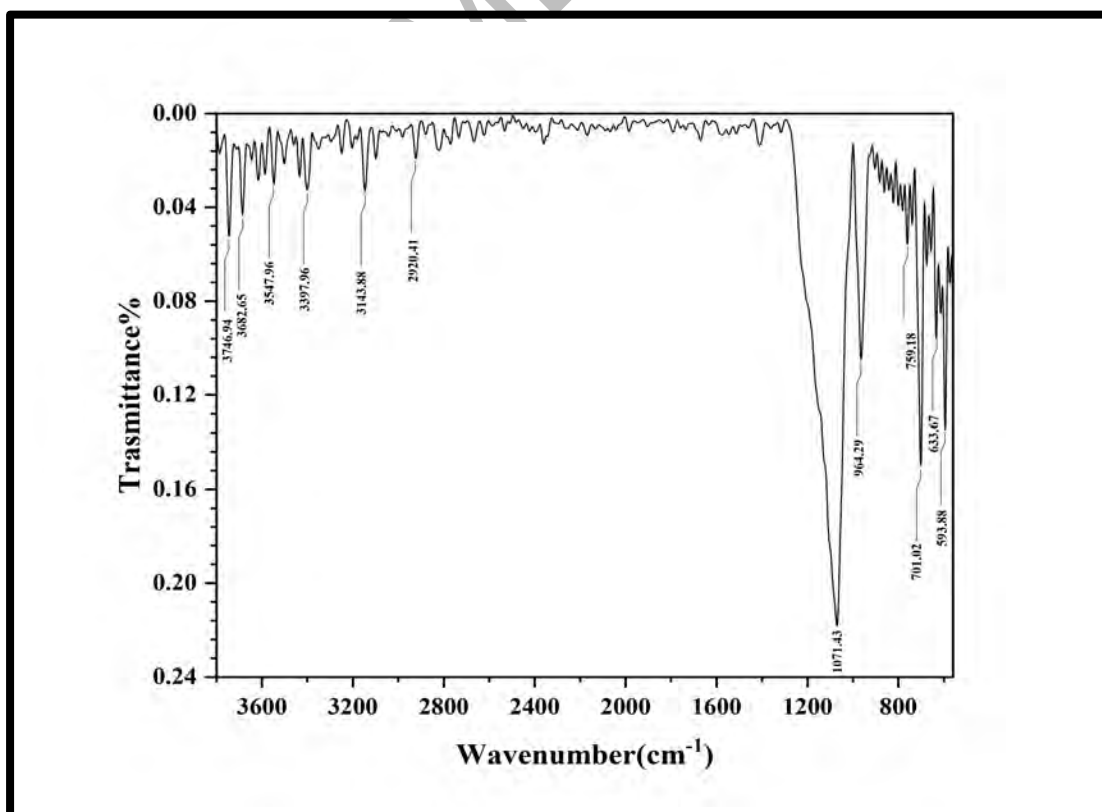
Figure 3.4.4 FT-IR of CuO green nano-catalyst
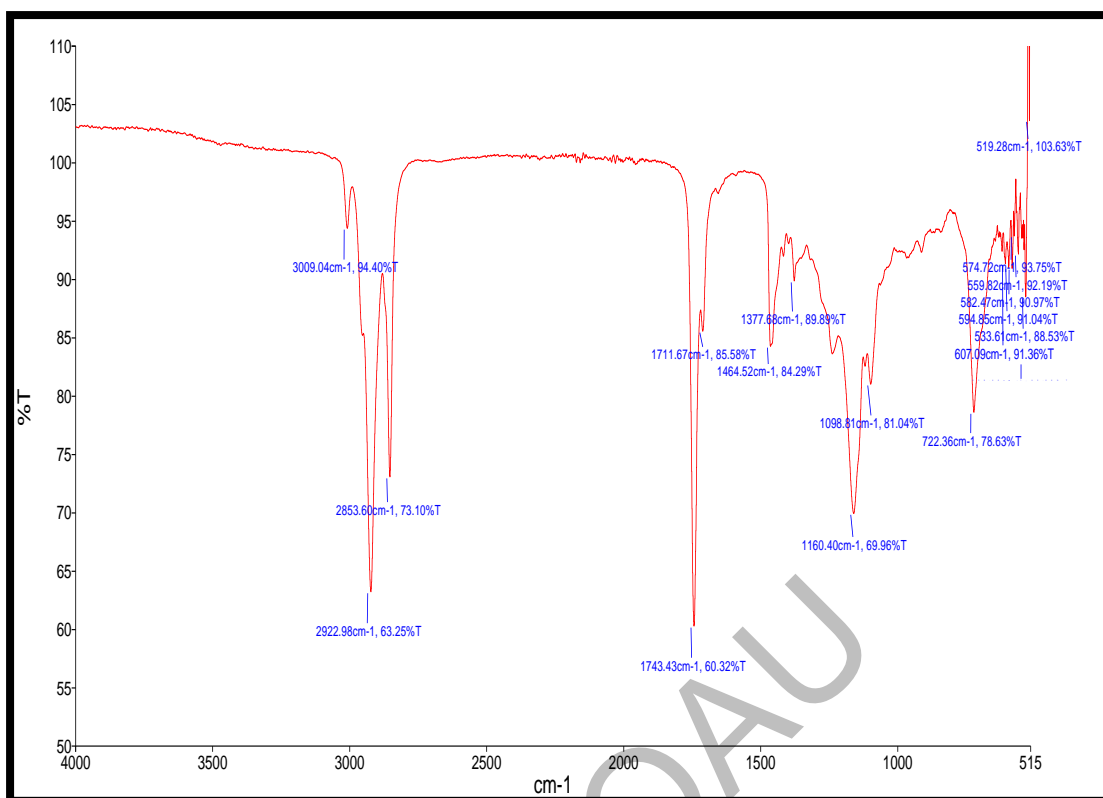
Figure 3.4.5 FT-IR spectrum of PFBD
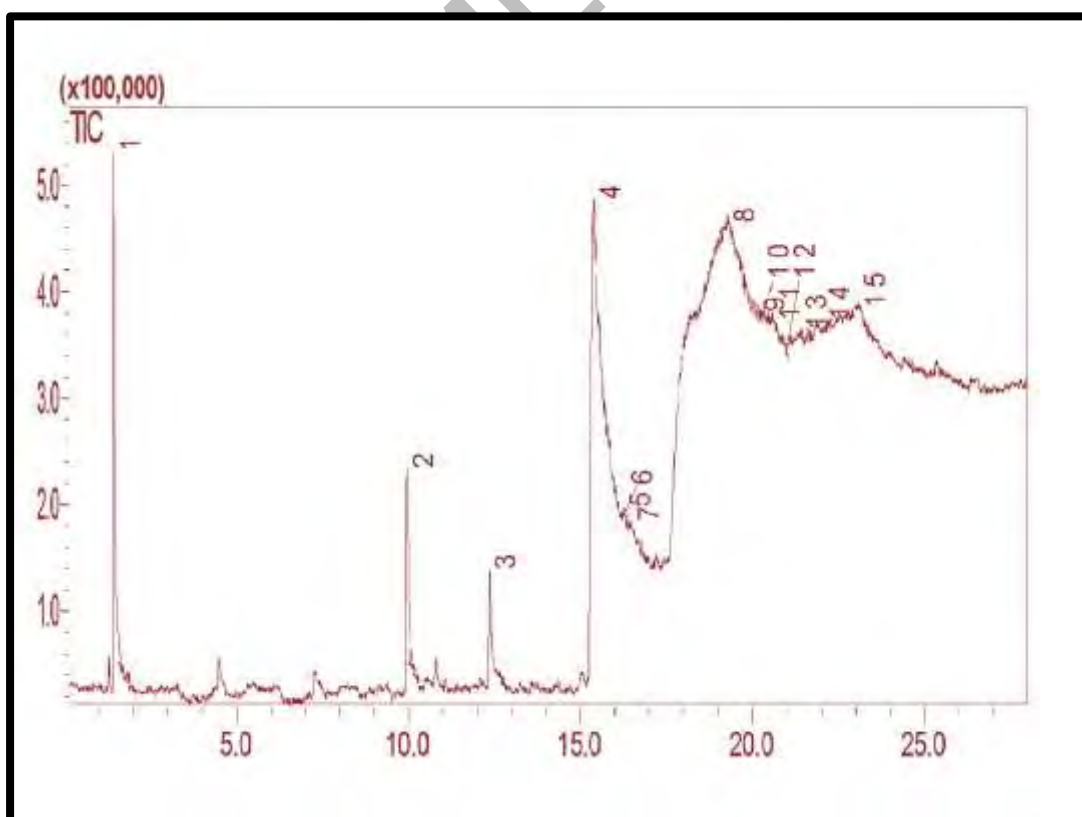
Figure 3.4.6 GC-MS spectrum of PFBD
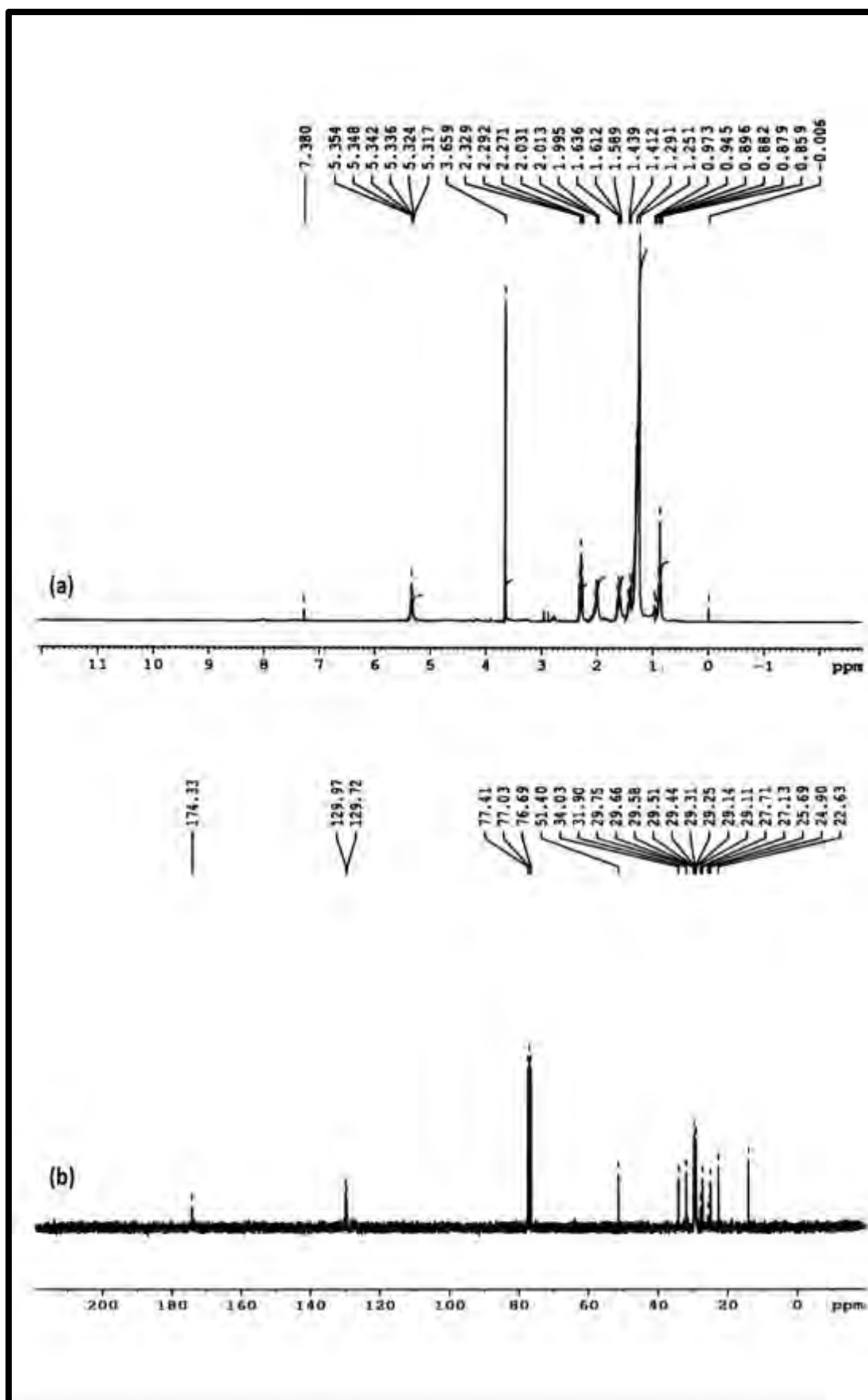
Figure 3.4. 7 (a) ^{1}HNMR **(b)** ^{13}CNMR spectra of PFBD
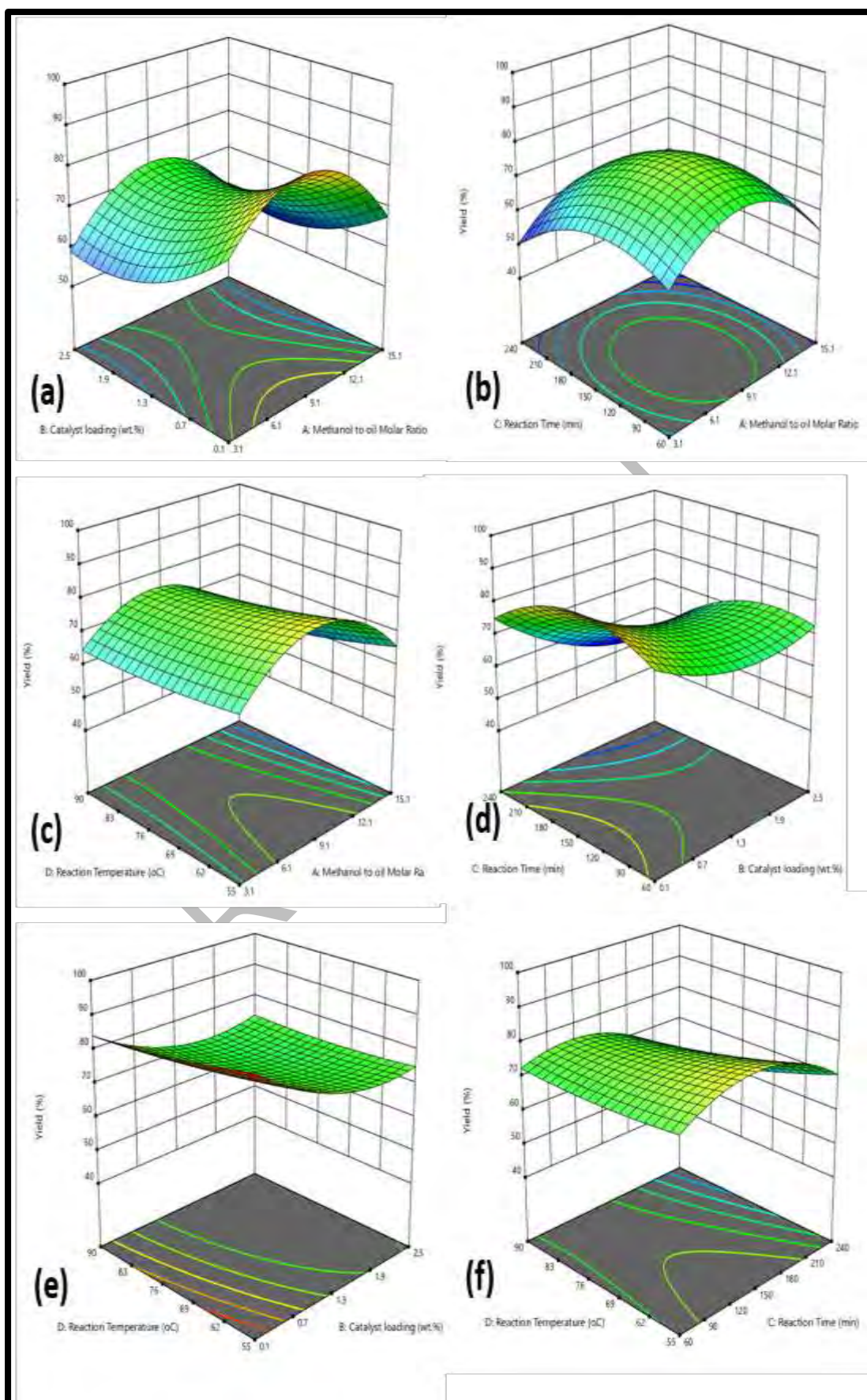
Figure 3.4.8 Influence of reaction variables on PFBD
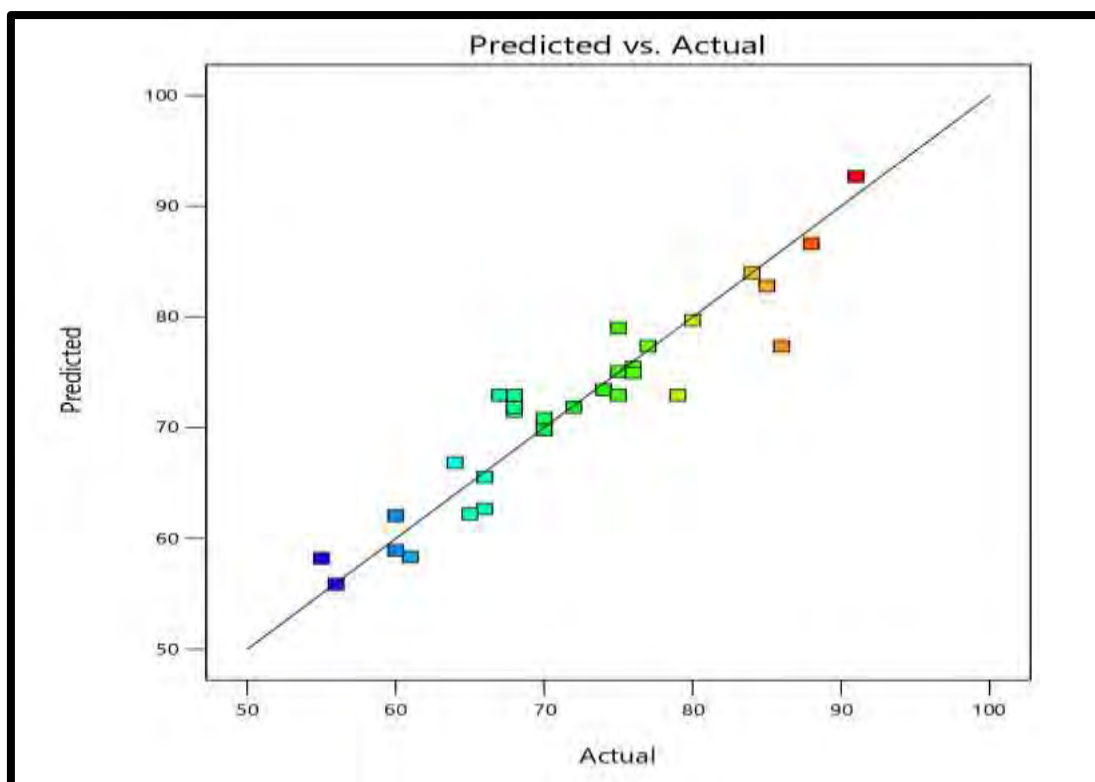
Figure 3.4.9 Predicted yield vs actual yield of PFBD

Table 3.4.1 Fuel properties of PFBD

TESTS	METHOD	PF B-100
Color	Visual	2
Density @ 15 °C Kg/L	ASTM D-1298	0.89
Kinematic Viscosity @ 40 °C c St	ASTM D-445	4.52
Pour point °C	ASTM D-97	-12
Flash point °C(PMCC)	ASTM D-93	70
Cloud point °C	ASTM D-2500	-8
Total Acid No. mg KOH/gm	ASTM D-4294	0.36
Sulphur % wt.	ASTM D-974	0.0063

Table 3.4.2 Experimental yield of PFBD

Run	Methanol to Oil Molar Ratio	Catalyst Loading (wt. %)	Reaction Time (min)	Reaction Temp. (°C)	PFBD Yield (%)
1	9.1	0.1	60	72.5	80
2	3.1	2.5	60	90	66
3	9.1	0.1	60	90	75
4	3.1	2.5	150	55	55
5	15.1	2.5	60	90	60
6	3.1	0.1	150	90	74
7	15.1	1.3	150	55	60
8	9.1	1.3	150	72.5	75
9	9.1	0.1	240	55	84
10	15.1	1.3	150	72.5	56
11	3.1	1.3	150	55	77
12	15.1	0.1	240	55	64
13	9.1	0.1	240	72.5	76
14	15.1	0.1	150	90	65
15	15.1	0.1	60	55	66
16	9.1	1.3	240	72.5	68
17	9.1	1.3	150	55	86
18	9.1	0.1	150	90	68
19	9.1	0.1	150	55	91
20	3.1	0.1	240	55	70
21	3.1	1.3	150	72.5	79
22	9.1	1.3	60	55	68
23	15.1	0.1	150	55	76
24	9.1	2.5	150	90	72
25	3.1	0.1	60	55	70
26	9.1	2.5	240	55	61
27	9.1	2.5	150	55	75
28	15.1	1.3	150	90	67
29	9.1	0.1	60	55	85
30	9.1	0.1	150	72.5	88

Table 3.4.3 Analysis of Variance (ANOVA) of PFBD

Source	Sum of Squares	df	Mean Square	F-value	p-value	
Model	2266.22	14	161.87	8.66	< 0.0001	significant
A-Methanol to oil Molar Ratio	27.34	1	27.34	1.46	0.2453	
B-Catalyst loading	670.22	1	670.22	35.84	< 0.0001	
C-Reaction Time	183.32	1	183.32	9.80	0.0069	
D-Reaction Temperature	93.41	1	93.41	5.00	0.0410	
AB	20.76	1	20.76	1.11	0.0087	
AC	0.0180	1	0.0180	0.0010	0.0356	
AD	25.07	1	25.07	1.34	0.0250	
BC	77.12	1	77.12	4.12	0.0604	
BD	26.96	1	26.96	1.44	0.0485	
CD	39.16	1	39.16	2.09	0.1684	
A^2	1194.34	1	1194.34	63.87	< 0.0001	
B^2	115.34	1	115.34	6.17	0.0253	
C^2	334.70	1	334.70	17.90	0.0007	
D^2	4.66	1	4.66	0.2494	0.6247	
Residual	280.48	15	18.70			
Lack of Fit	133.23	10	13.32	0.4524	0.8662	not significant
Pure Error	147.25	5	29.45			
Cor Total	2546.70	29				

SECTION: V

Biodiesel Synthesis from *Luffa acutangula* Using Cadmium Oxide Green Nano-catalyst

3.5. Biodiesel Synthesis from *Luffa acutangula* Using Cadmium Oxide Green Nano-catalyst

3.5.1 Characterization of Cadmium Oxide Green Nano-catalyst

(a) XRD of CdO

Diffraction peaks absorbed at 2θ were visible in the XRD patterns of the CdO nanostructure (Figure 3.5.1). The Scherrer equation, written as follows, was used to determine the grain size from the obvious peaks:

D = (Kλ)/(β cosθ)

λ = 1.542 Å, β= FWHM, θ= diffraction angle, K= 0.9 (Sankaran & Kumaraguru, 2020).

The relative intensity peak (220) for CdO nanoparticles was used to measure the grain size, which was found to be 48 nm. An elevation in the sharpness of the Xrd patterns shows that the particles are crystalline. The reference patterns for CdO are clearly visible in the (111), (200), (220), (311), and (222) reflections (Joint Committee for Powder Diffraction Studies (JCPDS) File No. 05-0640). The polycrystalline nature of the particles and the random orientation of the nanostructure are both shown by the strong XRD peaks. Our results are in close concordance with previous work (Aldwayyan *et al.*, 2013; Vidhya *et al.*, 2020)

(b) SEM of CdO

The SEM image of the prepared CdO nanoparticles that corresponds to the XRD pattern in Figure 3.5.2 It is evident that the prepared CdO nanoparticles have a regular spherical shape and uniform size, with an average size of 50 nm and one can notice some coalescing nanoparticles with a size of around 98 nm. Aldwayyan and coworkers prepared CdO nanoparticles with spherical shape within size range of 40-50nm (Aldwayyan *et al.*, 2013). Similar SEM results published by Kaveh et al. (2021) depict spherical CdO nanoparticles with particle size around 70nm (Kaveh *et al.*, 2021).

(c) EDX of CdO

The EDX image depicts the composition of the green nano-catalyst, which is made of the two distinct components cadmium and oxygen (Figure 3.5.3). The peaks

that closely approximate the optical absorption of the generated nano-catalyst were identified by EDX analysis. The nano-elemental catalyst analysis revealed that it included 70.25% cadmium and 29.75% oxygen. CdO nanostructures were synthesized and analyzed by (Abbas *et al.*, 2021).

(d) FT-IR of CdO

The efficient tool of Fourier Transform Infrared Spectroscopy (*FT-IR*) is used to recognize the functional groups present in the material under investigation. The FT-IR spectrum was used to analyses the modes of vibration of the chemical bonds found in the CdO nano-powder, and the functional groups were noted in the 400–4000 cm^{-1} range (Figure 3.5.4). O-H stretching linked with CdO causes a wide band range in the region of 3600-3250 cm^{-1}. The O-H stretching vibration of the hydroxyl groups in CdO is related to a potent band at 3563.27 cm^{-1}, as is seen from the FT-IR spectra of the CdO nanopowder. It is determined that CH symmetric stretching vibration is responsible for the peak at 3009.18 cm^{-1}. The oxygen matrix peak at 1732.65 cm^{-1}, where nano-CdO is present, is confirmed by it. The FT-IR spectroscopy investigation confirms that is attributed to C=O stretching while increasing the nano-CdO is functioning as a catalyst for the oxidation process in the CdO backbone. The distinctive bands in the 400-700 cm-1 range, with peaks from 526.53, 547.96, 587.76, 664.29 cm^{-1} correspond to the CdO mode. New absorption bands, specifically 664.29, 811.22, and 982.65 cm^{-1}, are assumed to have emerged in the wavelength range of 1000-600 cm-1 as a result of the metal-oxygen stretching of CdO. Our results coincide with the FT-IR results of Arun *et al.*, 2015 and Kaviyarasu *et al.*, 2014 where CdO nanopowder was synthesized and analyzed via FT-IR spectroscopy with characteristic peaks appeared in similar range (Arun *et al.,* 2015; Kaviyarasu *et al.,* 2014).

3.5.2 Characterization of *Luffa acutangula* Biodiesel (LABD)

(a) FT-IR of LABD

It is a quick analytical approach for the straightforward identification of methyl esters of fatty acids. It has been used as fingerprinting as it aids in identifying the biodiesel chemical bonds and functional groups. The mid-infrared FT-IR spectra of LABD is shown in Figure 3.5.5 The FAMEs (biodiesel) have two specific properties: methoxy-carbonyl group and C-O stretch-based absorptions. Two most pronounced

peaks at 1743.48.64 cm^{-1} and 1160.07 cm^{-1} indicate that C=O ester group is present. Bukkarapu and krishasamy (2021) confirmed the ester functional groups i.e. –C=O and –COC stretch at 1743 cm^{-1}and 1169 cm^{-1} in synthesized biodiesel samples (Bukkarapu & Krishnasamy, 2021). Since this absorption peak suggests that illustrates the efficient production of the carbonyl group in the LABD and triglyceride (fatty acid) conversion to the corresponding fatty acid methyl esters (Figure 3.5.5). At 2922.18 cm^{-1} the (sp2) C-H stretching and (sp3) C-H stretching exists at 2853.23 cm^{-1} in the FT-IR range. The vibrational bending of (methyl group) appear on 1,464.61 cm^{-1} (-CH$_3$) and 1,377.55 cm^{-1} (-CH$_2$) respectively. However, at 3,008.09 cm^{-1}, a stretching peak of alkenes is evident. Our results resemble with a lot of studies involving FT-IR analysis with sharp absorption peaks appearance at 1743 cm^{-1} to detect ester in biodiesel sample (Bibi *et al.*, 2022; Perumal & Mahendradas, 2022; Utami *et al.*, 2022).

(b) GC-MS of LABD

The chemical composition, structure, and fragmentations of FAMEs in manufactured biodiesel have all been comprehensively quantified using GC-MS. Library match software (NO. NIST02) was used to identify the 14 significant CPBD peaks that were seen. Figure 3.5.6 shows a sample eicosenoic acid, methyl ester mass-spectrum with significant fragmentations ion. In GC-MS spectrum of biosynthesized LABD remarkable fatty acid methyl esters include hexadecanoate (C$_{17}$H$_{34}$O$_2$), 9-octadecanoate(C$_{19}$H$_{36}$O$_2$), 9,12-Octadecadienoate (C$_{19}$H$_{34}$O$_2$), 6-octadecenoate (C$_{19}$H$_{36}$O$_2$), Methyl stearate (C$_{19}$H$_{38}$O$_2$), cis-13-Eicosenoate (C$_{21}$H$_{40}$O$_2$), cis-11-Eicosenoate (C$_{21}$H$_{40}$O$_2$), Eicosanoate(C$_{21}$H$_{40}$O$_2$), and 13-Docosenoate (C$_{23}$H$_{44}$O$_2$) with retention time of 24.00, 26.07, 25.80, 25.87, 26.07, 27.77, 27.82, 27.95, 29.56 minutes respectively (Figure 3.5.6).

(d) NMR of LABD

The use of ^{1}HNMR to assess the fuel qualities for LABD was explored in this work. FAME synthesis from oil has been established because a distinctive singlet peak at 3.656 ppm corresponds to the methoxy protons (-OCH3). When triglycerides are transesterified and transform into the appropriate alkyl esters depending on the type of alcohol used. When glycerol is substituted with alcohol, an NMR signal appears that ranges from 5.3 to 3.3 ppm, and this distinctive peak that appears at 3.656 ppm (-OCH3) indicates the presence of hydrogen next to the electronegative atom in the biodiesel

spectrum (Figure 3.5.7a). Previous studies are evidence of the presence of methoxy at this position (Chatterjee *et al.*, 2021; Doudin 2021; Islam *et al.*, 2022) Other conspicuous peaks include 0.826 and 0.854ppm showing terminal methyl protons (–CH3), 2.036-2.786 ppm α-methylene protons (–CH2), 1.271–1.636 ppm for β-methylene protons (–CH2) No peak observed in range of 4.0-4.2 ppm showing absence of methylene glyceridic protons, 5.324–5.356 ppm depicts Olefinic protons (–HC=CH), respectively. These detected signals indicate different methyl esters present in the biodiesel sample (Daimary *et al.*, 2022). Figure 3.5.7b depicts ^{13}CNMR of LABD and presents that the methoxy carbon resonated at 51.64 ppm which it is attributed to the principal distinctive peak in the biodiesel ^{13}C NMR. Other noticeable peaks in LABD include those at 130.06 ppm and 127.27 ppm, which are ascribed to the olefinic carbons of C-11 and C-12, respectively, as well as multiple peaks in the range of 127.67 ppm to 130.06 ppm brought on by the existence of other unsaturated carbon chains. The most noteworthy peak of biodiesel ester at 173.23ppm (-COO-), 129.69 ppm (-CH=CH-), 29.33ppm (-CH2-), 14.15 (-CH3-). Our results coincide with NMR study of *Raphanus raphanistrum* seed oil biodiesel produced by (Munir *et al.*, 2021).

3.5.3 Biodiesel Yield Optimization via Response Surface Methodology

To display the overall impact of reaction parameters, response surface methodology has been employed to develop 3D graphics (Figure 3.5.8 a-f). Under ideal reaction circumstances, it is typical to anticipate an increase in methyl ester yield. Biodiesel yield abruptly dropped below optimum levels. The interconnected ramifications of the transesterification reaction could be thoroughly explained in later subsections (Table 3.5.2). The transesterification process frequently employs reaction parameters. It is necessary to examine the perfect transesterification reaction conditions in order to create the highest quality biodiesel. Using four independent transesterification variables with lower and higher values, such as the molar ratio of 3:1–12:1 (A), the catalyst concentration of 0.5-2 wt. % (B), the reaction time of 1–3 h (C), and the temperature of 65–90 °C (D), the Central Composite Design (CCD) for our current study was created by DOE (Design of Experiment). The comparison of the predicted and actual transesterification yield is depicted in Figure 3.5.9. The distribution of the predicted and actual values is discovered to be close to the straight line, indicating a strong correlation between them. The results of the response surface

quadric model statistical analyses of variance (ANOVA) are shown in Table 3.5.3. The model adequate precision was found to be more than 4. (5.8531). The current experimental model higher value of acceptable precision showed how effectively it can be used to estimate biodiesel yield. Following polynomial equation used in the quadric model.

Yield $= +58.43 + 6.36*A - 10.06*B + 5.41*C - 2.01*D + 0.0055*AB - 1.71*AC - 1.04*AD + 1.30*BC - 2.71*BD - 1.47*CD + 5.95*A^2 + 1.16*B^2 + 2.59*C^2 + 0.1327*D^2$ **(8)**

3.5.3.1 Interaction between methanol to oil molar ratio and catalyst loading

Molar ratio and catalyst loading (AB) are essential reaction parameters that have an impact on the biodiesel synthesis process during the transesterification process. To quickly turn oil or fat into biodiesel, a large amount of methanol is needed. A 3D-plot of the combined effects of the catalyst loading and oil to methanol molar ratio is shown in Figure3.5.8a. The highest yield (93%) was achieved at 3:1 (Met: Oil) with 0.5 wt. % catalyst loading (run 25), however both reaction time and reaction temperature were kept constant at 3h and 65°C. With a slight upsurge in catalyst concentration, a sudden drop in biodiesel yield to 65% (run 15) was noticed. This can be explained by the side reaction of saponification that affected biodiesel yield in optimization reactions. When methanol to oil ratio was increased to 12:1 at other constant parameters, biodiesel yield declination from 93 % to 85% was recorded (run 27). Due to the reversibility of transesterification, an excessive amount of methanol in the reacting mixture dilutes the catalyst concentration and favors glycerolysis (a reversible reaction). Therefore, reformation of monoglycerides results from the recombination of glycerol with FAMEs. When both the molar ratio and catalyst loading were increased to 7.1 and 1.25 then a yield reduction of up to 88% was observed (run 6). However, further increase in methanol to 12:1 resulted in mixing of glycerol, soap and biodiesel. Hence due to solubilization the product separation became a difficult task and low percentage of biodiesel (70%) was obtained (run 3). Our ANOVA show significant ration between two factors with p-values (0.0385) < 0.05.

3.5.3.2 Interaction between oil to methanol molar ratio and reaction time

Molar ratio (Met: oil) and reaction time (AC) both collectively influence the FAME yield as a critical optimization parameter. In our study, the interactive influence

is depicted by Figure3.5.8b. The highest yield (93%) was obtained at a ratio of 3:1 (Met: Oil) and a reaction time of 3 hours (run 25), while keeping the catalyst amount constant at 0.5 wt. % and 65°C. With a minor increase in molar ratio to 7:1 while keeping other parameters constant (at 0.5 wt.% , 3 h and 65°C.), methyl ester yield reduced to 72% (run 5). With a molar ratio of 7:1 and a 2 h reaction time, just 58% biodiesel yield was achieved (run 10) due to deficiency of reaction time provided to the reactants. However, when the molar ratio increased to the maximum fixed limit, i.e., 12:1, then a decline in biodiesel was witnessed in 1 h of reaction and 55 % yield was recorded (run 14). Because higher molar ratios did not favor the FAME yield and high methanol content made separation more difficult as a result of dilution and the synthesis of undesirable byproducts therefore a low conversion yield was attained. The ANOVA results depicted a significant and a strong correlation between these two parameters with p- value < 0.05 (i.e. 0.0242).

3.5.3.3 Interaction between methanol to oil molar ratio and reaction temperature

The interactive effect of methanol to oil molar ratio (Met: Oil) and reaction temperature (AD) has been explained in Figure3.5.8c. The highest yield (93%) was achieved at 3:1 (Met: Oil) with 65°C reaction temperature (run 25) with constant catalyst loading (0.5 wt. %) and reaction time (3 h). At higher molar ratios (7:1 and 12:1) with higher temperatures 77.5°C and 90°C, the biodiesel yield decreased to 87% and 75% respectively at run 11 and 29. This declination could be ascribed to the dilution due to the high methanol amount and temperature beyond the methanol boiling point, triggering its vaporization. ANOVA outcomes depict this interactive effect significant with p-value < 0.05 (0.0454). Recent findings have thus prompted the conclusion that the combined influence of molar ratio and temperature is vital and must be taken into account during transesterification.

3.5.3.4 Interaction between catalyst loading and reaction time

The 3D RSM graph Figure3.5.8d depicts the interactive relationship between catalyst concentration and reaction time (BC). With a catalyst concentration of 0.5 wt. % and a reaction time of 3 h, the highest biodiesel production (93%) was achieved (run 25). When reaction time was set at 1 h by keeping other parameters constant, then 67% biodiesel yield was observed because the triglycerides could not be converted into respective methyl esters within the given time that was insufficient for the reactants to

combine properly (run 28). However, when both catalyst concentration and reaction time were adjusted at 1.25 wt. % and 2 h respectively, the biodiesel yield was recorded as 76% (run 7). Because a high catalyst concentration results in soap formation, this yield is not as low as in run 28 because reactants were provided with a 2 h reaction time that supported their effective reactions. Hence, in run 25, the catalyst load was lowered to 0.5% and reaction time was raised to 3 h, which resulted in the highest FAME yield (93%). According to ANOVA results, catalyst loading and reaction time have a significant mutual influence (p-value < 0.05), i.e. 0.0498

3.5.3.5 Interaction between catalyst loading and reaction temperature

The comprehensive interactive relationship between catalyst concentration and the reaction temperature is displayed in a 3D plot (BD) Figure3.5.8e. By adjusting catalyst concentration at 0.5 wt. % and reaction temperature at 65 °C, the highest biodiesel yield (93 %) was attained. When methanol to oil ratio (1:3) and reaction time (3 h) were kept constant, a rise in reaction temperature to 90°C resulted in just 77% biodiesel yield (run 21) This reduction in FAME yield is attributed to the higher temperature than the boiling point of methanol because most of the reactant remained in a vaporized state even in the presence of a condenser. By adjustment of reaction temperature at 77.5 °C along with catalyst concentration (1.25 wt. %) produced considerably low biodiesel yield (69 %) was achieved (run 19). A further decline in FAME yield (50%) was noticed when catalyst concentration was increased to 2 wt. % (run16). This drop could be due to synthesis of undesirable products such as soap and methanol vaporization at high temperature. Our ANOVA results showed a significant relation with p-value (0.0318) <0.05.

3.5.3.6 Interaction between reaction time and reaction temperature

The combined impact of reaction time and temperature on biodiesel yield is depicted in the Figure3.5.8f. It is clear that temperature (65 °C) and reaction time (3 h) have a substantial impact on biodiesel yield (93 %, Run 25). A decrease in yield would result from raising the temperature further (77.5 °C and 90 °C) and shortening the reaction time (1 h and 2 h). As it is clear from the output of run 8, just 67% biodiesel yield was achieved in 2 h of reaction time and 65°C reaction temperature because the short reaction time did not favor the forward reaction. A further decrease in reaction time to 1 h and an increase in reaction temperature to 90°C resulted in only 58%

biodiesel yield (run 20) at constant molar ratio (1:3) and catalyst loading (0.5 wt.%). The output of biodiesel has dropped as a result of the endothermic nature of the transesterification phase. The maximum biodiesel production of 93% was thus achieved at 65°C with a reaction time of 2.5 h owing to the complete mixing of oil and methanol, followed by the simple and direct separation of glycerol and end product. The amount of biodiesel that may be created would be decreased by higher temperatures, which may increase the hydrolysis of alkyl esters to produce acids and lose the polarity of methanol. The combined effect of reaction time and temperature on the ultimate biodiesel output is not significant with a P-value (0.5745) > 0.05.

3.5.4 Fuel Properties of LABD

Before consuming biodiesel produced from non-edible seed oils in diesel engines, it is vital to take into account the fuel important fuel parameters, such as kinematic viscosity, density, sulphur content, and flash point. The results of the current study analysis of the fuel properties of LABD in comparison to American (ASTM D-6751) and other international standards are shown in Table 3.5.1. In order to demonstrate the coherence in their properties with some slight changes, the properties of the biodiesel synthesized in the present study were also compared with previous work by Fadhil *et al.*., 2017. The amount of FFAs in the fuel is related to the acid number. Higher acid numbers, however, have a negative impact on engine performance by producing engine corrosion. The acid value of the biodiesel in this investigation (0.246 mg KOH/g) is within the acceptable limit for international standards i.e. 0.5 mg KOH/g. But as compared to biodiesel produced from *Silybum marianum* L. seed oil (0.08 mgKOH/g) and *Nicotiana tabbacum* seed oil (0.66 mgKOH/g), LABD has a higher acid value. By measuring the density, it is possible to have an insight in to the fatty acid composition and biodiesel purity profile. The fuel density can affect how the fuel atomizes during combustion. If fuels have a higher density, there could be issues with their operation in the engine due to viscosity concerns. FAMEs should have a density between 0.86 and 0.90, which is somewhat greater than the density of petro-diesel, according to American (ASTM). The biodiesel density in the current study (0.8722) is likewise within the international standard tolerances, demonstrating that using biodiesel as a diesel fuel alternative in a diesel engine can be done without harming the engine or the environment. Fadhil *et al.*. (2017) stated that *Silybum mariaum* biodiesel had a density of 0.8810 g/mL, which is marginally higher than our findings. One of the most

crucial characteristics of biodiesel is its viscosity. Fuel spray, mix formation, and combustion all depend on kinematic viscosity. The greater viscosity could lead to deposition and incomplete combustion in the engine. Kinematic viscosity must be low and t 40 °C, the LABD has a kinematic viscosity of 5.45 cSt. that is within the ASTM range of 1.9-6.0. The LABD flash point was 90 °C within ASTM range 60-100°C, which likewise falls within acceptable parameters per American (ASTM). When compared to biodiesel made from *Silybum marianum* L. seed oil, it is lower (88°C) (Table 3.5.1). Regarding hazardous flammability, fuels with flash points higher than 66 °C are considered to be safe. Pour point and Cloud point were checked according to ASTM D-97 and ASTM D-2500 and was found as -13 and -9 respectively, exactly within the ASTM range -15-16 and -3-12°C. Sulphur content (% wt.) was tested according to ASTM D-4294 and found to be 0.00432 (Akhtar *et al.,* 2022; Ameen *et al.,* 2018).
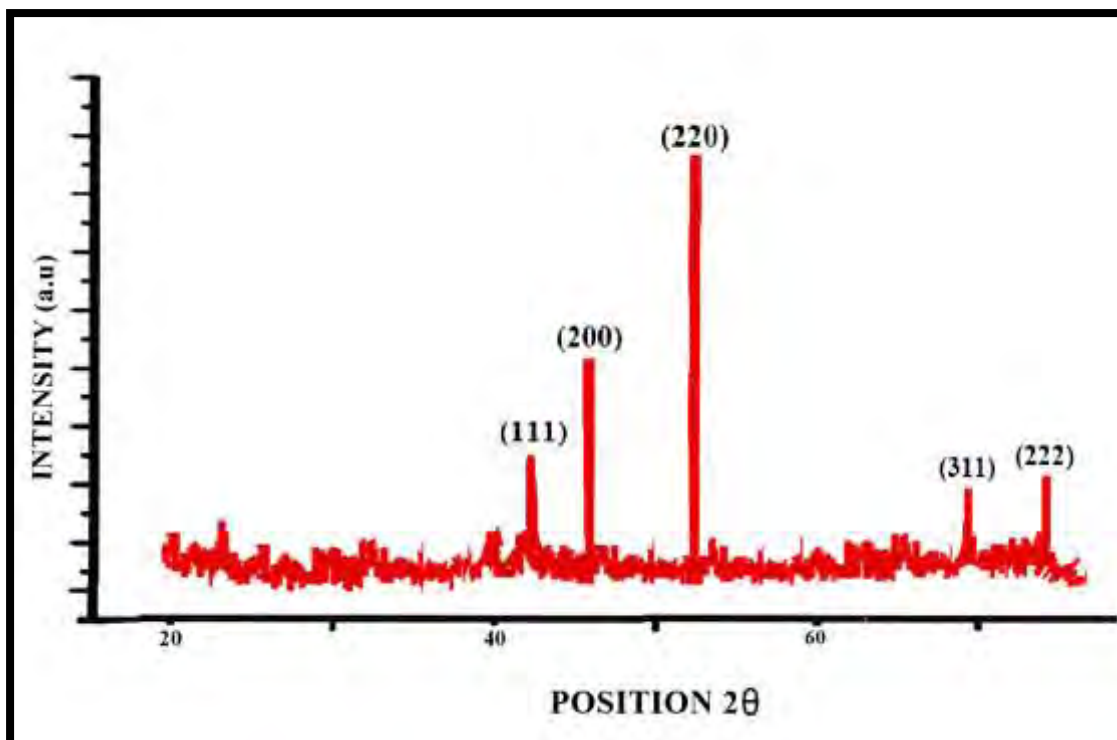
Figure 3.5.1: XRD of CdO green nano-catalyst
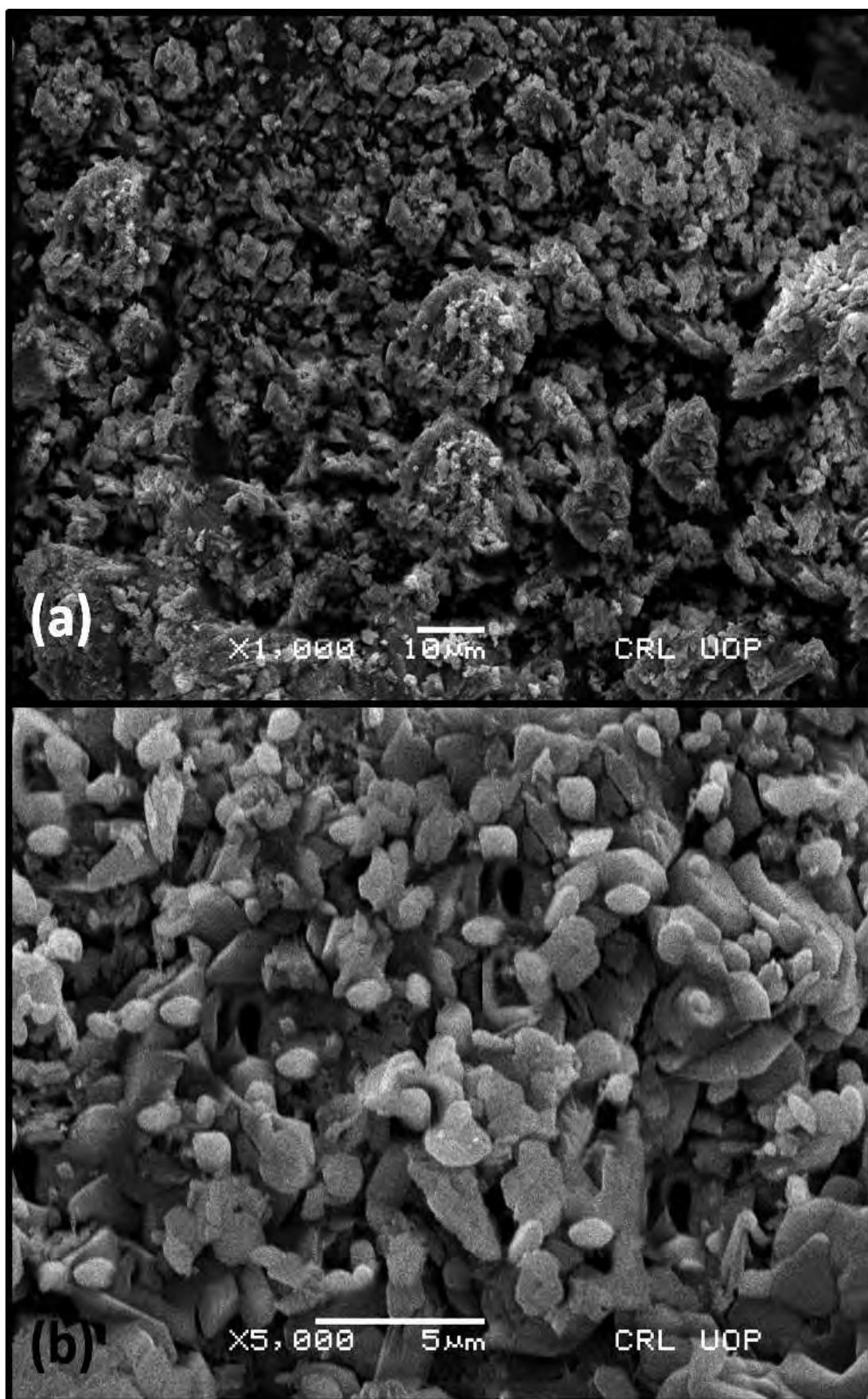
Figure 3.5.2: SEM of CdO green nano-catalyst
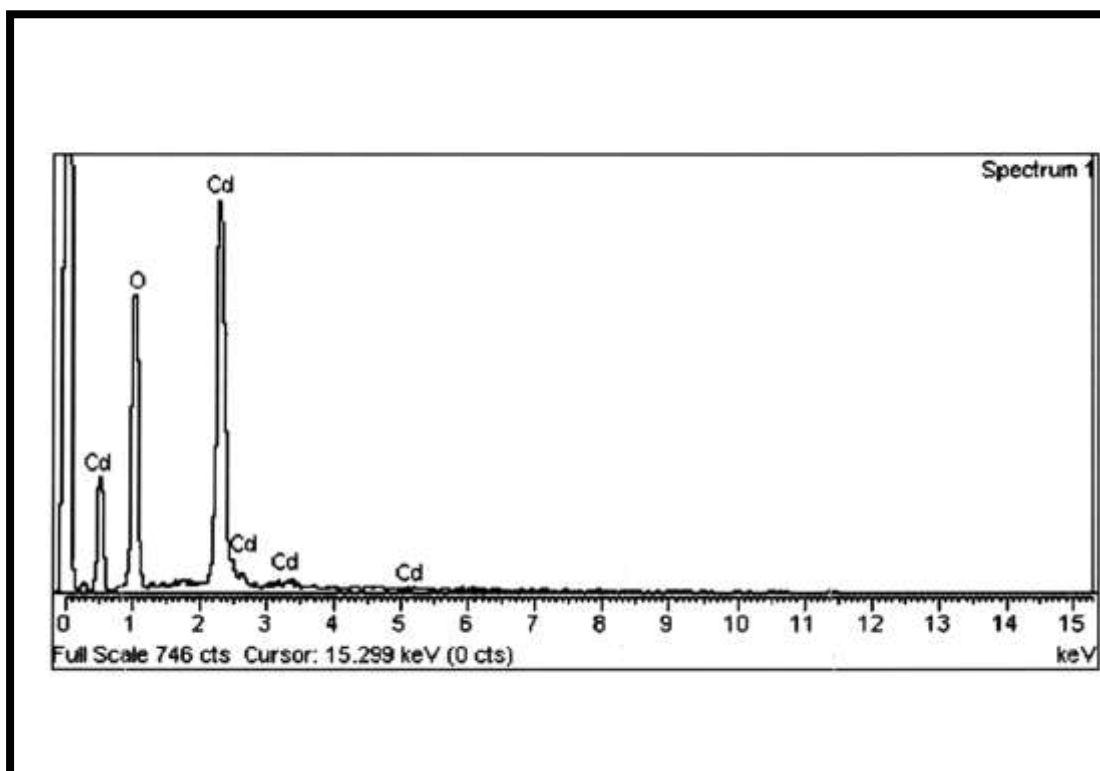
Figure 3.5.3: EDX of CdO green nano-catalyst
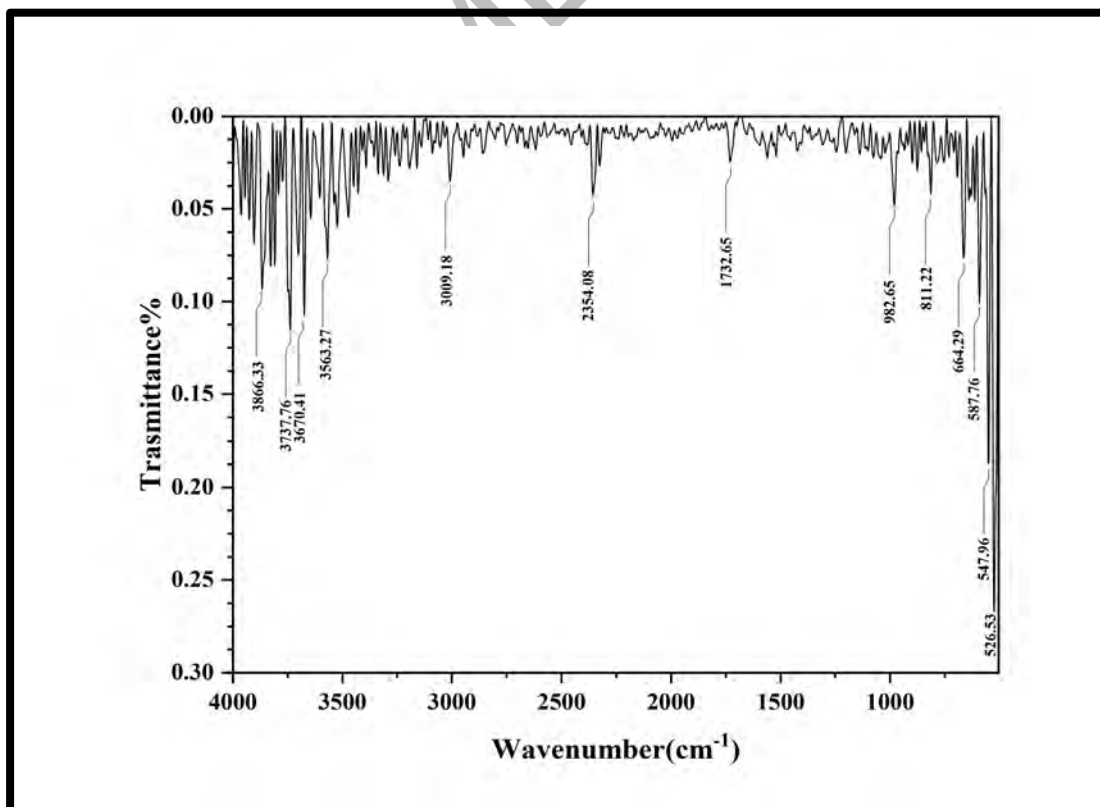
Figure 3.5.4: FT-IR of CdO green nano-catalyst
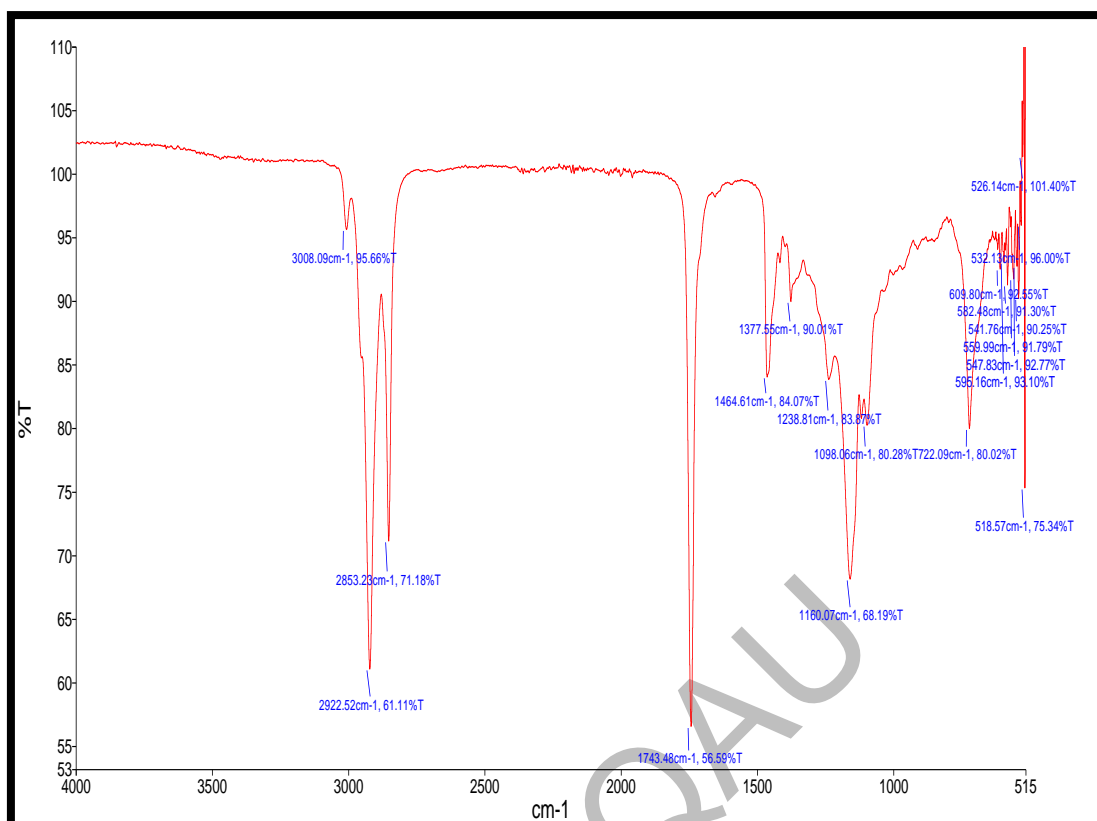
Figure 3.5.5: FT-IR spectrum of LABD
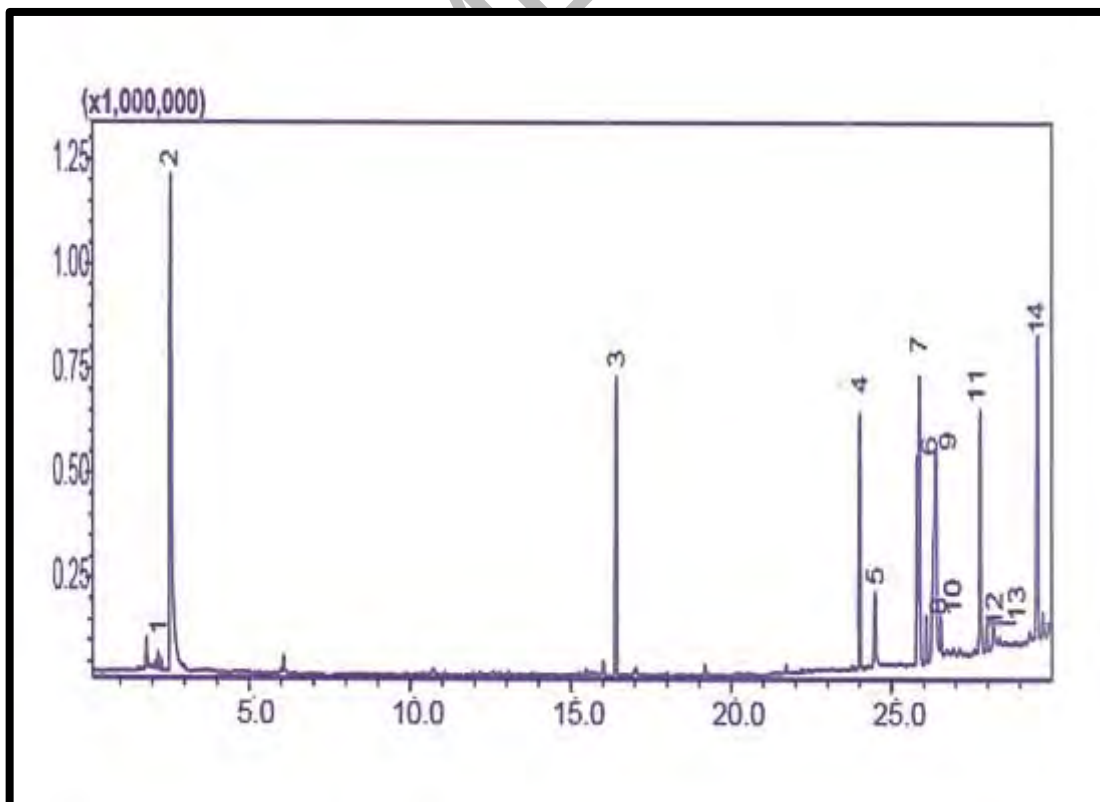
Figure 3.5.6: GC-MS spectrum of LABD
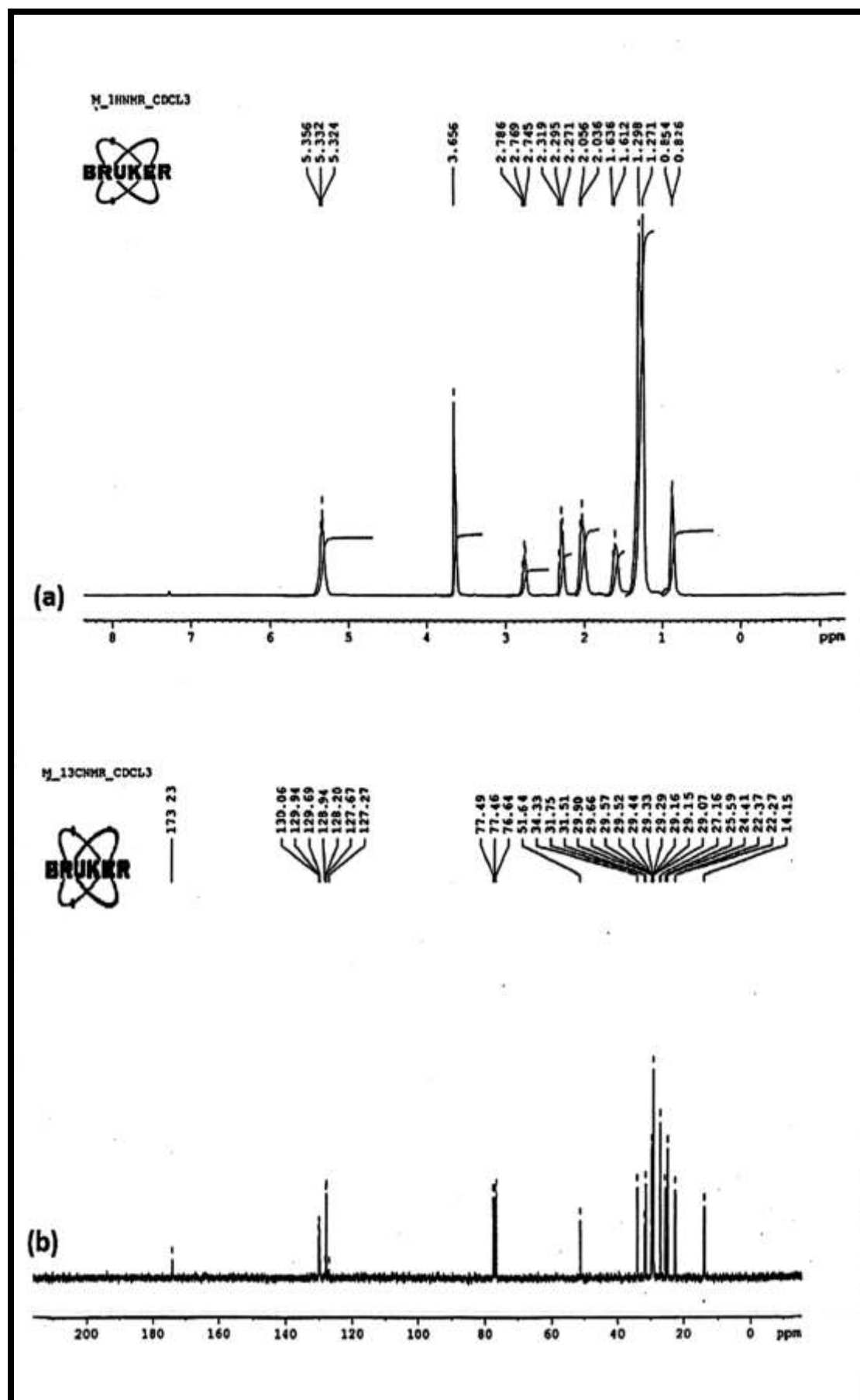
Figure 3.5.7: (a) ^{1}HNMR and (b) ^{13}CNMR spectra of LABD
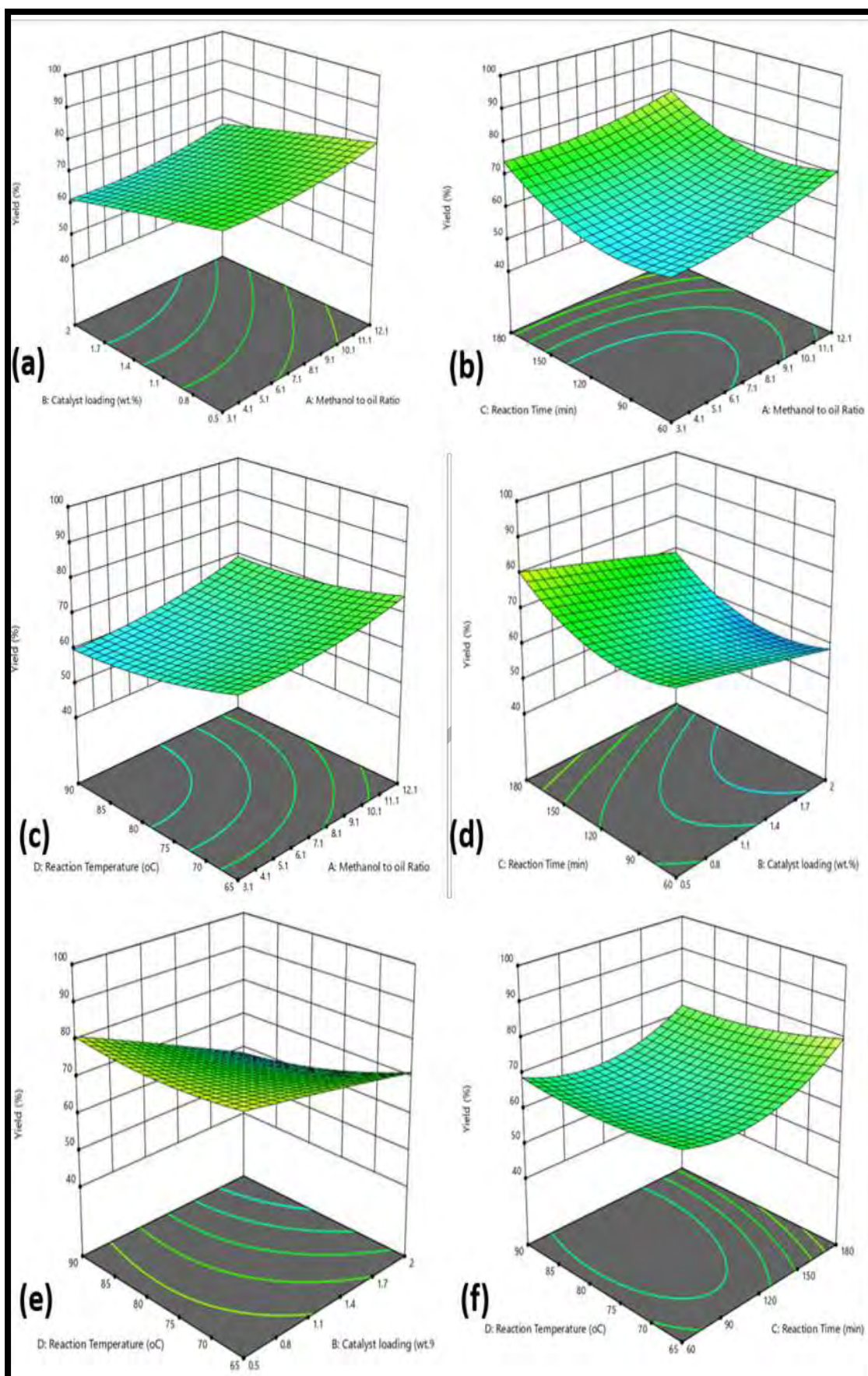
Figure 3.5.8: Influence of reaction variables on LABD
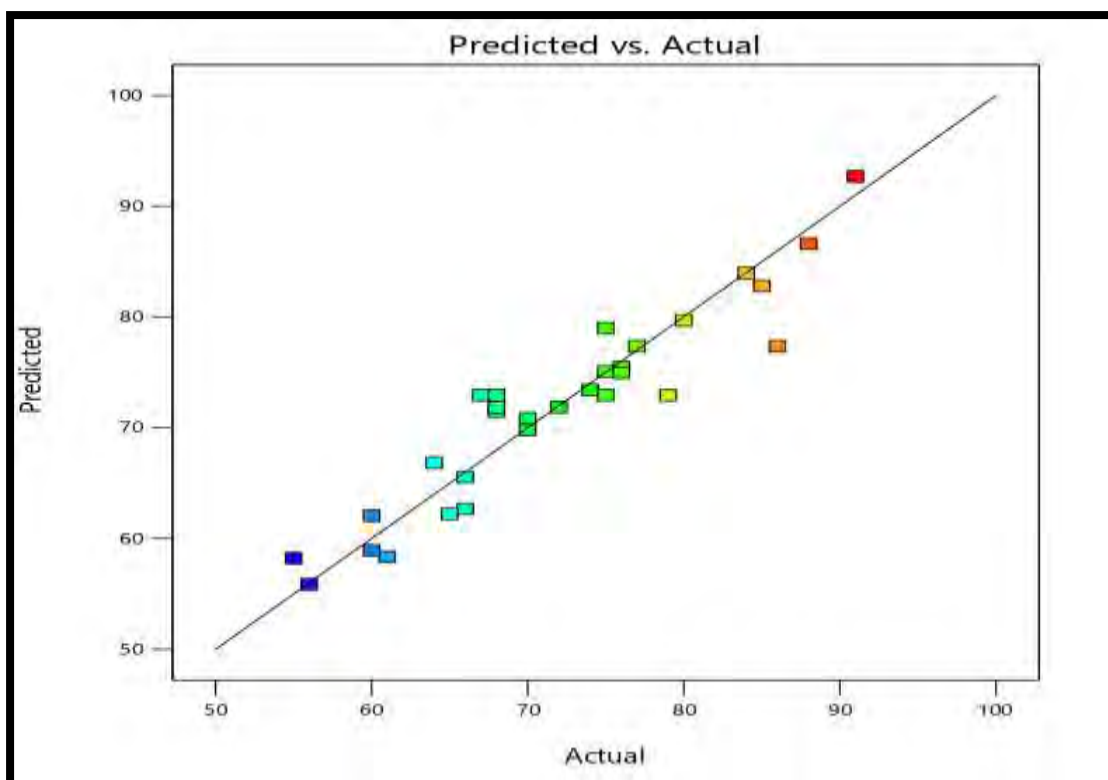
Figure 3.5.9: Predicted yield vs actual yield of LABD

Table 3.5.1: Fuel properties of LABD

TESTS	METHOD	LA B-100
Color	Visual	2
Density @ 15 °C Kg/L	ASTM D-1298	0.8722
Kinematic Viscosity @ 40 °C c St	ASTM D-445	5.45
Pour point °C	ASTM D-97	-13
Flash point °C(PMCC)	ASTM D-93	90
Cloud point °C	ASTM D-2500	-9
Total Acid No. mg KOH/gm	ASTM D-4294	0.246
Sulphur % wt.	ASTM D-974	0.00432

Table 3.5.2: Experimental yield of LABD

Run	Methanol to Oil Molar Ratio	Catalyst Loading (wt. %)	Reaction Time (min)	Reaction Temp. (°C)	LABD Yield (%)
1	3.1	1.25	120	77.5	60
2	12.1	2	180	77.5	
3	12.1	1.25	180	65	70
4	7.1	1.25	120	77.5	57
5	7.1	0.5	180	65	72
6	7.1	1.25	180	65	88
7	3.1	1.25	120	65	76
8	3.1	0.5	120	65	67
9	12.1	0.5	60	90	80
10	7.1	0.5	120	65	58
11	12.1	0.5	180	90	75
12	12.1	2	180	90	57
13	12.1	1.25	120	77.5	60
14	12.1	0.5	60	65	55
15	3.1	2	180	65	65
16	3.1	2	180	77.5	50
17	12.1	2	60	65	58
18	7.1	1.25	120	90	66
19	3.1	1.25	180	77.5	69
20	3.1	0.5	60	90	58
21	3.1	0.5	180	90	77
22	7.1	2	60	65	70
23	12.1	2	120	65	73
24	7.1	1.25	120	65	65
25	3.1	0.5	180	65	93
26	12.1	2	180	65	85
27	12.1	0.5	180	65	85
28	3.1	0.5	60	65	67
29	7.1	0.5	180	77.5	87
30	12.1	1.25	60	65	65

Table 3.5.3: Analysis of Variance (ANOVA) of LABD

Source	Sum of Squares	df	Mean Square	F-value	p-value	
Model	2547.61	14	181.97	2.98	0.0021	significant
A-Methanol to oil Ratio	313.78	1	313.78	5.14	0.0386	
B-Catalyst loading	486.31	1	486.31	7.96	0.0129	
C-Reaction Time	225.32	1	225.32	3.69	0.0140	
D-Reaction Temperature	34.00	1	34.00	0.5566	0.0472	
AB	0.0002	1	0.0002	3.457E-06	0.0385	
AC	25.98	1	25.98	0.4253	0.0242	
AD	9.73	1	9.73	0.1594	0.0454	
BC	13.11	1	13.11	0.2147	0.0498	
BD	47.49	1	47.49	0.7775	0.0318	
CD	20.12	1	20.12	0.3295	0.5745	
A²	95.39	1	95.39	1.56	0.2306	
B²	3.72	1	3.72	0.0610	0.0083	
C²	15.13	1	15.13	0.2477	0.2259	
D²	0.0584	1	0.0584	0.0010	0.3757	
Residual	916.26	15	61.08			
Lack of Fit	575.26	8	71.91	1.48	0.3105	not significant
Pure Error	341.00	7	48.71			
Cor Total	3463.87	29				

SECTION: VI

Biodiesel Synthesis from *Diospyros lotus* Using Nickel Oxide Green Nano-catalyst

3.6. Biodiesel Synthesis from *Diospyros lotus* Using Nickel Oxide Green Nano-catalyst

3.6.1 Characterization of Nickel Oxide Green Nano-catalyst

(a) XRD of NiO

XRD is a quick analytical method for determining crystalline phase of material. The phenomena of monochromatic X-ray interference on crystalline material is done by XRD. The XRD spectrum of nickel oxide green nano-catalyst is shown in Figure 3.6.1. This spectrum reveals that the nano-catalyst that was created is crystalline with three diffraction peaks being intense and sharp, found at 37.43° (111), 43.4°(200), and 62.89°(220), hence the green nickel oxide nano-diffractogram demonstrates face-centered cubic phase of the particles and that the lattice disorder as well as Oxygen vacancies are responsible for appearance of broad peak in XRD spectrum. Debye Scherer eq. used to estimate NiO crystal size at (200) plane. The nanoparticles appeared to be 18 nm in size. This is because extract contains a number of phytochemicals that have potential reducing and capping properties, resulting in the formation of green nano-metal oxides. Recently XRD study by Ezhilarasi *et al.*, (2018) reported phase-centered cubic phase and crystalline structure of green NiO nanparticles (Ezhilarasi *et al.*, 2018)

(b) SEM of NiO

To study shape and surface morphology of prepared green nickel oxide, SEM was implicated. Figure 3.6.2 portrays the NiO nano-catalyst general shape, external structure and appearance at various resolutions. The findings demonstrate that the particles are noticeable agglomerized with cubic and spherical shapes, which supports the presence of magnetic interactions and polymeric adherence between nanoparticles (Ezhilarasi *et al..*, 2018). According to another study by Panday and Manivannan (2015) comprising synthesis of green NiO nanoparticles that were 200 nm in size and had an agglomerated shape (Pandey & Manivannan, 2015). Gebretinsae *et al..* (2021) took SEM images of NiO biosynthesized from cactus plant extract, the nanoparticles were spherical with some degree of agglomeration, which may be related to the high surface energy and high surface tension of NiO nanoparticles (Gebretinsae *et al.*, 2021). The NiO NPs produced by *Euphorbia heterophylla* were observed by Lingaraju *et al..*

(2020) via the scanning electron microscope and found rhombohedral NiO nanoparticle that were agglomerated together with other particles on the surface (Lingaraju *et al..*, 2020).

(C) EDX of NiO

In conjunction with SEM, EDX is employed and On passing the beam of electrons across the object, any constituent may be seen individually. Digital image often involves few hour shifts because of the weak X-ray intensity. The EDX can be used to figure out the composition or mass of particular metallic ions existing with in nanocrystals close to and along the exterior. (Titus *et al..*, 2019)

As demonstrated in Figure 3.6.3, nickel oxide phytonano-catalyst clearly identified two distinct elements, 60.25% nickel and 39.75% oxygen were found in the nickel oxide nano-catalyst after an elemental analysis. According to the results of the EDX examination, the created nano-catalyst is in a highly purified state and is suitable for use in the transesterification that catalyze the reaction effectively. By using EDX analysis, former researchers investigated the purity and chemical make-up of the produced green NiO nanoparticles (Anand *et al..*, 2020; Ezhilarasi *et al..*, 2018; Singh *et al..*, 2022).

(d) FT-IR of NiO

Strong peaks appeared at 514.29 cm^{-1} and 551.20 cm^{-1} demonstrate the presence of stretching vibration of nickel oxide, in the biosynthesized green nano-catalyst (Suresh *et al..*, 2018). The C-O bond stretching and bending mode revealed by strong absorption (1013.27 cm^{-1}). Because extract contains a number of phytochemicals causes stretching vibration, as the peak at 1607.14 cm^{-1} matches to aromatic constituent (-C=C-).The hydroxyl group, demonstrates water molecules' adsorption on surface of nano-catalyst, is seen in the stretching band at 3532.65 cm^{-1}. The adsorption of water by the nano-catalyst demonstrates the significant increase in surface area of the produced NiO.

Hence, the achieved FT-IR outcomes being consistent to XRD as well as EDX, eventually supports green synthesis of a highly pure NiO. The FT-IR of synthesized NiO phytonano-catalyst is shown in Figure 3.6.4.

3.6.2 Characterization of *Diospyros lotus L.* Biodiesel (DLBD)

(a) FT-IR of DLBD

FT-IR is a potential approach for verifying the identity of pure chemicals, however it is not particularly effective for compound mixtures. The method is based on the discovery of functional groups within molecules, where these groups vibrate (either through stretching or bending in different ways) when exposed to particular light wavelengths. A FT-IR spectrum is created by plotting the frequency of light (cm^{-1}) to which the material is subjected against the vibration intensity (% transmission). The substance under test-specific portions i.e. fingerprint region of the FT-IR spectrum. By means of the mid-IR area, FT-IR analysis is utilized to identify a number of constituents in substance under study (Chandravanshi *et al.*, 2022). Spectrum showing various stretching vibrations that correspond to the production of FAME, were seen. The distinctive peaks seen at 2922.80 cm^{-1} and 2853.38 cm^{-1} indicate the presence of methyl groups and alkane groups, respectively (Figure 3.6.5). The carbonyl group results in two high peaks at 1743.34cm^{-1} as well as 1159.46cm^{-1} representing C-O stretching vibration of esters (Bukkarapu & Krishnasamy, 2021) that was identified with an IR shift. This specific peak denotes the transformation of DLSO into biodiesel. Peak of 1463.91cm^{-1} represents the presence of the alkane group (C-H), At 1098.63 cm^{-1}, the aliphatic amine group was detected. The presence of carboxylic acid is confirmed by the medium-sized peak at 1098.63 cm^{-1} (O-H), A band, 721.61cm^{-1},besides, denotes alkane group (C-H), respectively (Ahmad *et al.*, 2022; Bukkarapu & Krishnasamy, 2021).

. **(b) GC-MS of DLBD**

A synthesized biodiesel sample is subjected to GC-MS in order to quantify as well as characterize the different esters. In GC-MS chromatogram for DLBD (Figure 3.6.6), various peaks of FAME can be seen, identified via comparison with software i.e. default NIST-11. The fuel chromatogram revealed the presence of six methyl fatty acids esters (peak 3, 6,7,8,9,13, 14), such as Methyl palmitate($C_{17}H_{34}O_2$), Methyl octadeca-2,4-dienoate($C_{19}H_{39}O_2$), Methyl 9-octadecenoate($C_{19}H_{34}O_2$), Methyl stearate($C_{19}H_{38}O_2$), 9-Octadecenoic acid($C_{19}H_{36}O_2$), Methyl 12 hydroxy methylesters ($C_{19}H_{36}O_3$), 13-Docosenoic acid methyl ester ($C_{23}H_{44}O_2$) were detected with retention time 23.542, 25.344, 25.709, 25.798, 26.090, 28.073, 30.33 minutes. Hence, *Diospyros*

lotus biodiesel (DLBD) was confirmed by all of the peaks discussed above (Munir *et al..*, 2020; Ameen *et al..*, 2022; Shaheen *et al..*, 2018).

(c) NMR of DLBD

NMR is chemical characterization technique typically established on basis of external radiation radiofrequency and nuclear interaction. Nuclear spin shift results from the net energy exchange that occurs during this interaction. ^{1}HNMR clarifies type of H-atom and is determined by chemical shift, integration yields results for each type of H atom and splitting reveals which H atoms (and how many) exist on adjacent C atoms. The largest importance is displayed by the methoxy signals (between 5.25 and 5.50 ppm) and the characteristic peak for biodiesel at 3.6ppm followed by the aliphatic signals (below 3.0 ppm) in a full spectrum (between 0.4 and 9.0 ppm) (Portela *et al..*, 2016). Figure 3.6.7a shows the ^{1}H-NMR spectra of DLBD with the following chemical shifts (ppm): 0.805(t,-CH3), 1.680(m,-CH2-CH2-), 2.794(t,-CH2-COO-), 5.205(t, -CH=CH-), and strong signal indicating –OCH$_3$ at 3.667ppm. The peak position is consistent with earlier research (Ameen *et al..*, 2022; Islam *et al..*, 2022). Despite the fact that ^{1}H NMR makes it possible to identify the mono-, di-, and triacetin components of glycerol, not all of the molecules may be detected and quantified simultaneously because of overlapping signals. Thus, the detection and quantification of these compounds using ^{13}C NMR becomes the most suited method (Portela *et al..*, 2016).

Figure 3.6.7b represents ^{13}C-NMR spectrum that displays the following distinctive signals and chemical shifts: (ppm): 29.49 (-CH2-)n, 77.49 (-C-O), 129.85 (-CH=CH-), and 174.63 (-COO-). 51.07 (-O-CH3). The signals for the aliphatic methylene carbons (-CH2-s) range from 34.02-27.26 ppm and –CH$_3$ signal in the terminal chain is at 25.55 ppm. Hence, both ^{1}HNMR and ^{13}C-NMR proved the specifications of *Diospyros lotus* L. biodiesel as high quality fuel.

3.6.3 Biodiesel Yield Optimization via Response Surface Methodology

RSM was used to construct 3D graphs to show the overall impact of reaction parameters (Figure 3.6.8 a-f). Such graphs understand how diverse factors interact collectively, therefore they determine the ideal limits of each parameter for peak response as detailed in the following subsections (Table 3.6.2)

The transesterification process frequently employs reaction parameters. It is necessary to examine the perfect conditions for the highest quality biodiesel. Transesterification parameters, such as the Methanol/Oil of 3:1–16:1 (A), the catalyst concentration (0.5-2wt. %) (B) Time (1–3h) (C), the temp. 50–80 °C (D), design of our current study was created by DOE (Design of Experiment). The comparison of the transesterification yield (predicted/actual) is shown in Figure 3.6.9. The distribution of points is discovered to be close to line, indicating strong connection between them. The outcome of response surface quadric model statistical analyses ANOVA are presented in Table 3.6.3. A low p-value of (0.0041) indicated, significant quadric model. The lack of fit F-value of experimental model, 0.7819, statistically insignificant compared with pure error. The good lack of fit value for the quadric model is one that is not statistically significant, and there is a 78.19% possibility that noise may cause such a huge lack of fit F-value. According to the results in Table 3.6.3, this was estimated that the R2 value would be 0.5269, which is closer to the adjusted R2 value of 0.6807 with a variance of 0.2. The appropriate precision was discovered to be more than 4. (5.8689). the current experimental model higher degree of allowable precision demonstrated how well it can be used to the estimation yield. The quadric model use of the given polynomial equation.

Yield $= +82.66 + 2.38*A + 4.65*B - 3.75*C + 0.2700*D + 1.90*AB + 9.78*AC + 14.01*AD + 7.86*BC - 3.57*BD - 7.91*CD - 3.34*A^2 - 12.73*B^2 - 8.06*C^2 - 2.82*D^2$ **(9)**

3.6.3.1 Interaction between methanol to oil molar ratio and catalyst loading

Significant reaction parameters that affect the transesterification step of the biodiesel synthesis process are the Methanol/Oil and catalyst conc. (AB). Process to convert oil or fat into biodiesel is accelerated by using excess of methanol. Mutual interaction of catalyst and Oil/Methanol are showed in a 3D Figure 3.6.8a. The maximum yield (87%) was attained at 9:1 (Methanol/Oil) with 1.25 wt. % catalyst (run 6) while keeping other parameters constant with 2 h and 65°C. Due to alcohol potential to convert triglycerides into mono glycerides, it has been found that the yield increases with high alcohol content; however, this effect only persisted up to a certain point, and any additional addition of methanol past this point significantly reduced the yield of biodiesel (Rehan *et al*., 2018). Low yield of 55% was achieved with high catalyst of 1.25 weight percent and Methanol/Oil 16:1 (Run 30). Excess methanol causes the reaction to move toward the unfavourable condition of transesterification, speeding up

the reverse reaction and resulting in a low yield of methyl ester as a result (Mofijur *et al..*, 2021; Ong *et al..*, 2020). It was discovered that a 3:1 Methanol/Oil and a 1.25 weight percent catalyst were insufficient to carry out biodiesel synthesis, and a drop in the percentage yield of biodiesel up to 80% was seen (Run 19). When molar ratio was kept at two extreme limits i.e. 3:1 and 16:1 and catalyst load at minimum optimal level 0.5 wt. %, a sudden drop in biodiesel yield to 65% and 66% in run 21 and 27 respectively. This decline can be explicated by less active sites availability for reactants and also by reduced or amplified methanol content. Lower molar ratios are insufficient to drive transesterification however higher molar ratios make the product separation a difficult task and favor the reversible reaction of glycerolysis. When both molar ratio and catalyst were increased to the maximum i.e. 16:1 and 2 wt. %, biodiesel yield decreased to 60% for two reasons; glycerolysis and saponification (run 25). Our current investigation indicated that the combined influence of the Methanol/Oil and catalyst concentration was significant for the synthesis of methyl esters with a p-value (0.0345) < 0.05.

3.6.3.2 Interaction between oil to methanol molar ratio and reaction time

As a fundamental optimization parameter, the Methanol/Oil and the time (AC) both jointly affect the FAME production. Figure 3.6.8b illustrates the interactive influence. The highest yield (87%) was achieved at 9:1 (Methanol/Oil) and 2 h time and maximum yield was achieved (run 3). It was noticed the yield increases initially with increase in molar ratio and time but up to certain limit it goes on decreasing. With collective decrease in Methanol/Oil and time to minimal set limit i.e. 3:1 and 1 h respectively by keeping other parameters constant, just 68% methyl ester yield was achieved. Because a transesterification reaction requires a sufficient chemical interaction between oil and alcohol, an acceptable time is necessary to enable efficient mixing with proper stirring at constant rate (Naveenkumar & Baskar, 2020).

After a specific limit was exceeded, even a high molar ratio (16:1) and prolonged time (3 h) preferred reversible reaction, and 68 % biodiesel yield was produced (run 18). ANOVA results show a p-value of 0.0125 <0.05, hence the combined effect of Methanol/Oil and time on biodiesel yield was found to be significant.

3.6.3.3 Interaction between methanol to oil molar ratio and reaction temperature

Figure 3.6.8c shows the mutual influence of temperature and Methanol/Oil. At a 9:1 Methanol/Oil, a reaction temperature of 65 °C, a constant reaction period of 2 h, and a catalyst concentration of 1.25 wt. %, the percentage yield of biodiesel was found to be 87 % (run 3). A lower yield (78 %) was obtained with the same Methanol/Oil and temperature drop (50 °C) (run 17). It is ascribed to the oil, methanol, and catalytic compact mass transfer rate because all three components are immiscible at low temperatures and require adequate kinetic energy to react properly and increase productivity in a shorter amount of time. With a 3:1 Methanol/Oil and an ambient temperature of 80°C, produced a noticeably low yield of methyl ester (55%) because there was not enough methanol present perform transesterification and the higher temperature caused the methanol to vaporize (run 28). A rise of Methanol/Oil up to 16:1 and lowering temp. to 50 °C led to production of 65% biodiesel (Run 9), due to enhanced solubilization of the reactants and the low kinetic energy of reactant molecules at lower temperatures. Similar findings have already been reported (Li *et al.*, 2019). With a p-value of 0.0451 (>0.05), Methanol/Oil and temperature interactive effect was determined to be significant.

3.6.3.4 Interaction between catalyst loading and reaction time

The amount of catalyst and time (BC) interaction has been mention as 3D RSM graph Figure 3.6.8d. A highest yield (87%) obtained via 1.25 wt. % catalyst and 2 h time (run 6). Under the constant conditions of 9:1 molar ratio, 2 h of time, and 65 °C, a considerable reduction in biodiesel output to 83 and 70 % was seen when catalyst amount was decreased or increased above the optimal level (1.05wt %) to 0.5 wt. % (minimum) and 2 wt. % (maximum) in run 2 and 24 respectively. The decline can be explained by low catalytic concentration that offered less availability of catalytic sites for transesterification and excess of catalyst triggered a side reaction of saponification. As amount was elevated to 2 wt. % and the time was increased to 3 h, while maintaining other parameters constant, a striking reduction in the biodiesel yield (73 %) was observed. This sudden reduction is attributed to the long duration provided to the reaction mixture that initiated reversible transesterification (run 29). The similar results were supported by earlier study, when low product yield recorded in less given time (Elkelawy *et al.*, 2019). Decreasing the catalyst to 0.5 wt. % and time to 1 h resulted

in just 57 % biodiesel yield (run 26). Because efficient mixing with an adequate time is necessary to ensure the transesterification reaction, the oil and alcohol must be stirred properly and at a steady rate. ANOVA results show the significant mutual influence of catalyst and time (p-value < 0.05) i.e. 0.0238.

3.6.3.5 Interaction between catalyst loading and reaction temperature

A 3D plot shows the overall interactive relationship of catalyst and temp. (BD) (Figure 3.6.8e). The maximum biodiesel yield (87%) was achieved with 1.25 wt. % catalyst and 65 °C. By keeping optimization parameters constant (9:1 molar ratio and 2 h time) with catalyst amount (0.5 wt.%) resulted in yield declination to 79 % and 57% in run 1 and 4 respectively. Because both extreme adjusted temperatures i.e. 50 °C and 80 °C do not favor the transesterification reaction. However, when both catalyst conc. and temperature were increased from 1.25 wt. % to 2 % and temperature from 65 to 80°C respectively, just 54 % yield was achieved (run 54). The reason is saponification and methanol evaporation. Increased catalyst and temperature are evidently speeding up hydrolysis and consequential $-CH_3OH$ and a diminishing percentage yield of biodiesel. ANOVA results show their significant mutual effect by having p-value (<0.05) i.e. 0.0254.

3.6.3.6 Interaction between reaction time and reaction temperature

The relationship between temperature and time (CD) has been mentioned as a 3D RSM graph (Figure 3.6.8f) while keeping both molar ratio and catalytic load constant at 9:1 and 1.25 wt. % respectively. The maximum biodiesel yield (87%) was achieved in 2 h and 65 °C. However, when temperature is decreased to 50°C with 3 h time, a decline in conversion percentage (65%) was observed (run 14). When the reaction parameters (time and temperature) were set at lower extremities, i.e. 1 h and 50 °C, a considerably low yield (69%) was recorded (run 23). Improper mixing of three fundamental components; catalyst, methanol, and oil due to inadequacy of process time, resulted in low yield. Moreover, viscosity of oil is high at low temperatures and the reactant molecules cannot change into their desired products due to limited kinetic energy and a short time. However with an increase in temperature up to 80°C, a conversion yield of 50% was obtained in even 3 h of time (run 7). Although reactant molecules have enough time to collide and convert in to products but reversible transesterification is initiated that decreases the biodiesel yield. Moreover, high

temperature (80°C) causes methanol vaporization and hinders the forward reaction of biodiesel production. P-value of 0.0185 < 0.05, according to the ANOVA results, exhibited this good correlation.

3.6.4 Fuel Properties of DLBD

Diospyros lotus L. biodiesel fuel properties were checked according to ASTM procedures and the findings are shown in Table. 3.6.3. The result showed that the DLBD Flash point is 90°C when the ASTM D-93 flash point technique was applied. Because it has a higher flash point than petroleum diesel, hence biodiesel is safer to use, transport, and store. According to ASTM D-1298 test procedure, the density for DLBD was determined to be 0.8643 Kg/L. Biodiesel density typically fluctuates within constrained ranges of 0.86 and 0.90 g/cm3. The kinematic viscosity of DLBD was found to be 5.46cSt. and it falls in the ASTM 1.9-6.0 cSt values at 40 °C. According to ASTM D-97 testing procedure, the pour point or freezing point of biodiesel is -12 °C. Since DLBD has a substantially lower pour point, it is significantly viable in cold climates. Furthermore, the pour point of DLBD is in the range of -15 to 16°C when compared to ASTM D 6751. The cloud point was determined to be -11°C using the ASTM D-2500 technique. Biodiesel is regarded as sustainable fuel because to its minimal Sulphur content. According to ASTM D-4294, sulphur (% wt.) was tested and found to be 0.0004. The ASTM D-974 method was used to test the total acid number, and the findings showed that is 0.247 mg KOH/gm. This number is much below 0.8 and falls within the acceptable range of ASTM D-6751, or 0.8. The *Diospyros* lotus L. biodiesel entire fuel profile complied with all applicable international biofuel criteria.
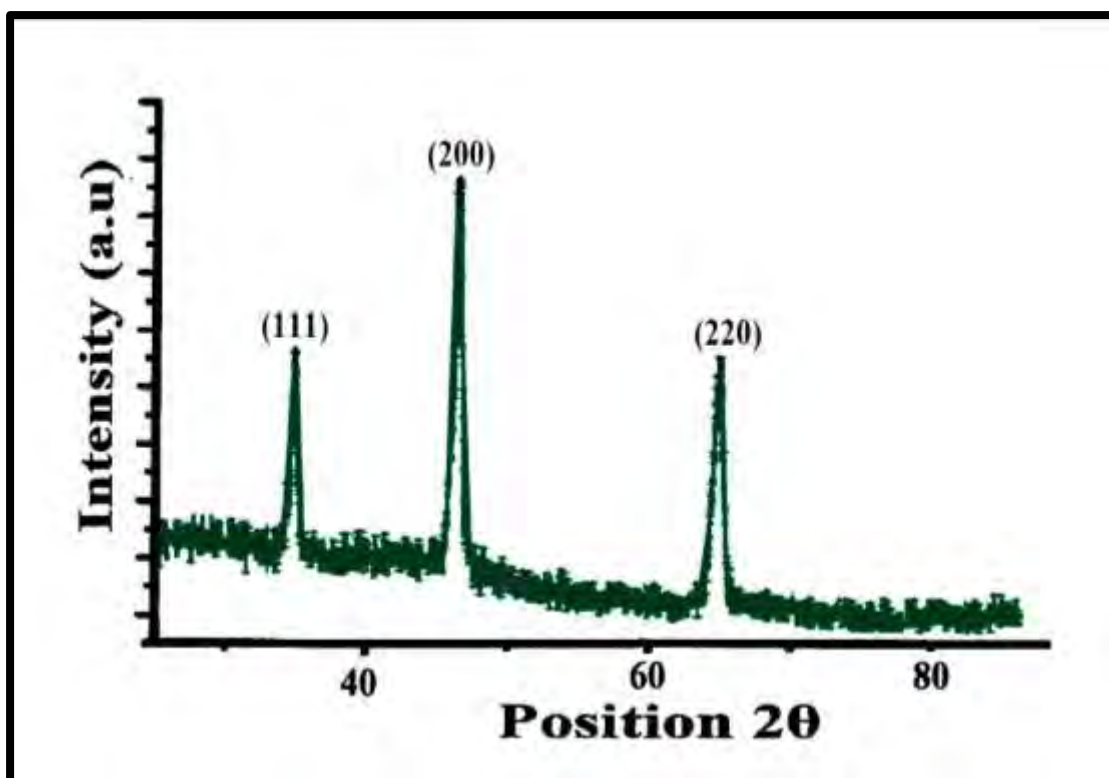
Figure 3.6.1: XRD of NiO green nano-catalyst
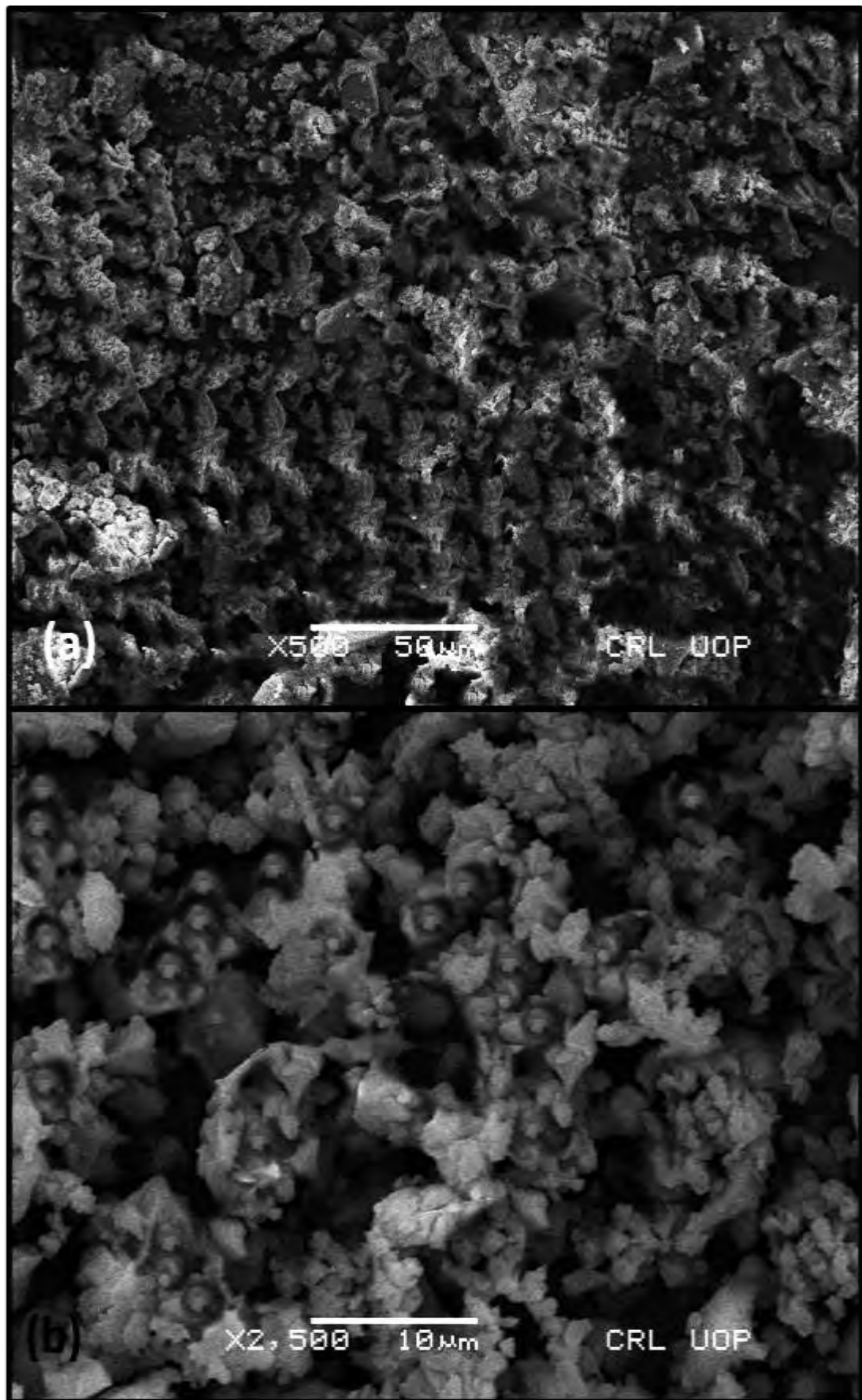
Figure 3.6.2: SEM of NiO green nano-catalyst
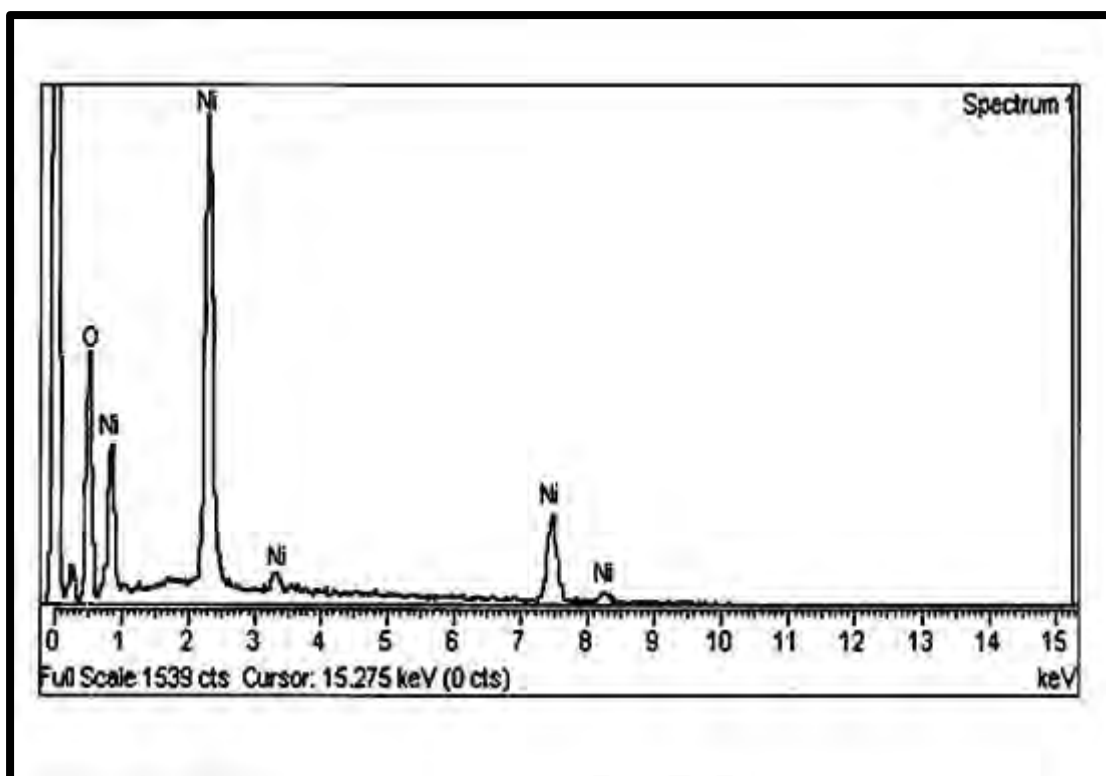
Figure 3.6.3: EDX of NiO green nano-catalyst
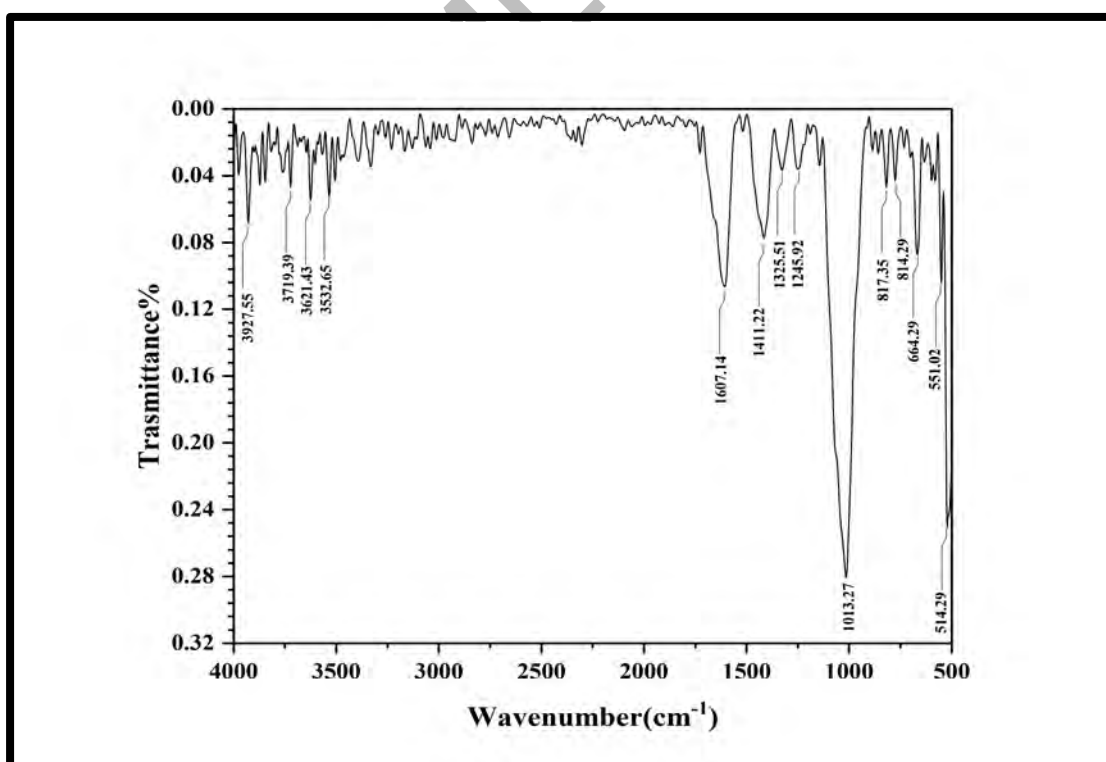
Figure 3.6.4: FT-IR of NiO green nano-catalyst
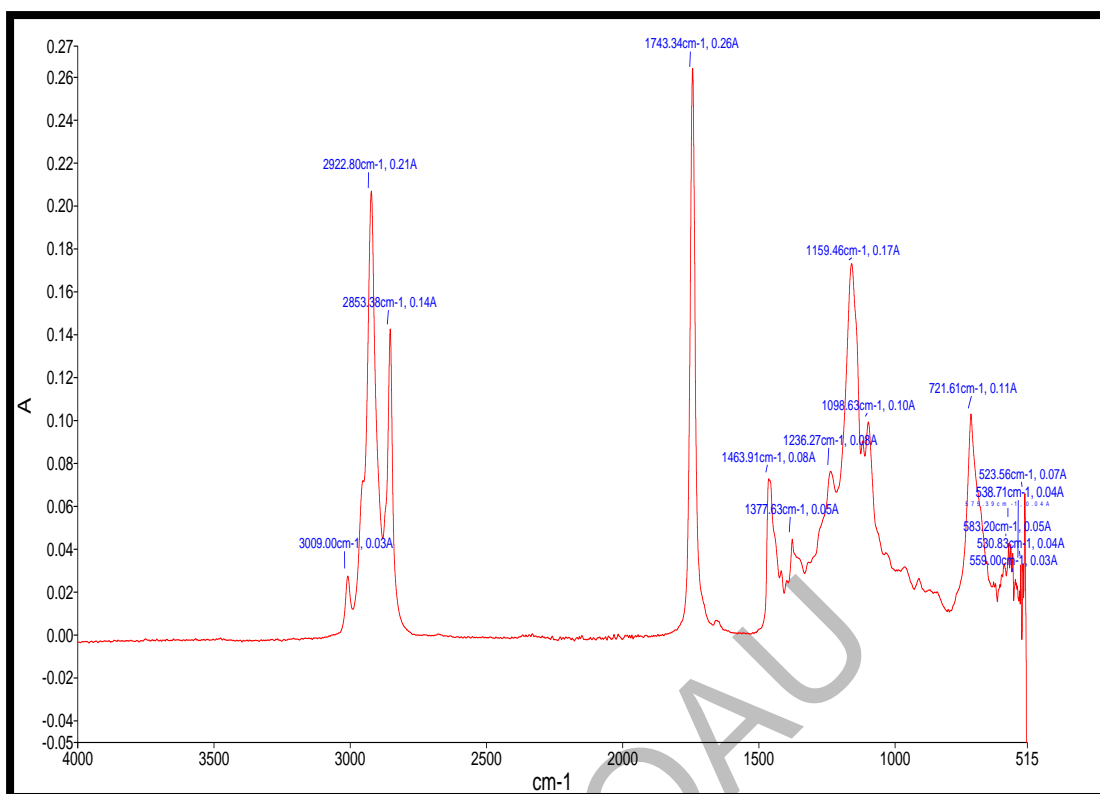
Figure 3.6.5: FT-IR spectrum of DLBD
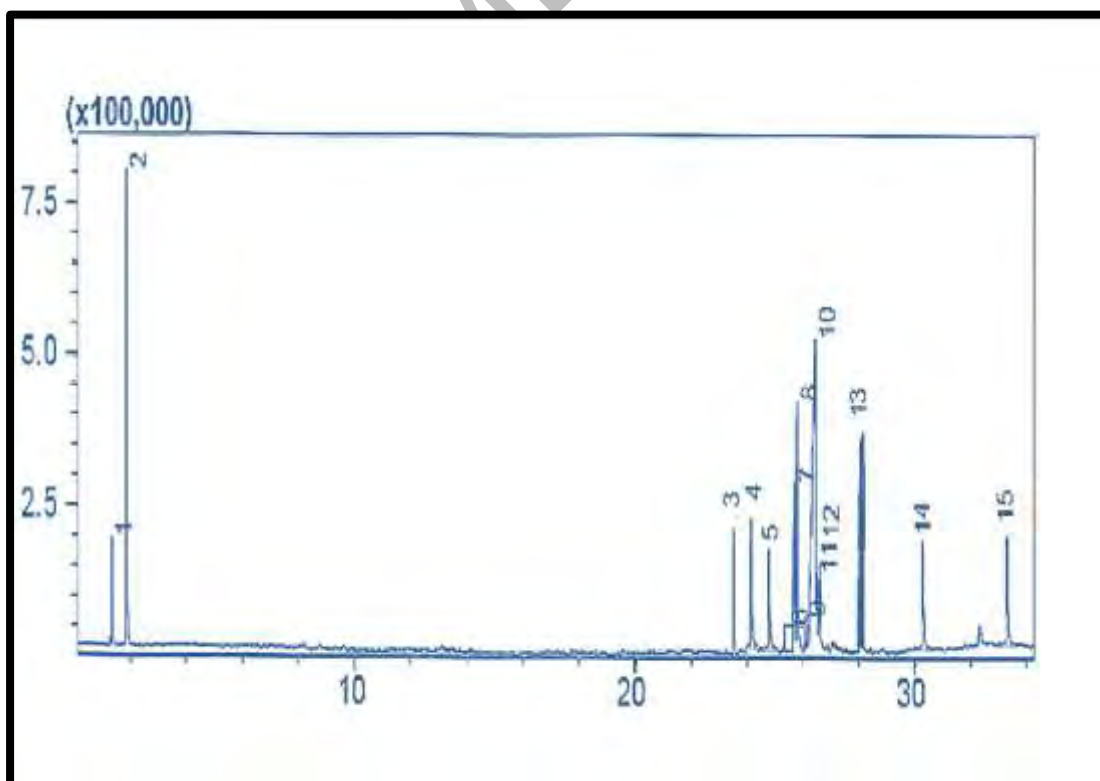
Figure 3.6.6: GC-MS spectrum of DLBD
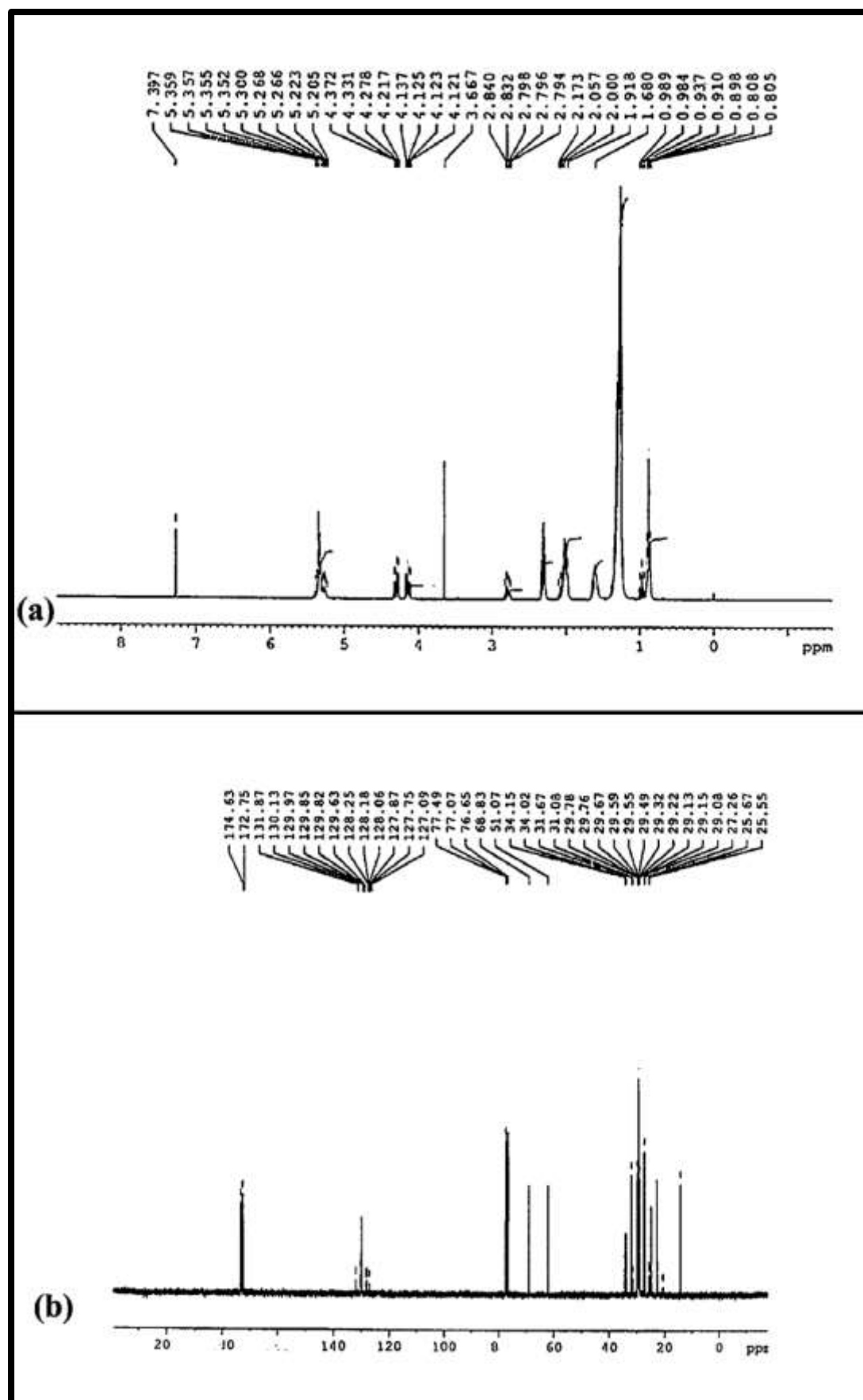
Figure 3.6.7: (a) ¹HNMR (b) ¹³CNMR spectra of DLBD
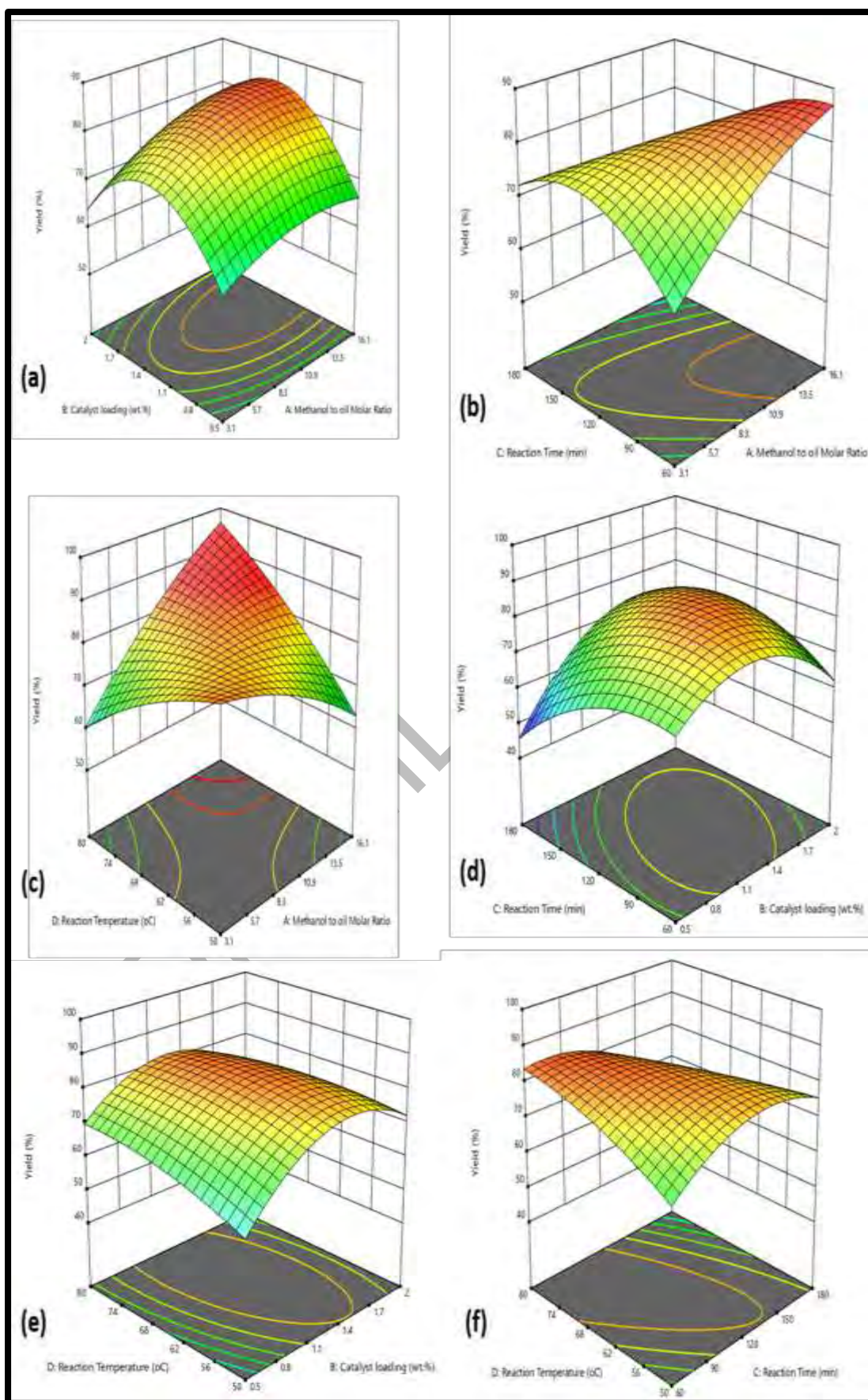
Figure 3.6.8: Influence of reaction variables on DLBD
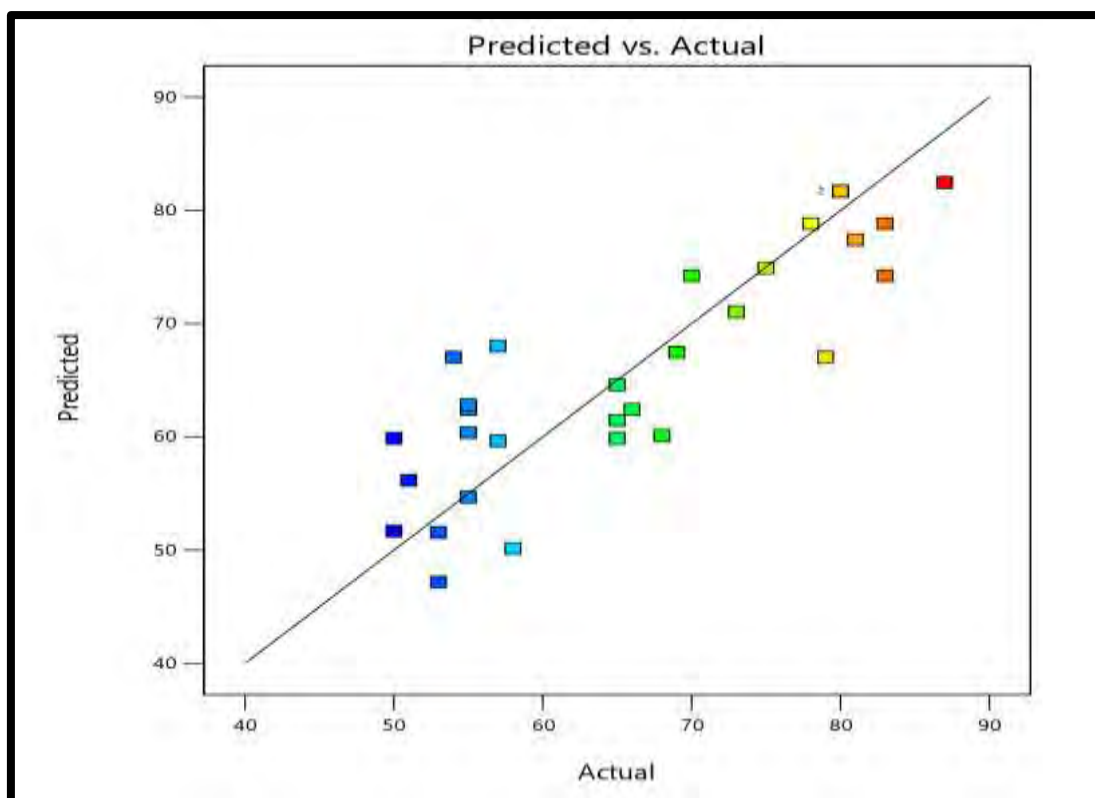
Figure 3.6.9 Predicted vs. actual yield of DLBD

Table 3.6.1 Fuel Properties of DLBD

TESTS	METHOD	DL B-100
Color	Visual	2
Flash point °C(PMCC)	ASTM D-93	90
Density @ 15 °C Kg/L	ASTM D-1298	0.8643
Kinematic Viscosity @ 40 °C cSt	ASTM D-445	5.46
Pour point °C	ASTM D-97	-12
Cloud point °C	ASTM D-2500	-11
Sulphur % wt	ASTM D-4294	0.0004
Total Acid No. mg KOH/gm	ASTM D-974	0.247

Table 3.6.2: Experimental yield of DLBD

Run	Methanol to Oil Molar Ratio	Catalyst Loading (wt. %)	Reaction Time (min)	Reaction Temp. (°C)	DLBD Yield (%)
1	9.1	0.5	120	80	79
2	9.1	0.5	120	65	83
3	16.1	2	60	50	50
4	9.1	0.5	120	50	57
5	3.1	2	60	50	53
6	9.1	1.25	120	65	87
7	9.1	1.25	180	80	50
8	16.1	0.5	60	50	53
9	16.1	1.25	120	50	65
10	9.1	2	120	80	54
11	9.1	1.25	120	80	83
12	9.1	1.25	60	65	81
13	16.1	2	180	50	51
14	9.1	1.25	180	50	65
15	3.1	1.25	180	65	75
16	3.1	1.25	60	65	55
17	9.1	1.25	120	50	78
18	16.1	1.25	180	65	68
19	3.1	1.25	120	65	80
20	3.1	0.5	60	80	58
21	3.1	0.5	120	65	65
22	3.1	0.5	60	50	55
23	9.1	1.25	60	50	69
24	9.1	2	120	65	70
25	16.1	2	120	65	60
26	9.1	0.5	60	65	57
27	16.1	0.5	120	65	66
28	3.1	1.25	120	80	55
29	9.1	2	180	65	73
30	16.1	1.25	120	65	55

Table 3.6.3 Analysis of Variance (ANOVA) of DLBD

Source	Sum of Squares	df	Mean Square	F-value	p-value	
Model	2952.33	14	210.88	2.92	0.0041	significant
A-Methanol to oil Molar Ratio	47.07	1	47.07	0.6511	0.0323	
B-Catalyst loading	194.34	1	194.34	2.69	0.0219	
C-Reaction Time	128.12	1	128.12	1.77	0.0030	
D-Reaction Temperature	0.6038	1	0.6038	0.0084	0.0284	
AB	22.58	1	22.58	0.3124	0.0345	
AC	292.82	1	292.82	4.05	0.0125	
AD	345.28	1	345.28	4.78	0.0451	
BC	147.41	1	147.41	2.04	0.0238	
BD	48.53	1	48.53	0.6713	0.0254	
CD	119.23	1	119.23	1.65	0.0185	
A²	44.12	1	44.12	0.6103	0.0468	
B²	857.65	1	857.65	11.86	0.0036	
C²	178.98	1	178.98	2.48	0.0365	
D²	26.90	1	26.90	0.3721	0.0510	
Residual	1084.34	15	72.29			
Lack of Fit	501.84	9	55.76	0.5744	0.7819	not significant
Pure Error	582.50	6	97.08			
Cor Total	4036.67	29				

SECTION: VII

Biodiesel Synthesis from *Cucumis melo* var. *cantalupensis* Using Calcium Oxide Green Nano-catalyst

3.7. Biodiesel Synthesis from *Cucumis melo* var. *cantalupensis* Using Calcium Oxide Green Nano-catalyst

3.7.1 Characterization of Calcium Oxide Green Nano-catalyst

(a) XRD of CaO

A non-destructive analytical method for analyzing crystalline materials based on their diffraction pattern is X-ray diffraction (XRD). Crystal orientations (texture), ideal crystal structures, phase identification, and other structural features such as grain-size estimation, crystallization degree, strain, and crystal defects, are among the information it produces. The CaO nano-crystalline and structural state determined by means of the XRD and sample displayed a high degree of crystalline structure.

Fig. 3.7.1 shows the XRD pattern, which has sharp peaks at 2θ values and corresponding to the lattice plane, of 34.8° (111), 38.30° (200), 53.80° (202), and 64.07° (311) (JCPD 77–9574). A 35nm size of CaO nano-catalyst showing the characteristic of green nano-particles with large surface area (Attari *et al..,* 2022; Das *et al..,* 2020; Gaurav & Sharmac; Velusamy *et al..,* 2021).

(b) SEM of CaO

The surface morphology of CaO was examined via SEM at magnifications of 5 and 10µm. A SEM image of a CaO nano-catalyst shows its shape to be square and cubic (Figure 3.7.2). The polarity of nanoparticles and electrostatic attraction are responsible for the little aggregation of particles that may be seen in micrographs. Additionally, different particle sizes showed that nanoparticles have more active sites and a larger surface area for carrying out the transesterification activity (Ramli *et al..,* 2019).

Such analytical test was performed to examine the morphological characteristics, diameter, porous nature, and form of the synthesised calcium oxide by Ramli *et al..* (2021). This process was mediated by the *Hylocereus Polyrhizus* and the biosynthesized CaO had fiber-like particle shapes, and their diameters ranged from 50 to 121 nm on average, with an average of 81.45 nm, allowing them to be categorised as nanoparticle materials (100 nm) (Ramli *et al..,* 2019).

(c) EDX of CaO

A microanalysis technique referred as EDX is used to identify nanoparticles based on the generation of distinct X-Rays. EDX does not qualify as a surface science method because the X-rays are produced in a zone that is only a few microns deep X-ray energy diffraction employed to analyze elemental constituency of CaO nanoparticles (NPs) (Titus *et al..*, 2019; Zul *et al..*, 2021).

EDX of CaO-NPs is shown in Figure 3.7.3. Peaks in the EDX spectrum at 0.3, 3.8, 4.0 and 0.6 keV are linked to binding energies of Ca and O respectively. The purity of the CaO nanoparticles that were manufactured was demonstrated by the EDX results, which showed that there was no extra element in the spectrum. Calcium has an atomic percentage of 70.51 (w/w %) compared to oxygen atomic percentage of 39.49 (w/w %).

(d) FT-IR of CaO

One effective method for giving a fundamental understanding of molecular vibrations or transitions in vibrational modes is FT-IR that nalyzes the high resolution information covering a wide spectrum. This spectroscopy relies on interference of electromagnetic radiation and aids in detailed investigation of several functional groupings in play on nanoparticles surface (Ramola *et al..*, 2019). FT-IR spectroscopic analysis was applied for detecting the the various functional groups.

Figure 3.7.4 shows the FT-IR of CaO NPs (4000-500 cm^{-1}, mid IR region). Asymmetry within the carbon - containing unit involving CaOCa (stretch) linkages are shown by a peak at 817.35 cm^{-1} (Singh & Verma, 2019). Band at 982.65 cm^{-1} indicates the existence of calcium oxide (Cholapandian *et al..,* 2022). Ca-O group was detected as vibrating by the strong and distinct characteristic band at 520.51 cm^{-1} (Habte *et al..*, 2019).

IR bands at 3006.12cm^{-1} and 2354.08cm^{-1} denote the carboxyl group along with hydroxyl group, respectively, show that phytol could be present plant extract in order to stabilize CaO nanoparticles. Noteworthy peaks (cm^{-1}) appeared at 3569.39 and 1726.53 show that -N-H and C=O in the calcium oxide nanopowder, respectively. On the other hand, CaO nanoparticles displayed C-O characteristic peaks around 1064.51cm^{-1} (Cholapandian *et al..,* 2022; Singh & Verma, 2019).

3.7.2 Characterization of *Cucumis melo* var. *cantalupensis* Biodiesel (CMCBD)

(a) FT-IR of CMCBD

Monitoring the composition of polymers is made especially convenient by FT-IR that can identify elements of a chemical process by using its capacity to identify chemical components by fingerprint (Ahmed *et al.*, 2021; Helmi *et al.* 2021). There were distinctive stretching vibrations in the biodiesel sample, which correspond to the development of several functional groups (Figure 3.8.6). Since the specific peaks at $2922.52 cm^{-1}$ and $2853.16 cm^{-1}$ indicate $-C-H$ and CH_3 correspondingly, $3007.99 cm^{-1}$ refers to production of aromatic alkynes. The carbonyl(C=O) is responsible for high band $1743.57 cm^{-1}$ revealed with an IR shift. This specific peak denotes the transformation of CMC seed oil into biodiesel however $1160.18 cm^{-1}$ denotes $-RX$ (alkyl halide), the peaks at $1464.69 cm^{-1}$ and $1377.48 cm^{-1}$ show the -CH3 and -CH2 vibrations. At $1098.00 cm^{-1}$ $1097.89 cm^{-1}$, the aliphatic amine group was detected. The $721.78 cm^{-1}$ indicates alkane (C-H) and the alkyl halides radical is represented by the region between 518.68 and $532.54 cm^{-1}$, respectively .

(b) GC-MS of CMCBD

The most popular and well accepted method for determining the structure, chemical composition and kind of (FAMEs) present in synthetic biodiesel is gas chromatography-mass spectrometry (GC-MS). The gas chromatogram of *Cucumis melo* var. *cantalupensis* Biodiesel (CMCBD) reveals the structure of the methyl esters (Figure 3.7.6). The gas chromatogram revealed distinct peaks that were further identified by comparing them to standards from the NIST library 11, which are very compatible with the FAMEs found. Many peaks (2-15) exhibit existence of 14 FAMEs such as Methyl palmitate($C_{17}H_{34}O_2$), Methyl oleate($C_{19}H_{36}O_2$),Methyl stearate($C_{19}H_{38}O_2$), Methyl 9,12,15-octadecatrienoate($C_{19}H_{32}O_2$), 9-Octadecenoic acid($C_{19}H_{36}O_2$), Methyl *cis,cis,cis*-9,12,15 octadecatrienoate($C_{19}H_{32}O_2$), Methyl ricinoleate($C_{19}H_{36}O_3$); methyl esters of Cis-13-Eicosenoic acid($C_{21}H_{40}O_2$), Cis-11-Eicosenoic acid ($C_{21}H_{40}O_2$), Eicosenoic acid($C_{21}H_{42}O_2$); Methyl Brassidate ($C_{23}H_{44}O_2$); methyl esters of Docosenoic acid($C_{23}H_{46}O_2$), 15-Teracosanoic acid($C_{25}H_{48}O_2$), Teracosanoic acid($C_{25}H_{50}O_2$) with retention time 23.452, 26.089, 26.257, 27.439, 27.682, 27.976, 28.125, 28.365, 28.387, 28.679, 30.635, 30.655, 32.485, 32.546

minutes. Our results correlate with GC-MS analysis performed by Ameen *et al.* (2018) where 14 different methyl esters were noticed in prepared biodiesel sample (Ameen *et al..*, 2018)

(c) NMR of CMCBD

NMR spectroscopy has developed into one of the most effective methods for determining interactions, dynamics and the structures of compounds. Figure 3.7.7a illustrates the ^{1}H and ^{13}C NMR spectra to describe the CMCBD. The characteristic singlet, appeared in ^{1}HNMR and revealed protons (methoxy i.e.-OCH3; 3.65ppm), supported the hypothesis that seed oil had certainly been converted into respective FAMEs. A triplet of alpha methylene protons (α-CH2), terminal methyl protons (-CH3), olefinic hydrogen (-CH2) and β-methyl protons (β-CH2) were all detected at ppm: 2.010-2.782, 0.850-0.905, 1.248-1.994 were recorded whereas Olefinic hydrogen (-CH2) concentrations ranged from 5.314 to 5.383 ppm. Hence, detected signals show that CMCBD contains a range of methyl esters. However, assigning a chemical shift to each carbon in a given molecule is the basis of ^{13}C-NMR spectroscopy (Bikash *et al..* 2018). Figure 3.7.7b shows ^{13}CNMR to investigate the carbon based compositional properties of CMCBD. The typical peaks in the ^{13}C NMR spectrum of biodiesel sample, were detected at 173.23 ppm and 51.40 ppm account for carbons of carbonyl of ester and methoxy –groups i.e. -COOR and -OMe respectively. Specifying(C=C) in CMCBD are 130.15ppm and 127.87ppm peaks. The other peaks 14.11 and 14.07 ppm in the same frequency absorption sequence correspond to the terminal methyl carbons whereas long carbon chain containing -CH$_2$ produced signals at 25.60 to 34.15 ppm, respectively. The previous work of Ogunbusola *et al.*, (2017) matches this study who reviewed the cucurbits potential for biodiesel production via NMR spectroscopy (Ogunbusola *et al..* 2017).

3.7.3 Biodiesel Yield Optimization via Response Surface Methodology

It has been used to produce 3D graphs to show the overall effect of reaction parameters (Figure 3.7.8 a-f). Such graphs comprehend the collective interaction between various factors therefore establish the optimal limits of each parameter for peak response as specified in the next subsections (Table 3.7.2) During the transesterification procedure, reaction parameters are regularly used. In order to

produce highest biodiesel, it is required to analyze the ideal transesterification reaction conditions. Four optimization factors i.e. Methanol/Oil3:1-15:1 (A), Catalyst load 2-0.1wt. % (B),Time 1–5 h (C),Temperature of 50–70 °C (D), the Central Composite Design (CCD) for our current study was created by DOE (Design of Experiment). The comparison of transesterification yield (predicted/actual) is illustrated by Figure3.7.9. The distribution of the values is discovered as close to the line, indicating strong correlation. The results of the response surface quadric model and statistical analyses of variance (ANOVA) are shown in Table 3.7.3. A low p-value of (0.0016) indicated significant quadric model. Lack of fit (0.8928) statistically insignificant compared with 0.6936 predicted R^2 value with <0.2 difference as of adjusted R^2 i.e. 0.8415 (Table3.7.3). The model adequate precision was found to be more than 4. (5.5802). The current experimental model with higher value of acceptable precision showed how effectively it can be used to estimate biodiesel yield. The following is the polynomial equation used in the quadric model.

Yield =+74.53+2.56*A-2.04*B-0.2947*C+3.75*D-0.8750*AB-0.8750*AC-2.75*AD+1.07*BC-0.4244*BD+3.02*CD-11.02*A²-7.48*B²-0.6719*C²+2.46*D²   **(10)**

3.7.3.1 Interaction between methanol to oil molar ratio and catalyst loading

The Methanol/Oil and catalyst load(AB) are significant variable yield during the transesterification process. To quickly convert oil or fat into biodiesel, a large amount of methanol is needed. A 3D-plot shows how the catalyst loading and Oil/Methanol interact (Figure 3.7.8a). The highest yield (98%) was obtained with a 1.05 wt. % catalyst and 9:1 (Methanol/Oil) (run 19). When molar ratio was increased to 15:1, then yield reduction up to 74% was observed (run 14). This decrease in conversion yield is related to glycerolysis, which causes glycerol to solubilize and recombine with methyl esters, resulting in monolglycerides reformation. When molar ratio was decreased to 3:1 and by adjusting other variables at constant values, the yield was decreased to 60% (run 8). Correspondingly with upsurge in catalyst concentration to 2% the decrease in biodiesel yield was noted i.e. 70% (run 24) and the synthesis of undesirable byproducts is the cause of the yield decline. The collective interaction of molar ratio and catalyst (0.0166) was significant with p-value less than 0.05. Moreover, the separate Methanol/Oil and catalyst were also found significant i.e. 0.0371 and 0.0175 respectively (Table 3.7.3).

3.7.3.2 Interaction between oil to methanol molar ratio and reaction time

Molar ratio (Methanol/Oil) and time (AC) both collectively influence the FAME yield as a critical optimization parameter. In our study, the interactive influence is showed by Figure 3.7.8b. The highest yield (98%) was achieved at 9:1 (Methanol/Oil) and 3 h time (run 19). The low molar ratio (1:3) and short time (1 h) at constant 70°C temperature and 1.05 wt. % catalyst amount, gave considerably smaller yield (56%) as happened in run 3. This decrease in FAME yield is explained by inadequate time, which resulted in incomplete transesterification process. With optimum molar ratio (1:9) and 3h time, the maximum yield 98% was achieved because of an increase in transesterification due to an improved interaction between methanol excess and triglycerides. When both parameters were increased such as molar ratio (1:15) along with time (5 h) then the yield achieved was (72%). The cause may have been the creation of undesirable byproducts, which caused the reaction to move backward and made the separation more challenging (run 9). The ANOVA results defined a highly significant and a strong correlation between these two parameters with p- value < 0.05 (i.e. 0.0466) (Table 3.7.3).

3.7.3.3 Interaction between methanol to oil molar ratio and reaction temperature

The interactive effect of Methanol/Oil and temperature (AD) has been mentioned in Figure 3.7.8c. The highest yield (98%) was achieved at 9:1 (Methanol/Oil) with 70°C temperature (run 19). In our optimizations, the low temperature i.e. 60 °C resulted in yield decline to 69% (run 2) when all other three parameters were constant (i.e. 9:1 Methanol/Oil, 3 h time and 1.05 wt. % catalyst) due to reduced oil miscibility of methoxide at low temperatures. By lowering both variables such as Methanol/Oil to 3:1 and temperature to 50°C, the yield reduced to 60% (run 10). By increasing molar ratio to 15:1 and a slight rise in temperature to 60°C, the biodiesel yield also increased to 68% (run 22) and it is attributed to excess of methanol that effectively lowers the viscosity of feedstock oil and slightly high temperature that results in more effective collisions between reactant molecules with high kinetic energy. ANOVA outcomes represent this interactive effect highly significant with p-value < 0.05 (0.0306). Hence, it is certain that the combined impact is essential while optimizing the transesterification reaction.

3.7.3.4 Interaction between catalyst loading and reaction time

Interactive effect of amount of catalyst and time (BC) has been mention as 3D RSM graph (Figure 3.7.8d). The highest biodiesel yield was attained with 1.05 wt. % catalyst and 3 h time (run 19). When catalyst amount was increased and time were decreased below the optimized level i.e. from 1.05 to 2 wt. % and from 3 h to 1 h respectively, a remarkable reduction in biodiesel yield (55%) was noticed even under same 9:1 molar ratio and 70 °C (run 17). As high catalyst concentration caused saponification, and a short reaction period prevents a proper interaction between the catalyst and the oil, partially converting the reactants into products. Similarly, increasing both variables i.e. the catalyst load up to 2 wt. % as well as time from 3h to 5 h, the biodiesel yield declined (70%). Because reversible transesterification decreases the product concentration in the reaction mixture when the time restriction exceeds the ideal level. Run 6 made it very evident how time and the catalyst combined influence worked. As catalyst amount and time increased, there was a definite drop in biodiesel yield. Furthermore, the rise in time up to 5 h while keeping other parameters constant, the yield reduction to 80 % was noticed (run 11). ANOVA results mention the significant mutual influence of catalyst and time (p-value < 0.05) i.e. 0.0286.

3.7.3.5 Interaction between catalyst loading and reaction temperature

A 3D plot shows the overall interactive relationship between the amount of catalyst and the temperature (BD) (Figure 3.7.8e).The maximum biodiesel yield (98%) was achieved with 1.05 wt. % catalyst and 70 °C. It is ascribed to high molecular kinetic energy, which causes effective molecular collisions that ultimately convert molecules to their corresponding methyl esters as a result of a constant increase in reaction rate. When both Oil/Methanoland time were kept constant (1:9 and 3h) both catalyst conc. and temperature were decreased from 1.05 % to 0.1 wt. % and temperature from70°C to 60 °C respectively, just 66 % yield was achieved (run 23). At this point, the low concentration of catalyst is not enough to lower the activation energy barrier, and the reaction is proceeding slowly due to the lack of catalytic active sites needed to accommodate a large number of substrate molecules, which results in a poor product yield. Similar to low temperature, low reaction rate and markedly low FAME yield occur from molecules insufficient kinetic energy to support their effective collisions. Our findings are consistent with earlier research (Abbah *et al..,* 2016). When

concentration of catalyst was increased more than 1.05% i.e. 2 wt. % and temperature was further lowered i.e. 50 °C, it lead to declination of yield at constant ratio (1:9) and time (3h), Biodiesel yield reduction up to 60% was noticed (run 29). More catalyst is added, which speeds up the reaction by lowering the activation energy of the reactant. As a result, more triglycerides are transformed into their corresponding methyl esters, which increases the production of biodiesel. However, up to a point, the increase in catalyst concentration reduces the ester yield due to the unwanted saponification process. ANOVA results show their significant mutual effect by having p-value (<0.05) i.e. 0.0468.

3.7.3.6 Interaction between reaction time and reaction temperature

The cumulative impact of a change in either of the factors was thoroughly investigated (while keeping both molar ratio and catalytic load constant at 1:9 and 1.05 wt. % respectively). In form of 3D RSM graph, the interaction between time and temperature (CD) has been mentioned in figure 3.7.8f. The highest yield (98%) was achieved in 3h at 70°C however considerably low yield was observed when the reaction parameters (time and temperature) were set at lower extremities, i.e. 1 h and 50 °C, and was recorded as 70% (run 1). Poor mixing of three basic parameters i.e. catalyst, methanol and oil was the cause of the low yield (as viscosity of oil is high at low temp.). As a result, the reactant molecules are unable to react properly and change into their desired products due to a lack of energy in short time. However, when time was increased to 3 h even though other reaction conditions were same as for run 1, the biodiesel yield rise was noticed i.e. 83% (run 4) Because, the high temperature for long time resulted in vaporization of methanol prevent the chemical reaction of two liquids (oil and methanol) under given conditions. But this yield is not as high as in run 19 (98% yield) since the temperature in run 4 is low comparatively. Similarly, more time (5 h) with low temperature (50°C) gave extremely low yield i.e. 50% (run 25). The reason for low yield is backward reaction leading to less product that occurs when time is notably high. When temperature is slightly high i.e. 60°C, the yield improved up to 62 % even in just 1 h, as reactant had enough kinetic energy for effective collisions hence biodiesel yield is high.

ANOVA shows significant effect of time and temperature (p-value < 0.05) i.e. 0.0129 (Table 3.7.1).

3.7.3 Fuel Properties of CMCBD

CMCBD qualities were examined in order to determine the fuel quality and the possibility of using it in diesel engines. CMCBD fuel properties were studied (as per ASTM D-6751). Since it immediately affects spark-ignition machinery at low temperatures, kinematic viscosity is thought to be one of the most important characteristics of biodiesel. It is an essential component in the atomization and burning of fuel.

The higher viscosity of the gasoline results in a decrease in fluidity. The K. viscosity of CMCBD at 40 °C is 5.31 cSt., which is much lower than that of traditional biodiesel and complies with ASTM criteria. High density more pollutants and incomplete combustion. The fluid density must be kept within the normal range since using high density fluid in fuel injection systems requires using more fuel. CMCBD density (0.8126 kg/L at 15 °C), which is acceptable by international ASTM standards.

Two qualities that are related to the storage and security of fuel are flash and fire point. Flash point of CMCBD is 80°C and a higher fire point that is outside the acclaimed range although being considerably less expensive than petro-diesel. CMCBD has lower flash and fire points than conventional biodiesels since it is more volatile than *Pongamia pinnata, Ricinus communis, Eruca sativa,* etc. (Shaheen *et al.,* 2018).

Cloud point (-12°C) and pour point (-11°C) were within the range of HSD (Ameen *et al.,* 2018). The total acid number was discovered to be 0.243

The total sulphur compounds within gasoline recorded by measuring theits Sulphur (%). Fuel sulphur has the ability to raise emissions by corroding engine parts. Sulfur concentration for CMCBD 0.00048% shows that better quality standards were used in the biodiesel preparation (Table 3.7.1).
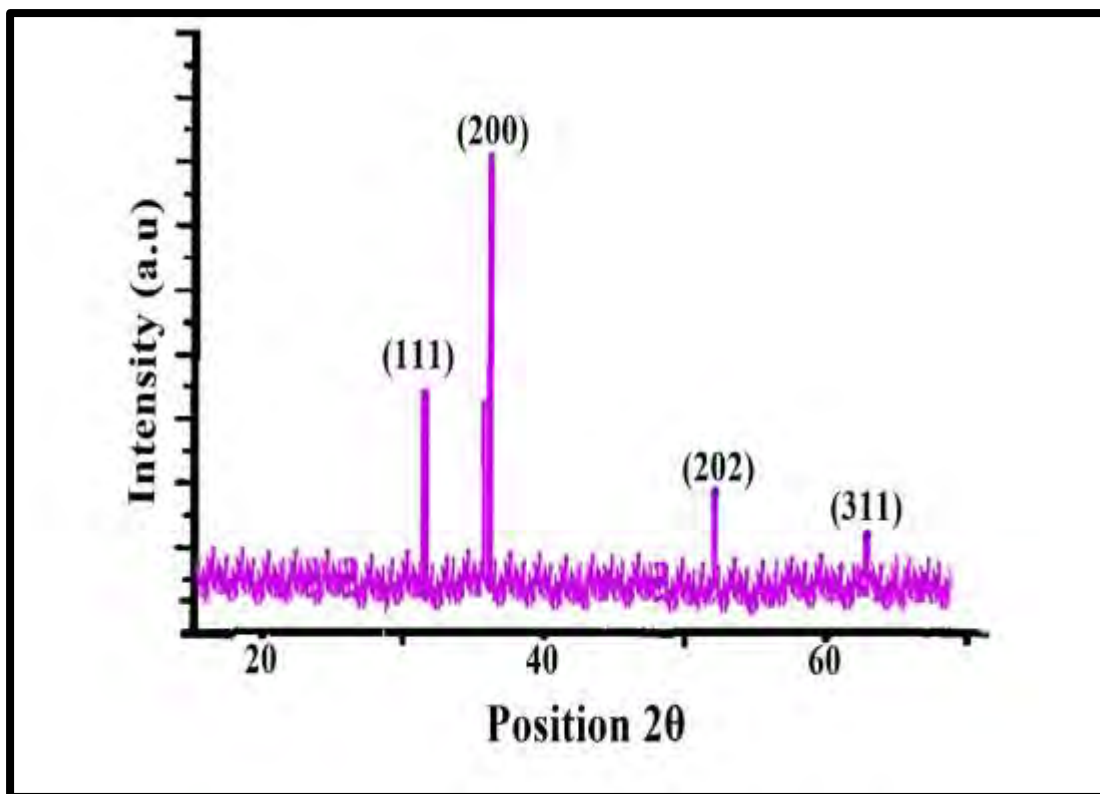
Figure 3.7.1: XRD of CaO green nano-catalyst
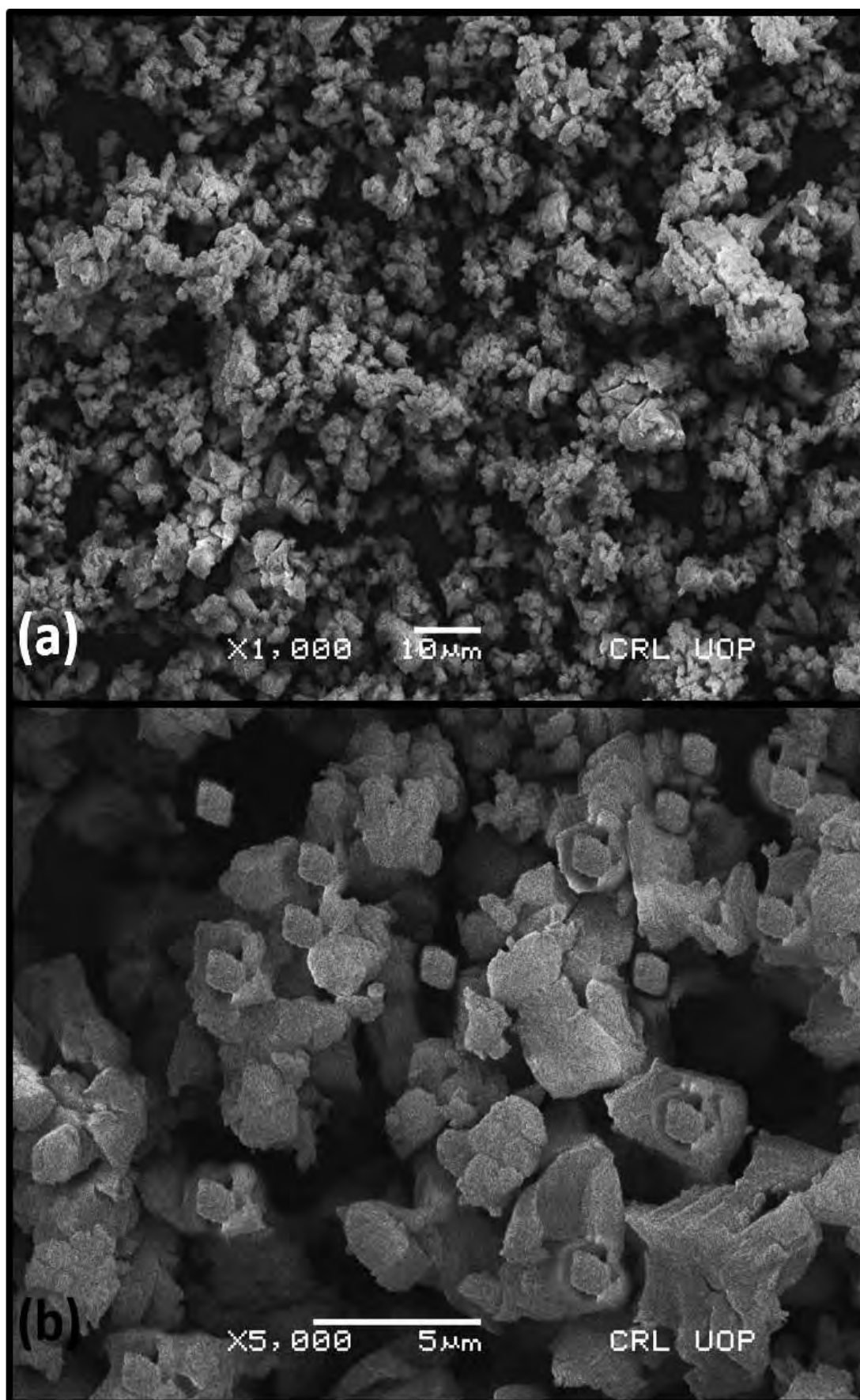
Figure 3.7.2: SEM of CaO green nano-catalyst
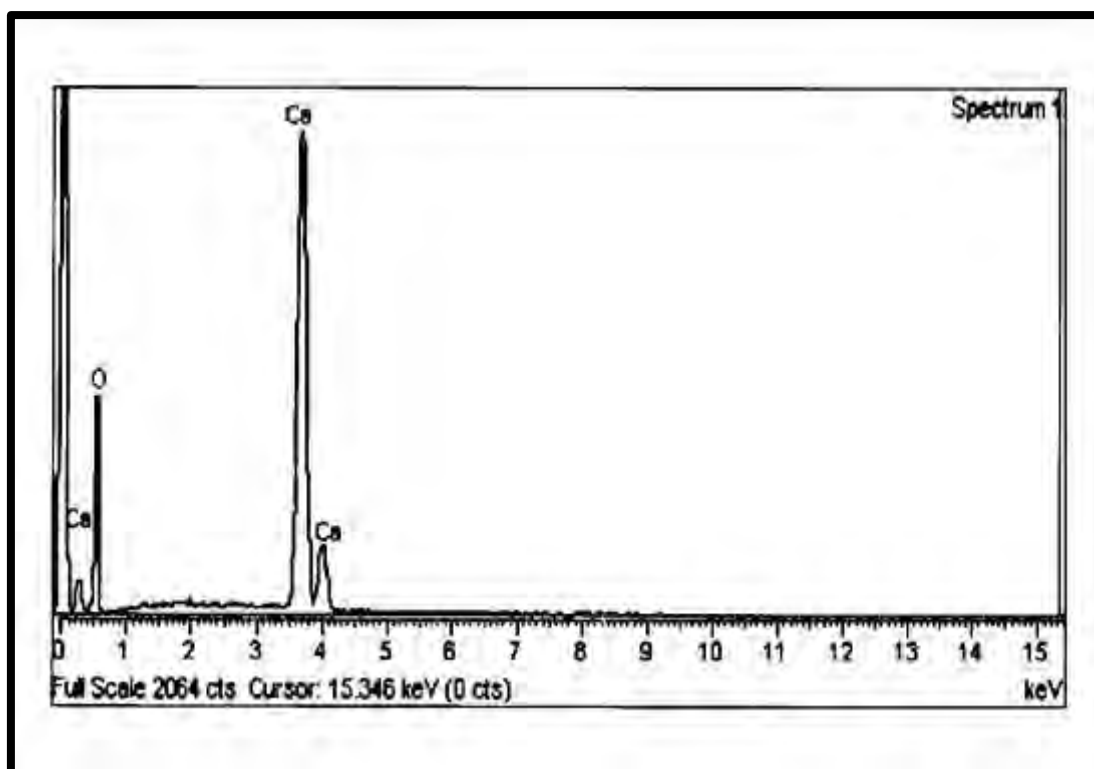
Figure 3.7.3: EDX of CaO green nano-catalyst
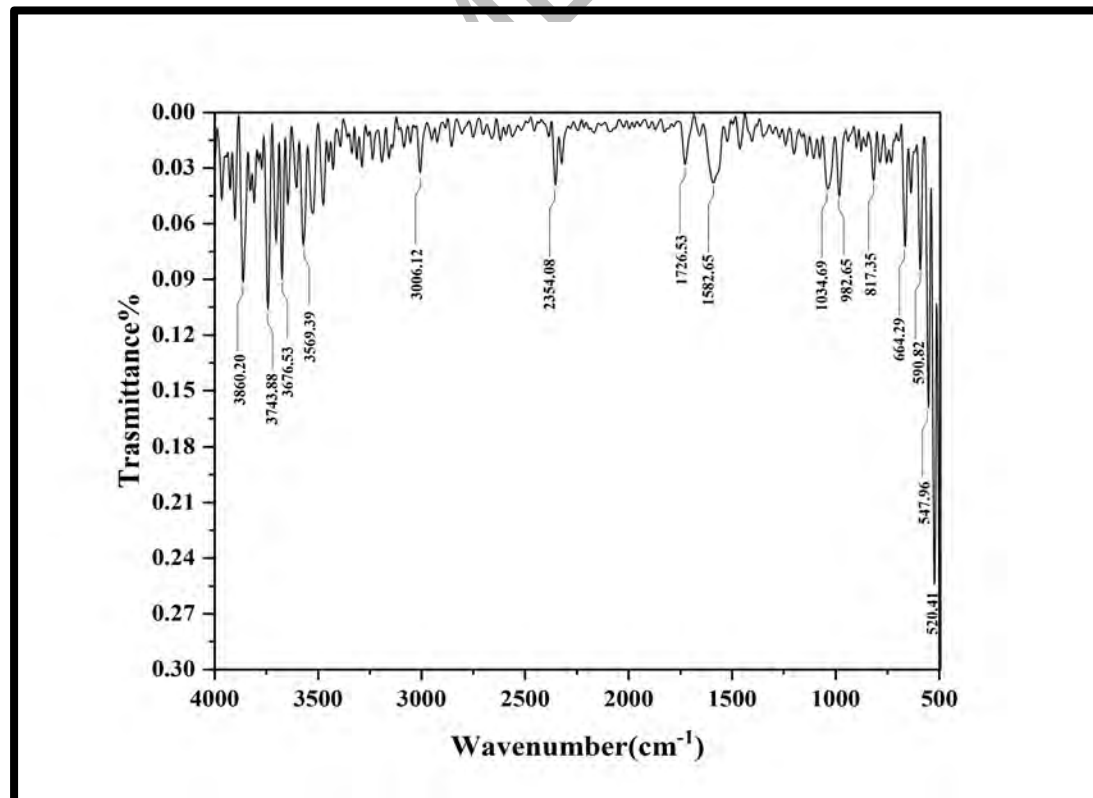
Figure 3.7.4: FT-IR of CaO green nano-catalyst
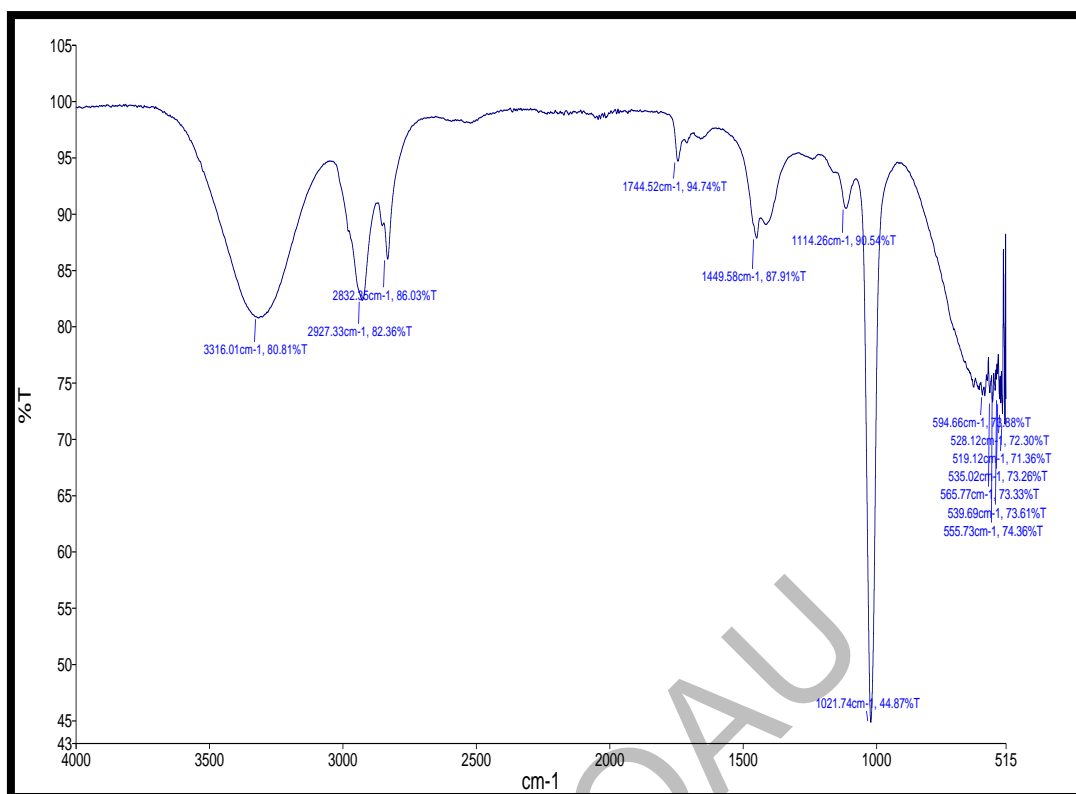
Figure 3.7.5: FT-IR spectrum of CMCBD
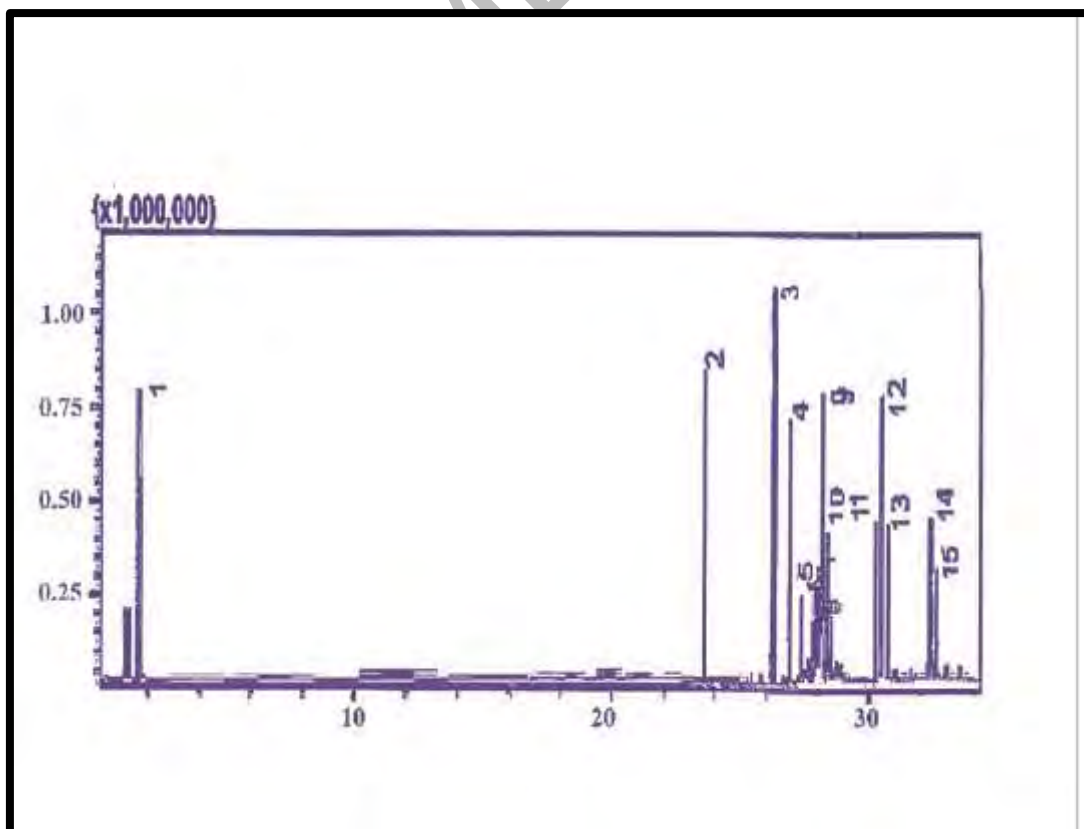
Figure 3.7.6: GC-MS spectrum of CMCBD
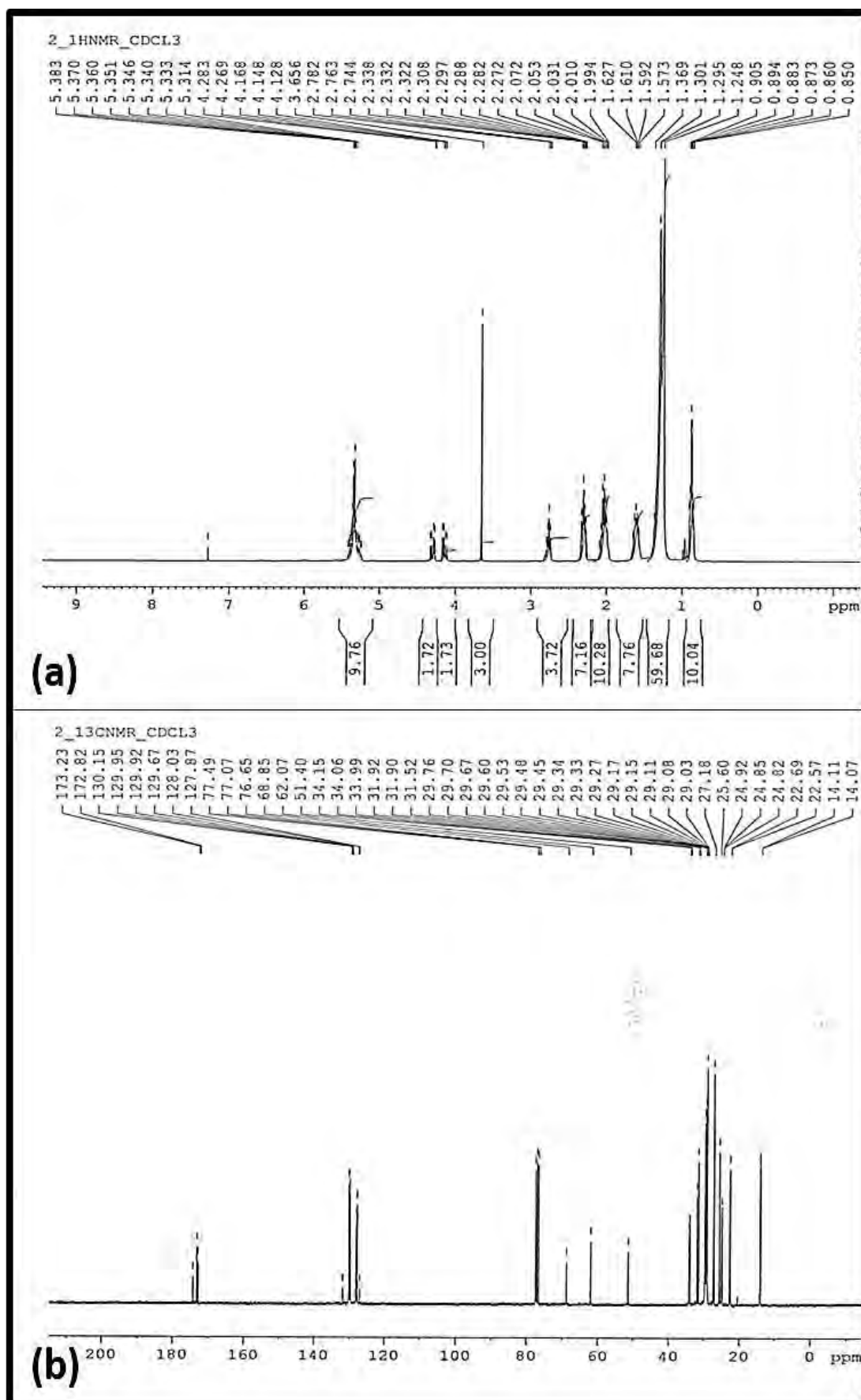
Figure 3.7.7: (a) ¹HNMR **(b)** ¹³CNMR spectra of CMCBD
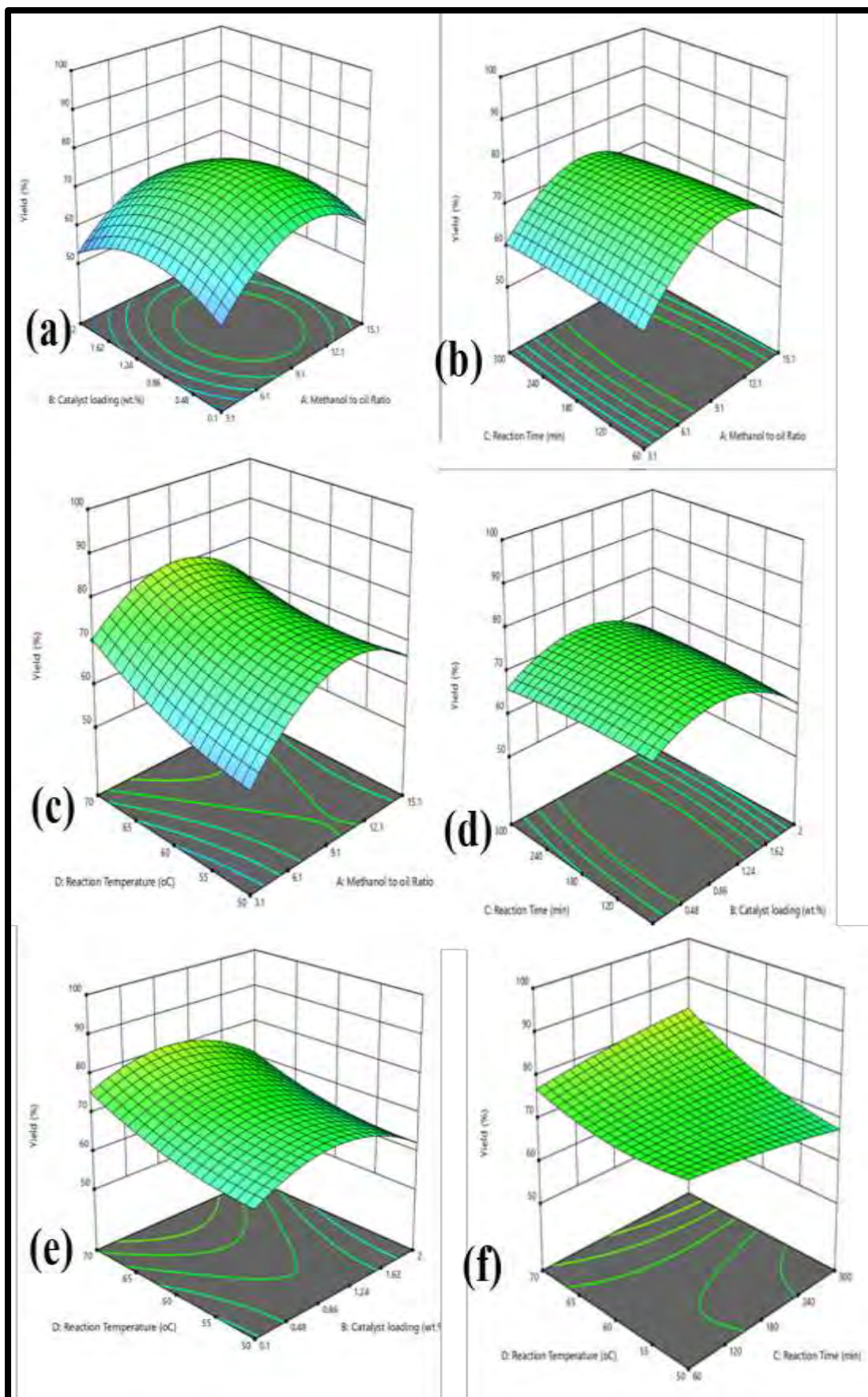
Figure 3.7.8: Influence of reaction variables on CMCBD
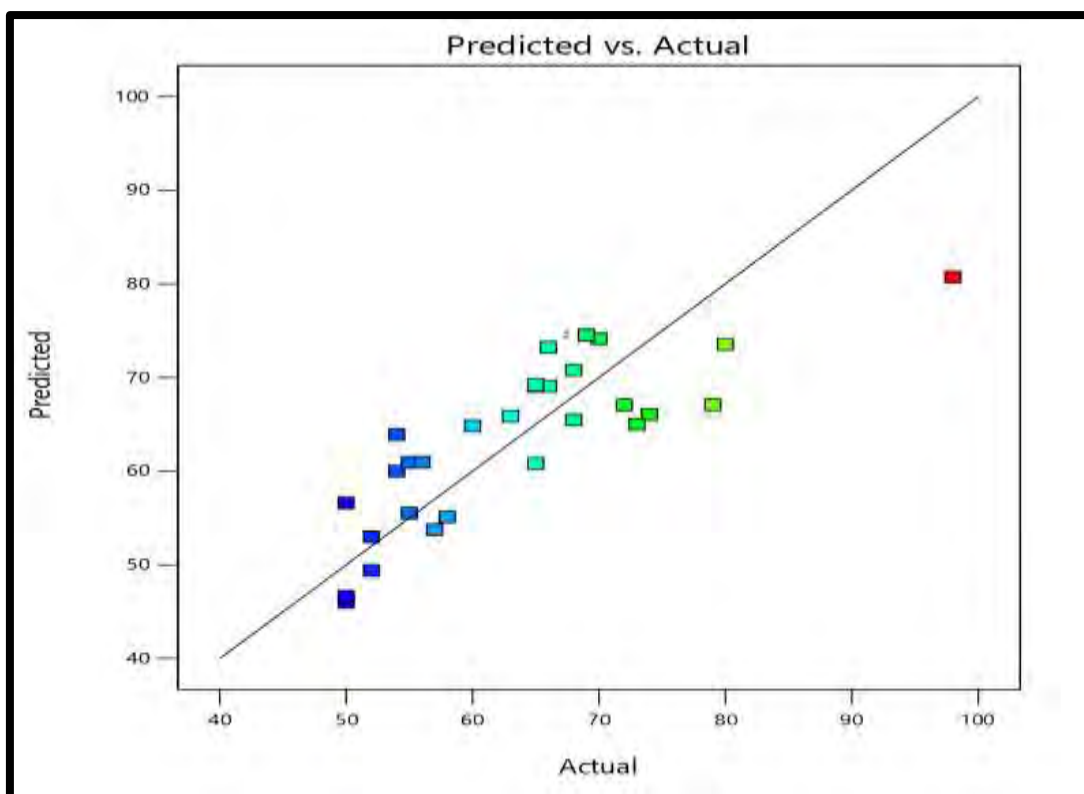
Figure 3.7.9: Predicted vs. actual yield of CMCBD

Table 3.7.1 Fuel Properties of CMCBD

TESTS	METHOD	CMC B-100
Color	Visual	2
Density @ 15 °C Kg/L	ASTM D-1298	0.8126
Kinematic Viscosity @ 40 °C cSt	ASTM D-445	5.31
Pour point °C	ASTM D-97	-12
Flash point °C(PMCC)	ASTM D-93	80
Cloud point °C	ASTM D-2500	-11
Total Acid No. mg KOH/gm	ASTM D-4294	0.243
Sulphur % wt.	ASTM D-974	0.00048

Table 3.7.2 Experimental yield of CMCBD

Run	Methanol to Oil Molar Ratio	Catalyst Loading (wt. %)	Reaction Time (min)	Reaction Temp. (°C)	CMCBD Yield (%)
1	9.1	1.05	60	50	70
2	9.1	1.05	180	60	69
3	3.1	1.05	60	70	56
4	9.1	1.05	180	50	83
5	15.1	2	60	70	58
6	9.1	2	300	70	70
7	15.1	0.1	300	50	50
8	3.1	1.05	180	70	60
9	15.1	1.05	300	70	72
10	3.1	1.05	180	50	60
11	9.1	1.05	300	70	80
12	9.1	1.05	60	60	62
13	3.1	0.1	60	50	52
14	15.1	1.05	180	70	74
15	15.1	0.1	300	70	68
16	3.1	2	300	70	60
17	9.1	2	60	70	55
18	3.1	0.1	300	50	50
19	9.1	1.05	180	70	98
20	3.1	1.05	300	70	85
21	15.1	2	60	50	54
22	15.1	1.05	180	60	68
23	9.1	0.1	180	60	66
24	9.1	2	180	70	70
25	9.1	1.05	300	50	50
26	15.1	0.1	60	70	54
27	15.1	2	300	70	55
28	15.1	2	300	50	57
29	9.1	2	180	50	60
30	3.1	2	60	50	52

Table 3.7.3 Analysis of Variance (ANOVA) of CMCBD

Source	Sum of Squares	df	Mean Square	F-value	p-value	
Model	2250.75	14	160.77	2.07	0.0016	significant
A-Methanol to oil Ratio	117.56	1	117.56	1.52	0.0371	
B-Catalyst loading	82.87	1	82.87	1.07	0.0175	
C-Reaction Time	1.66	1	1.66	0.0215	0.0454	
D-Reaction Temperature	271.11	1	271.11	3.50	0.0011	
AB	12.25	1	12.25	0.1580	0.0166	
AC	12.25	1	12.25	0.1580	0.0466	
AD	121.00	1	121.00	1.56	0.0306	
BC	18.90	1	18.90	0.2438	0.0286	
BD	2.99	1	2.99	0.0386	0.0468	
CD	151.14	1	151.14	1.95	0.0129	
A^2	451.32	1	451.32	5.82	0.0291	
B^2	230.81	1	230.81	2.98	0.0049	
C^2	1.64	1	1.64	0.0211	0.0863	
D^2	22.14	1	22.14	0.2857	0.0008	
Residual	1162.62	15	77.51			
Lack of Fit	1162.12	13	89.39	357.58	0.8928	Not significant
Pure Error	0.5000	2	0.2500			
Cor Total	3413.37	29				

SECTION: VIII

Biodiesel Synthesis from *Solanum surratense* Using Silver Oxide Green Nano-catalyst

3.8. Biodiesel Synthesis from *Solanum surattense* Using Silver Oxide Green Nano-catalyst

3.8.1 Characterization of Silver Oxide Green Nano-catalyst

(a) XRD of Ag$_2$O

The structural characteristics and crystalline size of the produced green silver oxide nano-catalyst (Ag$_2$O) were determined using the powder XRD analysis. The structural characteristics of Ag$_2$Owere determined using X-ray diffraction in the angle range of 2θ from 15° to 75°. The XRD results of Ag$_2$O is displayed as Figure 3.8.1. This spectrum shows that the synthesized nano-catalyst is highly crystalline and that its diffraction peaks were strong and distinct. At 2θ angle three strong diffraction peaks 38.14° (111), 44.36° (200) and 64.61° (220) were found. Our results coincide with Al-Zahrani et al. (2021) who produced 48nm Ag$_2$O nanoparticles with face centered cubic (FCC) shape (Al-Zahrani *et al..*, 2021). In the diffractogram of the manufactured green silver oxide nano-catalyst, which shows face centered cubic phase. Debye-Scherrer formula was used to determine the silver oxide nanoparticles crystallite size, which was found to be 39 nm. In a prior study, XRD analysis revealed that nano-units were 18.6 nm (Sagadevan, 2016) Another study revealed that silver oxide nanoparticles made from *Callistemon lanceolatus* leaf extract formed a face-centered cubic shape (Ravichandran *et al..*, 2016). According to Jalees et al. (2018), silver oxide nanoparticles made from mango peel extract with crystallite 6.2nm in size and a face-centered cubic layout (Jalees *et al..*, 2018).

(b) SEM of Ag$_2$O

SEM was used to examine the surface properties as well as crystalline size of the fabricated Ag$_2$O nano-catalyst. Figure 3.8.2 illustrates SEM images of Ag$_2$O nano-catalyst at various resolutions. The findings indicate that the particles are cube in shape with aggregate much, which supports the presence of magnetic interactions and polymeric adhesion between nanoparticles. According to calculations, the typical nano-catalyst particle size lies between 40 and 45 nm in diameter. Green Silver oxide nanoparticles in another study were 18.3 nm in size and had a spherical shape (Sagadevan, 2016). From *Carica papaya* root extract, Yadav *et al..* (2018) create green silver oxide nanoparticles and describe their spherical morphology using scanning

electron microscopy (Yadav *et al..,* 2018). Rashmi et al. (2020) synthesized green silver oxide naoparticles (Ag$_2$O NPs), analyzed by SEM and evideced spherical shaped Ag$_2$O NPs from SEM micrographs (Rashmi *et al..*, 2020).

(C) EDX of Ag$_2$O

EDX is analytical technique that examines and calculates proportions and composition of elements on different to provide sample record. The EDX analysis of silver oxide nano-catalyst clearly demonstrates that the manufactured nano-catalyst was composed of two separate elements, namely silver and oxygen (Figure 3.8.3). The peaks that closely approximate the optical absorption by fabricated particles were identified. Elemental analysis of nano-catalyst revealed that it included 85.08% silver and 14.92% oxygen, indicating that it was produced in the purest possible manner. Through EDX analysis, Ravichandran et al. (2016) assessed the quality of green silver oxide produced from *Callistemon lanceolatus* leaf extract (Ravichandran *et al..*, 2016). Nainawal and Pant (2021) used EDX analysis to study chemical composition of biosynthesized silver oxide nanoparticles (Nainwal & Pant, 2021)

(d) FT-IR of Ag$_2$O

Materials of diverse variety are investigated via FT-IR including liquids and solid form of matter for analyzing features depending on their quality along with quantity. 11mm units are certainly studied by focusing the top ~1 micrometer layer or the sample as a whole. In the current study, FT-IR spectral analysis was conducted to pinpoint the prospective and potential biomolecules in plant extract that are accountable for bioreducing and capping the silver nanoparticles. As stabilising agents in the design of nanoparticles, plant extracts serve a dual purpose. Further, the FT-IR data demonstrate that the presence of terpenoids, flavones, phenolics, and polysaccharides components in the plant extracts caused the reduction of silver ion (Chand *et al..*, 2020; Thangamani & Bhuvaneshwari, 2019). The bands at 3410.20 cm^{-1} are attributable to phenol molecules. While the peak seen at 1784.69cm^{-1} belonged to (-C-C-), bond at 759.18 cm^{-1} also represented the (H-bonded) O-H. Strong band at 832.65 cm^{-1} represent C-H bending in aromatic ring. The typical bands with lattice vibration observed at approximately 508.16 to 554.08 cm^{-1} as reported earlier (Liu *et al..*, 2019; Pawar *et al..*, 2016). Ag$_2$O nanoparticles presence is confirmed by the strong and distinct peak at 1337.76 cm^{-1}. Following reductive as well as synthesis phases, Chand et al. (2021)

determined that a certain rise around 1630-1380cm^{-1} attributed to the microfiber oscillations for compounds N-H, suggests a phase purity pf Ag$_2$O nanocrystals capping by biocompatible units like polyphenols etc.(Chand *et al.*, 2021). Thus, Ag$_2$O obtained from herbal material comprises CH, -OH, N-H, and C=C, each of which possesses the ability to accomplish the stabilization, reduction and capping (Chand *et al.*, 2021).

3.8.2 Characterization of *Solanum surratense* Biodiesel (SSBD)

(a) FT-IR of SSBD

Via this advanced technique for monitoring the composition of polymers is made especially convenient by FT-IR. It can identify elements in a composite by using its capacity to identify chemical components by fingerprint (Ahmed *et al.*, 2021; Helmi *et al.*, 2021). There were distinctive stretching vibrations in the biodiesel sample, which correspond to the development of several functional groups (Figure 3.8.6). Since the specific peaks at 2922.52cm^{-1} and 2853.16cm^{-1} indicate presence of -CH and -CH$_3$ respectively, 3007.99 cm^{-1} indicates the production of aromatic alkynes (C-H). The carbonyl being responsible for high band 1743.57cm^{-1} revealed with an IR shift. This specific peak denotes the transformation of *Solanum surratense* seed oil into biodiesel while 1160.18cm^{-1} denotes the formation of –R-X redicle, at 1464.69cm^{-1} and 1377.48cm^{-1} show the -CH$_3$ and -CH$_2$ vibrations. At 1098.00 cm^{-1},1097.89 cm^{-1}, the aliphatic amine group was detected. The –C-H is represented by 721.78 cm^{-1}, and alkyl halides radical is represented by the region between 518.68 and 532.54 cm^{-1}, respectively. Similar FT-IR results were found by Dawood *et al.,* 2022 when silver oxide green nano-catalyst was synthesized for carrying out biodiesel production from *Prunus bokhariensis* (Dawood *et al.,* 2022).

(b) GC-MS of SSBD

To determine occurrence of diverse FAMEs and assess the quality of synthesized biodiesel, as in SSBD conducted. Each raw material used to make biodiesel has a unique fatty acid structure. Quantity of altered fatty acids in the oil supply, from which biodiesel is prepared, heavily influences nearly all of its important fuel qualities. Therefore, it is necessary to thoroughly study FAMEs; therefore accorded using their retention times with NIST02 software. Figure 3.8.6 shows an SSBD chromatogram that displays six distinct peaks, including the methyl esters of both saturated and unsaturated

fatty acids. Various peaks (4,5,7,8,9,14) indicate the presence of six FAMEs such as Dodecanoic acid methyl ester ($C_{13}H_{26}O_2$), Methyl palmitate($C_{17}H_{34}O_2$), Methyl lineolate($C_{19}H_{34}O_2$), Methyl oleate($C_{19}H_{36}O_2$), Methyl stearate($C_{19}H_{38}O_2$), trans-13-Docosenoate($C_{23}H_{44}O_2$) with retention time 19.179, 23.985, 25.802, 25.839, 26.177 and 29.337 minutes respectively. Hence, the seed oil of *Solanum surratense* has an effective conversion ability into FAMEs and used for extensive biodiesel production, as showed by GC/MS analysis in this study.

(c) NMR of SSBD

NMR analysis has been employed in various biofuel investigations, including fatty acid analysis, monitoring the progress of transesterification reactions, and determining the presence of free glycerol, mono-, and diglycerides. Figure 3.8.7a displays ^{1}H NMR spectrum of SSBD. A distinctive signal 3.626ppm that resulted from the methyl ester moiety, is accountable for biodiesel to be distinguished from pure diesel. Clear signals appeared (ppm) at 0.8,1.2,1.6,2.0,2.3,2.8,5.3 correspond to –**CH$_3$** (hydrogen), -**CH$_2$**(carbon), carbonyl(-CH$_2$), α-carbonyl(-CH$_2$), allylic, bisallylic, and oleific(hydrogen)(Figure 3.8.7a). The structural characterisation of methyl esters in SSBD was studied using ^{13}C NMR spectroscopy (Figure 3.8.7b). The distinctive peaks of methoxy carbon (-OMe) and ester carbonyl group (-COOR) emerged in the ^{13}C NMR spectrum at 173.62 and 51.08 ppm, respectively. In SSBD (C=C)is indicated by the peaks that emerged at 131.22 and 127.50 ppm. The other peaks in the same frequency absorption sequence correspond to carbons (-CH3) i.e. 27.01 ppm and the long carbon chain ethylene carbons (-CH2-) at 29.08–34.17 ppm, respectively. Our results are in close accord with the NMR results of *Solanum nigrum* seed oil biodiesel by (Kasirajan *et al.*. 2017).

3.8.3 Biodiesel Yield Optimization via Response Surface Methodology

Figure 3.8.8 a-f show three-dimensional response surface plots of reaction parameter data. These plots were discovered to be helpful in evaluating the various interacting impacts of four factors, supporting in the identification of extreme response levels. Typically, an ideal reaction should result in an increase in methyl ester yield. Abrupt decline in biodiesel output past optimum levels was seen (Table 3.8.2). Reaction parameters are always in action while performing transesterification. Hence,

it is indispensable to analyze best condition to achieve high biodiesel product. Reaction parameters chosen were Methanol/Oil(A)2:1–15:1; the catalyst concentration(B)0.5-2wt.%; the time(C)1–5h; and the temperature(D)50–80 °C, the Central Composite Design (CCD) for our current study was created by DOE (Design of Experiment). The distribution of the predicted/actual values is revealed as close to line, indicating strong correspondence between values(Figure 3.8.9). Table 3.8.3 refers to the response surface quadric model statistical analyses of variance (ANOVA). A p-value (0.0060) defines significance of quadric model (less than0.05). Compared to error, a lack of fit statistically insignificant i.e. 0.2683. Good lack of fit value is one that is not statistically significant and has a chance 26.83%. Predicted R^2(0.7680) being near to adjusted R^2(0.6582)and has<0.2variance(Table 3.8.3). An adequate precision was found to be more than 4. (5.7158). A higher value of acceptable precision showed how effectively it can be used to estimate biodiesel yield. The following is the polynomial equation used in the quadric model.

Yield = +76.18+3.47*A+1.80*B-2.49*C+1.55*D+1.51*AB-2.35*AC+1.63*AD+3.43*BC-4.19*BD-1.12*CD-5.14*A²-8.13*B²+2.84*C²-6.82*D²   **(11)**

A successive subsections could thoroughly clarify the interaction consequences of the transesterification reaction.

3.8.3.1 Interaction between methanol to oil molar ratio and catalyst loading

Transesterification is significantly influenced by the Methanol/Oil and the catalyst (AB). It has been demonstrated in the three-dimensional plot design used for their mutual effects (Figure 3.8.8a). With a 8:1 molar ratio (Methanol/Oil), 1.25 (wt.%)catalyst, duration 3h at 65 °C, as in run 8, 89% yield was attained. Over these limits, a yield diminution was noted (15:1 and 2 wt.%), as in run 13, with 78% esters. A key reaction parameter that increases biodiesel output is methanol/oil. Consequently, 2:1 and 0.5 wt. % usual decreased yield marked at 55% (run 18). Hence, a considerably low yield was achieved at both extremes i.e., by simultaneous rise and decline in molar ratio and catalyst concentration as compared to optimal levels. It was discovered that Run 26 produced 60% yield with a lower molar ratio of 2:1 and the same amount of catalyst (1.25 wt.%). A low yield of 66% was achieved at 0.5 wt. % catalyst and 15:1 ratio. (Run 22). The reaction mixture favors glycerolysis, a process can cause it to reverse, in case of high molar ratios. and dilutes the catalyst concentration (a reversible

reaction) (Foroutan *et al.*, 2021). As per ANOVA, there exists significant correlation (0.0355 < 0.05)

3.8.3.2 Interaction between oil to methanol molar ratio and reaction time

The parametric correlation of the Methanol/Oil and time was thoroughly examined, when catalyst and time set at 1.25 wt. % and 65°C. Biodiesel is significantly impacted by the interaction of these reactions factors (Figure 3.8.8b). At 8:1 for 3h, a high yield of 89% was attained (Run 8) however at 15:1 for 5h produced a FAMEs yield declined up to 78%. (Ma *et al.*, 2021). At Run 29, a decrease in minimum fixed limit(2:1) with maximum processing time (5 h) led to a reduced yield of 72%. Insufficient time prevents the reactants from properly mixing and reaching an equilibrium state, which leads to an inefficient conversion of the reactants into products. (Shaheen *et al.*, 2018). A minimum ratio (2:1) and a minimum time (1h), a yield reduction up to 64% was recorded at Run 20. ANOVA outcomes with a p-value < 0.05 (0.0488), revealed this significant interaction.

3.8.3.3 Interaction between methanol to oil molar ratio and reaction temperature

Methanol/Oil and temperature (AD) have been mentioned in (Figure 3.8.8c) to illustrate their interactive influence. With optimized 8:1 (Methanol/Oil) and 65°C temperature, the highest yield (89%) was obtained (run 8). 85 °C temp. accelerated the bulk transference of the three insoluble phases—the catalyst, oil, and CH_3OH—and increased productivity by giving the molecules that are interacting more kinetic energy. However, at Run 7, the yield was severely reduced to 66% owing to 80 °C temp. (Considerably high) and 15:1 ratio (a maximum set). The soap formation and methanol evaporation above 65°C at this point considerably reduced the amount of methyl ester that could be produced. Similar results have published by Ahmad and Zafar 2021 as well as Ameen *et al.,* 2022 where rise in temperature resulted in saponification and solvent evaporation leading to yield declination (Ahmad and Zafar 2021; Ameen *et al.,* 2022)

With 50 °C (in general low) and 15:1 (noticeably high) in run 27, a minor conversion of 62% of biodiesel was obtained. A remarkably low yield (58%) was obtained at Run 21 with a ratio (lower) 2:1 and at 80 °C. As aforementioned in present studies, a combined outcome being tremendous so must be taken into account

throughout applied work. ANOVA with a p value (0.0550) > 0.05 revealed that there is no significant correlation between molar ratio and temperature.

3.8.3.4 Interaction between catalyst loading and reaction time

Interactive effect of amount of catalyst and time (BC) has been mention as 3D RSM graph (Figure 3.8.8d). The highest biodiesel yield was attained with 1.25 wt. % catalyst and 3 h time (run 8). At catalyst 1.25 wt. % and 3 h, the highest yield of 89% was obtained (Run 8). At Run 24, a 65% yield was achieved at 2 wt. % in 5h. The fluid viscosity is enhanced by excess amount of catalyst and resultant reduced mass transference across all phases, is responsible for yield drop at this run in transesterification. A yield of 55% was achieved with 0.5 wt. % and a maximum set duration i.e. 5h (run 15). Increased product was noticed to 69% in 1 h with a 2 wt. % catalyst addition (Run 30). According to ANOVA, there is the significant interaction with (p-value0.0364<0.05) (Table 3.8.3).

3.8.3.5 Interaction between catalyst loading and reaction temperature

Relating interactive effects (catalyst loading with temperature) investigated with an 8:1 constant molar ratio and a 3 h reaction duration. Temperature and catalyst during transesterification interact mutually, which is comprehended in (Figure 3.8.8e). When catalyst 1.25 (wt. %) at 65°C adjusted, an 89%yield was seen (run8). With same amount of catalyst (1.25 weight percent) and the lowest temperature of 50°C, around 70% return attained, showing that the low temperature managed to convert triglycerides into methyl esters (Run 2). At Run 28, the yield was reduced to 63% because the catalyst of 0.5wt.% and high temperature of 80 °C were insufficient to complete the transesterification reaction. Furthermore, 65°C(b.p. CH_3OH) or above temperature slows down accelerative course of chemical reaction. Similar to this, a low yield of 50% was obtained at the lowest temperature of 50 °C and with a catalyst of 0.5 wt. % (Run 5). At Run 17, 64% product was achieved with 2 wt. % conc. at 50°C. The ANOVA results showed that these parameters possess significant mutual interaction (0.0094<0.05).

3.8.3.6 Interaction between reaction time and reaction temperature

At methanol/oil 8:1with 1.25wt.%, collective influence of time with temp. were investigated. The combined impact of time and temperature on biodiesel yield is shown

in (Figure 3.8.8f). It is clear that the conversion (89%) upsurges considerably to a limit (i.e. with 1.5 wt.% at 65°C) that a little additional rise (up to 5h at 80 °C) would result in yield drop (82%,Run4), possibly due to reversible transesterification over an extended period of time and methanol vaporization. According to our research, the output of biodiesel increases up to a specific temperature, at which point it significantly decreases. Because the transesterification reaction is endothermic, the biodiesel yield has decreased. As oil and CH_3OH get well blended, followed by conveniently separation of product from byproduct, allowed for the maximum biodiesel production of 89% to be attained at 65 °C with a 3 h reaction period. However, higher temperatures of 80 °C even in 1 hour of time (81%, Run 1) may encourage ester hydrolysis to form acidic compound together with CH_3OH polarity, hence reducing biodiesel output. The output is significantly reduced to 67% at 50°C and 1 hour of minimum time (run 12). It was concluded that low temperature reduced biodiesel yield (by 70%) even after 5 h of time (run 6), since reactant molecules needed a higher temperature to build up enough kinetic energy to collide successfully and form the corresponding methyl esters. As a result, this interaction and the final yield is significant (p-value0.0621< 0.05).

3.8.4 Fuel Properties of SSBD

Fuel properties were compared to international standards with ASTM, method D6751 to ensure biodiesel (B100) purity before its utilization in either pure or blended form (biodiesel-petrodiesel). Fuel properties of SSBD are given in Table3.8.1.

The density has a massive concern associated with biodiesel and it was found to be 0.8860Kg/L that lie within the range (0.86-0.90) g/cm^3. Due to composition of FAMEs and biodiesel purity, density is higher as compared to regular petro-diesel (Munir *et al.,* 2021).

The Kinematic Viscosity checked according to ASTM D-445 and results (4.21@ 40 °C c. St.) were found within the range (1.9-6.0)(Munir *et al.*., 2021).

Pour point is minimum temp. for liquid to lose its flowing property while cloud point is the minimum temp. where wax crystal formation happens. Our results signify the pour point and cloud point of SSBD as -8 and -7°C respectively The biodiesel combustion is also affected by its flash point (PMCC). Flash point (PMCC) of SSBD

(70 °C) is quite within the range i.e. 60-100 °C, hence safer to be used as alternate of petro-diesel (Ameen *et al.,* 2018).

Total Acid No. of SSBD was matched with ASTM D-4294 standard and was found as 0.34 mg KOH/gm that should be less than 0.5 in order to meet the international standards. SSBD has extraordinarily low Sulphur content (0.00097 wt. %) compared with ASTM D-974 (Dawood *et al.,* 2021).

Biodiesel takes several benefits above traditional petro-fuel since burns cleanly and without pollutants because to its low Sulphur content of less than 0.05 parts per million (ppm). Furthermore, the minimal Sulfur content makes biodiesel environmentally sustainable due to the decreased SO2 emissions while biodiesel burning in automobile engines (Ahmad *et al.,* 2021).

The fuel properties were found compatible with physicochemical characteristics of already reported feedstock from family Solanceae (Raj *et al.*., 2022) such as *Datura metel* (Muhammad *et al.*., 2019).
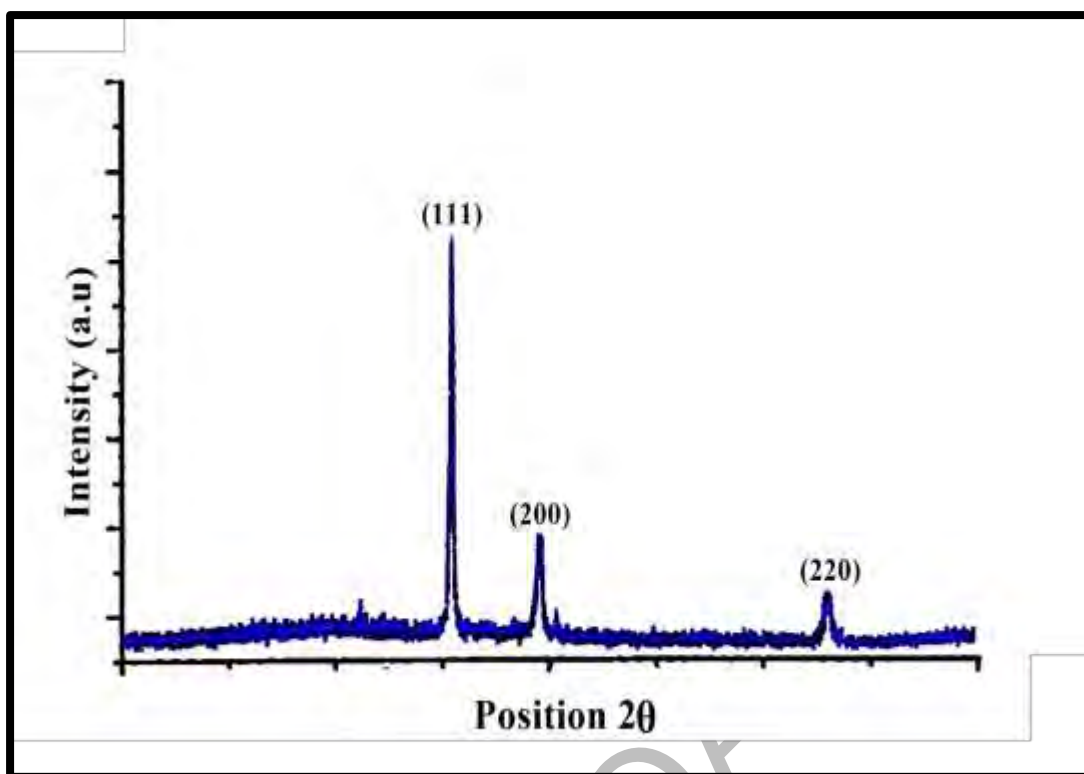
Figure 3.8.1: XRD of Ag$_2$O green nano-catalyst
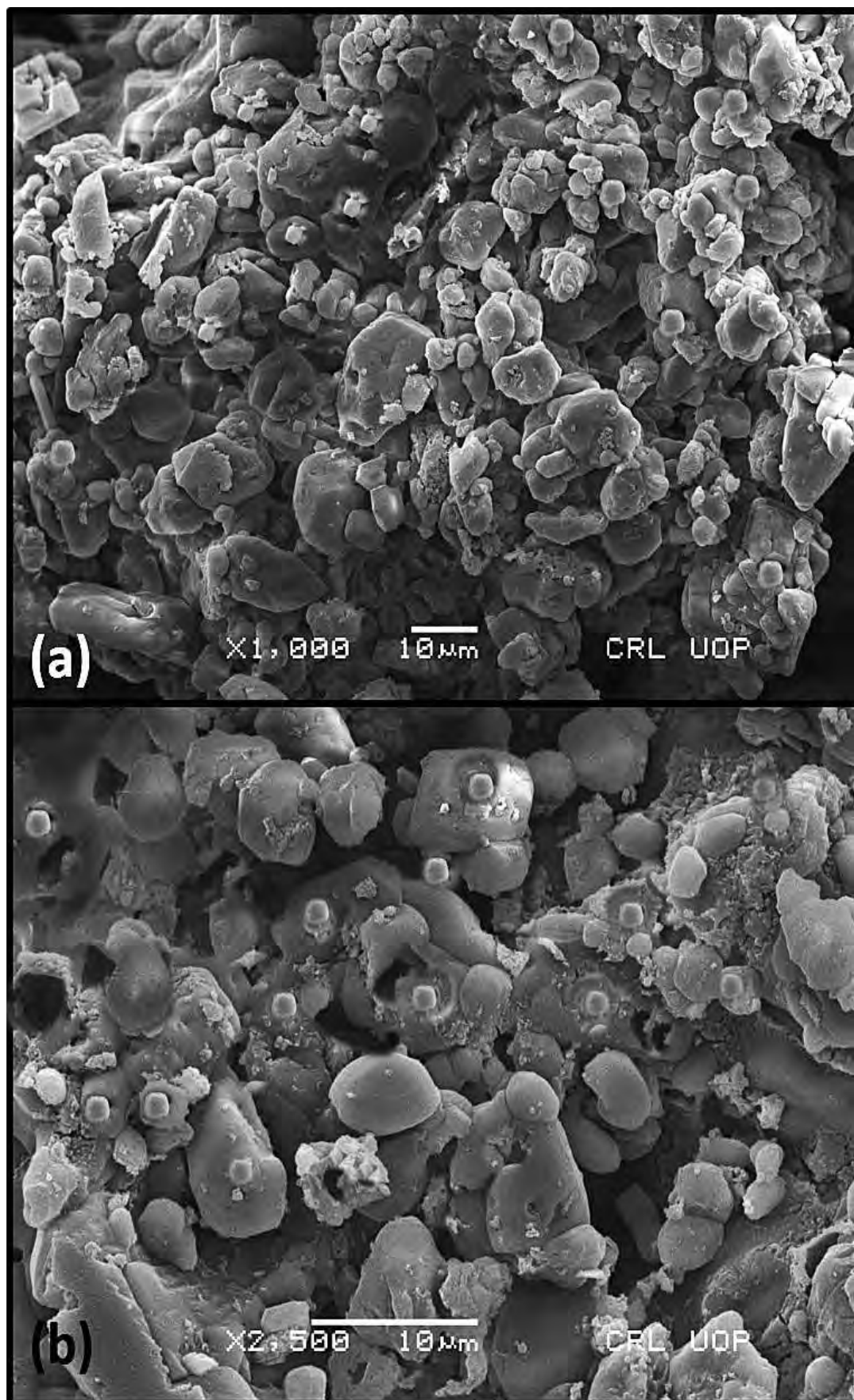
Figure 3.8.2: SEM of Ag$_2$O green nano-catalyst
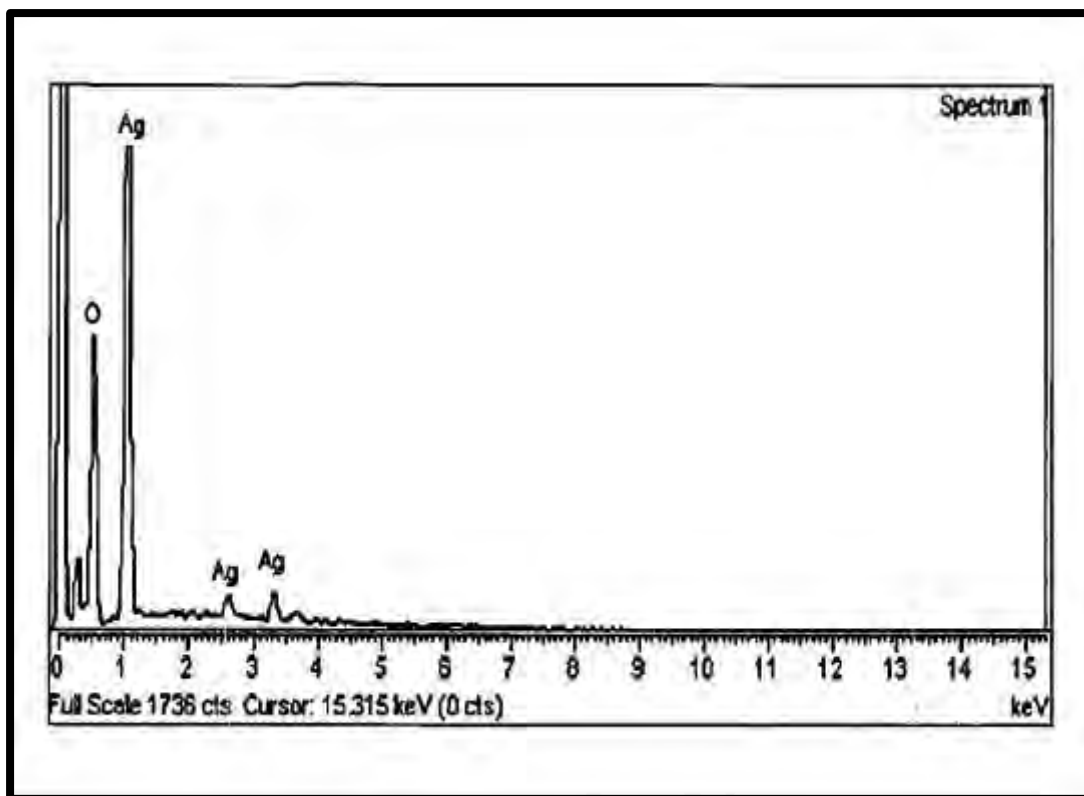
Figure 3.8.3: EDX of Ag₂O green nano-catalyst
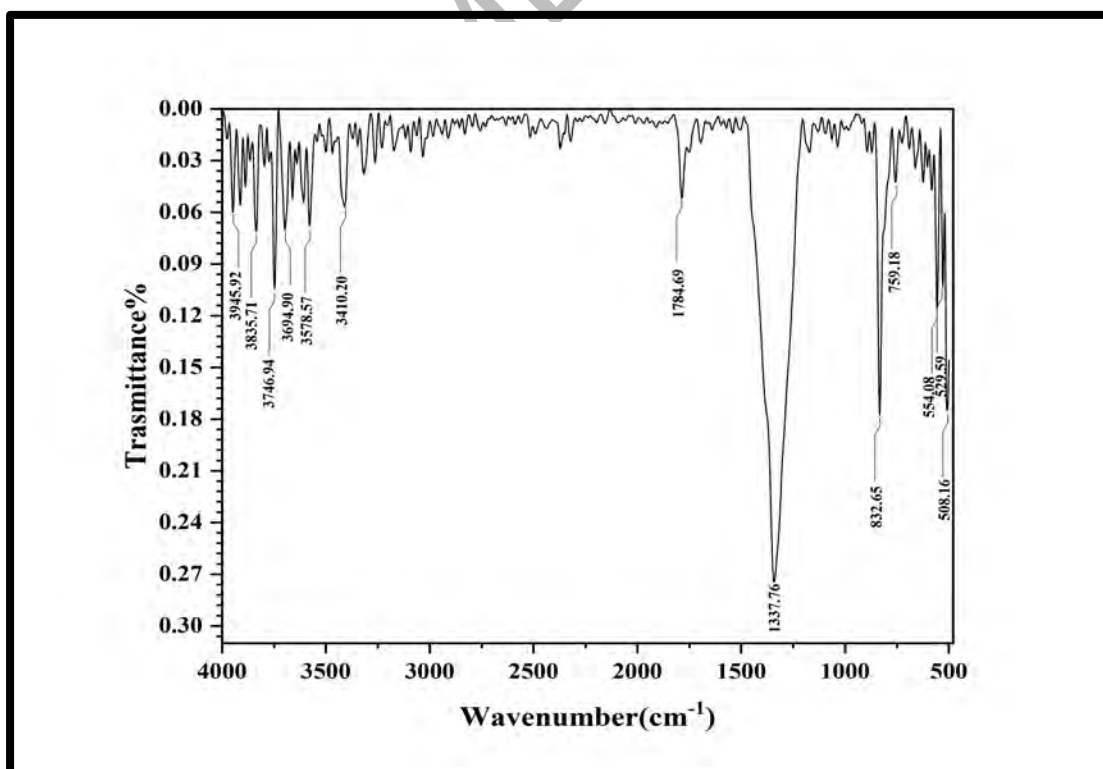
Figure 3.8.4: FT-IR of Ag₂O green nano-catalyst
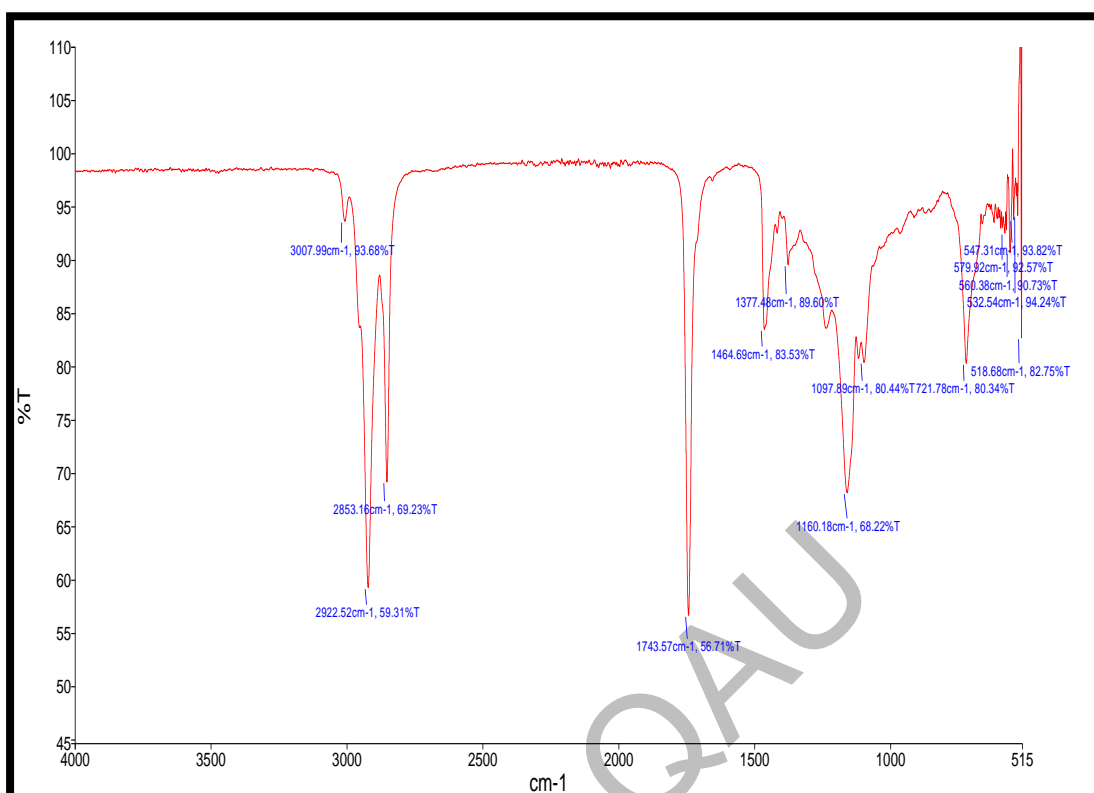
Figure 3.8.5: FT-IR of *Solanum surrantense* Biodiesel
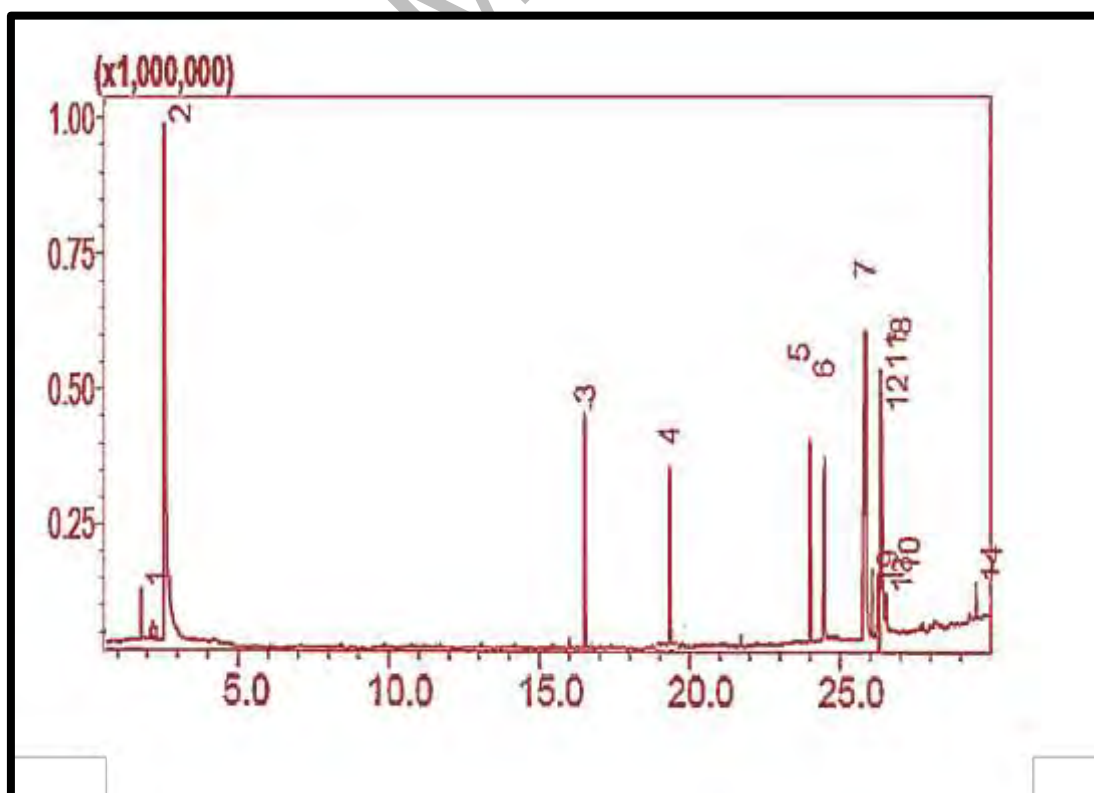
Figure 3.8.6: GC-MS of *Solanum surratense* Biodiesel
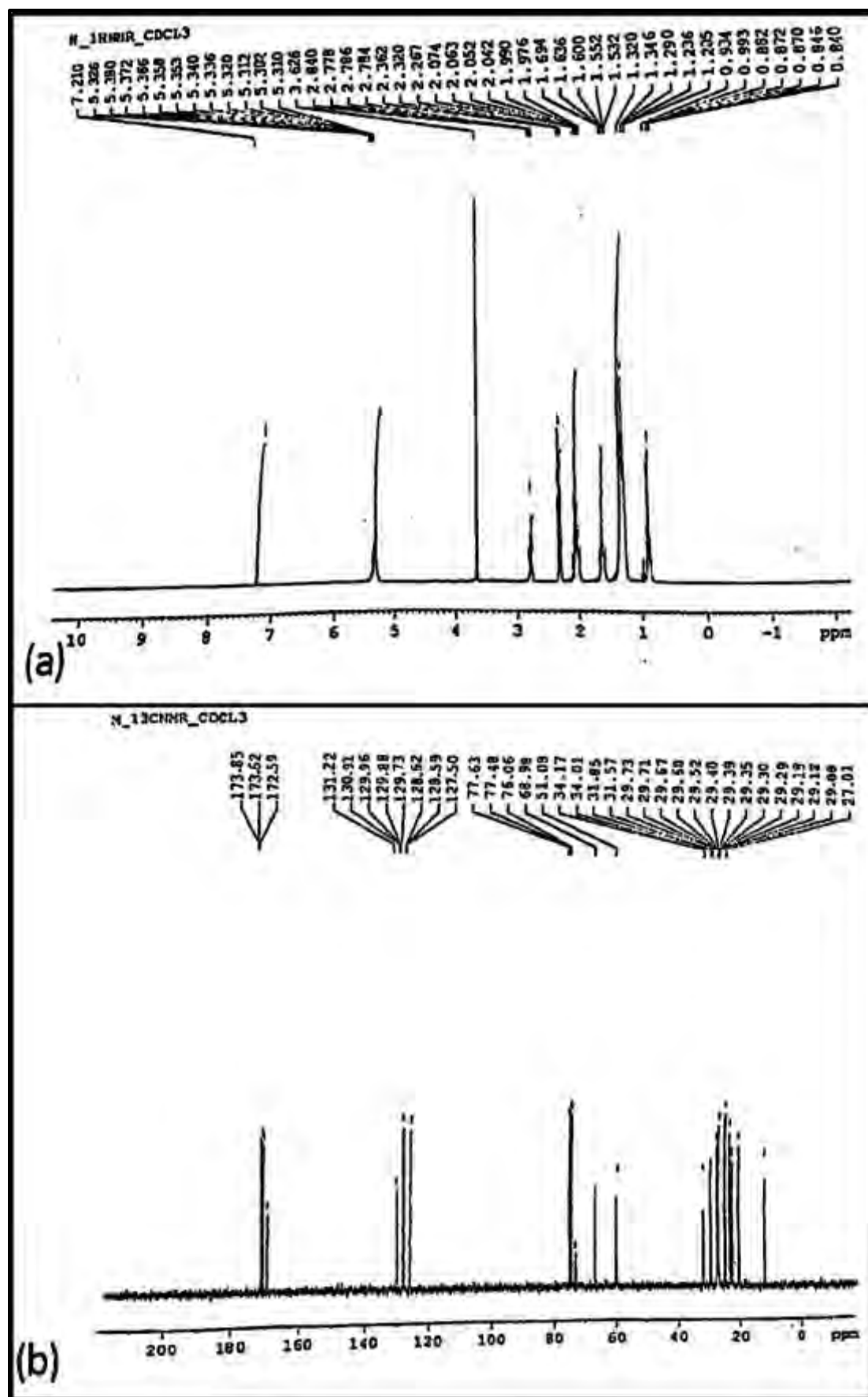
Figure 3.8.7: (a) ^{1}HNMR **(b)** ^{13}CNMR of *Solanum surrantense* Biodiesel
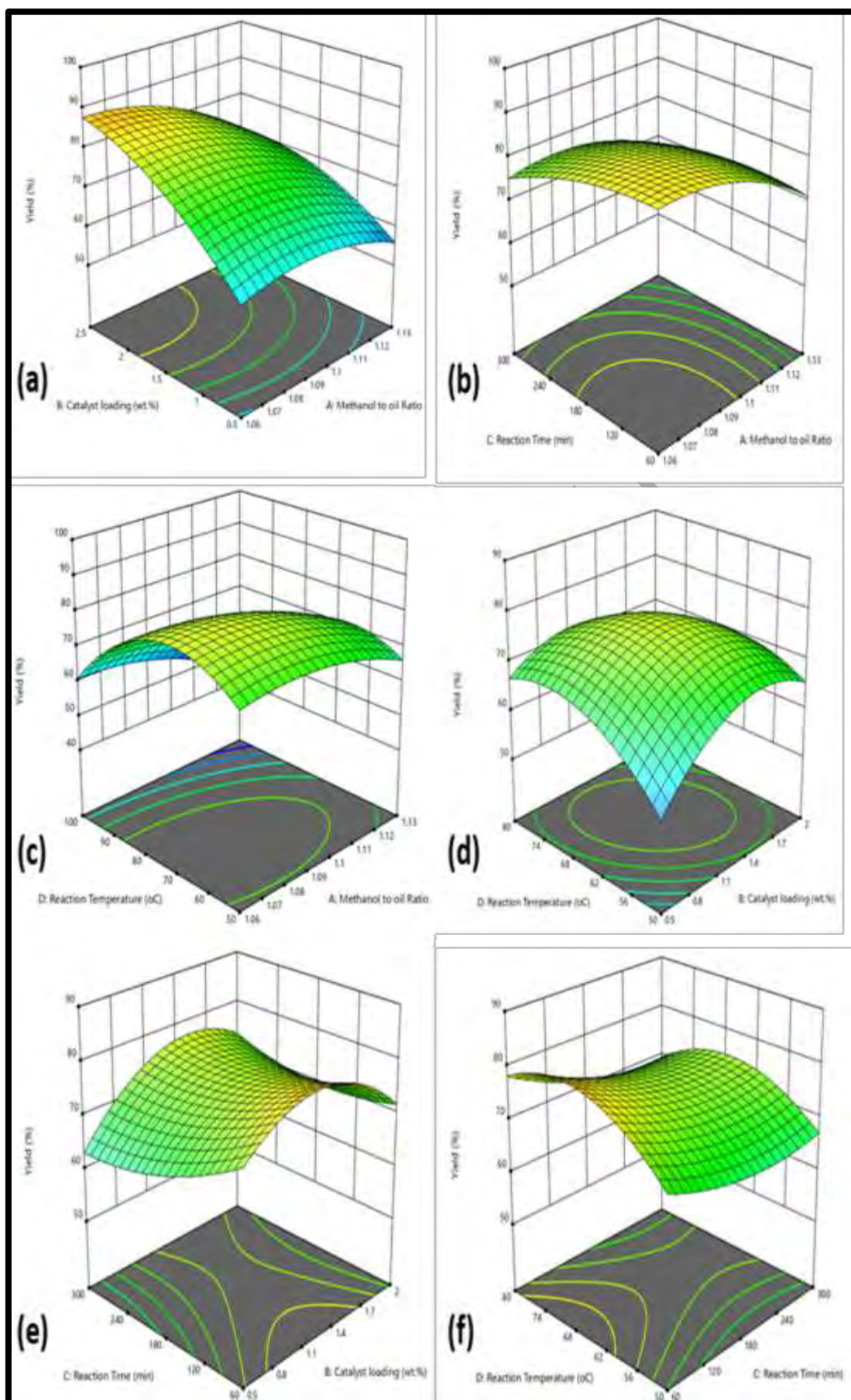
Figure 3.8.8: Influence of reaction variables on SSBD
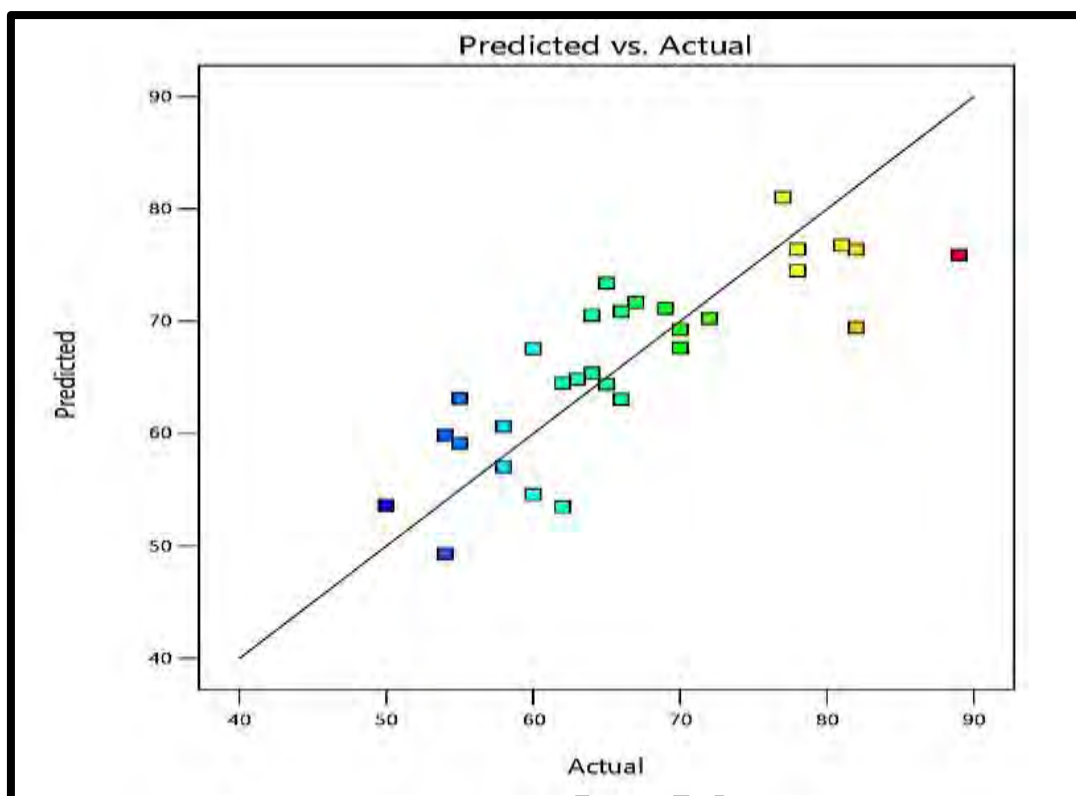
Figure 3.8.9: Predicted vs. actual yield of SSBD

Table 3.8.1: Fuel properties of SSBD

TESTS	METHOD	SS B-100
Color	Visual	2
Density @ 15 °C Kg/L	ASTM D-1298	0.8860
Kinematic Viscosity @ 40 °C c St	ASTM D-445	4.21
Pour point °C	ASTM D-97	-8
Flash point °C(PMCC)	ASTM D-93	70
Cloud point °C	ASTM D-2500	-7
Total Acid No. mg KOH/gm	ASTM D-4294	0.34
Sulphur % wt.	ASTM D-974	0.00097

Table 3.8.2: Experimental yield of SSBD

Run	Methanol to Oil Molar Ratio	Catalyst Loading (wt. %)	Reaction Time (min)	Reaction Temp. (°C)	SSBD Yield (%)
1	8.1	1.25	60	80	81
2	8.1	1.25	180	50	70
3	15.1	0.5	300	80	58
4	8.1	1.25	300	80	82
5	8.1	0.5	180	50	50
6	8.1	1.25	300	50	70
7	15.1	1.25	180	80	66
8	8.1	1.25	180	65	89
9	2.1	2	300	50	65
10	15.1	1.25	300	65	78
11	8.1	2	180	65	82
12	8.1	1.25	60	50	67
13	15.1	2	180	65	78
14	2.1	0.5	300	80	60
15	8.1	0.5	300	65	55
16	2.1	0.5	60	50	62
17	8.1	2	180	50	64
18	2.1	0.5	180	65	55
19	8.1	1.25	60	65	77
20	2.1	1.25	60	65	64
21	2.1	1.25	180	80	58
22	15.1	0.5	180	65	66
23	2.1	2	60	80	54
24	8.1	2	300	65	65
25	8.1	2	180	80	54
26	2.1	1.25	180	65	60
27	15.1	1.25	180	50	62
28	8.1	0.5	180	80	63
29	2.1	1.25	300	65	72
30	8.1	2	60	65	69

Table 3.8.3: Analysis of Variance (ANOVA) of SSBD

Source	Sum of Squares	df	Mean Square	F-value	p-value	
Model	1858.11	14	132.72	2.16	0.0060	significant
A-Methanol to oil Molar Ratio	85.69	1	85.69	1.39	0.0264	
B-Catalyst loading	28.78	1	28.78	0.4675	0.0046	
C-Reaction Time	54.35	1	54.35	0.8830	0.0323	
D-Reaction Temperature	28.85	1	28.85	0.4687	0.0040	
AB	7.29	1	7.29	0.1185	0.0355	
AC	18.78	1	18.78	0.3051	0.0488	
AD	12.79	1	12.79	0.2078	0.0550	
BC	49.00	1	49.00	0.7960	0.0364	
BD	105.87	1	105.87	1.72	0.0094	
CD	5.85	1	5.85	0.0951	0.0621	
A^2	147.00	1	147.00	2.39	0.0131	
B^2	407.79	1	407.79	6.62	0.0212	
C^2	43.53	1	43.53	0.7071	0.0136	
D^2	326.17	1	326.17	5.30	0.0361	
Residual	923.36	15	61.56			
Lack of Fit	915.36	14	65.38	8.17	0.2683	not significant
Pure Error	8.00	1	8.00			
Cor Total	2781.47	29				

SECTION: IX

Biodiesel Synthesis from *Cucumis melo* var. *Agrestis* using Magnesium Oxide Green Nano-catalyst

3.9. Biodiesel Synthesis from *Cucumis melo* var. *Agrestis* using Magnesium Oxide Green Nano-catalyst

3.9.1 Characterization of Magnesium Oxide Green Nano-catalyst

(a) XRD of MgO

In order to identify the crystalline phase of the produced nanocatalyst, X-ray diffraction method was applied. Peaks of various intensities were seen in the MgO spectra to gauge the size and form of the crystals (Figure 3.9.1). Peaks were seen to be being acquired at angles of 2°. The diffraction peaks, which correspond to the (101), (102), and (103) planes, were found at 38.40°, 42.22°, and 63.07°, respectively (JCPDS-89-7746). The average particle size was determined using the Debye Scherer.

$$D = \frac{K \; x \; \lambda \; (nm)}{FWHM \cos \theta}$$

Where;

D = Crystalline Size in nanometer; λ = Wavelength in nanometer; FWHM = Full Width at Half Maximum and θ= Braggs angle θ.

It was determined that the typical particle size was 30 nm. The cubic shape of the particles is demonstrated by the XRD pattern of synthetic MgO.

MgO nanoparticles with a size range of 70–90 nm were employed by Dawood et al. (2018) to transform yellow oleander into biodiesel. Similar to this, Shaheen et al. (2018) created a 13 nm MgO nano-catalyst and used it to turn Silybum eburneum seed oil into biodiesel (Shaheen et al., 2018).

(b) SEM of MgO

Figure 3.9.2 displays SEM images of calcined MgO catalyst at various magnifications. The catalyst was found to have a smooth, porous lamellar surface with a range of sized particles. Small particle aggregation is another phenomenon that supports the smaller particle size. The MgO nano-catalyst is depicted by SEM as having a more compact, irregularly cubical shape with aggregated nano entities. The looser and

more porous structure of the MgO nano-catalyst was described by Du and colleagues (Du et al., 2019)

(C) EDX of MgO

The chemical composition of calcined catalyst was also observed by EDX analysis Figure 3.9.3. It shows 54.62 % O, 30.72 % Mg, 10.11 % N, and 4.55 % Al. The results indicate that the synthesized MgO catalyst has a high composition of two elements: oxygen and magnesium, as reported (Dawood *et al.,* 2018). The presence of N and Al is attributed to phytochemicals in plant extract used as capping agent.

(d) FT-IR of MgO

FT-IR characterizes functional groups in addition to chemical bonds. The visible peaks in the FTIR spectrum (Figure 3.9.5), which represent C-H stretching vibrations, including the 2981.08 cm^{-1} peak. O-H bending vibrations have a peak at 1431.57 cm^{-1}. Stretching vibrations of C-O have a wavelength of 1150.43 cm^{-1}. Mg-O vibrations have a peak at 550.96 cm^{-1}. Major peaks at 449 cm^{-1}, 511 cm^{-1}, 584 cm^{-1}, and 671 cm^{-1} were observed by Tamilselvi et al. in 2013 and proved the existence of Mg-O vibrations. In our research, the stretching vibration of Mg-OH is attributed to a peak at 578.56 cm^{-1}. The absence of the 3686 cm^{-1} strong peak due to anti-symmetric stretching vibrations in the crystal structure of (MgOH)$_2$ is further evidence that hexagonal Mg(OH)$_2$ is transformed into cubic MgO during calcination (600 °C, 4h), as shown by other investigations (Shaheen et al., 2018).

3.9.2 Characterization of *Cucumis melo* var. *Agrestis* Biodiesel (CMABD)

(b) FT-IR of CMABD

Infrared radiations are used in the sophisticated technology known as FT-IR to identify chemical bonds and functional groups in each substance. The composition of biodiesel was examined in the current work by sample scanning in the mid-IR range, or 400–4000 cm^{-1}, and distinctive peaks of particular molecular bonds were seen. Figure 3.9.5 displays the prepared biodiesel's FT-IR spectra. Peaks at 1448.81 cm^{-1} (C-H stretching) corresponding to the methyl group and 2941.87 cm^{-1} (corresponding alkane) proved the presence of fatty acid methyl esters (FAMEs). The primary peak, which verifies the presence of biodiesel, was seen at 1114.74 cm^{-1}.

(c) GC-MS of CMABD

Gas chromatography and mass spectrometry were used to analyse the biodiesel to determine its chemical composition (GC-MS). Using library software (NO. NIST02), seven significant peaks in the biodiesel sample were found (Figure 3.9.6). Octanoic acid, methyl ester, methyl 8-octanoate, nonanoic acid, 9-oxo, dodecanoic acid, and 10-oxodecanoic acid were some of the FAMEs found. Other FAMEs included 2-(3-oxocyclohexyl) thio propionic acid. High temperatures speed up peroxidation, which causes engine blockage. Therefore, it is believed that a biodiesel feedstock with a lot of polyunsaturated fat is impractical. Due to mono-unsaturated acids' low affinity for oxygen, peroxidation occurs. Prior research has previously been done on these main methyl esters (Laskar *et al.,* 2020).

(d) NMR of CMABD

In this investigation, the potential of H1NMR and 13CNMR to assess the fuel characteristics of *Cucumis melo* var. *Agrestis* biodiesel was investigated (Munir et al., 2021). FAME synthesis from oil has been established thanks to the identification of the methoxy protons (-OCH3) as a distinctive singlet peak at 3.655 ppm. The existence of esters was confirmed by peaks in the range of 3.3 to 4.1 that displayed aliphatic hydrogen and alkoxy groups. Depending on the alcohol employed, triglyceride is transformed into the appropriate alkyl ester during transesterification, and the substitution of alcohol for the glycerol component causes an NMR signal to arise in the range of 5.3–3.3 ppm.

Faraguna et al. (2017) noted peaks in ^{1}HNMR spectra with ascribed biodiesel and protons of several alcohols used to make biodiesel, ranging from 4.3 to 3.5 ppm. In the biodiesel spectrum, a noticeable peak at 3.6 indicates the presence of hydrogen next to the electronegative atom corresponding to methoxy (-OCH3). Studies from the past support the presence of methoxy at this location. Other notable peaks include those at 0.876–0.884 ppm, which represent terminal methyl protons (CH3), 2.033–2.786 ppm, 1.252–1.636 ppm for methylene protons (CH2), and 5.322–5.350 ppm, which represent olefinic protons (HC=CH), respectively. As shown in Figure 3.9.7a, these signals indicate the presence of various methyl esters in the biodiesel sample.

A preferable analytical method for examining the structural makeup of FAMEs and their spectrum is ^{13}C NMR spectroscopy. According to Figure 3.9.7b, the 13C NMR spectrum exhibits signals of 51.35 and 174.21 ppm, which represent the typical ester

methoxy carbon (-OMe) and carbonyl group (-COOR), respectively. These indications show that the methyl esters in the biodiesel sample contain a variety of carbons. The unsaturated double bonds (C=C) in methyl esters are visible as peaks at 130.13 and 127.07 ppm. The terminal carbon of methyl groups (CH3) is shown by a peak at 14.03, while the long carbons of ethylene (CH2) are shown by peaks at 25.59 and 34.04 ppm. Our findings concur with ^{13}CNMR spectra of sunflower oil and fatty acid ester, a study by Li et al., 2017.

3.9.3 Biodiesel Yield Optimization via Response Surface Methodology

To transesterify *Cucumis melo* var. *Agrestis* seed oil and produce FAMEs, the MgO was utilized as a solid green nanocatalyst. The significant oil content (29.1% with 0.64 mg/g KOH) points to a base-catalyzed transesterification reaction that occurs in a single step. The 20% oil content of seeds used as feedstock is the economically optimal level, and the FFA concentration must be below 3% to achieve high-rate conversion efficiency. However, when saponification is greater than 3%, FAME yield rapidly decreases, and the separation procedure eventually becomes troublesome.

To make biodiesel, transesterification was carried out utilizing an MgO green nanocatalyst. Comprehensive experimental findings of the biodiesel synthesis procedure are shown in Table 3.9.2. For optimizing biodiesel yield (%), quadratic polynomial equation in terms of coded factors is as follow:

Biodiesel yield (wt: %) = +82.65+4.11 A+2.67 B-2.26 C-2.12 D- 0.3125 AB -0.6875 AC +0.9375 AD +1.69 BC +0.0625 BD +1.33 CD -12.54 A^2 +2.46 B^2 -18.21 C^2 +1.50 D^2 **(12)**

The results of the analysis of variance (ANOVA) for the quadratic model of the response surface methodology are shown in Table 3.9.3.

The ANOVA findings show the statistical relationship between the yield of biodiesel and four factors. To determine the importance of the associated coefficient, the P-value and F-value were computed. Probability value (<0.05) is used to indicate the model's significance, and ANOVA findings with a p-value of 0.0087 reveal that the model is significant in terms of accurately forecasting the biodiesel production. R^2 coefficient of determination is a measure of how accurately response values can be predicted. The corrected R2 value was 0.7741 while the predicted R^2 value was 0.6723. (Satisfactory).

Quadratic term A^2 (Met:Oil) and C^2 catalyst loading is significant (p-value < 0.05) whereas B^2 reaction time and D^2 reaction temperature were found insignificant (p-value>0.05). The quality of the model may be improved if these quadratic terms were eliminated. However, these quadratic terms have a connection to model hierarchy. These are therefore included. The high precision number (6.2860) quantifies the signal to noise ratio, in accordance with the obligation. A negligible lack of fit value (16.83) demonstrates that it is not regarded as equivalent to pure error when determining the significance of the model. In Figure 3.9.9, there is depiction of the straight-line graph demonstrates the high degree of concordance between experimental and anticipated yields.

3.9.3.1 Interaction between methanol to oil molar ratio and catalyst loading

Alcohol to oil ratio is a significant component that affects the transesterification reaction. Using a software for design of experiments, response surface 3D plots were produced from experimental data. These response surface graphs show how parametric interactions impact the yield of biodiesel. At their unique centres, other optimization parameters were kept.

Figure 3.9.8a shows the 3D graph of oil/methanol with catalyst loading. According to the research findings, a mole of triglycerides in oil and three moles of alcohol react, resulting in the production of three moles of fatty acid alkyl esters. By employing high alcohol concentrations that result in triglyceride monoglycerides, one can make large amounts of biodiesel. However, too much alcohol makes it more challenging to purify biodiesel by increasing glycerol solubility. According to many studies, methanolysis is fueled by certain oil to methanol molar ratios. When the catalyst quantity was 2%, the greatest FAME yield was achieved by increasing the molar ratio from 1:3 to 1:9. The extra methanol may be responsible for the increase in yield because it renews the catalysts' surface and produces methoxy species, which cause the process to move forward (Li *et al.,* 2017).

At oil to methanol molar ratios greater than 1:9, it was observed that the yield of FAME decreased, which can be attributable to product and by-product dilution by biodiesel and glycerol, respectively. The yield is subsequently reduced as a result of the shifting reaction it induces in the opposite direction It is evident that an increase in catalysts reduces the yield of biodiesel due to the production of undesirable reaction

products. Low product yield is caused by methanol-induced catalyst dilution and interference with the separation of glycerol from FAMEs (Musa, 2016).

3.9.3.2 Interaction between oil to methanol molar ratio and reaction time

Another crucial reaction parameter that has a significant impact on biodiesel yield is the molar ratio of the oil to the methanol and the reaction time. While other reaction variables like temperature (90 °C) and catalyst loading (2 wt%) were held constant, Figure 3.9.8b shows the combined effect of oil to methanol molar ratio (A) and reaction time (B). At a 1:9 molar ratio and a 360 minute time period, a maximum yield of 93% was noted. It can be credited for enhancing the long-term interaction of extra methanol with triglycerides. However, a shorter transesterification time (210 min) and low molar ratio (3:1) result in a comparably lower biodiesel production (55%), compared to other methods (run 29). Most likely, there wasn't enough time for the reactants to adequately react, which led to an incomplete conversion of reactants into products. Due to an excess of methanol, which shifted the reaction towards an undesirable reaction condition and facilitated reverse reaction, a reduction in the biodiesel yield (78%) was observed at higher oil to methanol ratios of 1:15 with times of 210 min at run number. This resulted in a low yield of biodiesel.

3.9.3.3 Interaction between methanol to oil molar ratio and reaction temperature

High temperature increases the reaction rate within the defined optimal range since it has a substantial impact on the biodiesel synthesis process. According to numerous studies, high yields are attained between 60 and 70 °C (Deshmane & Adewuyi, 2013). A 3D depiction of the relationship between reaction time and esters generation at constant catalyst loading of 2 weight percent and 360 min is shown in Figure 3.9.8c. Different temperatures were chosen appropriately during the transesterification process utilizing MgO (2% w/w) for 3 h to examine its impact on FAME yield. According to the findings of the experimental study, a slow temperature rise has a noticeable impact on the pace of response, although after a certain point, it continues to decrease. The ideal temperature for transesterification was 90 °C, and the reason for the increase in reaction rate at high temperatures is because the activation energy has decreased, leading to more interaction between the catalyst and the reactants and a faster conversion of reactants into products. The products did, however, significantly decline as the temperature was raised over the ideal level. This may be due

to the methanol evaporating over the threshold temperature (90°C), producing a low yield of biodiesel. Lower temperature causes lower yields since oil, methanol, and catalyst all have slower mass transfer rates because they are immiscible at lower temperatures and require more kinetic energy to react properly and boost productivity more quickly. The current study shows that the combined impact of molar ratio and temperature is important to take into account during the transesterification reaction.

3.9.3.4 Interaction between catalyst loading and reaction time

Figure 3.9.8d shows, while maintaining all reaction parameters constant, the combined effect of reaction time (B) and catalyst loading (C) on transesterification. Due to equilibrium in the transesterification reaction, a maximum yield of 93% was attained at the optimum duration (360min) and catalyst amount (2%), during run 26. It was also shown that the biodiesel production decreased due to the catalytic quantity and optimal level response time. When the ideal parameters, such as a 1:9 oil to methanol molar ratio, 2 weight percent catalyst, and 90°C temperature, are fulfilled, a short period of time (210 min) results in a biodiesel yield (70%) (run 22). Due to the partial conversion of reactant into product within the same time period of 210 minutes, 9:1 molar ratio, and 90°C temperature, a low biodiesel yield (65%) was obtained at a high catalyst concentration (run 18).

3.9.3.5 Interaction between catalyst loading and reaction temperature

In Figure 3.9.8e, the combined impact of the catalyst and temperature is shown. Under controlled reaction conditions with 1:9 Oil:Methanol, at 90 °C and 360 min, catalyst amount was changed from 0.5% to 3.5% during the synthesis of FAMEs from seed oil in order to examine its impact on biodiesel yield. It was found that the FAME yield improved to 93% when the catalyst concentration was increased from 0.5 weight percent to 2 weight percent of the oil used in transesterification. With a catalyst content of 0.5%, the lowest FAME yield of 40% was produced as some of the triglycerides' biodiesel conversion (run 25). And 120°C was the reaction temperature. While the largest yield of methyl esters was reached at 2 weight percent, this rise may have been brought on by the presence of additional active sites on the catalyst surface.

Nevertheless, the yield was obtained reduced by the addition of more initial concentrations from above, likely due to a rise in the viscosity of the reaction medium brought on by a decrease in catalytic activity. As a result, the catalyst's interaction with the reaction system was reduced, resulting in a low product concentration (Musa, 2016).

Thus, 2 wt.% was identified as the ideal catalyst loading to achieve the highest FAME yield possible through trans-esterification. The yield of FAME in soybean oil increased with an increase in MgO content from 0.5 to 2%, but thereafter, the biodiesel yields declined with a higher concentration. As a result, these findings are in perfect agreement with the conclusions of recent study. According to a previous study by Eevera and colleagues, low FAME production resulted from subsequent temperature increases that cause saponification (Eevera et al., 2009).

3.9.3.6 Interaction between reaction time and reaction temperature

The combined impact of reaction temperature and time is shown in Figure 3.9.8f for a constant oil to methanol molar ratio, or 1:9 and 2% catalyst. Reaction time, like reaction temperature, is a crucial component that influences the transesterification reaction since it determines how much biodiesel will cost to produce. In this communication, a reaction time range of 60 to 360 minutes has been noted. After 360 minutes at 90 °C, the yield of FAME grew noticeably to 93%, and any further increases after the optimal period caused a sharp decline in yield. It is understandable that after an hour of reaction time, chemical equilibrium had not been reached because all of the reactants did not have enough opportunity to interact with the catalyst, resulting in a lower product. It is evident that the yield was 70% at a 9:1 methanol to oil molar ratio, 2 weight percent catalyst, and 90 °C for 60 minutes (run 22) Increase in time to 210 minutes improved the productivity to 89% (run 20), and In optimum time duration (360min), the reaction moved forward, equilibrium was attained, and highest production, i.e., 93%, was observed. Decreased yield is attributed to less time duration and insufficient time required to achieve maximum yield (run 26). A longer period of time did not, however, result in a higher FAME output. Longer hours of reaction time, however, showed a modest decrease in products due to backward reaction's conversion to reactants. Numerous research have examined how reaction time affects biodiesel output (Eevera et al., 2009). Several research revealed that reaction time has an impact on product yield (Okwundu et al., 2019). As an illustration, a steady elevation in FAME yield was seen with an increase in reaction time and increasing yield; however, after a certain period of time, it decreased as a result of reversible transesterification reaction.

3.9.4 Fuel Properties of CMABD

The fuel characteristics of synthetic biodiesel were identified and evaluated against ASTM norms. Investigations were conducted on fuel qualities including total

acidity, flash point, sulphur content, cloud point, kinematic viscosity, pour point, and density (Akhtar et al., 2019; Mallah & Sahito, 2020). ASTM specifications state that the *Cucumis melo* var. *Agrestis* biodiesel is visually colored. A liquid at a particular lowest temperature in the air near that liquid forms an ignitable combination when exposed to a spark or flame. This flashpoint provides a measurement of a liquid's ability to combine with another substance to ignite. Fuel with a high flash point can be moved, stored, or handled safely when it is needed for use. (Dawood et al., 2021). The fuel is safe to use based on the recorded value of (73.5°C) using ASTM-93, as diesel has a flashpoint of 53 °C and high-speed diesel has a flashpoint range of 60–80 °C (HSD). The density of the fuel is defined as the mass measured in a vacuum per unit of volume. Density is a simple way to determine the quality of biodiesel because it immediately affects fuel efficiency and is significantly correlated with viscosity and cetane number. The ASTM D-1298 standard was used to calculate the density of biodiesel, which was found to be 0.800 kg/L while the density of HSD is 0.834 kg/L (Arshad *et al.,* 2023).

Hence *Cucumis melo* var. *agrestis* biodiesel has less density as compared to HSD. It acts as a sign to show the capability of liquid to run (Table 3.9.1). The high viscosity of the fuel has a significant impact on engine performance. Instead of using highly viscous crude oil directly, it is now necessary and practical to reduce its viscosity through the esterification process. Vegetable oil has a viscosity between 27.2 and 53.6 mm^2/s, while the biodiesel it produces has a viscosity between 3.6-4.6 mm^2/s. To achieve very small fuel droplets and for simple drainage, less viscous oil is needed. (Razavi et al., 2019). According to ASTM D -445 standards, the kinematic viscosity of *Cucumis melo* var. *agrestis* biodiesel is 4.23 @ 40 °C. Biodiesel of rapeseed oil and palm oil biodiesel is 4.2 and 4.3-4.5 @ 40 ᵒC, respectively, similar to or higher than the kinematic viscosity of *Cucumis melo* var. *agrestis* biodiesel. As K. Viscosity (4.23 mm^2/s) lies between the standards values (i.e., 1.9-6.0 mm^2/s). The cloud point is the lowest temperature at which paraffin crystallises or has a tendency to separate under proposed conditions in cold temperatures. The term "pour point" refers to the temperature at which gasoline can flow. In biodiesel made from sesame seed oil, Saydut and colleagues reported these parameters as -6 °C and -14 °C, respectively (Saydut *et al.,* 2008). In the current study, the determination of cloud point and pour point was carried out using ASTM D-2500, and ASTM D-97 standards. According to ASTM standards, the value of pour point was -7 °C and its cloud point were -12 °C higher than HSD. In polluted areas, the fuel having less sulfur contents is considered ideal. Low

sulfur content is indispensable for the environment and the engine's life. As a result, the sulphur concentration of *Cucumis melo* var. *Agrestis* biodiesel is 0.0001 by weight, which is low compared to the 0.05 requirement set forth by ASTM D-4292. The biodiesel is superior to HSD, as seen by the declining sulphur content. The amount of carboxylic acid necessary to neutralize FAME, measured as mg KOH/gm, or the presence of FFA in a fuel sample is known as the acid or neutralization number (1g). It outlines how to confirm a specific fuel's ability to age and/or an appropriate synthesis procedure, as well as how to determine whether heat degradation caused fuel degradation. Diesel fuel becomes more acidic if the FFA content is high; otherwise, diesel lacks an acidic quality. The engine efficiency is impacted by the excessive number of acid values. It causes corrosion inside the engine components and in the system. The *Cucumis melo* var. *Agrestis* biodiesel has an acid value of 0.167, which is within the acceptable range (0.5) of ASTM D-974 i.e. global standard.
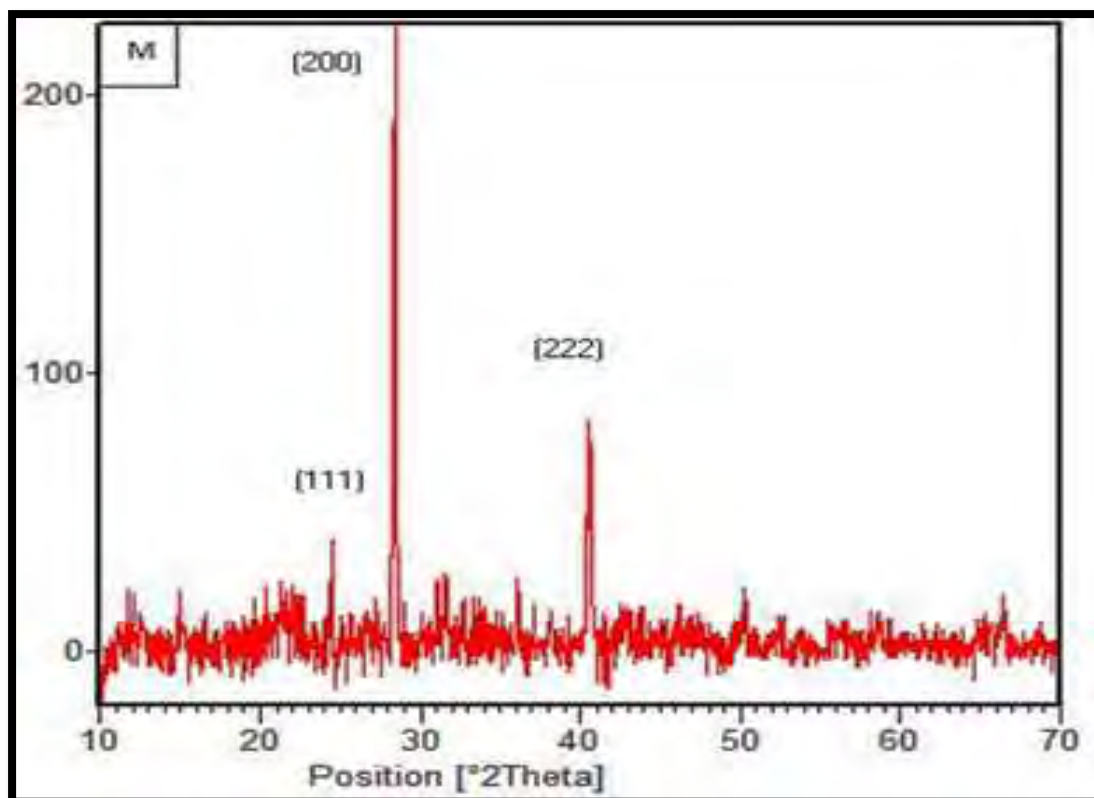
Figure 3.9.1: XRD of Magnesium Oxide Green Nanocatalyst
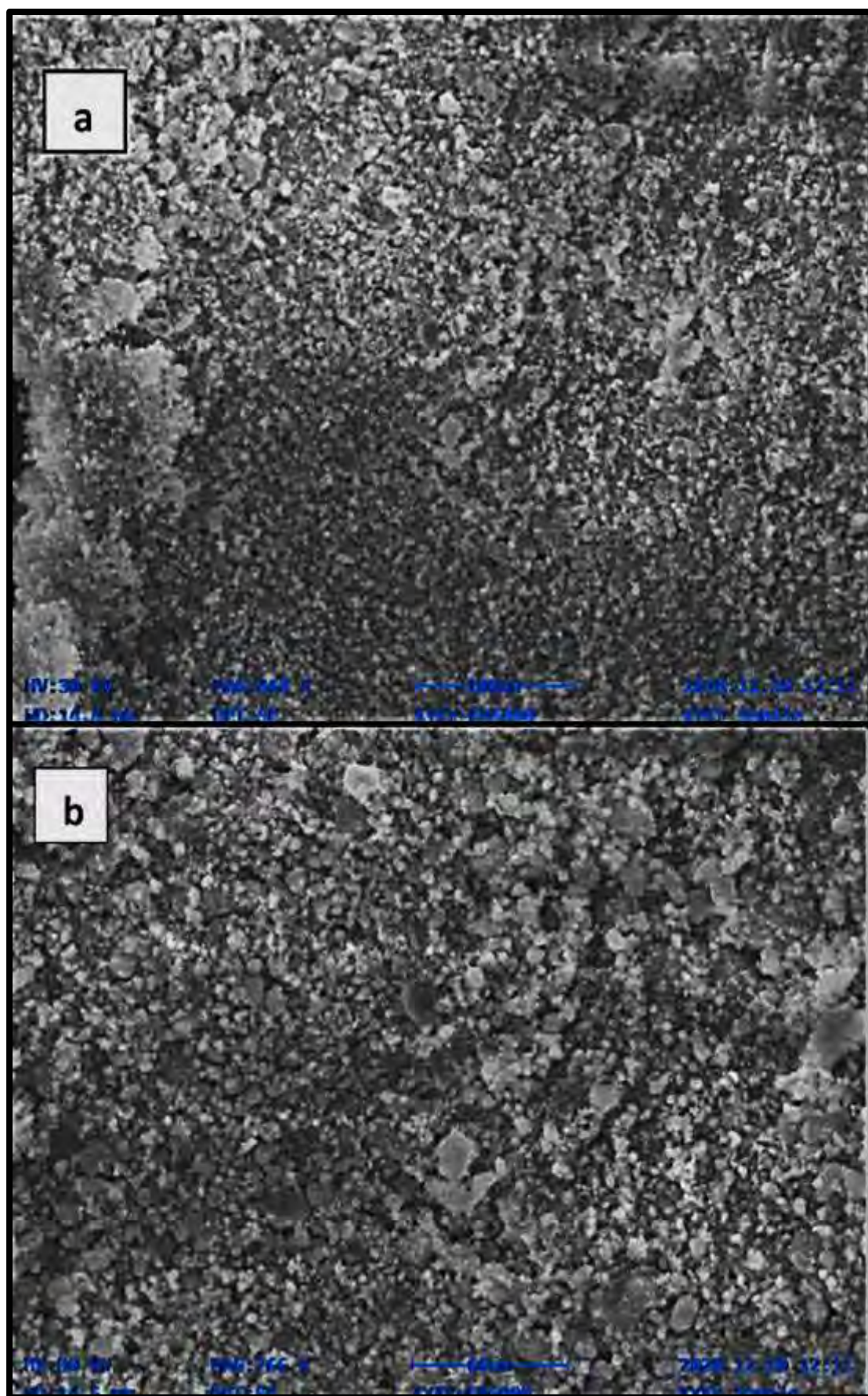
Figure 3.9.2: SEM of Magnesium Oxide Green Nanocatalyst
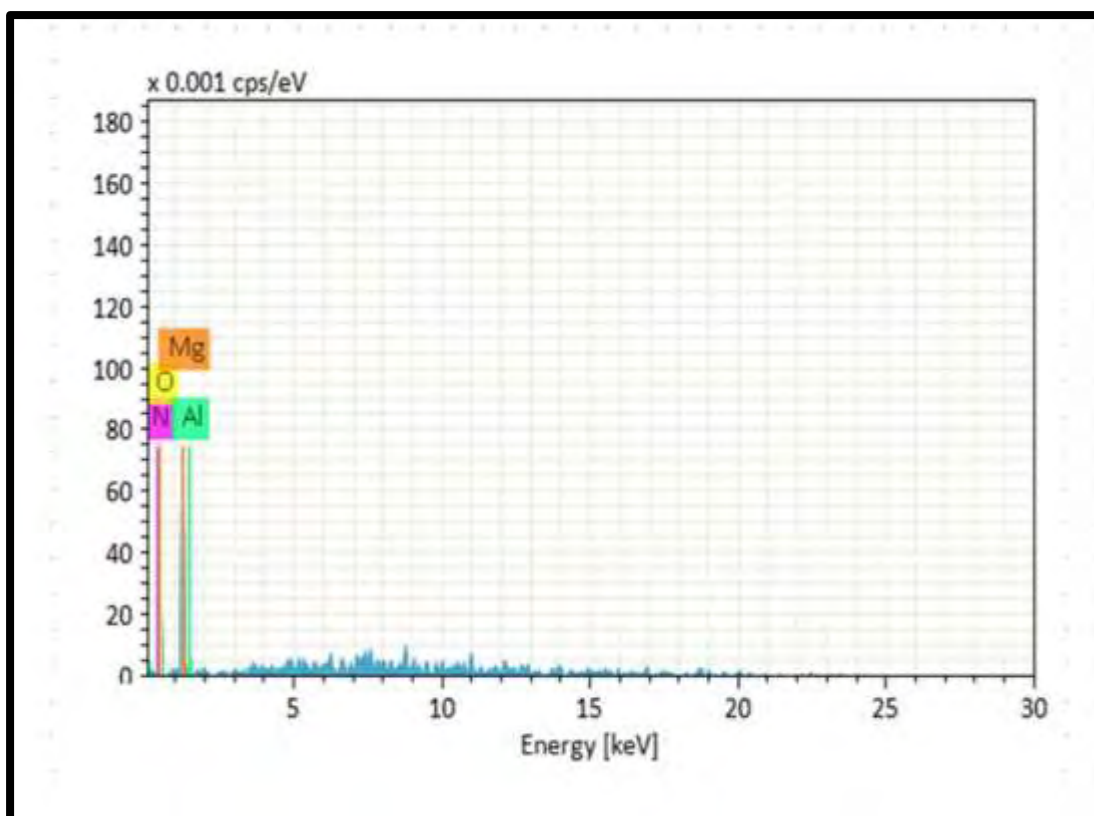
Figure 3.9.3: EDX of Magnesium Oxide Green Nanocatalyst
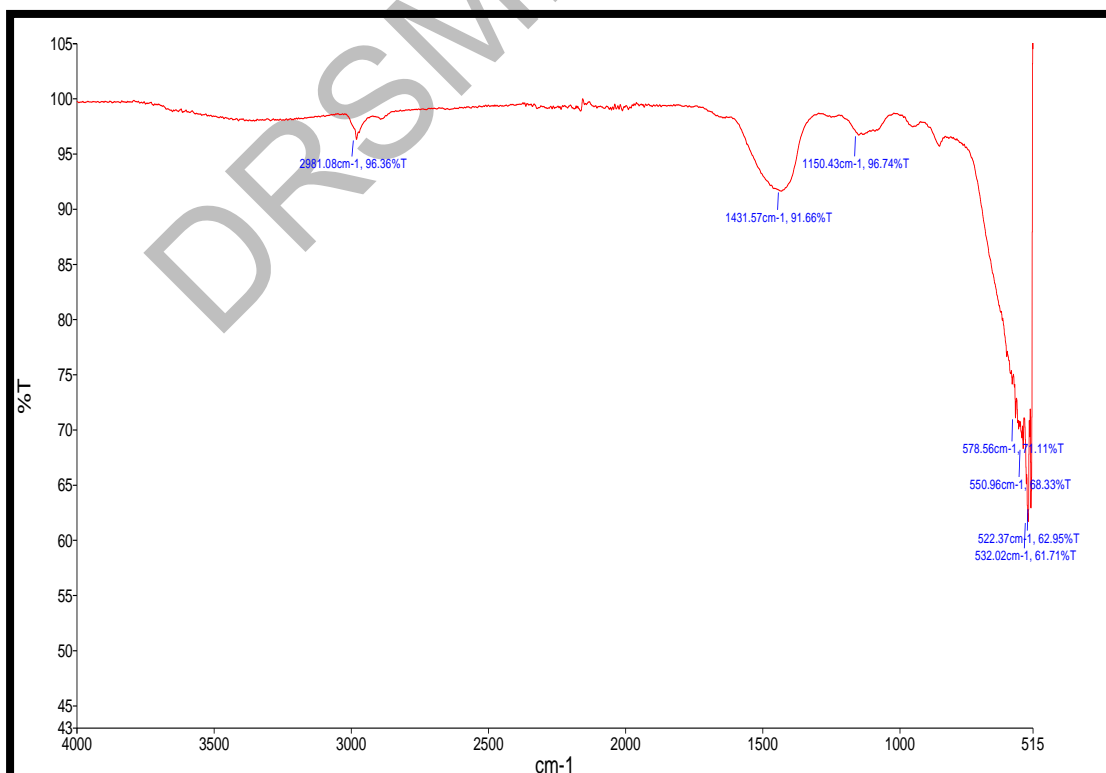
Figure 3.9.4: FT-IR of Magnesium Oxide Green Nanocatalyst
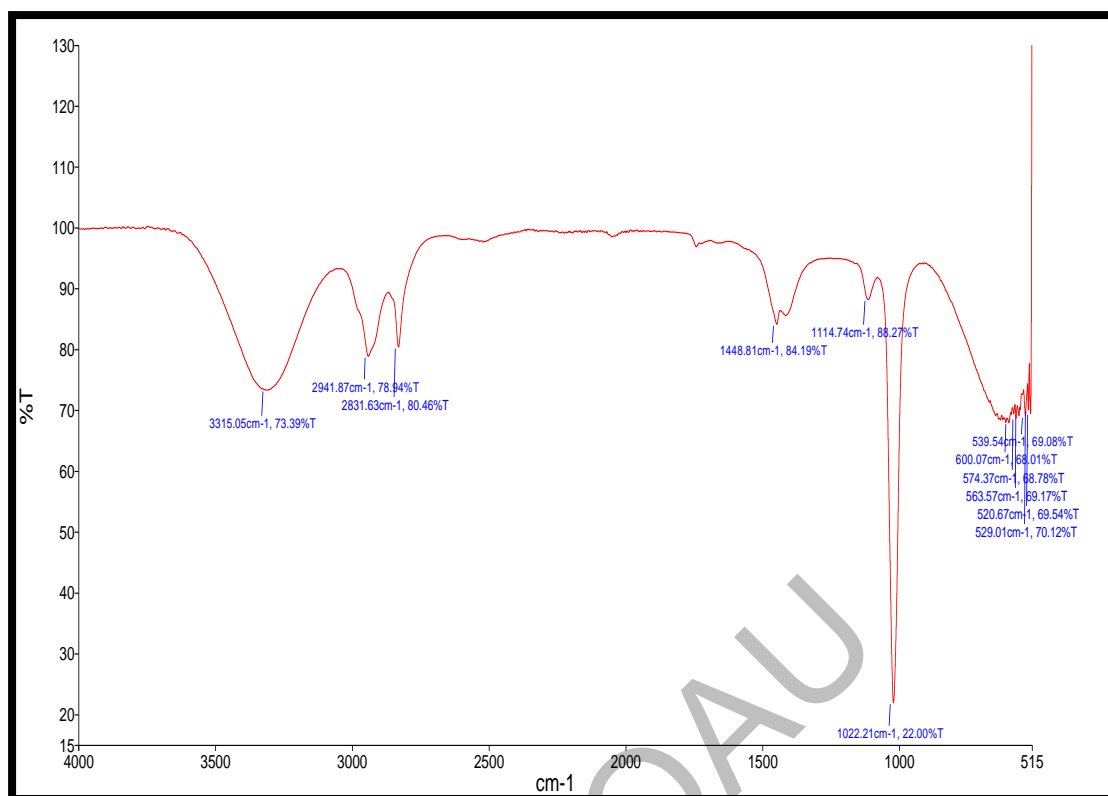
Figure 3.9.5: FTIR spectrum of CMABD
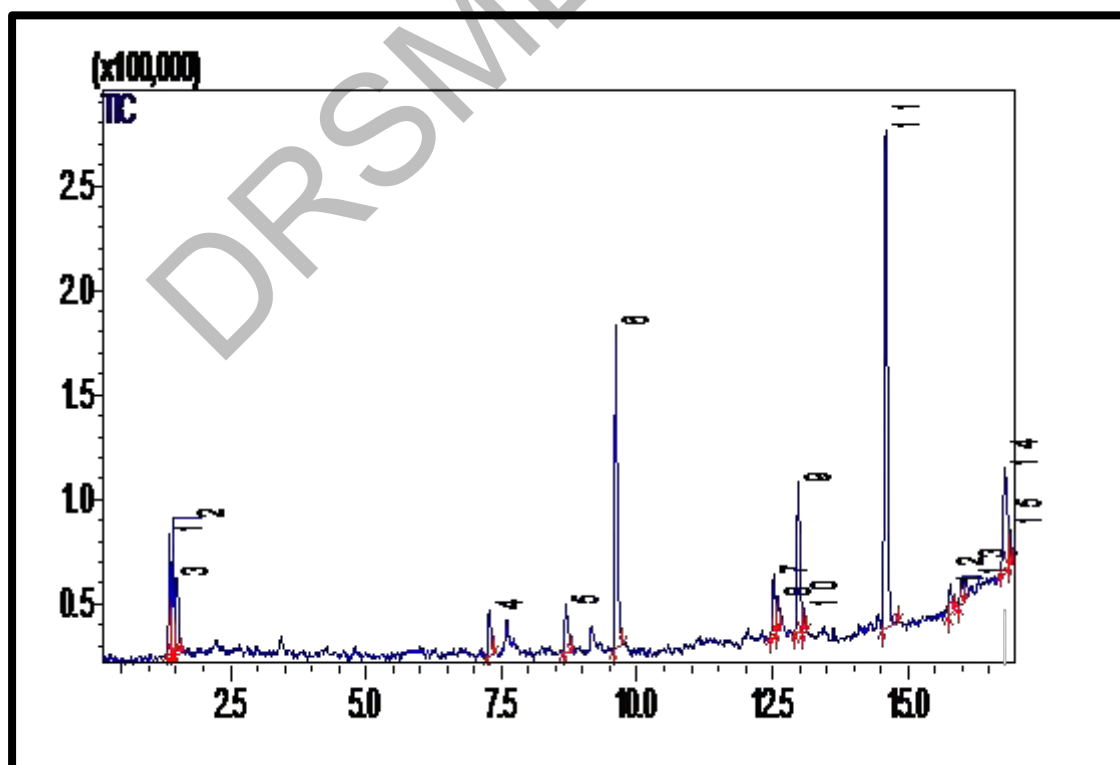
Figure 3.9.6: GC-MS spectrum olf CMABD
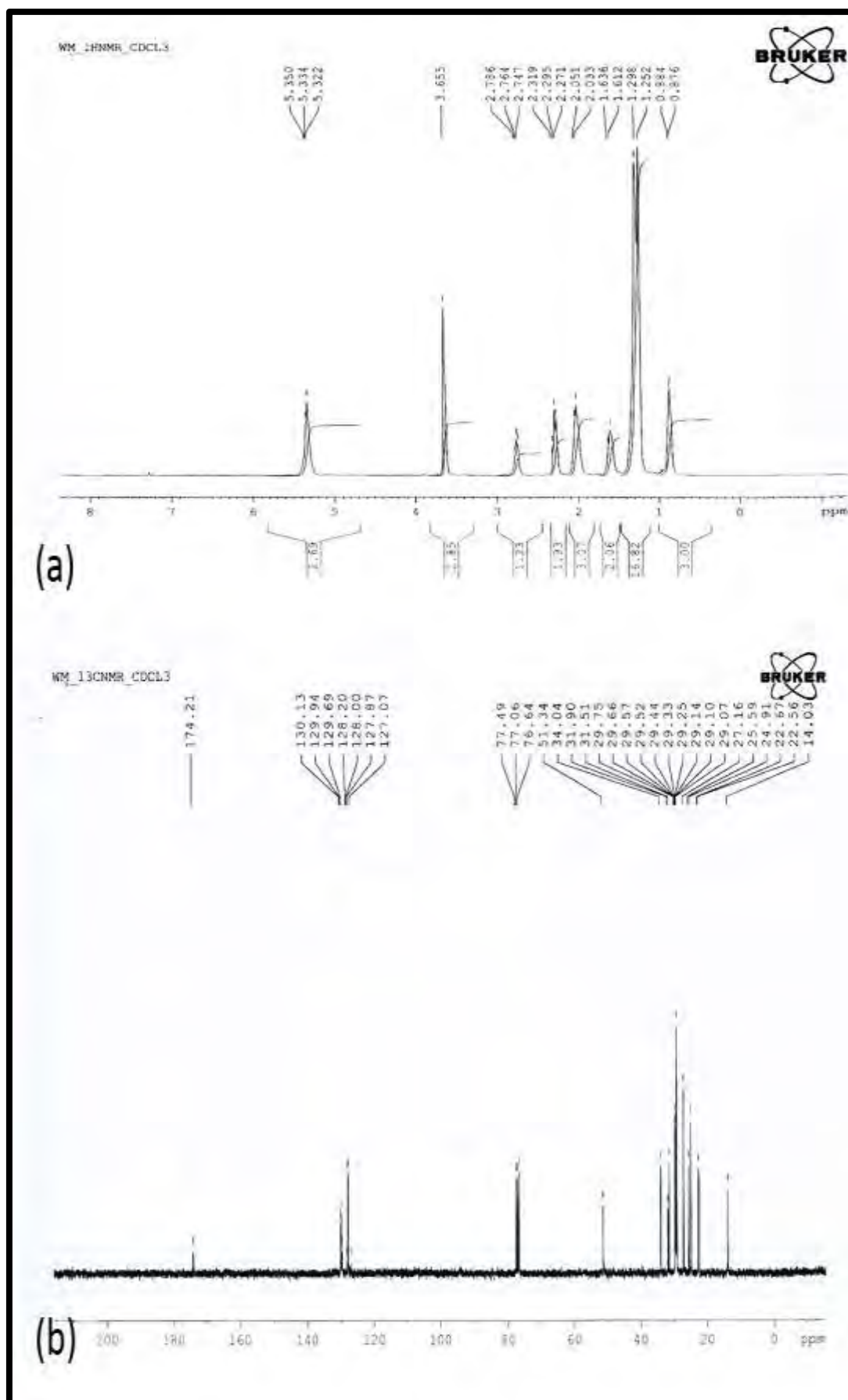
Figure 3.9.7: (a) ¹HNMR **(b)** ¹³CNMR spectra of CMABD
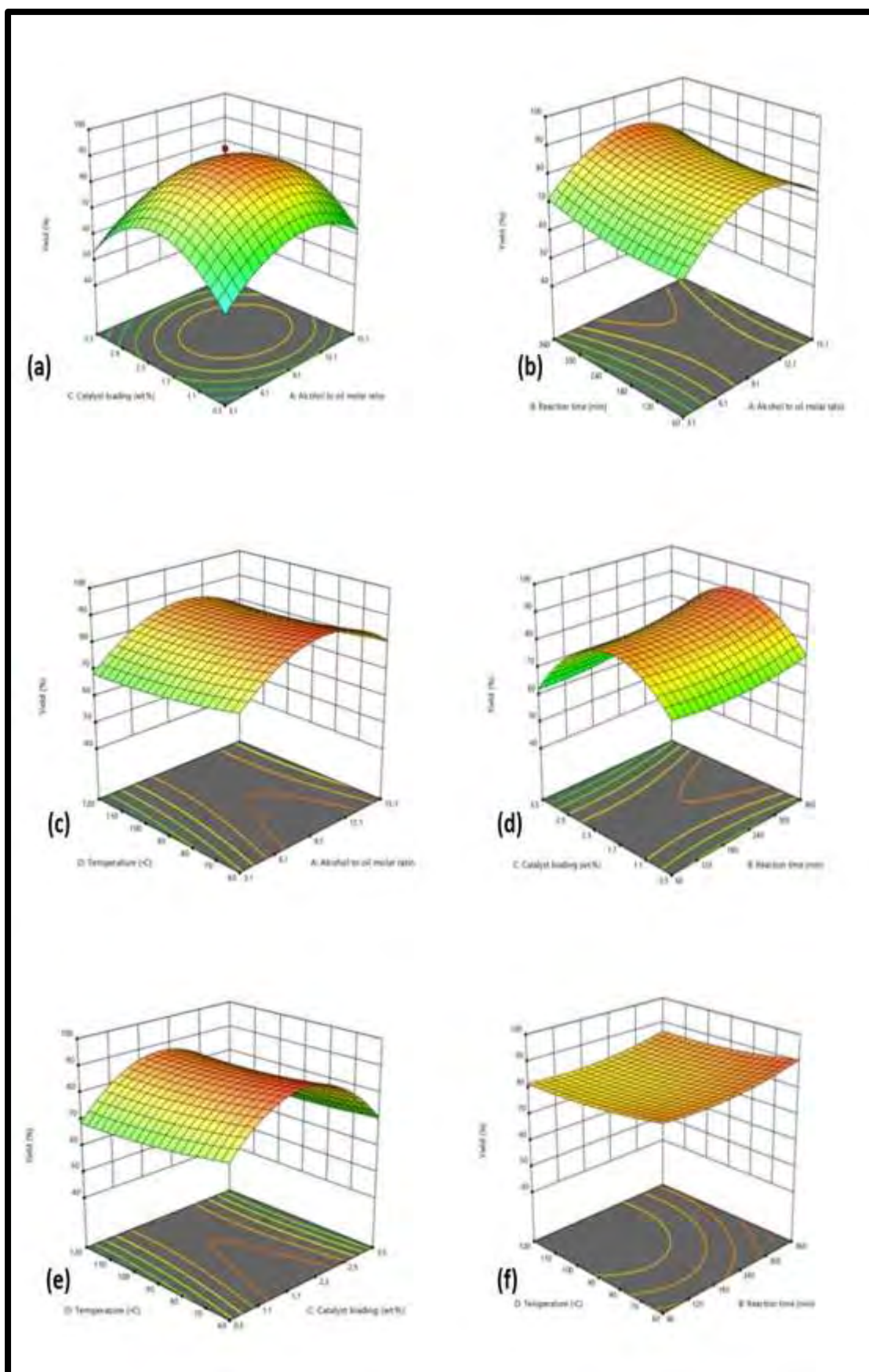
Figure 3.9.8 (a-f): The influence of reaction variables on CMABD
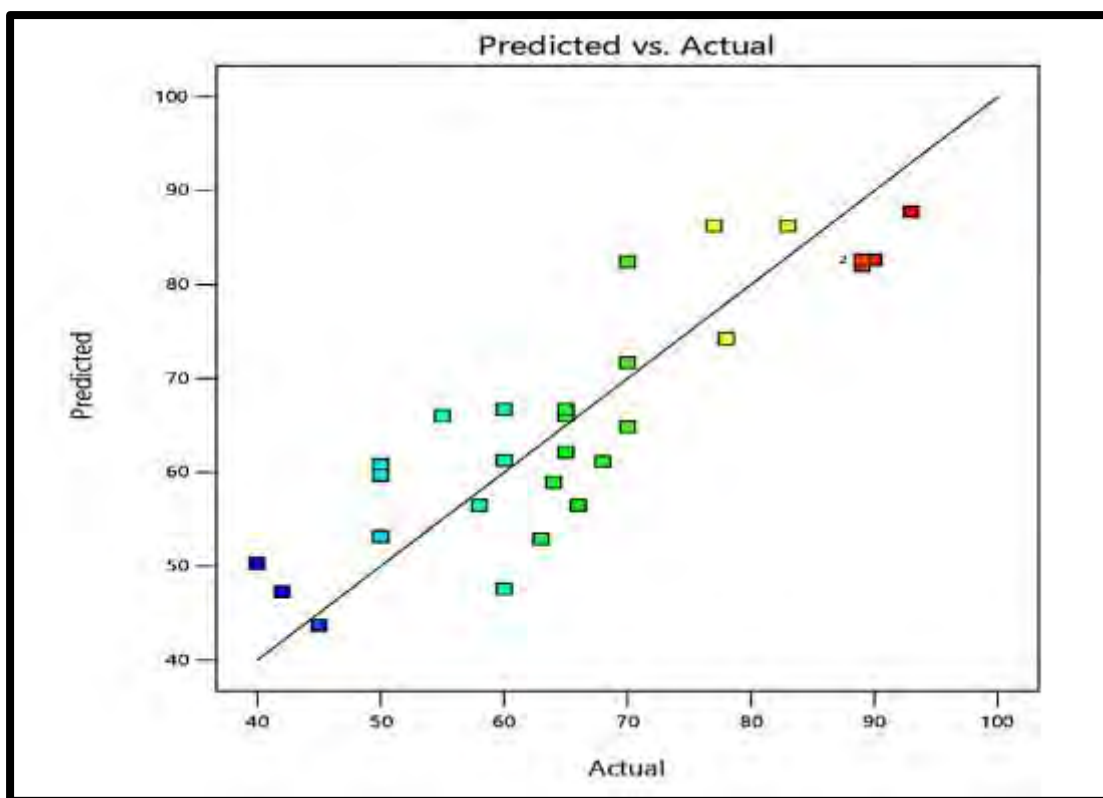
Figure 3.9.9: Predicted vs. actual yield of CMABD

Table 3.9.1: Fuel properties of CMABD

TESTS	METHOD	CMA B-100
Color	ASTM D-1500	Visual
Flash Point ℃(PMCC)	ASTM D-93	73.5
Density @15°C Kg/L	ASTM D-1298	0.800
K. Viscosity @ 40°C cSt	ASTM D-445	4.23
Pour Point °C	ASTM D-97	-7
Cloud Point °C	ASTM D-2500	-12
Sulphur % wt.	ASTM D-4294	0.0001
Total Acid No. mg KOH/gm	ASTM D-974	0.167

Table 3.9.2: Experimental yield of CMABD

Run	A:Alcohol to oil molar ratio	B:Reaction time (Min)	C: Catalyst loading (wt. %)	D:Temperature °C	Yield %
1	9:1	210	2	120	89
2	9:1	210	0.5	60	70
3	3:1	60	0.5	120	60
4	15:1	360	0.5	120	68
5	15:1	360	3.5	120	60
6	15:1	360	0.5	60	65
7	15:1	360	3.5	60	50
8	9:1	210	2	60	77
9	15:1	60	3.5	60	63
10	9:1	210	2	90	89
11	3:1	360	0.5	60	64
12	3:1	360	3.5	60	66
13	15:1	60	0.5	60	70
14	3:1	60	3.5	120	45
15	3:1	60	0.5	60	58
16	9:1	210	2	90	90
17	15.1	210	2	90	78
18	9:1	210	3.5	90	65
19	15:1	60	0.5	120	50
20	9:1	210	2	90	89
21	9:1	210	2	60	83
22	9:1	60	2	90	70
23	9:1	210	0.5	90	65
24	3:1	60	3.5	60	42
25	3:1	360	0.5	120	40
26	9:1	360	2	90	93
27	3:1	360	3.5	120	50
28	9:1	210	0.5	90	60
29	3:1	210	2	90	55
30	15:1	60	3.5	120	50

Table 3.9.3: Analysis of Variance (ANOVA) for CMABD

Source	Sum of Squares	df	Mean Square	F-value	p-value	
Model	5049.59	14	360.69	3.67	0.0087	significant
A-Alcohol to oil molar ratio	304.22	1	304.22	3.10	0.0988	
B-Reaction time	128.00	1	128.00	1.30	0.2715	
C-Catalyst loading	97.40	1	97.40	0.9918	0.3351	
D-Temperature	85.47	1	85.47	0.8703	0.3657	
AB	1.56	1	1.56	0.0159	0.0013	
AC	7.56	1	7.56	0.0770	0.7852	
AD	14.06	1	14.06	0.1432	0.0104	
BC	45.56	1	45.56	0.4639	0.5062	
BD	0.0625	1	0.0625	0.0006	0.0802	
CD	29.70	1	29.70	0.3024	0.5905	
A²	467.73	1	467.73	4.76	0.0454	
B²	18.00	1	18.00	0.1833	0.6747	
C²	1225.55	1	1225.55	12.48	0.0030	
D²	8.32	1	8.32	0.0847	0.7751	
Residual	1473.21	15	98.21			
Lack of Fit	1442.04	11	131.09	16.83	0.0075	significant
Pure Error	31.17	4	7.79			
Cor Total	6522.80	29				

R^2 0.7741, Std. Dev 9.91, C.V. % 15.06, Adeq. Precision 6.2860

4. CONCLUSION AND RECOMMENDATIONS

In this study, eight different oil yielding seeds have been identified systematically on the basis of morphological characters and scanning electron microscopic analysis. To address energy crises, particularly in Pakistan and globally, a thorough analysis of the viability of synthesizing biodiesel using various catalysts has been conducted. Selected feedstock for biodiesel production included *Bischofia javanica, Eryobotrya japonica, Praecitrullus fistulosus Luffa acutangula, Diospyros lotus*, *Cucumis melo* var. *Cantalupensis*, *Solanum surattense* and *Cucumis melo* var. *Agrestis.* Eight different, affordable, stable and efficient green nano-catalysts (ZrO_2, CoO, CuO, CdO, NiO, CaO, Ag_2O and MgO) were synthesized from same feedstock using the biosynthesis method. Response surface methodology was applied to test the effectiveness of these catalysts during the transesterification of seeds oil under ideal conditions.Light microscopy reveal the seeds are 3-4 mm in length and 14-16 mm in width with remarkable variation in seed color with various shades from yellow to brown and gray to black were also observed. SEM ultrastructure analysis of seeds reveals significant variation in seed size, color, sculpturing, form, and arrangement of the periclinal wall and other characteristics. Seed shape varies from ovoid, obovoid, ovate, obovate, semi-spheroid, oblong, and discoid. Surface sculpturing varied from verrucate, reticulate, wrinkled, striate, ruminate and thickened. Seeds wall ornamentation exhibits great variation from thin to very thick, concave, convex, buttressed, raised, undulate pattern and seed hilum was visible and invisible, sub-terminal to terminal, depressed or raised with lateral or dorsoventral compression. Prior to transesterification, physico-chemical characteristics of seeds were determined. The findings revealed that acid content of seeds oil ranges from 0.78-6.91 mg KOH/g. To prevent saponification, sulphuric acid (1% H_2SO_4) was used as a catalyst in acid esterification to lower the acid value of the oil before transesterification.

In comparative analysis, except for the non-edible seed oils of *Luffa acutangula* (3.91 mg/KOH) and *Diospyros lotus* (6.91 mg/KOH), which require pretreatment for FFA reduction, all selected seed oils contain less than 3% FFA content. The results showed that *Cucumis melo var. Cantalupensis* produced the best biodiesel output (98%) when employing a calcium oxide (CaO) green nano-catalyst However, the *Diospyros lotus* was found to have the lowest biodiesel yield (87%) when reaction was catalyzed by nickel oxide (NiO) green nano-catalyst.

Using various catalysts on various seed oils, the overall key findings were as follows:

a. The optimum conditions for novel, waste and non-edible *Bischofia javanica* seed oil (BJSO) using ZrO_2 green nano-catalyst were 1:6 oil to methanol ratio, 2.5 wt. % catalyst amount at 70°C for 3h giving 95.8% yield of *Bischofia javanica* biodiesel (BJBD).

b. For non-edible *Eryobotrya japonica* seed oil (EJSO), the transesterification reaction was optimized by using CoO green nano-catalyst with 1:7 oil to methanol ratio, 0.1 wt. % catalyst amount at 60°C for 3h with 96 % yield of *Eryobotrya japonica* biodiesel (EJBD).

c. The *Praecitrullus fistulosus* seed oil (PFSO) was transesterified via CuO green nano-catalyst were 1:9 oil to methanol ratio, 0.1 wt. % catalyst amount at 55°C for 2.5h produced 91 % yield of *Praecitrullus fistulosus* biodiesel (PFBD).

d. Ideal conditions for *Luffa acutangula* seed oil (LASO) using CdO green nano-catalyst were 1:3 oil to methanol ratio, 0.5 wt. % catalyst amount at 65°C for 3h, a 93% yield of *Luffa acutangula* biodiesel (LABD) was achieved.

e. The novel non-edible seed oil of *Diospyros lotus* (DLSO) was converted *Diospyros lotus* biodiesel (DLBD) under optimum conditions of 1:9 oil to methanol ratio, 1.25 wt. % of NiO green nano-catalyst at 65°C for 2h and highest yield of 87% DLBD was obtained.

f. However, *Cucumis melo* var. *Cantalupensis* seed oil (CMCSO) was efficiently converted into biodiesel (CMCBD) with CaO green nano-catalyst with 1:9 oil to methanol ratio, 1.05 wt. % catalyst amount at 70°C for 3h and 98% yield of *Cucumis melo* var. *Cantalupensis* biodiesel (CMCBD) was attained.

g. For transesterification of *Solanum surattense* seed oil (SSSO) with Ag_2O, the adjusted operating parameters were 1:8 oil to methanol ratio, 1.25 wt. % catalyst amount at 65°C for 3h that resulted in 89 % yield of *Solanum surattense* biodiesel (SSBD).

h. Finally, *Cucumis melo* var. *Agrestis* seed oil (CMASO) converted into biodiesel (CMABD) under ideal working settings (9:1 methanol to oil ratio, 2 wt. % catalysts at 90°C for 6h), a total biodiesel output of 93% was managed.

All of the synthesized biodiesel samples, produced from eight different seed oils, were evaluated for physicochemical properties and it was confirmed that these features complied with ASTM D-6751, a global biodiesel standard.

The findings from the current investigation would, however, recommend that SEM could be a helpful technique in revealing hidden micro-morphological aspects among various oil-producing seeds, assisting the researchers in making the right decisions for future seed exploration, identification, authentication and classification. It can be proposed on the basis of outcomes of the current research that this feedstock can be used extensively for the mass production of high quality biodiesel. However, the study also suggests mass cultivation of non-edible feedstock that can be grown at large scale on waste, marginal, saline, and wet soil. These plants may thrive in settings of low fertility, low moisture content, and marginal, degraded and waste land. Therefore, these seeds with non-edible oil as biodiesel feedstock have a great potential for synthesizing environment friendly biodiesel fuel to significantly reduce economic, environmental and social problems. The emission analysis of synthesized biodiesel is also recommended. This study also offers improving the quality and yield of biodiesel for industrial implication and the global market through the synthesis of advance green nano-composites employing inexpensive metals at a commercial level.

CHAPTER: 4

REFERENCES

Abbah, E., Nwandikom, G., Egwuonwu, C., & Nwakuba, N. (2016). Effect of reaction temperature on the yield of biodiesel from neem seed oil. *American Journal of Energy Science, 3*(3), 16-20.

Abbas, S., Basma, H., Al Boukhari, J., & Awad, R. (2021). Characterization of CdO nanoparticles prepared by co-precipitation method under different pH and calcination temperatures. *Applied Physics A, 127*(7), 1-17.

Abbasi, B. A., Iqbal, J., Khan, Z., Ahmad, R., Uddin, S., Shahbaz, A., Kanwal, S. (2021). Phytofabrication of cobalt oxide nanoparticles from Rhamnus virgata leaves extract and investigation of different bioactivities. *Microscopy Research and Technique, 84*(2), 192-201.

Abdullah, A., Ahmed, A., Akhter, P., Razzaq, A., Hussain, M., Hossain, N., Park, Y.-K. (2021). Potential for sustainable utilisation of agricultural residues for bioenergy production in Pakistan: An overview. *Journal of Cleaner Production, 287*, 1-14.

Abdullah, F. B. (2020). A Model for strategizing energy security dimensions and indicators selection for Pakistan. *Abdullah, FB, Hyder, SI, & Iqbal*, 558-569.

Abdullah, R. F., Rashid, U., Hazmi, B., Ibrahim, M. L., Tsubota, T., & Alharthi, F. A. (2022). Potential heterogeneous nano-catalyst via integrating hydrothermal carbonization for biodiesel production using waste cooking oil. *Chemosphere, 286*, 1-16

Adekunle, A. S., Oyekunle, J. A., Durosinmi, L. M., Oluwafemi, O. S., Olayanju, D. S., Akinola, A. S., Ajayeoba, T. A. (2020). Potential of cobalt and cobalt oxide nanoparticles as nanocatalyst towards dyes degradation in wastewater. *Nano-Structures & Nano-Objects, 21*, 100405.

Ahmad, A. F., Zulkurnain, N., Rosid, S. J. M., Azid, A., Endut, A., Toemen, S., Abdullah, W. N. W. (2022). *Characterization of coconut oil (Cocos nucifera L.) from fresh and waste coconut pulp for biodiesel production via transesterification process.* Paper presented at the AIP Conference Proceedings.

Ahmad, M., Asif, S., Klemeš, J. J., Mubashir, M., Bokhari, A., Sultana, S., Ullah, S. (2022). Conversion of the toxic and hazardous Zanthoxylum armatum seed oil into methyl ester using green and recyclable silver oxide nanoparticles. *Fuel, 310*, 122296.

Ahmad, M., Elnaggar, A. Y., Teong, L. K., Sultana, S., Zafar, M., Munir, M., Abidin, S. Z. U. (2022). Sustainable and eco-friendly synthesis of biodiesel from novel and non-edible seed oil of Monotheca buxifolia using green nano-catalyst of calcium oxide. *Energy Conversion and Management: X, 13*, 100142.

Ahmad, M., Khan, A. M., Abbas, Q., Arfan, M., Mahmood, T., Zafar, M., Ameen, M. (2022). Implication of scanning electron microscopy as a tool for identification of novel, nonedible oil seeds for biodiesel production. *Microscopy Research and Technique, 85*(5), 1671-1684.

Ahmad, M., & Zafar, M. (2021). Conversion of waste seed oil of Citrus aurantium into methyl ester via green and recyclable nanoparticles of zirconium oxide in the context of circular bioeconomy approach. *Waste Management, 136*, 310-320.

Ahmad, M., Zafar, M., & Ali, N. (2019). Biodiesel synthesis and physiochemical analysis of Taraxacum officinale FH Wigg seed oil. International Journal of Environmental Science and Technology, 16, 4103-4112.

Ahmed, A., Hidayat, S., Abu Bakar, M. S., Azad, A. K., Sukri, R. S., & Phusunti, N. (2021). Thermochemical characterisation of Acacia auriculiformis tree parts via proximate, ultimate, TGA, DTG, calorific value and FTIR spectroscopy analyses to evaluate their potential as a biofuel resource. *Biofuels, 12*(1), 9-20.

Abbasi, T. U., Ahmad, M., Asma, M., Munir, M., Zafar, M., Katubi, K. M., ... & Bokhari, A. (2022). High efficient conversion of Cannabis sativa L. biomass into bioenergy by using green tungsten oxide nano-catalyst towards carbon neutrality. Fuel, 126796.

Ajaib, M., & Zaheer-ud-din, K. (2012). Bischofia javanica: A new record to the Flora of Pakistan. *Biologia (Pakistan), 58*(1&2), 179-183.

Akhtar, M. T., Ahmad, M., Asma, M., Munir, M., Zafar, M., Sultana, S., ... & Kalam, M. A. (2022). Efficient Production of Wild and Non-Edible Brassica juncea (L.) Czern. Seed Oil into High-Quality Biodiesel via Novel, Green and Recyclable NiSO4 Nano-Catalyst. Sustainability, 14(16), 10188.

Akhtar, T., Tariq, M. I., Iqbal, S., Sultana, N., & Wei, C. K. (2017). Production and characterization of biodiesel from Eriobotrya Japonica seed oil: an optimization study. International Journal of Green Energy, 14(6), 569-574.

Akintelu, S. A., Folorunso, A. S., Folorunso, F. A., & Oyebamiji, A. K. (2020). Green synthesis of copper oxide nanoparticles for biomedical application and environmental remediation. *Heliyon, 6*(7), e04508.

Alsaiari, M., Ahmad, M., Zafar, M., Sultana, S., Rizk, M. A., Almohana, A. I., ... & Akhtar, M. S. (2022). Treatment of Saussurea heteromalla for biofuel synthesis using catalytic membrane reactor. Chemosphere, 305, 135335.

Al-Snafi, A. E. (2019). A review on Luffa acutangula: A potential medicinal plant. *magnesium, 52*-53.

Al-Zahrani, S., Astudillo-Calderón, S., Pintos, B., Pérez-Urria, E., Manzanera, J. A., Martín, L., & Gomez-Garay, A. (2021). Role of synthetic plant extracts on the production of silver-derived nanoparticles. *Plants, 10*(8), 1671.

Ala'a, H., Osman, A. I., Kumar, P. S. M., Jamil, F., Al-Haj, L., Al Nabhani, A., Rooney, D. W. (2021). Circular economy approach of enhanced bifunctional catalytic system of CaO/CeO2 for biodiesel production from waste loquat seed oil with life cycle assessment study. *Energy Conversion and Management, 236*, 114040.

Alagarasan, D., Harikrishnan, A., Surendiran, M., Indira, K., Khalifa, A. S., & Elesawy, B. H. (2021). Synthesis and characterization of CuO nanoparticles and evaluation of their bactericidal and fungicidal activities in cotton fabrics. *Applied Nanoscience*, 1-10.

Aldwayyan, A., Al-Jekhedab, F., Al-Noaimi, M., Hammouti, B., Hadda, T., Suleiman, M., & Warad, I. (2013). Synthesis and characterization of CdO nanoparticles starting from organometalic dmphen-CdI2 complex. *Int. J. Electrochem. Sci, 8*(8), 10506-10514.

Ali, C. H., Asif, A. H., Iqbal, T., Qureshi, A. S., Kazmi, M. A., Yasin, S., Mu, B.-Z. (2018). Improved transesterification of waste cooking oil into biodiesel using calcined goat bone as a catalyst. *Energy Sources, Part A: Recovery, Utilization, and Environmental Effects, 40*(9), 1076-1083.

Alsaiari, M., Ahmad, M., Zafar, M., Sultana, S., Rizk, M. A., Almohana, A. I., Akhtar, M. S. (2022). Treatment of Saussurea heteromalla for biofuel synthesis using catalytic membrane reactor. *Chemosphere*, 135335.

Ameen, M., Ahmad, M., Zafar, M., Munir, M., Abbas, M. M., Sultana, S., Kalam, M. (2022). Prospects of Catalysis for Process Sustainability of Eco-Green Biodiesel Synthesis via Transesterification: A State-Of-The-Art Review. *Sustainability, 14*(12), 7032.

Ameen, M., Zafar, M., Ahmad, M., Shaheen, A., & Yaseen, G. (2018). Wild melon: a novel non-edible feedstock for bioenergy. *Petroleum Science, 15*(2), 405-411.

Ameen, M., Zafar, M., Nizami, A.-S., Ahmad, M., Munir, M., Sultana, S., Rehan, M. Biodiesel Synthesis from Cucumis melo var. agrestis Seed Oil: Towards Non-Food Biomass Biorefineries. *Frontiers in Energy Research*, 943.

Anand, G. T., Nithiyavathi, R., Ramesh, R., Sundaram, S. J., & Kaviyarasu, K. (2020). Structural and optical properties of nickel oxide nanoparticles: Investigation of antimicrobial applications. *Surfaces and Interfaces, 18*, 100460.

Anandan, K., Rajesh, K., & Rajendran, V. (2017). Enhanced optical properties of spherical zirconia (ZrO2) nanoparticles synthesized via the facile various solvents mediated

solvethermal process. *Journal of Materials Science: Materials in Electronics, 28*(22), 17321-17330.

Arshad, S., Ahmad, M., Munir, M., Sultana, S., Zafar, M., Dawood, S., ... & Show, P. L. (2023). Assessing the potential of green CdO2 nano-catalyst for the synthesis of biodiesel using non-edible seed oil of Malabar Ebony. Fuel, 333, 126492.

Arun, K., Kumar, K. S., Batra, A., Aggarwal, M., & Francis, P. (2015). Surfactant free hydrothermal synthesis of CdO nanostructure and its characterization. *Advanced Science, Engineering and Medicine, 7*(9), 771-775.

Attari, A., Abbaszadeh-Mayvan, A., & Taghizadeh-Alisaraie, A. (2022). Process optimization of ultrasonic-assisted biodiesel production from waste cooking oil using waste chicken eggshell-derived CaO as a green heterogeneous catalyst. *Biomass and Bioenergy, 158*, 106357.

AVSL, S. B., Subramaniapillai, N., Mohamed, M. S. B. K., & Narayanan, A. (2021). Effect of rubber seed oil biodiesel on engine performance and emission analysis. *Fuel, 296*, 120708.

Awang, M. S. N., Mohd Zulkifli, N. W., Abbas, M. M., Amzar Zulkifli, S., Kalam, M. A., Ahmad, M. H., ... & Daud, W. M. A. W. (2021). Effect of addition of palm oil biodiesel in waste plastic oil on diesel engine performance, emission, and lubricity. ACS omega, 6(33), 21655-21675.

Ayoman, E., Hossini, G., & Haghighi, N. (2015). Synthesis of CuO nanoparticles and study on their catalytic properties. *International Journal of Nanoscience and Nanotechnology, 11*(2), 63-70.

Aziz, A., Ahmad, M., Ullah, R., Bari, A., Khan, M. Y., Zafar, M., . . . Anar, M. (2022). Microscopic techniques for characterization and authentication of oil-yielding seeds. *Microscopy Research and Technique, 85*(3), 900-916.

Banković-Ilić, I. B., Stamenković, O. S., & Veljković, V. B. (2012). Biodiesel production from non-edible plant oils. *Renewable and Sustainable Energy Reviews, 16*(6), 3621-3647.

Barman, K., Dutta, P., Chowdhury, D., & Baruah, P. K. (2021). Green biosynthesis of copper oxide nanoparticles using waste colocasia esculenta leaves extract and their application as recyclable catalyst towards the synthesis of 1, 2, 3-triazoles. *BioNanoScience, 11*(1), 189-199.

Barros, S. d. S., Junior, W. A. P., Sá, I. S., Takeno, M. L., Nobre, F. X., Pinheiro, W., de Freitas, F. A. (2020). Pineapple (Ananás comosus) leaves ash as a solid base catalyst for biodiesel synthesis. *Bioresource technology, 312*, 123569.

Berra, D., Laouini, S., Benhaoua, B., Ouahrani, M., Berrani, D., & Rahal, A. (2018). Green synthesis of copper oxide nanoparticles by Pheonix dactylifera L leaves extract. *Digest Journal of Nanomaterials and Biostructures, 13*(4), 1231-1238.

Bibi, F., Ali, M. I., Ahmad, M., Bokhari, A., Khoo, K. S., Zafar, M., Show, P. L. (2022). Production of lipids biosynthesis from Tetradesmus nygaardii microalgae as a feedstock for biodiesel production. *Fuel, 326*, 124985.

Bikash, B., Choudhury, N. D., Bora, D. K., & Kalita, K. (2018). *Physicochemical assessment of Pumpkin (Cucurbita pepo L.) seed oil as a viable feedstock for biodiesel production.* Paper presented at the Conference proceedings of the second international conference on recent advances in bioenergy research.

BIOFUELS, I. G. O. (2020). " Production of Biodiesel from Non Edible Vegetable Oils. A Review.

Bukkarapu, K. R., & Krishnasamy, A. (2021). Fourier-transform-infrared-spectroscopy-based approach to predict engine fuel properties of biodiesel. *Energy & Fuels, 35*(9), 7993-8005.

Cao, M., Peng, L., Xie, Q., Xing, K., Lu, M., & Ji, J. (2021). Sulfonated Sargassum horneri carbon as solid acid catalyst to produce biodiesel via esterification. *Bioresource technology, 324*, 124614.

Chand, K., Cao, D., Fouad, D. E., Shah, A. H., Dayo, A. Q., Zhu, K., Dong, S. (2020). Green synthesis, characterization and photocatalytic application of silver nanoparticles synthesized by various plant extracts. *Arabian Journal of Chemistry, 13*(11), 8248-8261.

Chand, K., Jiao, C., Lakhan, M. N., Shah, A. H., Kumar, V., Fouad, D. E., Cao, D. (2021). Green synthesis, characterization and photocatalytic activity of silver nanoparticles synthesized with Nigella Sativa seed extract. *Chemical Physics Letters, 763*, 138218.

Chandravanshi, A., Paikra, A. S., Pandey, S., & Malviya, R. K. (2022). Experimental Investigation on FTIR Analysis of Produced Biodiesel and Performance and Emission Analysis of Diesel Engine Using Schleichera Oleosa Methyl Ester as Fuel with EGR *Innovations in Mechanical Engineering* (pp. 355-367): Springer.

Changmai, B., Vanlalveni, C., Ingle, A. P., Bhagat, R., & Rokhum, L. (2020). Widely used catalysts in biodiesel production: a review. *RSC advances, 10*(68), 41625-41679.

Chatterjee, R., Mukherjee, S. K., Paul, B., & Chattopadhyaya, S. (2021). Comparative Evaluation of Madhuca Longifolia and Jatropha Curcas Extracted Biodiesel.

Chaudhry, B., Akhtar, M. S., Ahmad, M., Munir, M., Zafar, M., Alhajeri, N. S., Bokhari, A. (2022). Membrane based reactors for sustainable treatment of Coronopus didymus L. by developing Iodine doped potassium oxide membrane under Dynamic conditions. *Chemosphere*, 135138.

Chia, S. R., Ahmad, M., Sultana, S., Zafar, M., Asif, S., Bokhari, A., ... & Show, P. L. (2022). Green synthesis of biodiesel from Citrus medica seed oil using green nanoparticles of copper oxide. *Fuel*, *323*, 124285.

Cholapandian, K., Gurunathan, B., & Rajendran, N. (2022). Investigation of CaO nanocatalyst synthesized from Acalypha indica leaves and its application in biodiesel production using waste cooking oil. *Fuel, 312*, 122958.

Chowdhury, M. R., Chowdhury, K. H., Hanif, N. B., Sayeed, M. A., Mouah, J., Mahmud, I., . . . Adnan, M. (2020). An integrated exploration of pharmacological potencies of Bischofia javanica (Blume) leaves through experimental and computational modeling. *Heliyon, 6*(9), e04895.

Chuah, L. F., Yusup, S., Abd Aziz, A. R., Bokhari, A., Klemeš, J. J., & Abdullah, M. Z. (2015). Intensification of biodiesel synthesis from waste cooking oil (Palm Olein) in a Hydrodynamic Cavitation Reactor: Effect of operating parameters on methyl ester conversion. *Chemical Engineering and Processing: Process Intensification, 95*, 235-240.

Daimary, N., Eldiehy, K. S., Boruah, P., Deka, D., Bora, U., & Kakati, B. K. (2022). Potato peels as a sustainable source for biochar, bio-oil and a green heterogeneous catalyst for biodiesel production. *Journal of Environmental Chemical Engineering, 10*(1), 107108.

Danlami, E. K., Okoye, I. G., & Ezeonu, C. S. (2022). Physicochemical Properties Of Shea Butter Synthesized Biodiesel. *Int J Petro Chem Natur Gas, 2 (1): 17, 22*, 3-5.

Das, V., Tripathi, A. M., Borah, M. J., Dunford, N. T., & Deka, D. (2020). Cobalt-doped CaO catalyst synthesized and applied for algal biodiesel production. *Renewable Energy, 161*, 1110-1119.

Dawood, S., Ahmad, M., Ullah, K., Zafar, M., & Khan, K. (2018). Synthesis and characterization of methyl esters from non-edible plant species yellow oleander oil, using magnesium oxide (MgO) nano-catalyst. Materials Research Bulletin, 101, 371-379.

Dawood, S., Ahmad, M., Zafar, M., Ali, M. I., Ahmad, K., Sultana, S., ... & Kilic, O. (2020). Identification of novel nonedible oil seeds via scanning electron microscopy for biodiesel production. Microscopy research and technique, 83(2), 165-175.

Dawood, S., Ahmad, M., Zafar, M., Asif, S., Klemeš, J. J., Bokhari, A., El-Bahy, Z. M. (2022). Biodiesel synthesis from Prunus bokhariensis non-edible seed oil by using green silver oxide nanocatalyst. *Chemosphere, 291*, 132780.

Dawood, S., Koyande, A. K., Ahmad, M., Mubashir, M., Asif, S., Klemeš, J. J., ... & Show, P. L. (2021). Synthesis of biodiesel from non-edible (Brachychiton populneus) oil in the presence of nickel oxide nanocatalyst: Parametric and optimisation studies. Chemosphere, 278, 130469.

Deori, K., & Deka, S. (2013). Morphology oriented surfactant dependent CoO and reaction time dependent Co 3 O 4 nanocrystals from single synthesis method and their optical and magnetic properties. *CrystEngComm, 15*(42), 8465-8474.

Deshmane, V. G., and Adewuyi, Y. G. (2013). Synthesis and Kinetics of Biodiesel Formation via Calcium Methoxide Base Catalyzed Transesterification Reaction in the Absence and Presence of Ultrasound. Fuel 107, 474–482.

Devarajan, Y., Nagappan, B., Mageshwaran, G., Kumar, M. S., & Durairaj, R. (2020). Feasibility study of employing diverse antioxidants as an additive in research diesel engine running with diesel-biodiesel blends. *Fuel, 277*, 118161.

Dobrucka, R. (2018). Antioxidant and catalytic activity of biosynthesized CuO nanoparticles using extract of Galeopsidis herba. *Journal of Inorganic and Organometallic Polymers and Materials, 28*(3), 812-819.

Doudin, K. I. (2021). Quantitative and qualitative analysis of biodiesel by NMR spectroscopic methods. *Fuel, 284*, 119114.

Du, J., Yuan, R.-k., Hu, R.-x., Zhang, H.-l., Qi, Y.-t., & Zhang, W.-n. (2022). Biodiesel production from Momordica cochinchinensis (Lour.) Spreng seed oil. *Fuel, 314*, 123047.

Du, L., Li, Z., Ding, S., Chen, C., Qu, S., Yi, W., et al. (2019). Synthesis and Characterization of Carbon-Based MgO Catalysts for Biodiesel Production from castor Oil. Fuel 258, 116122.

Elkelawy, M., Bastawissi, H. A.-E., Esmaeil, K. K., Radwan, A. M., Panchal, H., Sadasivuni, K. K., . . . Walvekar, R. (2019). Experimental studies on the biodiesel production parameters optimization of sunflower and soybean oil mixture and DI engine combustion, performance, and emission analysis fueled with diesel/biodiesel blends. *Fuel, 255*, 115791.

Eevera, T., Rajendran, K., and Saradha, S. (2009). Biodiesel Production Process Optimization and Characterization to Assess the Suitability of the Product for Varied Environmental Conditions. Renew. Energy 34 (3), 762–765.

Ezhilarasi, A. A., Vijaya, J. J., Kaviyarasu, K., Kennedy, L. J., Ramalingam, R. J., & Al-Lohedan, H. A. (2018). Green synthesis of NiO nanoparticles using Aegle marmelos leaf extract for the evaluation of in-vitro cytotoxicity, antibacterial and photocatalytic properties. *Journal of Photochemistry and Photobiology B: Biology, 180*, 39-50.

Fadhil, A. B., Al-Tikrity, E. T., & Albadree, M. A. (2017). Biodiesel production from mixed non-edible oils, castor seed oil and waste fish oil. *Fuel, 210*, 721-728.

Faraguna, F., Racar, M., Glasovac, Z., and Jukić, A. (2017). Correlation Method for Conversion Determination of Biodiesel Obtained from Different Alcohols by1H NMR Spectroscopy. Energy fuels. 31 (4), 3943–3948.

Farooq, M., Ramli, A., & Naeem, A. (2015). Biodiesel production from low FFA waste cooking oil using heterogeneous catalyst derived from chicken bones. *Renewable Energy, 76*, 362-368.

Foroutan, R., Mohammadi, R., Razeghi, J., & Ramavandi, B. (2021). Biodiesel production from edible oils using algal biochar/CaO/K2CO3 as a heterogeneous and recyclable catalyst. *Renewable Energy, 168*, 1207-1216.

Friesen, P. C., Fink, W., Slama, A., & Cattani, D. J. (2022). Third and fourth year biomass yields of Miscanthus x giganteus, switchgrass, big bluestem, and prairie cordgrass in southern Manitoba, Canada: Latitude of origin affects biomass yield among native grasses. *Biomass and Bioenergy, 160*, 106441.

Gaurav, P. K. P. J. R., & Sharmac, S. D. U. S. A Review on Production of Biodiesel by Transesterification using Heterogeneous Nanocatalyst.

Gebremariam, S., & Marchetti, J. (2021). Process simulation and techno-economic performance evaluation of alternative technologies for biodiesel production from low value non-edible oil. *Biomass and Bioenergy, 149*, 106102.

Gebretinsae, H., Tsegay, M., & Nuru, Z. (2021). Biosynthesis of nickel oxide (NiO) nanoparticles from cactus plant extract. *Materials Today: Proceedings, 36*, 566-570.

Gohain, M., Devi, A., & Deka, D. (2017). Musa balbisiana Colla peel as highly effective renewable heterogeneous base catalyst for biodiesel production. *Industrial Crops and Products, 109*, 8-18.

Gul, I., Khan, S. M., Mehmood, T., Ahmad, Z., Badshah, H., & Shah, H. (2020). Characterization of cobalt oxide and calcium-aluminum oxide nano-catalyst through

scanning electron microscopy, X-ray diffraction, and energy dispersive X-ray spectroscopy. *Microscopy Research and Technique, 83*(9), 1124-1131.

Habte, L., Shiferaw, N., Mulatu, D., Thenepalli, T., Chilakala, R., & Ahn, J. W. (2019). Synthesis of nano-calcium oxide from waste eggshell by sol-gel method. *Sustainability, 11*(11), 3196.

Hafeez, M., Shaheen, R., Akram, B., Haq, S., Mahsud, S., Ali, S., & Khan, R. T. (2020). Green synthesis of cobalt oxide nanoparticles for potential biological applications. *Materials Research Express, 7*(2), 025019.

Haider, S., Khan, S. U., Najeeb, J., Naeem, S., Rafique, H., Munir, H., Nazar, M. F. (2022). Synthesis of cadmium oxide nanostructures by using Dalbergia sissoo for response surface methodology based photocatalytic degradation of methylene blue. *Journal of Cleaner Production, 365*, 132822.

Hasni, K., Ilham, Z., Dharma, S., & Varman, M. (2017). Optimization of biodiesel production from Brucea javanica seeds oil as novel non-edible feedstock using response surface methodology. *Energy Conversion and Management, 149*, 392-400.

Hebbar, H. H., Math, M., & Yatish, K. (2018). Optimization and kinetic study of CaO nano-particles catalyzed biodiesel production from Bombax ceiba oil. *Energy, 143*, 25-34.

Helmi, M., Ghadiri, M., Tahvildari, K., & Hemmati, A. (2021). Biodiesel synthesis using clinoptilolite-Fe3O4-based phosphomolybdic acid as a novel magnetic green catalyst from salvia mirzayanii oil via electrolysis method: Optimization study by Taguchi method. *Journal of Environmental Chemical Engineering, 9*(5), 105988.

Henmi, A., Shoji, M., Nomura, M., & Inoue, T. (2019). Fatty acid composition and applications of Eriobotrya japonica seed oil. *Journal of Oleo Science*, ess18178.

Hosseinzadeh-Bandbafha, H., Nizami, A.-S., Kalogirou, S. A., Gupta, V. K., Park, Y.-K., Fallahi, A., . . . Aghbashlo, M. (2022). Environmental life cycle assessment of biodiesel production from waste cooking oil: A systematic review. *Renewable and Sustainable Energy Reviews,* 161, 112411.

Ibrahim, N. A., Rashid, U., Hazmi, B., Moser, B. R., Alharthi, F. A., Rokhum, S. L., & Ngamcharussrivichai, C. (2022). Biodiesel production from waste cooking oil using magnetic bifunctional calcium and iron oxide nanocatalysts derived from empty fruit bunch. Fuel, 317, 123525.

Indra, R., Bachheti, R. K., & Archana, J. (2013). Chemical composition, mineral and nutritional value of wild Bischofia javanica seed. International Food Research Journal, 20(4).

Inoue, M., Hayashi, S., & Craker, L. (2017). Culture, history, and applications of medicinal and aromatic plants in Japan. *Aromatic and Medicinal Plants-Back to Nature; El-Shemy, HA, Ed*, 95-110.

Iravani, S., & Varma, R. S. (2020). Sustainable synthesis of cobalt and cobalt oxide nanoparticles and their catalytic and biomedical applications. *Green Chemistry, 22*(9), 2643-2661.

Islam, M. S., Hart, C. R., & Casadonte, D. (2022). Ultrasound-assisted solid Lewis acid-catalyzed transesterification of Lesquerella fendleri oil for biodiesel synthesis. *Ultrasonics sonochemistry, 88*, 106082.

Jalees, M., Lawrence, R. S., Chhattree, A., Yadav, M., & Sailus, N. (2018). Green synthesis of silver oxide nanoparticles prepared from waste part of mango peels. *International Journal of Pure & Applied Bioscience, 6*(3), 502-508.

Kaliammal, R., Parvathy, G., Maheshwaran, G., Velsankar, K., Devi, V. K., Krishnakumar, M., & Sudhahar, S. (2021). Zephyranthes candida flower extract mediated green synthesis of silver nanoparticles for biological applications. *Advanced Powder Technology, 32*(11), 4408-4419.

Kamel, D. A., Farag, H. A., Amin, N. K., Zatout, A. A., & Ali, R. M. (2018). Smart utilization of jatropha (Jatropha curcas Linnaeus) seeds for biodiesel production: Optimization and mechanism. *Industrial Crops and Products, 111*, 407-413.

Kara, K., Ouanji, F., El Mahi, M., Kacimi, M., & Mahfoud, Z. (2019). Biodiesel synthesis from vegetable oil using eggshell waste as a heterogeneous catalyst. *Biofuels*.

Karaye, I., Hayatu, M., Mustapha, Y., & Sani, A. (2021). Oil Extraction and GC-MS Analysis of the Seeds oil of three Nigerian Cucurbits. *International Journal Of Science for Global Sustainability, 7*(3).

Kasirajan, R., Sime, W., Subramanian, N., & Renganathan, S. (2017). Solanum nigrum L. as a novel energy resource for biodiesel production through transesterification process using an open-system reactor. *Energy Sources, Part A: Recovery, Utilization, and Environmental Effects, 39*(16), 1791-1798.

Kaveh, S., Norouzi, B., Nami, N., & Mirabi, A. (2021). Phytochemical synthesis of CdO nanoparticles: fabrication of electrochemical sensor for quantification of cefixime. *Journal of Materials Science: Materials in Electronics, 32*(7), 8932-8943.

Kaviyarasu, K., Manikandan, E., Paulraj, P., Mohamed, S., & Kennedy, J. (2014). One dimensional well-aligned CdO nanocrystal by solvothermal method. *Journal of alloys and compounds, 593*, 67-70.

Khan, M. I., Akhtar, M. N., Ashraf, N., Najeeb, J., Munir, H., Awan, T. I., Kabli, M. R. (2020). Green synthesis of magnesium oxide nanoparticles using Dalbergia sissoo extract for photocatalytic activity and antibacterial efficacy. *Applied Nanoscience, 10*(7), 2351-2364.

Killner, M., Linck, Y. G., Danieli, E., Rohwedder, J., & Blümich, B. (2015). Compact NMR spectroscopy for real-time monitoring of a biodiesel production. *Fuel, 139*, 240-247.

Kumar, P. (2021). A review on the pharmaceutical activity of Solanum surattense. *GSC Advanced Research and Reviews, 7*(3), 038-044.

Kumari, S. C., Dhand, V., & Padma, P. N. (2021). Green synthesis of metallic nanoparticles: a review. *Nanomaterials*, 259-281.

Kuppusamy, P., Yusoff, M. M., Maniam, G. P., & Govindan, N. (2016). Biosynthesis of metallic nanoparticles using plant derivatives and their new avenues in pharmacological applications–An updated report. *Saudi Pharmaceutical Journal, 24*(4), 473-484.

Lalithamba, H., Raghavendra, M., & Yatish, K. (2022). Efficient Application of Green Synthesized CeO2 Nanoparticles for the Preparation of Selenoester Derivatives of Protected Amino Acids and Production of Biodiesel from Annona squamosa Oil. *Journal of Electronic Materials*, 1-10.

Laskar, I. B., Rokhum, L., Gupta, R., and Chatterjee, S. (2020). Zinc Oxide Supported Silver Nanoparticles as a Heterogeneous Catalyst for Production of Biodiesel from Palm Oil. Environ. Prog. 39 (3),

Lee, S., Ha, J., Park, J., Kang, E., Jeon, S.-H., Han, S. B., . . . Cho, S. (2021). Antioxidant and Anti-Inflammatory Effects of Bischofia javanica (Blume) Leaf Methanol Extracts through the Regulation of Nrf2 and TAK1. *Antioxidants, 10*(8), 1295.

Li, J., Vosegaard, T., and Guo, Z. (2017). Applications of Nuclear Magnetic Resonance in Lipid Analyses: An Emerging Powerful Tool for Lipidomics Studies. Prog. Lipid Res. 68, 37–56.

Li, S., Li, X., & Ho, S.-H. (2021). Microalgae as a solution of third world energy crisis for biofuels production from wastewater toward carbon neutrality: an updated review. *Chemosphere*, 132863.

Li, Z., Ding, S., Chen, C., Qu, S., Du, L., Lu, J., & Ding, J. (2019). Recyclable Li/NaY zeolite as a heterogeneous alkaline catalyst for biodiesel production: Process optimization and kinetics study. *Energy Conversion and Management, 192*, 335-345.

Lingaraju, K., Naika, H. R., Nagabhushana, H., Jayanna, K., Devaraja, S., & Nagaraju, G. (2020). Biosynthesis of nickel oxide nanoparticles from Euphorbia heterophylla (L.) and their biological application. *Arabian Journal of Chemistry, 13*(3), 4712-4719.

Liu, J., Wang, L., & Bao, H. (2019). A novel fluorescent probe for ascorbic acid based on seed-mediated growth of silver nanoparticles quenching of carbon dots fluorescence. *Analytical and bioanalytical chemistry, 411*(4), 877-883.

Liu, K., Devarajan, Y., Nithyanantham, V., Nalla, B. T., & Krishnamurthy, V. (2021). An experimental study on transesterification process and emission analysis of diesel engine propelled with Capparis spinosa biodiesel. *Biomass Conversion and Biorefinery*, 1-8.

Loy, A. C. M., Quitain, A. T., Lam, M. K., Yusup, S., Sasaki, M., & Kida, T. (2019). Development of high microwave-absorptive bifunctional graphene oxide-based catalyst for biodiesel production. *Energy Conversion and Management, 180*, 1013-1025.

Luisetto, I., Pepe, F., & Bemporad, E. (2008). Preparation and characterization of nano cobalt oxide. *Journal of Nanoparticle Research, 10*(1), 59-67.

Lüneburger, S., Gallina, A. L., Soares, L. C., & Benvegnú, D. M. (2022). Biodiesel production from Hevea Brasiliensis seed oil. *Fuel, 324*, 124639.

Ma, X., Liu, F., Helian, Y., Li, C., Wu, Z., Li, H., Lu, W. (2021). Current application of MOFs based heterogeneous catalysts in catalyzing transesterification/esterification for biodiesel production: A review. *Energy Conversion and Management, 229*, 113760.

Maham, M., Sajadi, S. M., Kharimkhani, M. M., & Nasrollahzadeh, M. (2017). Biosynthesis of the CuO nanoparticles using Euphorbia Chamaesyce leaf extract and investigation of their catalytic activity for the reduction of 4-nitrophenol. *IET Nanobiotechnology, 11*(7), 766-772.

Mallah, T. A., and Sahito, A. R. (2020). Optimization of castor and Neem Biodiesel Blends and Development of Empirical Models to Predicts its Characteristics. Fuel 262, 116341.

Mali, M., & Harsh, N. (2015). Nutritional value estimation of the leaves and seeds of Solanum surattense. *Journal of Medicinal Plants, 3*(1), 27-29.

Mendonça, I. M., Paes, O. A., Maia, P. J., Souza, M. P., Almeida, R. A., Silva, C. C., de Freitas, F. A. (2019). New heterogeneous catalyst for biodiesel production from waste tucumã peels (Astrocaryum aculeatum Meyer): Parameters optimization study. *Renewable Energy, 130*, 103-110.

Mitra, S., Ghose, A., Gujre, N., Senthilkumar, S., Borah, P., Paul, A., & Rangan, L. (2021). A review on environmental and socioeconomic perspectives of three promising biofuel

plants Jatropha curcas, Pongamia pinnata and Mesua ferrea. *Biomass and Bioenergy, 151*, 106173.

Miyuranga, K. V., Arachchige, U. S., Jayasinghe, R. A., & Samarakoon, G. (2022). Purification of Residual Glycerol from Biodiesel Production as a Value-Added Raw Material for Glycerolysis of Free Fatty Acids in Waste Cooking Oil. Energies, 15(23), 8856.

Mofijur, M., Siddiki, S. Y. A., Shuvho, M. B. A., Djavanroodi, F., Fattah, I. R., Ong, H. C., Mahlia, T. (2021). Effect of nanocatalysts on the transesterification reaction of first, second and third generation biodiesel sources-A mini-review. *Chemosphere, 270*, 128642.

Moghaddam, A. H., Nabavi, S. M., Nabavi, S. F., Bigdellou, R., Mohammadzadeh, S., & Ebrahimzadeh, M. A. (2012). Antioxidant, antihemolytic and nephroprotective activity of aqueous extract of Diospyros lotus seeds. *Acta Pol Pharm, 69*(4), 687-692.

Mohan, S., & Raj, S. (2022). Impact of high and low concentration of fly ash amended soil on physico-chemical properties of biodiesel produced from Jatropha curcas. *Environmental Progress & Sustainable Energy*, e13819.

Moradpoor, H., Safaei, M., Rezaei, F., Golshah, A., Jamshidy, L., Hatam, R., & Abdullah, R. S. (2019). Optimisation of cobalt oxide nanoparticles synthesis as bactericidal agents. *Open access Macedonian journal of medical sciences, 7*(17), 2757.

Muhammad, A. B., Jodi, L. M. a., Hassan, L. G., Abubakar, L., & Sokoto, A. M. (2019). Optimization of reaction variables of ultrasound-assisted transesterification of Abelmoscus esculentus seed oil into biodiesel. *Biofuels*.

Muhammad, C., Uba, A., Muktar, M., Opotu, M. O. A., Agada, F., Muhammad, A. U., Ahmed, A. B. (2019). Biodiesel production from thorn apple *(Datura metel)* seeds oil using naoh as catalyst. *Bima Journal Of Science And Technology* (2536-6041), 3(01), 213-227.

Mukhtar, A., Saqib, S., Lin, H., Shah, M. U. H., Ullah, S., Younas, M., Asif, S. (2022). Current status and challenges in the heterogeneous catalysis for biodiesel production. *Renewable and Sustainable Energy Reviews, 157*, 112012.

Munir, M., Ahmad, M., Mubashir, M., Asif, S., Waseem, A., Mukhtar, A., Khoo, K. S. (2021). A practical approach for synthesis of biodiesel via non-edible seeds oils using trimetallic based montmorillonite nano-catalyst. *Bioresource Technology, 328*, 124859.

Munir, M., Ahmad, M., Rehan, M., Saeed, M., Lam, S. S., Nizami, A., Zafar, M. (2021). Production of high quality biodiesel from novel non-edible Raphnus raphanistrum L.

seed oil using copper modified montmorillonite clay catalyst. *Environmental research, 193*, 110398.

Munir, M., Saeed, M., Ahmad, M., Waseem, A., Alsaady, M., Asif, S., ... & Show, P. L. (2023). Cleaner production of biodiesel from novel non-edible seed oil (Carthamus lanatus L.) via highly reactive and recyclable green nano CoWO3@ rGO composite in context of green energy adaptation. Fuel, 332, 126265.

Munir, M., Saeed, M., Ahmad, M., Waseem, A., Sultana, S., Zafar, M., & Srinivasan, G. R. (2022). Optimization of novel Lepidium perfoliatum Linn. Biodiesel using zirconium-modified montmorillonite clay catalyst. Energy Sources, Part A: Recovery, Utilization, and Environmental Effects, 44(3), 6632-6647.

Musa, I. A. (2016). The Effects of Alcohol to Oil Molar Ratios and the Type of Alcohol on Biodiesel Production Using Transesterification Process. Egypt. J. Petroleum 25 (1), 21–31.

Muthulakshmi, N., Kathirvel, A., Subramanian, R., & Senthil, M. (2022). Biofabrication of Zirconia Nanoparticles: Synthesis, Spectral Characterization and Biological Activity Evaluation against Pathogenic Bacteria. *Biointerface Research in Applied Chemistry*.13(02), 1-12.

Nainwal, P., & Pant, M. (2021). Study on the Efficacy of Silver Nanoparticle Leaf Extract of Pluchea lanceolata. *International Journal of Current Research and Review*. *13*(09), 125.

Nathani, S. (2021). Synthesis of metallic nanoparticles using plant derivatives. *AIJR Abstracts*, 166.

Naveenkumar, R., & Baskar, G. (2020). Optimization and techno-economic analysis of biodiesel production from Calophyllum inophyllum oil using heterogeneous nanocatalyst. *Bioresource technology, 315*, 123852.

Nisar, J., Razaq, R., Farooq, M., Iqbal, M., Khan, R. A., Sayed, M., ur Rahman, I. (2017). Enhanced biodiesel production from Jatropha oil using calcined waste animal bones as catalyst. *Renewable Energy, 101*, 111-119.

Ogunbusola, E., Fagbemi, T., & Osundahunsi, O. (2017). Fatty acid characterisation, sterol composition and spectroscopic analysis of selected Cucurbitaceae seed oils. *International Food Research Journal, 24*(2).

Okwundu, O. S., El-Shazly, A. H., and Elkady, M. (2019). Comparative Effect of Reaction Time on Biodiesel Production from Low Free Fatty Acid Beef Tallow: a Definition of Product Yield. SN Appl. Sci. 1 (2), 140.

Ong, H. C., Mofijur, M., Silitonga, A., Gumilang, D., Kusumo, F., & Mahlia, T. (2020). Physicochemical properties of biodiesel synthesised from grape seed, philippine tung, kesambi, and palm oils. *Energies, 13*(6), 1319.

Orege, J. I., Oderinde, O., Kifle, G. A., Ibikunle, A. A., Raheem, S. A., Ejeromedoghene, O., ... & Daramola, M. O. (2022). Recent advances in heterogeneous catalysis for green biodiesel production by transesterification. Energy Conversion and Management, 258, 115406.

Pandey, A., & Manivannan, R. (2015). A study on synthesis of nickel nanoparticles using chemical reduction technique. *Recent Patents on Nanomedicine, 5*(1), 33-37.

Pawar, O., Deshpande, N., Dagade, S., Waghmode, S., & Nigam Joshi, P. (2016). Green synthesis of silver nanoparticles from purple acid phosphatase apoenzyme isolated from a new source Limonia acidissima. *Journal of Experimental Nanoscience, 11*(1), 28-37.

Perea-Moreno, M. A., Manzano-Agugliaro, F., Hernandez-Escobedo, Q., & Perea-Moreno, A. J. (2020). Sustainable thermal energy generation at universities by using loquat seeds as biofuel. Sustainability, 12(5), 2093.

Perumal, G., & Mahendradas, D. K. (2022). Biodiesel production from Bauhinia variegata seeds oil using homogeneous catalyst. *Petroleum Science and Technology, 40*(7), 857-870.

Perumal, V., & Ilangkumaran, M. (2018). Water emulsified hybrid pongamia biodiesel as a modified fuel for the experimental analysis of performance, combustion and emission characteristics of a direct injection diesel engine. *Renewable Energy, 121*, 623-631.

Portela, N. A., Oliveira, E. C., Neto, A. C., Rodrigues, R. R., Silva, S. R., Castro, E. V., & Filgueiras, P. R. (2016). Quantification of biodiesel in petroleum diesel by 1H NMR: evaluation of univariate and multivariate approaches. *Fuel, 166*, 12-18.

Rafique, M. M., & Rehman, S. (2017). National energy scenario of Pakistan–Current status, future alternatives, and institutional infrastructure: An overview. *Renewable and Sustainable Energy Reviews, 69*, 156-167.

Rai, I., Bachheti, R., Joshi, A., & Pandey, D. (2013). Physicochemical properties and elemental analysis of some non cultivated seed oils collected from Garhwal region, Uttarakhand (India). *IJCRGG, 5*(1), 232-236.

Raj, S. P., Solomon, P. R., & Thangaraj, B. (2022). Solanaceae *Biodiesel from Flowering Plants* (pp. 543-549): Springer.

Ramli, M., Rossani, R. B., Nadia, Y., Darmawan, T. B., & Ismail, Y. S. (2019). *Nanoparticle fabrication of calcium oxide (CaO) mediated by the extract of red dragon fruit peels (Hylocereus Polyrhizus) and its application as inorganic–anti-microorganism materials.* Paper presented at the IOP Conference Series: Materials Science and Engineering.

Ramola, B., Joshi, N. C., Ramola, M., Chhabra, J., & Singh, A. (2019). Green synthesis, characterisations and antimicrobial activities of CaO nanoparticles. *Oriental Journal of Chemistry, 35*(3), 1154.

Ramos, M. D. N., Milessi, T. S., Candido, R. G., Mendes, A. A., & Aguiar, A. (2022). Enzymatic catalysis as a tool in biofuels production in Brazil: Current status and perspectives. *Energy for Sustainable Development, 68*, 103-119.

Rashmi, B., Harlapur, S. F., Avinash, B., Ravikumar, C., Nagaswarupa, H., Kumar, M. A., . . . Santosh, M. (2020). Facile green synthesis of silver oxide nanoparticles and their electrochemical, photocatalytic and biological studies. *Inorganic Chemistry Communications, 111*, 107580.

Raud, M., Kikas, T., Sippula, O., & Shurpali, N. (2019). Potentials and challenges in lignocellulosic biofuel production technology. *Renewable and Sustainable Energy Reviews, 111*, 44-56.

Ravichandran, S., Paluri, V., Kumar, G., Loganathan, K., & Kokati Venkata, B. R. (2016). A novel approach for the biosynthesis of silver oxide nanoparticles using aqueous leaf extract of Callistemon lanceolatus (Myrtaceae) and their therapeutic potential. *Journal of Experimental Nanoscience, 11*(6), 445-458.

Razavi, R., Bemani, A., Baghban, A., Mohammadi, A. H., and Habibzadeh, S. (2019). An Insight into the Estimation of Fatty Acid Methyl Ester Based Biodiesel Properties Using a LSSVM Model. Fuel 243, 133–141.

Rehan, M., Gardy, J., Demirbas, A., Rashid, U., Budzianowski, W., Pant, D., & Nizami, A. (2018). Waste to biodiesel: A preliminary assessment for Saudi Arabia. *Bioresource technology, 250*, 17-25.

Rezania, S., Mahdinia, S., Oryani, B., Cho, J., Kwon, E. E., Bozorgian, A., Mehranzamir, K. (2022). Biodiesel production from wild mustard (Sinapis Arvensis) seed oil using a novel heterogeneous catalyst of LaTiO3 nanoparticles. *Fuel, 307*, 121759.

Sagadevan, S. (2016). Synthesis, Structural, Surface Morphology, Optical and Electrical Properties of Silver Oxide Nanoparticles. *International Journal of Nanoelectronics & Materials, 9*(1).

Sahar, J., Farooq, M., Ramli, A., & Naeem, A. (2022). Feasibility of Biodiesel Production in Pakistan.

Salaheldeen, M., Aroua, M. K., Mariod, A., Cheng, S. F., Abdelrahman, M. A., & Atabani, A. (2015). Physicochemical characterization and thermal behavior of biodiesel and biodiesel–diesel blends derived from crude Moringa peregrina seed oil. *Energy Conversion and Management, 92*, 535-542.

Sankaran, A., & Kumaraguru, K. (2020). The novel two step synthesis of CuO/ZnO and CuO/CdO nanocatalysts for enhancement of catalytic activity. *Journal of Molecular Structure, 1221*, 128772.

Savale, A., Ghotekar, S., Pansambal, S., & Pardeshi, O. (2017). Green synthesis of fluorescent CdO nanoparticles using Leucaena leucocephala L. extract and their biological activities. *J. Bacteriol. Mycol. Open Access, 5*(5), 00148.

Saydut, A., Duz,M., Kaya, C., Kafadar, A., and Hamamci, C. (2008). Transesterified Sesame (Sesamum indicum L.) Seed Oil as a Biodiesel Fuel. Bioresour. Technol. 99 (14), 6656–6660.

Schaefer, H., & Renner, S. S. (2011). Phylogenetic relationships in the order Cucurbitales and a new classification of the gourd family (Cucurbitaceae). *Taxon, 60*(1), 122-138.

Sekoai, P. T., Ouma, C. N. M., Du Preez, S. P., Modisha, P., Engelbrecht, N., Bessarabov, D. G., & Ghimire, A. (2019). Application of nanoparticles in biofuels: an overview. *Fuel, 237*, 380-397.

Shaah, M. A. H., Hossain, M. S., Allafi, F. A. S., Alsaedi, A., Ismail, N., Ab Kadir, M. O., & Ahmad, M. I. (2021). A review on non-edible oil as a potential feedstock for biodiesel: physicochemical properties and production technologies. *RSC advances, 11*(40), 25018-25037.

Shaheen, A., Sultana, S., Lu, H., Ahmad, M., Asma, M., & Mahmood, T. (2018). Assessing the potential of different nano-composite (MgO, Al2O3-CaO and TiO2) for efficient conversion of Silybum eburneum seed oil to liquid biodiesel. *Journal of Molecular Liquids, 249*, 511-521.

Shammout, M., & Awwad, A. (2021). A novel route for the synthesis of copper oxide nanoparticles using Bougainvillea plant flowers extract and antifungal activity evaluation. MW Shammout and AM Awwad. A novel route for the synthesis of copper

oxide nanoparticles using Bougainvillea plant flowers extract and antifungal activity evaluation. *Chemistry International, 7*(1), 71-78.

Sharifi, S., Shakur, H., Mirzaei, A., & Hosseini, M. (2013). Characterization of cobalt oxide Co3O4 nanoparticles prepared by various methods: effect of calcination temperatures on size, dimension and catalytic decomposition of hydrogen peroxide. *International Journal of Nanoscience and Nanotechnology, 9*(1), 51-58.

Sharma, A., Kodgire, P., & Kachhwaha, S. S. (2019). Biodiesel production from waste cotton-seed cooking oil using microwave-assisted transesterification: Optimization and kinetic modeling. *Renewable and Sustainable Energy Reviews, 116*, 109394.

Sharma, S., Kundu, A., Basu, S., Shetti, N. P., & Aminabhavi, T. M. (2020). Sustainable environmental management and related biofuel technologies. *Journal of Environmental Management, 273*, 111096.

Siddiqui, V. U., Ansari, A., Chauhan, R., & Siddiqi, W. A. (2021). Green synthesis of copper oxide (CuO) nanoparticles by Punica granatum peel extract. *Materials Today: Proceedings, 36*, 751-755.

Singh, A., Goyal, V., Singh, J., Kaur, H., Kumar, S., Batoo, K. M., . . . Hussain, S. (2022). Structurally and morphologically engineered single-pot biogenic synthesis of NiO nanoparticles with enhanced photocatalytic and antimicrobial activities. *Journal of Cleaner Production, 343*, 131026.

Singh, D., Sharma, D., Soni, S., Inda, C. S., Sharma, S., Sharma, P. K., & Jhalani, A. (2021). A comprehensive review of physicochemical properties, production process, performance and emissions characteristics of 2nd generation biodiesel feedstock: Jatropha curcas. *Fuel, 285*, 119110.

Singh, D., Sharma, D., Soni, S., Sharma, S., Sharma, P. K., & Jhalani, A. (2020). A review on feedstocks, production processes, and yield for different generations of biodiesel. *Fuel, 262*, 116553.

Singh, T. S., & Verma, T. N. (2019). Taguchi design approach for extraction of methyl ester from waste cooking oil using synthesized CaO as heterogeneous catalyst: Response surface methodology optimization. *Energy Conversion and Management, 182*, 383-397.

Sodeifian, G., Ardestani, N. S., & Sajadian, S. A. (2019). Extraction of seed oil from Diospyros lotus optimized using response surface methodology. *Journal of forestry research, 30*(2), 709-719.

Srivastava, N., Srivastava, M., Gupta, V. K., Manikanta, A., Mishra, K., Singh, S., Mishra, P. (2018). Recent development on sustainable biodiesel production using sewage sludge. *3 Biotech, 8*(5), 1-11.

Stavarache, C., Vinatoru, M., Nishimura, R., & Maeda, Y. (2005). Fatty acids methyl esters from vegetable oil by means of ultrasonic energy. *Ultrasonics sonochemistry, 12*(5), 367-372.

Suresh, M., Jawahar, C., & Richard, A. (2018). A review on biodiesel production, combustion, performance, and emission characteristics of non-edible oils in variable compression ratio diesel engine using biodiesel and its blends. *Renewable and Sustainable Energy Reviews, 92*, 38-49.

Takase, M., Zhang, M., Feng, W., Chen, Y., Zhao, T., Cobbina, S. J., Wu, X. (2014). Application of zirconia modified with KOH as heterogeneous solid base catalyst to new non-edible oil for biodiesel. *Energy Conversion and Management, 80*, 117-125.

Tamilselvi, P., Yelilarasi, A., Hema, M., and Anbarasan, R. (2013). Synthesis of Hierarchical Structured MgO by Sol-Gel Method. Nano Bull. 2 (1), 130106.

Tariq, M., Qureshi, A. K., Karim, S., Sirajuddin, M., Abbas, N., Imran, M., & Shirazi, J. H. (2021). Synthesis, characterization and fuel parameters analysis of linseed oil biodiesel using cadmium oxide nanoparticles. *Energy, 222*, 120014.

Tasić, M. B. (2020). Disadvantages of herbaceous oil-bearing plants as feedstock in the biodiesel production. *Advanced Technologies, 9*(2), 88-97.

Tekuri, S. K., Pasupuleti, S. K., Konidala, K. K., Amuru, S. R., Bassaiahgari, P., & Pabbaraju, N. (2019). Phytochemical and pharmacological activities of Solanum surattense Burm. f.–A review. *J Appl Pharm Sci, 9*(03), 126-136.

Thangamani, N., & Bhuvaneshwari, N. (2019). Green synthesis of gold nanoparticles using Simarouba glauca leaf extract and their biological activity of micro-organism. *Chemical Physics Letters, 732*, 136587.

Thiyagarajan, S., Sonthalia, A., Geo, V. E., Prakash, T., Karthickeyan, V., Ashok, B., Dhinesh, B. (2020). Effect of manifold injection of methanol/n-pentanol in safflower biodiesel fuelled CI engine. *Fuel, 261*, 116378.

Titus, D., Samuel, E. J. J., & Roopan, S. M. (2019). Nanoparticle characterization techniques *Green synthesis, characterization and applications of nanoparticles* (pp. 303-319): Elsevier.

Tripathi, G., Jamal, A., Jamal, T., Faiyaz, M., & Farooqui, A. (2022). Phyco-Nanotechnology: An Emerging Nanomaterial Synthesis Method and Its Applicability in Biofuel

Production *Green Nano Solution for Bioenergy Production Enhancement* (pp. 169-200): Springer.

Tyagi, N., Sharma, G. N., & Hooda, V. (2012). Medicinal value of Praecitrullus fistulosus: an overview. *Int J Pharm Therap, 3*(2), 136-142.

Ullah, K., Jan, H. A., Ahmad, M., & Ullah, A. (2020). Synthesis and structural characterization of biofuel from Cocklebur sp., using zinc oxide nano-particle: A novel energy crop for bioenergy industry. Frontiers in Bioengineering and Biotechnology, 8, 756.

Ullah, K., Khan, K., & Ullah, A. (2021). Synthesis and structural characterization of energy crop peelu methyl esters, using hybrid metallic nano-particles. A step forward to bioenergy industry. Fuel, 300, 119241.

Ullah, K., Sharma, V. K., Ahmad, M., Lv, P., Krahl, J., & Wang, Z. (2018). The insight views of advanced technologies and its application in bio-origin fuel synthesis from lignocellulose biomasses waste, a review. Renewable and sustainable energy reviews, 82, 3992-4008.

Utami, M., Setiawan, P., Falah, I. I., Shidiq, M., Wijaya, K., Jarin, T., Chang, S. W. (2022). Synthesis of biodiesel from castor oil catalyzed by sodium hydroxide dispersed on bentonite. *Sustainable Energy Technologies and Assessments, 53*, 102526.

Veisi, H., Karmakar, B., Tamoradi, T., Hemmati, S., Hekmati, M., & Hamelian, M. (2021). Biosynthesis of CuO nanoparticles using aqueous extract of herbal tea (Stachys Lavandulifolia) flowers and evaluation of its catalytic activity. *Scientific Reports, 11*(1), 1-13.

Velusamy, K., Devanand, J., Kumar, P. S., Soundarajan, K., Sivasubramanian, V., Sindhu, J., & Vo, D.-V. N. (2021). A review on nano-catalysts and biochar-based catalysts for biofuel production. *Fuel, 306*, 121632.

Verma, P., Sharma, M., & Dwivedi, G. (2016). Impact of alcohol on biodiesel production and properties. *Renewable and Sustainable Energy Reviews, 56*, 319-333.

Vidhya, M., Archana, R., Sadayandi, K., Suresh, S., Gunasekaran, S., Podder, J., Oh, W. C. (2020). Comparison of sunlight-driven photocatalytic activity of semiconductor metal oxides of tin oxide and cadmium oxide nanoparticles. *Optik, 217*, 164878.

Vijayanandan, A. S., & Balakrishnan, R. M. (2018). Biosynthesis of cobalt oxide nanoparticles using endophytic fungus Aspergillus nidulans. *Journal of Environmental Management, 218*, 442-450.

Wang, D., Liu, J., Chen, J., Zhang, A., Zhang, X., Tong, Z., & Lu, Y. (2013). Analysis on seed and fatty acids components in Bischofia polycarpa. Journal of Zhejiang Forestry Science and Technology, 33(2), 29-33.

Wang, J., Singer, S. D., Souto, B. A., Asomaning, J., Ullah, A., Bressler, D., & Chen, G. (2022). Current progress in lipid-based biofuels: Feedstocks and production technologies. Bioresource Technology, 127020.

Yadav, M., RS, R. L., & Jalees, M. (2018). Biological synthesis and antibacterial activity of silver oxide nanoparticle prepared from Carica papaya root extract. *International Journal of Pure & Applied Bioscience, 6*(2), 1632-1639.

Yedurkar, S., Maurya, C., & Mahanwar, P. (2016). Biosynthesis of zinc oxide nanoparticles using ixora coccinea leaf extract—a green approach. *Open Journal of Synthesis Theory and Applications, 5*(1), 1-14.

Yu, S., Wu, S., Li, L., & Ge, X. (2020). Upgrading bio-oil from waste cooking oil by esterification using SO_4^{2-}/ZrO_2 as catalyst. *Fuel, 276*, 118019.

Yusuff, A. S., Gbadamosi, A. O., & Popoola, L. T. (2021). Biodiesel production from transesterified waste cooking oil by zinc-modified anthill catalyst: parametric optimization and biodiesel properties improvement. *Journal of Environmental Chemical Engineering, 9*(2), 104955.

Zamberi, M. M., Haminudin, N. F., Ani, F. N., Said, M. F. M., Haizal, M., Husin, M., & Zakaria, T. I. T. (2022). Physicochemical properties of high FFA Hevea brasiliensis oil for biodiesel production. *Proceedings of ICE-SEAM 2021: Special Edition*, 41.

Zhang, H., Zhang, L.-L., Tan, X., Li, H., & Yang, S. (2021). Catalytic high-yield biodiesel production from fatty acids and non-food oils over a magnetically separable acid nanosphere. *Industrial Crops and Products, 173*, 114126.

Zhu, Z., Liu, Y., Cong, W., Zhao, X., Janaun, J., Wei, T., & Fang, Z. (2021). Soybean biodiesel production using synergistic CaO/Ag nano catalyst: Process optimization, kinetic study, and economic evaluation. *Industrial Crops and Products, 166*, 113479.

Zul, N. A., Ganesan, S., Hamidon, T. S., Oh, W.-D., & Hussin, M. H. (2021). A review on the utilization of calcium oxide as a base catalyst in biodiesel production. *Journal of Environmental Chemical Engineering, 9*(4), 105741.

PUBLISHED PAPERS

RESEARCH OUTCOMES

Sr. No.	Title	Impact Factor
1.	Ameen, M., Zafar, M., Ramadan, M. F., Ahmad, M., Makhkamov, T., Bokhari, A., ... & Show, P. L. (2023). Conversion of novel non-edible Bischofia javanica seed oil into methyl ester via recyclable zirconia-based phyto-nanocatalyst: A circular bioeconomy approach for eco-sustenance. Environmental Technology & Innovation, 30, 103101	7.758
2.	Ameen, M., Zafar, M., Ahmad, M., Ramadan, M. F., Eid, H. F., Makhkamov, T., ... & Majeed, S. (2023). Assessing the Bioenergy Potential of Novel Non-Edible Biomass Resources via Ultrastructural Analysis of Seed Sculpturing Using Microscopic Imaging Visualization. Agronomy, 13(3), 735.	3.949
3.	Ameen, M., Zafar, M., Ahmad, M., Shaheen, A., & Yaseen, G. (2018). Wild melon: a novel non-edible feedstock for bioenergy. Petroleum Science, 15, 405-411.	4.757
4.	Ameen, M., Zafar, M., Nizami, A. S., Ahmad, M., Munir, M., Sultana, S.... & Rehan, M. (2022). Biodiesel Synthesis from *Cucumis melo var. agrestis* Seed Oil: Towards Non-Food Biomass Biorefineries. *Frontiers in Energy Research*, 943.	4.008
5.	Ameen, M., Ahmad, M., Zafar, M., Munir, M., Abbas, M. M., Sultana, S., ... & Kalam, M. A. (2022). Prospects of catalysis for process sustainability of eco-green biodiesel synthesis via transesterification: a state-of-the-art review. *Sustainability*, *14*(12), 7032	3.889

Conversion of novel non-edible *Bischofia javanica* seed oil into methyl ester *via* recyclable zirconia-based phyto-nanocatalyst: A circular bioeconomy approach for eco-sustenance

Maria Ameen [a], Muhammad Zafar [a], Mohamed Fawzy Ramadan [b], Mushtaq Ahmad [a,*], Trobjon Makhkamov [c], Awais Bokhari [d,e,*], Muhammad Mubashir [f], Lai Fatt Chuah [g,*], Pau Loke Show [h,i,j,k,**]

[a] Biofuel Laboratory Department of Plant Sciences, Quaid-i-Azam University Islamabad, 45320, Pakistan
[b] Department of Clinical Nutrition, Faculty of Applied Medical Sciences, Umm Al-Qura University, Makkah, 21955, Saudi Arabia
[c] Department of Forestry and Landscape Design, Tashkent State Agrarian University, 2 A., Universitet Str., Kibray district, 100700, Tashkent region, Uzbekistan
[d] Department of Chemical Engineering, COMSATS University Islamabad, Lahore Campus, 54000, Pakistan
[e] Sustainable Process Integration Laboratory, SPIL, NETME Centre, Faculty of Mechanical Engineering, Brno University of Technology, VUT Brno, Technická 2896/2, 616 00, Brno, Czech Republic
[f] Department of Petroleum Engineering, School of Engineering, Asia Pacific University of Technology and Innovation, 57000 Kuala Lumpur, Malaysia
[g] Faculty of Maritime Studies, Universiti Malaysia Terengganu, 21030 Terengganu, Malaysia
[h] Zhejiang Provincial Key Laboratory for Subtropical Water Environment and Marine Biological Resources Protection, Wenzhou University, Wenzhou 325035, China
[i] Department of Chemical Engineering, Khalifa University, P.O. Box 127788, Abu Dhabi, United Arab Emirates
[j] Department of Chemical and Environmental Engineering, Faculty of Science and Engineering, University of Nottingham Malaysia, 43500 Semenyih, Selangor, Malaysia
[k] Department of Sustainable Engineering, Saveetha School of Engineering, SIMATS, Chennai 602105, India

ARTICLE INFO

ABSTRACT

The current study assesses *Bischofia javanica* Blume's potential as novel non-edible seed oil for environmentally benign biodiesel production using phyto-nanocatalyst, i.e., green nanoparticles (NPs) of zirconium oxide (ZrO_2) synthesized with aqueous leaf extract of the same plant *via* the biological method. Using response surface methods, the maximum yield (95.8 wt.%) was obtained at a 1:6 oil-to-methanol molar ratio, 2.5 wt.% catalyst loading, 70 °C reaction temperature and 2 h of reaction time. In addition, advanced analytical techniques such as Fourier transform infrared spectroscopy (FTIR), X-ray diffraction (XRD) and scanning electron microscopy (SEM) with energy dispersive X-ray (EDX) were used to characterize green nanoparticles. Six peaks in the GC–MS spectrum were identified, showing the presence of six different methyl esters such as methyl palmitate, methyl linoleate, methyl oleate, methyl stearate, methyl linolenate and methyl 11-eicosenoate. In addition, ^{1}HNMR and ^{13}CNMR confirmed the high conversion yield of the esters group with distinct peaks at 3.649 ppm and 174.19 ppm. Biodiesel prepared from *Bischofia javanica* has fuel qualities that meet international standards. Fuel properties were found analogous to international standards

* Corresponding authors.
** Corresponding author at: Faculty of Maritime Studies, Universiti Malaysia Terengganu, 21030 Terengganu, Malaysia.
E-mail addresses: mushtaq@qau.edu.pk (M. Ahmad), awaisbokhari@cuilahore.edu.pk, bokhari@fme.vutbr.cz (A. Bokhari), lfchuah@umt.edu.my (L.F. Chuah), pauloke.show@nottingham.edu.my, PauLoke.Show@ku.ac.ae, showpauloke@gmail.com (P.L. Show).

Assessing the Bioenergy Potential of Novel Non-Edible Biomass Resources via Ultrastructural Analysis of Seed Sculpturing Using Microscopic Imaging Visualization

Maria Ameen [1], Muhammad Zafar [1,*], Mushtaq Ahmad [1,2], Mohamed Fawzy Ramadan [3], Heba F. Eid [4], Trobjon Makhkamov [5], Akramjon Yuldashev [6], Oybek Mamarakhimov [7], Maxsuda Nizomova [8], Rima J. Isaifan [9], Shaista Jabeen [1] and Salman Majeed [1,10]

[1] Biofuel Laboratory, Department of Plant Sciences, Quaid-i-Azam University, Islamabad 45320, Pakistan
[2] Pakistan Academy of Sciences, Islamabad 44000, Pakistan
[3] Department of Clinical Nutrition, Faculty of Applied Medical Sciences, Umm Al-Qura University, Makkah 24382, Saudi Arabia
[4] Faculty of Science, Al-Azhar University, Cairo 4434003, Egypt
[5] Department of Forestry and Landscape Design, Tashkent State Agrarian University, 2 A., Universitet Str., Kibray District, Tashkent 100700, Uzbekistan
[6] Department of Ecology and Botany, Andijan State University, 129, Universitet Str., Andijan 170100, Uzbekistan
[7] Department of Ecology Monitoring, National University of Uzbekistan, 4 University Street, Tashkent 100174, Uzbekistan
[8] Department of Medicinal Plants, Tashkent State Agrarian University, 2 A., Universitet Str., Kibray District, Tashkent 100700, Uzbekistan
[9] Division of Sustainable Development (DSD), College of Science and Engineering, Hamad Bin Khalifa University/Qatar Foundation (QF), Education City, Doha P.O. Box 5825, Qatar
[10] Department of Botany, University of Mianwali, Mianwali 42200, Pakistan
*   Correspondence: zafar@qau.edu.pk

Abstract: Recently, intensifying energy crises accompanying ecological crises due to the decline in fossil-fuel reserves and extensive greenhouse gas emissions have triggered the exploration of renewable substitutes for petro-diesel. In this scenario, biodiesel is the best alternative to non-renewable finite conventional fuels due to its cost-effectiveness, sustainability, renewability, biodegradability, and eco-friendly nature. Hence, the current research was designed to utilize scanning electron microscopy to investigate and identify the micro-morphological characteristics of selected seed-bearing crops. Light-microscopy (LM) indicated discrete variations in macro-morphological characters such as seed shape (ovoid, ovate, oblong, semi-spheroid, or discoid), seed size (3.5–14 mm in length and 2.25 to 6.5 mm in width), seed color (yellow to black), and number of seeds per kilogram (from 6000 to 260,000). Chemical extraction via Soxhlet apparatus resulted in the estimation of oil content within the range of 20.3–48.0% (wt./wt.), FFA content (0.63–6.91 mg KOH/g), and maximum product, i.e., 98% biodiesel yield was achieved. Multivariate analysis via principal component analysis (PCA) was done using PAST 3 software to investigate similarities and differences among factors/variables. SEM examination exhibited ultra-morphological characters and distinct variation in cell-wall ornamentation; hilum occurrence, position, and level; wall-sculpturing variations such as ruminate, verrucate, wrinkled, or striate; cell arrangement (anticlinal or periclinal); and cell shape and margins. To conclude, SEM could be an advanced technique to disclose the ultra-micromorphological characteristics of oil-bearing energy crops providing a convenient way for scientists to determine correct identification, authentication, and classification.

Keywords: energy crises; seed crops; seed morphology; LM and SEM; biodiesel potential

1. Introduction

The energy that directly streamlines industry, power generation, and the transportation sector determines the economic success, development, and sustainability of a country [1]. In

ORIGINAL PAPER

CrossMark

Wild melon: a novel non-edible feedstock for bioenergy

Maria Ameen[1] · Muhammad Zafar[1] · Mushtaq Ahmad[1] · Anjuman Shaheen[1,2] · Ghulam Yaseen[1]

Abstract

In the present research work, a non-edible oil source *Cucumis melo* var. *agrestis* (wild melon) was systematically identified and studied for biodiesel production and its characterization. The extracted oil was 29.1% of total dry seed weight. The free fatty acid value of the oil was found to be 0.64%, and the single-step alkaline transesterification method was used for conversion of fatty acids into their respective methyl esters. The maximum conversion efficiency of fatty acids was obtained at 0.4 wt% NaOH (used as catalyst), 30% (methanol to oil, v/v) methanol amount, 60 °C reaction temperature, 600-rpm agitation rate and 60-min reaction time. Under these optimal conditions, the conversion efficiency of fatty acid was 92%. However, in the case of KOH as catalyst, the highest conversion (85%) of fatty acids was obtained at 40% methanol to oil ratio, 1.28 wt% KOH, 60 °C reaction temperature, 600-rpm agitation rate and 45 min of reaction time. Qualitatively, biodiesel was characterized through Fourier transform infrared spectroscopy (FTIR) and gas chromatography and mass spectroscopy (GC–MS). FTIR results demonstrated a strong peak at 1742 cm^{-1}, showing carbonyl groups (C=O) of methyl esters. However, GC–MS results showed the presence of twelve methyl esters comprised of lauric acid, myristic acid, palmitic acid, non-decanoic acid, hexadecanoic acid, octadecadienoic acid and octadecynoic acid. The fuel properties were found to fall within the range recommended by the international biodiesel standard, i.e., American Society of Testing Materials (ASTM): flash point of 91 °C, density of 0.873 kg/L, viscosity of 5.35 cSt, pour point of −13 °C, cloud point of −10 °C, total acid number of 0.242 mg KOH/g and sulfur content of 0.0043 wt%. The present work concluded the potential of wild melon seed oil as excellent non-edible source of bioenergy.

Keywords *Cucumis melo* var. *agrestis* · Wild melon seed oil (WMSO) · Transesterification · Bioenergy · Characterization · Fuel properties

1 Introduction

The ecological balance of natural resources has been disrupted to alarming levels due to exponential growth of human population and many other anthropogenic activities (Eryilmaz and Yesilyurt 2016; Chang et al. 1996). The recent trends in urbanization and industrialization have not only increased fuel consumption but also led to depletion of finite fossil fuel resources (Ilkilic et al. 2011). The

increased rate of fossil fuel consumption has resulted in increased carbon emissions, intensified local air pollution, ozone depletion and acid precipitation as well as magnified global warming up to alarming conditions (Ahmad et al. 2013). Therefore, the search for eco-friendly, renewable energy resources that may be substitutes for fossil fuels has become indispensable for a sustainable future. In the present scenario, biodiesel has a considerable attraction because of its many favorable properties: non-flammable, non-toxic, less pollutant emission, good lubricity and high flash point (Ahmad et al. 2011). Approximately, a 78% reduction in overall CO_2 has been observed in various analyses of biodiesel because of its closed carbon cycle (Ahmad et al. 2011). In addition to the high biodegradability of biodiesel, its high rate of combustion efficiency and low viscosity (measure of resistance of fluid to gradual deformation by shear or tensile stress) are its other major advantages (Ahmad et al. 2007; Atabani et al. 2012). In many earlier studies, biodiesel had been synthesized from

✉ Muhammad Zafar
zafar@qau.edu.pk

1   Biofuel Laboratory, Department of Plant Sciences, Quaid-i-Azam University, Islamabad, Pakistan

2   Department of Environmental Science, Female Campus, International Islamic University Islamabad, Islamabad, Pakistan

🌲 Springer

Biodiesel Synthesis From *Cucumis melo* Var. *agrestis* Seed Oil: Toward Non-food Biomass Biorefineries

Maria Ameen[1], Muhammad Zafar[1], Abdul-Sattar Nizami[2,3]*, Mushtaq Ahmad[1], Mamoona Munir[1,4], Shazia Sultana[1], Anwar Usma[1] and Mohammad Rehan[3]

[1]Biofuel Laboratory, Department of Plant Sciences, Quaid-i-Azam University, Islamabad, Pakistan, [2]Sustainable Development Study Center, Government College University, Lahore, Pakistan, [3]Centre of Excellence in Environmental Studies (CEES), King Abdulaziz University, Jeddah, Saudi Arabia, [4]Department of Botany, Rawalpindi Women University, Rawalpindi, Pakistan

This study aims to examine the potential of non-edible seed oil (*Cucumis melo* var. *agrestis*), seed oil content 29.1%, FFA 0.64 (mg KOH/g) for biodiesel production via nano-catalyst. The catalyst was characterized using X-ray diffraction spectroscopy (XRD), Fourier transform infrared spectroscopy (FTIR), scanning electron microscopy (SEM), and energy dispersive X-ray spectroscopy (EDX). The maximum biodiesel yield (93%) was attained under optimized conditions, i.e., 9:1 methanol to oil molar ratio, 2 wt% catalyst (MgO) at 60°C. The synthesized biodiesel yield was optimized through response surface technology via Box Behnken design (BBD). Biodiesel was characterized by advanced analytical techniques, including gas chromatography and mass spectroscopy, FTIR, and nuclear magnetic resonance (NMR). Fuel properties of synthesized biodiesel, including density (0.800 kg/L), K. viscosity @ 40°C (4.23 cSt), cloud point −12°C, pour point −7°C, sulfur content (0.0001%), flash point (73.5°C), total acid no (0.167 mg KOH/g) were found in lines with international standard of American Society of Testing Materials (ASTM). *Cucumis melo* var. *agrestic* seed oil and nano MgO catalyst appeared as economical, sustainable, and feasible candidates to overcome global energy glitches and environmental issues. The study findings involving unpalatable seed oil will be a promising step toward non-food biomass biorefinery.

Keywords: Cucumis melo var. agrestris, nano-catalyst, transesterification, biorefinery, fuel characterization

1 INTRODUCTION

Due to economic development, energy demand has increased with time. Overpopulation, urbanization, and deforestation have laid the foundation for this energy gap (Mahlia et al., 2020). Moreover, it has deteriorated the ecosystem by creating severe environmental concerns such as intensifying local air pollution, ozone depletion, acid rain, and global warming (Rahman et al., 2017). It is due to the emission of hazardous gases like CO_2, SO_x, NO_x, CO, and hydrocarbons produced during fossil fuel combustion that cause the greenhouse effect (Ahmad et al., 2011a; 2013; Mumtaz et al., 2021). The primary source for fulfilling basic energy needs is regular non-renewable petroleum-based fuel (Ullah et al., 2018). Finite deposits of conventional fuel are squeezing and exhausting fast due to continuous indiscriminate consumption and overexploitation (Cheema et al., 2021). This hasty decline of natural fuel reserves and linked petroleum price hikes have searched for alternative energy sources indispensable and accelerated their exploration and utilization (Dai et al.,

Prospects of Catalysis for Process Sustainability of Eco-Green Biodiesel Synthesis via Transesterification: A State-Of-The-Art Review

Maria Ameen [1], Mushtaq Ahmad [1,*], Muhammad Zafar [1,*], Mamoona Munir [1,2], Muhammad Mujtaba Abbas [3,*], Shazia Sultana [1], Rozina [1], Samah Elsayed Elkhatib [4], Manzoore Elahi M. Soudagar [5] and M. A. Kalam [6]

[1] Biofuel Lab, Department of Plant Sciences, Quaid-i-Azam University, Islamabad 15320, Pakistan; mameen@bs.qau.edu.pk (M.A.); mamoona.munir@iiu.edu.pk (M.M.); shaziaflora@hotmail.com (S.S.); rozinaroshni@yahoo.com (R.)

[2] Department of Biological Sciences, International Islamic University, Islamabad 44000, Pakistan

[3] Department of Mechanical Engineering, University of Engineering and Technology (New Campus), Lahore 54890, Pakistan

[4] Department of Mechanical Engineering, Faculty of Engineering & Technology, Future University in Egypt, New Cairo 11845, Egypt; samah.elmetwally@fue.edu.eg

[5] Department of Mechanical Engineering and University Centre for Research & Development, Chandigarh University, Mohali 140413, Punjab, India; me.soudagar@gmail.com

[6] Faculty of Engineering and IT, University of Technology Sydney, Sydney, NSW 2007, Australia; mdabul.kalam@uts.edu.au

* Correspondence: mushtaq@qau.edu.pk (M.A.); zafar@qau.edu.pk (M.Z.); m.mujtaba@uet.edu.pk (M.M.A.)

Abstract: Environmental pollution caused by conventional petro-diesel initiates at time of crude oil extraction and continues until its consumption. The resulting emission of poisonous gases during the combustion of petroleum-based fuel has worsened the greenhouse effect and global warming. Moreover, exhaustion of finite fossil fuels due to extensive exploitation has made the search for renewable resources indispensable. In light of this, biodiesel is a best possible substitute for the regular petro-diesel as it is eco-friendly, renewable, and economically viable. For effective biodiesel synthesis, the selection of potential feedstock and choice of efficient catalyst is the most important criteria. The main objective of this bibliographical review is to highlight vital role of different catalytic systems acting on variable feedstock and diverse methods for catalysis of biodiesel synthesis reactions. This paper further explores the effects of optimized reaction parameters, modification in chemical compositions, reaction operating parameters, mechanism and methodologies for catalysts preparation, stability enhancement, recovery, and reusability with the maximum optimum activity of catalysts. In future, the development of well-planned incentive structures is necessary for systematic progression of biodiesel process. Besides this, the selection of accessible and amended approaches for synthesis and utilization of specific potential catalysts will ensure the sustainability of eco-green biodiesel.

Keywords: biodiesel; esterification; transesterification; nanocatalysts; biocatalysts

1. Introduction

A specific portion of economic development of a country can be represented by its fuel consumption, since fuel plays a role in many commercial sectors such as the transport sector, where Petro-diesel is in particularly high demand. In addition, the emission of poisonous gases during fuel combustion has also become a matter of parallel concern because these gases are directly contributing to global warming as the greenhouse effect is becoming progressively worse. In this developing era, extensive research has been conducted with the objective of producing renewable and sustainable substitutes as a backup for non-renewable and exhausting fossil fuel either partially or completely. In this scenario, biodiesel is considered as successor for regular diesel produced by petroleum fractionation.

BOOK CHAPTER (ELSEVIER)

Prospects of Bioenergy Development in Future

Maria Ameen and Muhammad Zafar, Biofuel Laboratory Department of Plant Sciences, Quaid, i-Azam University, Islamabad, Pakistan

Mushtaq Ahmad, Biofuel Laboratory Department of Plant Sciences, Quaid, i-Azam University, Islamabad, Pakistan and Pakistan Academy of Sciences, Islamabad, Pakistan

Shazia Sultana, Biofuel Laboratory Department of Plant Sciences, Quaid, i-Azam University, Islamabad, Pakistan

Trobjon Makhkamov, Department of Forestry and Landscape Design, Tashkent State Agrarian University, Tashkent region, Uzbekistan

Akramjon Yuldashev, Department of Ecology and Botany, Andijan State University, Andijan, Uzbekistan

Oybek Mamarakhimov, Department of Ecology Monitoring, National University of Uzbekistan, Tashkent, Uzbekistan

Muhtor Nasirov, International Relations Office Samarkand State University, University Boulevard, Samarkand, Uzbekistan

Omer Kilic, Department of Pharmacy, Pharmacy Faculty Adıyaman University, Adıyaman, Turkey

Fethi A Ozdemir, Bingöl University Faculty of Science and Literature, Department of Molecular Biology and Genetics, Turkey

Yusufjon Gafforov, New Uzbekistan University, Tashkent, Uzbekistan; Tashkent International University of Education, Tashkent, Uzbekistan; and Institute of Botany, Academy of Sciences of Republic of Uzbekistan, Tashkent , Uzbekistan

Abstract

The contribution of bioenergy to the global energy system is substantial and indispensable. Because of the population explosion, global energy demand has increased along with fossil fuel consumption. In this scenario, energy derived from biomass may significantly lower carbon emissions, exclusively in difficult-to-decarbonize industries like manufacturing, heavy transportation, and aviation. However, expanding the use of bioenergy with sustainability in the global energy grid is a great challenge due to the need for cleaner production methods and stakeholder governance. This chapter will provide an overview of sustainable bioenergy with special emphasis to focus on the generation of biodiesel, biogas and bioethanol. The main objectives highlight the advances in various modern techniques for producing economically feasible bioenergy in future. Moreover, this chapter will cover affluences of clean and renewable energy production from non-edible oil seeds for bioenergy (raw materials shouldn't compete with food production). The overview of bioenergy, modern production methods, challenges, prospects, and future work in bioenergy development are all emphasized. These factors should all be taken into account for a smooth transition to a bioenergy economy.

Key Points

- This chapter aims to provide a comprehensive scenario of bioenergy development and the challenges encompassing it.
- To apprehend biomass feedstocks and bioenergy products that are now thought to be sustainable or likely to be in the near future due to the current momentum in technological and economic development of energy (biogas, biodiesel and bioalcohol)
- To conduct a thorough analysis of the scale of bioenergy, biomass supply, impacts, and associated challenges through this chapter.
- Exploration of status and challenges in socio-econo-environmental impact of bioenergy in modern era and future.